Clickmers and Aptamers as versatile tools for drug testing and fluorescence microscopy techniques

Dissertation

zur
Erlangung des Doktorgrades (Dr. rer. nat.)
der
Mathematisch-Naturwissenschaftlichen Fakultät
der
Rheinischen Friedrich-Wilhelms-Universität Bonn
vorgelegt von

Malte Rosenthal
aus
Bergisch Gladbach

Bonn 2020

Angefertigt mit Genehmigung der Mathematisch-Naturwissenschaftlichen Fakultät der Rheinischen Friedrich-Wilhelms-Universität Bonn

1. Gutachter: Prof. Dr. Günter Mayer
2. Gutachter: Prof. Dr. Christoph Thiele
Tag der Promotion: 13.07.2020
Erscheinungsjahr: 2020

Parts of this thesis have been published in:

Rosenthal M, Pfeiffer F, Mayer G**.** A receptor-guided design strategy for ligand identification. Angew Chem Int Ed Engl, **58**, 10752-10755. doi:10.1002/anie.201903479 (2019).

Pfeiffer, F., Rosenthal, M., Siegl, J., Ewers, J. & Mayer, G. Customised nucleic acid libraries for enhanced aptamer selection and performance. *Curr. Opin. Biotechnol.* **48**, 111-118, doi:10.1016/j.copbio.2017.03.026 (2017).

Tolle, F., Rosenthal, M., Pfeiffer, F. & Mayer, G. Click Reaction on Solid Phase Enables High Fidelity Synthesis of Nucleobase-Modified DNA. *Bioconjug. Chem.* **27**, 500-503, doi:10.1021/acs.bioconjchem.5b00668 (2016).

Contents

List of Figures

List of Tables

List of Abbreviations

11-OH-THC	11-hydroxy-tetrahydrocannabinol
AM11542	(−)-7′-Bromo-1′,1′-dimethylheptyl-Δ^8-tetrahydrocannabinol
2-AG	2-arachidonoylglycerol
ACN	acetonitrile
AEA	anandamide
APS	Ammonium peroxodisulphate
BAC	blood alcohol concentration
Bn-dU	benzyl-deoxyuridine
CB1	cannabinoid receptor 1
CB2	cannabinoid receptor 2
CBD	cannabidiol
CNS	central nervous system
CuAAC	copper-catalysed alkyne-azide cycloaddition
cAMP	cyclic adenosine monophosphate
DFHBI	2,5-difluoro-4-hydroxybenzylidene imidazolinone
DNA	deoxyribnucleic acid
dP	2-amino-8-(1′-β-D-2-deoxyribofuranosyl)-imidazo[1,2-a]-1,3,5-triazin-4(8H)one
DRUID	driving under the influence of drugs, alcohol, and medicines
Ds	7-(2-thienyl)imidazo[4,5- b]pyridine
dZ	6-amino-5-nitro-3-(1′-β-D-2′-deoxyribofuranosyl)-2(1H)-pyridone
eDFHBI	enlarged DFHBI ((Z)-4-((E)-3-(3,5-difluoro-4-hydroxyphenyl)allylidene)-1,2-dimethyl-1H-imidazol-5(4H)-on)
EdU	5-ethynyl-2’-deoxyuridine
ECS	endocannabinoid system
EIA	enzyme immunoassay
FACS	Fluorescence activated cell sorting
FISH	fluorescence in situ hybridization
FLAP	Fluorescent llight-up aptamer
FP	Fluorescent protein
GC-MS	Gas chromatography-mass spectrometry
HBI	(Z)-4-(4-hydroxybenzylidene)-1,2-dimethyl-1H-imidazol-5(4H)-one
HEK	Human embryonic kidney
HEPES	4-(2-hydroxyethyl)-1-piperazineethanesulfonic acid
HPLC-MS	High performance liquid chromatography – mass spectrometry
IL-1	interleukin-1
IL-6	interleukin-6
K_D	dissociation constant
LB	lysogeny broth
MS	multiple sclerosis
Nap-dU	naphthyl-deoxyuridine
NGF	nerve growth factor
NGS	next-generation sequencing
ONBY	*o*-nitrobenzyl-O-tyrosine
PA-DFHBI	Photoactivatable 2,5-difluoro-4-hydroxybenzylidene imidazolinoneIHB
PAFPs	photoactivatable fluorescent proteins
PAGFP	photoactivatable green fluorescent protein
PAH	solycyclic aromatic hydrocarbons

PALM	photoactivated localization microscopy
PAmCherry1	photoactivatable mCherry1
PCR	polymerase chain reaction
PDB	protein data bank
PDGF(-BB)	platelet-derived growth factor (B)
PEG	polyethylene glycol
PNK	Polynucleotide kinase
PPG	Photolabile protective group
RESOLFT	reversible saturatable optical linear fluorescence transition
RNA	ribnucleic acid
ROSITA	roadside testing assessment
rsFPs	Reversibly switchable fluorescent proteins
RT-PCR	reverse transcription polymerase chain reaction
SAM	S-adenosylmethionine
SAMHSA	Substance Abuse Mental Health Service Administration
SELEX	systematic evolution of ligands by exponential enrichment
SOMAmer	small off-rate modified aptamer
SRP	super resolution microscopy
STED	stimulated emission depletion
TfnR	transferrin receptor
THC	Δ9-tetrahydrocannabinol
THCA	Δ9-tetrahydrocannabinolic acid
THC-COOH	11-nor-9-carboxy-tetrahydrocannabinol
TPP	thiamine pyrophosphate

Abstract

Δ^9-tetrahydrocannabinol (THC) is the main psychotropic compound of the plant *cannabis sativa*. THC consumption provokes several physical impairments, which in turn might reduce the capability of consumers, to drive vehicles. Hence, test-devices for the police are needed, that reliably detect small amounts of THC in biological matrices as*, e.g.,* saliva. To date, most road-side test devices are based on antibodies and often lack the desired specificity and sensitivity. Therefore, chemically modified aptamers (clickmers) could serve as alternative biomolecules functioning as sensors in drug-test devices.
Chemically modified aptamers are able to bind a multitude of targets with high affinity and specificity. Click-SELEX enables the modular modification of DNA libraries during the selection process. The incorporated building blocks ideally support the interaction of the oligonucleotides with the target molecule, which might increase the prospect of the selection-success. In this thesis a Click-SELEX approach was applied for THC, which had been immobilised on magnetic particles for the selection procedure. A benzyl-functionalised DNA-library was utilized for the selection of clickmers. The click-SELEX resulted in a G-rich sequence, capable to bind THC-modified beads with a dissociation constant of about 100 nM. Further characterisation of its binding properties resulted in a 41 nt long oligonucleotide only containing one relevant benzyl-modified position. Binding was clearly dependent on the introduced aromatic residues. However, the determined affinity of the identified sequence to THC in solution is not sufficient for the construction of a road side test-device. Nonetheless, it could be demonstrated, that click-SELEX is a suitable method for the selection of ligands for difficult to address target molecules like THC. Additional click-selections with adapted selection conditions potentially could lead to clickmers that fulfil the criteria for a road-side test.

To study the location and dynamics of RNA sequences of interest fluorescent, light-up aptamer (FLAP) systems have been developed. FLAPs consist of RNA aptamers that specifically bind and enhance the fluorescence of inherently almost non-fluorescent organic dyes. To date, green, yellow, and red fluorescent light-up aptamer systems have been developed and the development of more FLAPs is in progress. One prominent FLAP is the Spinach-DFHBI complex. It has been shown, that slight modifications on the DFHBI structure in combination with already existing aptamers result in slightly red-shifted fluorescence emission of these complexes.
In this thesis a derivative of DFHBI (called eDFHBI) with an enlarged aromatic system was synthesized with the aim to develop a FLAP with red-shifted emission properties. In complex with Baby-Spinach eDFHBI showed a distinct red-shifted fluorescence. However, the affinity of Baby-Spinach to eDFHBI was drastically reduced. Thus, to develop a new FLAP system an RNA SELEX for eDFHBI has been undertaken. Yet the selection did not lead to the identification of the desired aptamer, thus the development of a red FLAP system was not successful.

Furthermore, a photoactivatable derivative of DFHBI, called PA-DFHBI was synthesized here. The combination of Spinach or Spinach-derived aptamers with PA-DFHBI would result in a photoactivatable FLAP. Such photoactivatable systems might be advantageous in super resolution microscopy techniques. Indeed, *in vitro* characterisation of PA-DFHBI with DFHBI binding aptamers revealed the functionality of such a photoactivatable system. However, in mammalian cells the PA-DFHBI-aptamer complex immediately emitted green fluorescence and thus the photoactivatable character of this system was lost. The reason for this problem could not be determined

Zusammenfassung

Δ^9-Tetrahydrocannabinol (THC) ist eine psychotrope Verbindung aus der Pflanze *Cannabis Sativa*. Der Konsum von THC führt zu deutlichen körperlichen Beeinträchtigungen, welche die Fähigkeit der Konsumenten zum Führen von Fahrzeugen herabsetzen können. Daher werden THC-Schnelltests für die Polizei benötigt, welche in der Lage sind, kleine Mengen an THC in biologischen Proben wie z.B Speichel zu erkennen. Aktuelle Testgeräte basieren meistens auf der Antikörper-Erkennung von THC. Oft fehlt es ihnen an der gewünschten Spezifität und Empfindlichkeit. Chemisch modifizierte Aptamere (Clickmere) könnten daher als alternative Biomoleküle dienen, die als Sensoren in Drogentestgeräten fungieren sollen.
Chemisch modifizierte Aptamere können eine Vielzahl von Zielmolekülen mit hoher Affinität und Spezifität binden. Click-SELEX ermöglicht die modulare Modifikation von DNA-Bibliotheken während des Selektions-Prozesses. Die so eingebauten Bausteine unterstützen idealerweise die Wechselwirkung der Oligonukleotide mit dem Zielmolekül, was die Aussicht auf den Selektionserfolg erhöhen könnte. In dieser Arbeit wurde ein Click-SELEX Ansatz für die Selektion von Clickmeren für THC verwendet. Hierfür wurde eine Benzyl-modifizierte DNA-Bibliothek eingesetzt. Die Click-SELEX resultierte in einer G-reichen Sequenz, welche in der Lage war, konzentrationsabhängig an die THC-modifizierten magnetischen Partikel zu binden. Weitere Charakterisierungen der Bindungseigenschaften führten zu einem verkürzten, 41 nt langen Oligonukleotid, welches eine einzige relevante benzyl-modifizierte Position enthielt. Die Affinität des Clickmers zu immobilisiertem THC lag bei etwa 100 nM. Die ermittelte Affinität des Clickmers zu THC in Lösung reicht jedoch nicht aus, um dieses als Sensormolekül in einem Drogen-Schnelltest zu verwenden. Zukünftig ausgeführte Click-SELEX könnten allerdings zum gewünschten Erfolg führen.

Mit Hilfe von neu entwickelten „fluorescent light-up Aptamer“ Systemen (FLAPs) kann die Lokalisation und Dynamik von RNA-Sequenzen von Interesse untersucht werden. FLAPs bestehen aus RNA-Aptameren, welche inhärent kaum fluoreszierenden organischen Farbstoffen spezifisch binden können und somit deren Fluoreszenz drastisch verstärken. Bisher wurden FLAPs von grüner, gelber und roter Fluoreszenz entwickelt, und die Entwicklung weiterer FLAPs ist im Gange. Eine wohl bekanntes FLAP ist der Komplex aus dem Spinach-Aptamer und DFHBI. Es wurde gezeigt, dass geringfügige Modifikationen der DFHBI-Struktur zu einer leicht rotverschobenen Fluoreszenzemission führen, wenn diese DFHBI-Derivate von den bekannten Aptameren gebunden werden.
In dieser Arbeit wurde ein DFHBI-Derivat mit einem erweiterten aromatischen System synthetisiert (eDFHBI), um einen FLAP mit rotverschobenen Emissionseigenschaften zu entwickeln. Das eDFHBI zeigte eine deutliche rotverschobene Fluoreszenz im Komplex mit Baby-Spinach. Jedoch war die Affinität von Baby-Spinat zu eDFHBI im Vergleich zu ursprünglichem DFHBI drastisch verringert. Daher wurde eine RNA

SELEX für eDFHBI durchgeführt mit dem Ziel ein rot fluoreszierendes FLAP System zu generieren. Die durchgeführte SELEX fphrte jedoch nicht zu dem gewünschten Ziel.

Außerdem wurde ein photoaktivierbares DFHBI-Derivat namens PA-DFHBI synthetisiert. Die Kombination von Spinach Aptameren mit PA-DFHBI würde theoretisch zu einem photoaktivierbaren FLAP führen. Derartige photoaktivierbare Systeme könnten in hochauflösenden Mikroskopietechniken Anwendung finden. *In-vitro*-Charakterisierungen von PA-DFHBI mit DFHBI bindenden Aptameren zeigten die Funktionalität eines solchen photoaktivierbaren Systems. In Säugetierzellen emittierte der PA-DFHBI-Aptamer-Komplex jedoch augenblicklich eine grüne Fluoreszenz. Somit ging der photoaktivierbare Charakter dieses Systems verloren. Der Grund für dieses Problem konnte nicht ermittelt werden.

1. Introduction

1.1 ∆9-Tetrahydrocannabinol

Marijuana, dope, weed, hemp, pot, ganja … the list of colloquial speech is large for the Δ^9-tetrahydrocannabinol (THC)-containing parts of the plant *Cannabis sativa* that, upon consumption leads to several psychotropic and physical effects on the human body. According to the World Health Organisation (WHO) around 2.5% of the world population consumes cannabis-products (annual prevalence) making it the most widely cultivated and used illicit drug worldwide[1–4]. Besides implementation of cannabis for medical purposes due to beneficial effects like the analgesic potency, its recreational application as a psychoactive drug is very popular especially among the younger part of the population in western countries[5,6]. Furthermore, recent years saw a general increasing acceptance of cannabis use, a decrease of criminalisation in some western countries and recreational legalisation of cannabis consumption in several US-states, Canada and Uruguay[7,8]. These new laws in Canada and some US-states in addition also have great economic influence, as can be seen by the success of several cannabis companies, e.g., , Canopy Growth, Aurora, and Apharia. Stock price for those companies are increasing since the beginning of 2017[9]. With increasing supply and widespread tolerance of cannabis use, there is a good chance for an escalating number of consumers. Some new studies already point into this direction and observe at least a slight increase in cannabis consumption upon legalisation[10–14].

Mainly responsible for the inebriant effects of cannabis is one of the contained cannabinoids, the (-)-(trans)-Δ^9-tetrahydrocannabinol (Δ^9-THC, or short: THC). It is the most intensively examined cannabinoid of over 500 different cannabinoids discovered in the plant *Cannabis sativa* to date. Actually, THC is a decay product of the carboxylic acid (-)-trans-tetrahydrocannabinolic acid (THCA), which in turn is the result of a complex biosynthetic route, involving the methylerithritol phosphate (MEP)-pathway as well as the polyketide pathway[15]. THCA itself does not induce any psychoactive effects. Due to its instability, heat or high light intensities cause a decarboxylation of THCA to yield psychoactive THC[16]. The bulk of the THC-content in the spadix (~20%) and the plants leaves (~ 5%) is initially existent as THCA.

1.1.1 THC, cannabinoids and the endocannabinoid system (ECS)

THC is the most extensively studied constituent of more than 100 phyto-cannabinoids found so far in *cannabis sativa*. Besides being mainly responsible for the psychoactive effects, it has been shown to provide several beneficial pharmacological properties justifying its application in medicine[17].

The medicative effects of phyto-cannabinoids and especially of THC can be explained by their influence on the endocannabinoid system (ECS)[18,19]. The ECS is known to

play a complex homeostatic role in body´s functions of “sleep, eat, forget, protect and relax”. These functions are kept running through an intricate interplay between the G-protein coupled cannabinoid receptors CB_1 and CB_2, their endocannabinoid ligands, e.g., sn-2-arachidonoyl-glycerol (2-AG) and anandamide, and presumably further G-protein coupled receptors[19–23]. Some of the discovered phyto-cannabinoids derived from *cannabis sativa* can imitate the effects of the body´s own endocannabinoids by binding to the same receptors. At the beginning of the 1990s it has been shown, that endocannabinoids have high affinities to cannabinoid receptors and furthermore induce behavioral effects similar to those observed for THC when injected into rodents[24]. A multitude of other endocannabinoids have since been discovered. Thus, phyto-cannabinoids do affect the endocannabinoid system by mimicking endocannabinoids. A selection of endocannabinoids and some phyto-cannabinoids is shown in **Figure 1.**

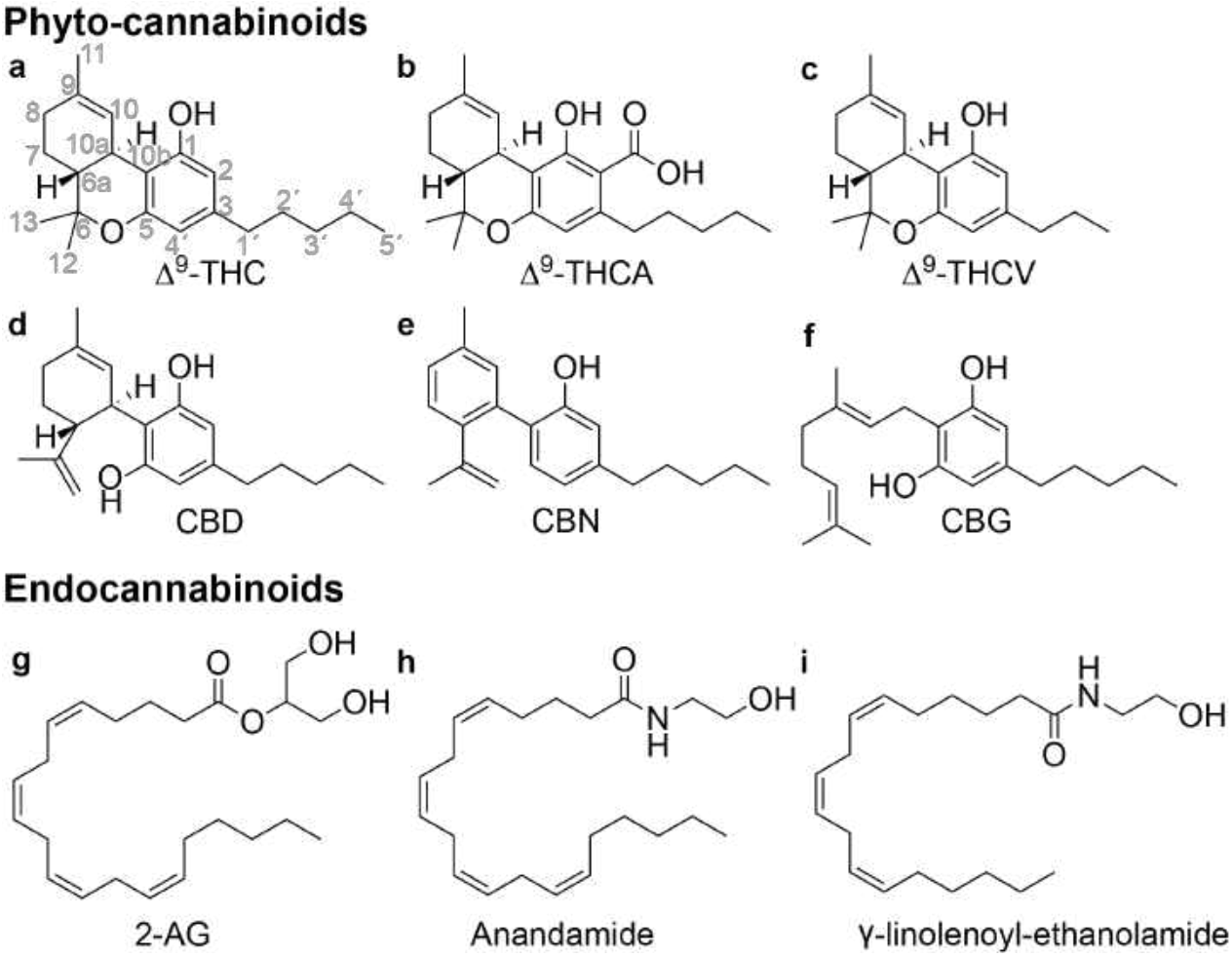

Fig.1. Overview of phyto- and endocannabinoids. Selection of phyto-cannabinoids with medicative effects: a) The psychoactive compound Δ^9-tetrahydrocannabinol (Δ^9-THC). Numbering of the tricyclic ring framework was done on the basis of the dibenzopyran system. b) Δ^9-tetrahydrocannabinoic acid (Δ^9-THCA), c) Δ^9-tetrahydrocannabivarin, d) cannabidiol (CBD), e) cannabinol (CBN), f) cannabigerol (CBG) g-i) Endocannabinoids: g) 2-arachidonylglycerol (2-AG), h) anandamide, i) γ-linolenoyl-ethanolamine.

Several phyto-cannabinoids have opposed effects, as some act as agonists, whereas others act as antagonists[25,26]. Anandamide, 2-AG, and THC function as (partial) agonists of the primary receptor CB_1, which is most abundantly expressed in the mammalian central nervous system (CNS). An important role of CB_1 apparently is the homeostasis of neuronal activity via modulation of neurotransmitter release upon binding of cannabinoids to the receptor[23]. CB_1 is most abundant in regions responsible for functioning as memory storage (hippocampus), motor function, movement control, and balance (cerebellum, basal ganglia) which explains most of the effects of psychotropic THC[20,21,27]. Furthermore, a low amount of CB_1 can be found in peripheral tissue, whereas CB_2, the second known cannabinoid receptor can primarily be found in cells of the immune and hematopoietic system and has functions in neuroprotection and immunosuppression[18–20,28].

Though the actual mode of interaction between THC and the cannabinoid receptor (CB_1) could not be completely clarified so far, several modelling studies during the last couple of years have elucidated some structural insight[29–31]. Binding of agonists leads to a conformational change resulting in the active state of the receptor.[31,32] Molecular dynamics simulation (MD) and two crystal structures agree on the fact that binding is mainly supported by hydrophobic or aromatic amino acids. However, co-crystallisation of CB_1 with Δ^9-THC itself was not successful yet. **Figure 2 a** shows a crystal-structure of CB_1 in complex with the agonist (−)-7′-Bromo-1′,1′-dimethylheptyl-Δ^8-tetrahydrocannabinol (AM11542). In addition, co-crystallisation and docking studies of various other CB_1 agonists and antagonists, which are not shown in **Figure 2**, have been published[32,33]. AM11542 has obvious similarities to THC like the tricyclic terpenoid ring system and the phenol-group at C1, as well as the same stereochemistry at the junction between ring B and C. The tricyclic ring system forms π-π-stacking interactions with phenylalanine-residues F177, F189, F268, and F379 whereas the phenolic hydroxyl group at C1 forms H-bonds with Serine-residue 383[32]. The likewise shown F200 seems more involved in a structural switch within the receptor upon receptor activation by a ligand[32]. On the basis of the CB_1-AM11542 structure, interaction of Δ^9-THC with CB_1 was investigated through docking and molecular dynamics validation. **Figure 2 b** depicts the high resemblance of THC-CB1-interaction to the CB_1-AM11542 structure. Again, the ring framework is in π-π-contact with phenylalanine residues[32]. Though there are discrepancies between several sources about the amount and position of amino acids important for ligand interactions, all studies published to date agree, that phenylalanine-residues play an important role in terms of π-π -stacking interactions[29,32–34]. Similarities could also be observed for the binding modes of the endocannabinoids anandamide and 2-AG compared to that of THC. Accordingly, the endocannabinoids adopt a C-shaped form and occupy a similar space in the same binding pocket of CB_1 as THC does[32–34].

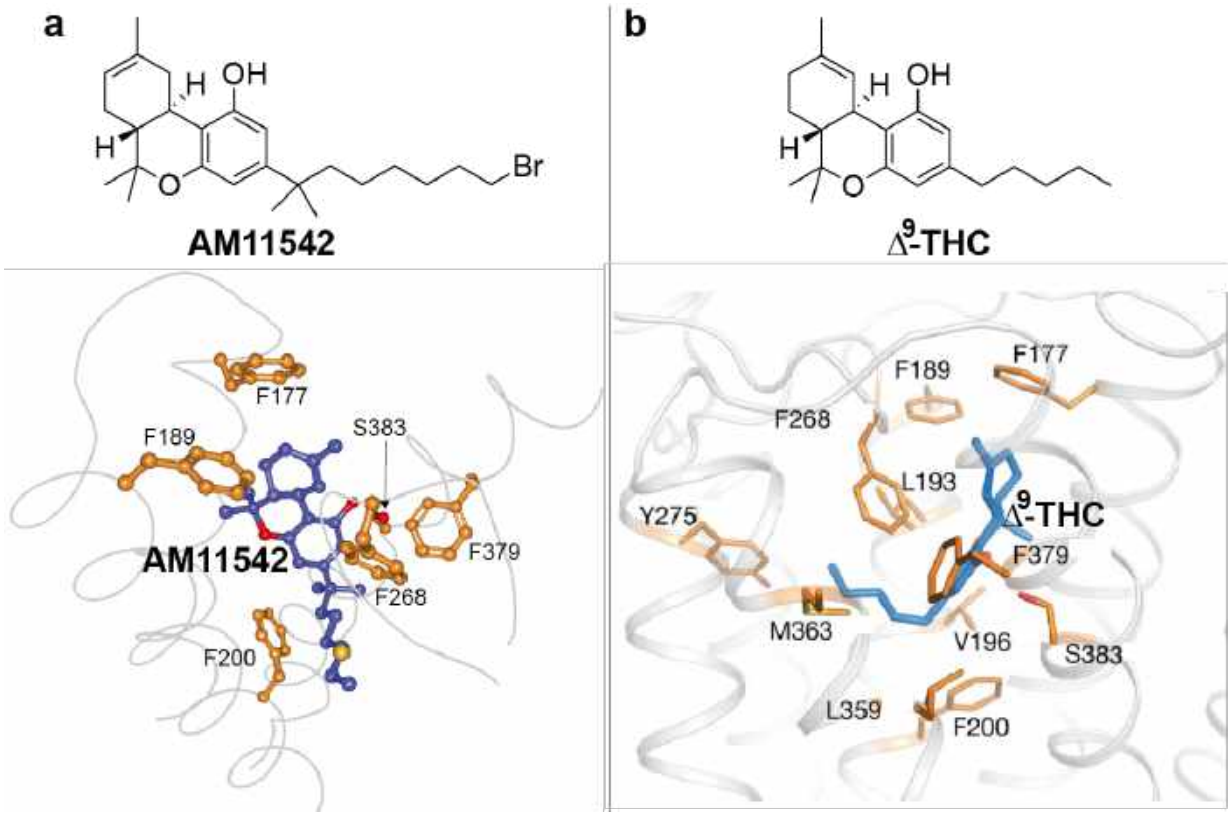

Fig. 2. Interaction studies of the ligands AM11542 and Δ^9-THC with the Cannabinoid receptor CB_1. a) CB_1-AM11542 ((−)-7′-Bromo-1′,1′-dimethylheptyl-Δ^8-tetrahydrocannabinol) crystal structure (PDB code 5XRA). Phenylalanine residues are depicted in orange. Structure of AM11542 is drawn in C=blue, O=red, Br=yellow. Structure was handled with the free software protein workshop. b) Molecular docking pose of Δ^9-THC. THC is drawn in blue, interacting amino acid residues are drawn in orange. Picture is modified after Hua et. al. 2017.

1.1.2 The History of Cannabis and THC

Cannabis sativa is known to be one of the earliest plants cultivated by men. Originating from central Asia, first reports about diverse fields of application in china date back several thousand years. Evidence of its cultivation for the production of fibres to manufacture ropes and textiles date back to 4000 B.C[35]. Also, the medical benefits have been known in Asian countries, long before the individual constituents responsible for those effects have been characterized [2]. The whole plant was used during that time to appease several complaints. Mainly its anaesthetic outcome led to its popularity and medical use for ages, while it spread around the world. According to the book *Pên-ts'ao Ching* it could be used for more than 100 ailments including gout, rheumatism, malaria, constipation, and absentmindedness (2700 B.C). Furthermore it was applied as analgesic during surgical operations, sometimes in combination with other sedative products as wine[35,36].

The psychoactive effects also played a role in several spiritual rituals of different cultures, particularly in India and Tibet but in later years also in some south American countries[35,36]. Especially in India the use of cannabis as medicine and recreational drug was widely spread dating back to around 1000 B.C[37]. In Hinduism and Buddhism the "sacred" cannabis was denoted as "bringer of freedom" and "source of happiness"[36].

For Africa, Arabia, Europe, and America archaeological evidence for cannabis use were found at later time points than for Asia. Intensified medical use is reported from the middle ages. Cannabis was used to treat, e.g., snakebites, malaria, epilepsy, and blood poisoning[36]. However, the risk that intense consumption might lead to addiction was also known and reported for the first time by Ibn al-Badri[35–38]. In the late eighteenths century, mainly the analgesic effects, the alleviating properties for several complaints, and the improvement of appetite and digestion led to a peak in cannabis use, followed by a decline in the first decades of the 20th century[35]. This reduction probably has been due to a combination of different reasons, e.g., the development of vaccines for a bunch of diseases, the discovery of synthetic analgesics[35,37], and increased usage of opiates[36]. Among American citizens, the 1930s saw an increase in recreational cannabis consumption, entailed by strongly increased taxes, and later on intensified restrictive legislation on recreational and medicinal cannabis use[35–37,39]. These restrictions further decreased medical interest in the plant, climaxing in the removal from the United States Pharmacopedia with the justification that cannabis had no medical use at all[39].

Renewed scientific interest occurred, with the identification of THC and other constituents in 1964 by Gaoni and Mechoulam[17,40]. THC is just one compound among a multiplicity of over 100 compounds, belonging to the so-called phyto-cannabinoids[41–43]. A multitude of pharmacological and clinical effects of those molecules could be investigated after the discovery of the endocannabinoid receptors CB_1 and CB_2 along with the ECS in the 1990s[44–46]. Going along with this renewed interest, decriminalization and even legalization of cannabis use is increasing in western countries again. In the USA, 30 states have passed laws for allowance of medical and recreational cannabis use within the last two decades[8]. Similar developments can be observed for some other western countries. Since 2018 Canada is the second country in the world (after Uruguay in 2013) that allows cannabis trade in addition to cultivation and consumption. In Europe legislation differs between countries. As cannabis consumption still is punishable with prison in France, Cyprus Greece, Hungary and Scandinavia several other European countries (e.g., Spain, Italy, and Germany) decriminalized its possession and consumption[8,47]. Moreover, medicinal products are nowadays authorized in 17 EU states[47]. This general development in legislation in western countries is reflected by the rapid growth of companies that legally cultivate and sell cannabis and cannabis products for medical purposes, as , e.g., Canopy Growth, Aurora, or Aphira[9].

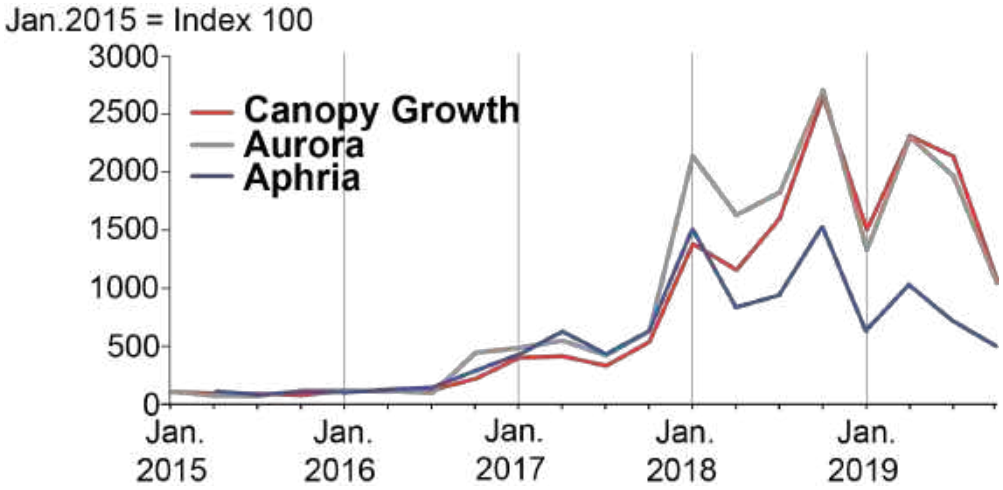

Fig. 3. Stock price development of the three largest cannabis producers over the last five years. Data were obtained and modified from https://www.onvista.de (25.11.2019)[9].

The stock prices for these three largest companies in cannabis business clearly increased since mid of 2016 (**Figure 3**). The trust of the investors seems justified as all three companies plan to further expand their cultivation area[48–50]. Hence, the available amount of recreational and medical cannabis products will probably further increase within the upcoming years.

1.1.3 Cannabis and THC in medicine

Medical cannabis is getting increasingly popular and represents promising alternatives to other medications, especially in the field of pain treatment. As already mentioned in **section 1.1.2,** the cannabis plant has found medical application within different cultures over thousands of years. With the discovery and investigations of several of the plant´s compounds, especially of the phyto-cannabinoids, the underlying reason for the healing effects were discovered[40]. The total impact of consumed cannabis on the human body is mediated through an interplay of different constituents. Among the several hundred phyto-cannabinoids, THC and cannabidiol (CBD) are the most abundant and most extensively studied compounds. As the psychotropic THC shows strong anti-inflammatory, analgetic and relaxing properties, in can alleviate, e.g., (spasm-induced) pain as in multiple sclerosis, arthritis, or cancer. The non-psychotropic CBD is known to antagonize some effects of THC. It can help to support the immune system and has additional anti-anxiety and anti-psychotic effects[51]. Furthermore, it shares anti-inflammatory and pain-killing properties, and thus potentiate those effects, already known from THC[51–54]. Besides the two mentioned molecules, further cannabinoids also seem to have therapeutic effects. Generally spoken, cannabis is a “synergistic shotgun” meaning that all the compounds within the plant might interact with the same, or different receptors[16]. Therefore, in Germany, 14 different cannabis strains can be used for the treatment of variable kinds of chronic pain, all of which differ slightly in composition of their main effectors THC and CBD[52,55–59]. In addition, medical cannabis preparations containing mixtures of phyto-

cannabinoids are available. The field of application is quite similar for all the preparations. Nabiximols (Sativex®) is a 1:1 mixture of THC and CBD and is used for chronic pain and spastic symptoms in multiple sclerosis (MS) patients and for pain treatment in patients where other medications , e.g., with opioids are ineffective[60]. Dronabinol (Marinol®) contains only THC and Nabilone (Canemes®), which is a synthetic THC-mimic are mainly prescribed for treatment of chronic pain, spastics, nausea, as well as anorexia. The pain-relievers can either be used as spray or pill[59]. Moreover, indications exist that cannabis or cannabis-based products have positive effects in treatment of diseases as epilepsy and Alzheimer[59,61,62].

The most common ways of cannabis consumption are smoking, inhalation or oral administration. By smoking or inhalation, THC is directly transferred from the lungs to the blood. The onset of THC´s effects occurs immediately (several seconds to minutes) after inhalation with a slow decline over about four hours. In contrast, effects start much later and last longer after oral administration[4]. Hence, for recreational purposes the most popular way of consumption is smoking of Marijuana (dried flower), or Hashish (resin from upper leaves and flower buds), since its relieving effects occur immediately, and the required dosage is therefore easy. In addition, overconsumption as can happen via oral intake can be avoided by smoking. However, bioavailability of THC is at only 10-27% or even lower when smoked, since 70% of existing THC will be destroyed during smoking via pyrolysis and additional losses of THC in side stream smoke further reduce availability, dependent on the individual user[63]. Individual smoking represented by the number, volume and intervals of inhalation dynamics are mainly responsible for the recorded differences regarding bioavailability[17,63–65]. A slightly more effective and healthier way of consumption is the utilization of vaporizers, wherefore they are favored for the medical administration[66]. Though by vaporization the plant is just heated to temperatures below combustion, which avoids the formation of hazardous compounds from pyrolysis. Nonetheless, the percentage of available THC remains low (~ 30%) as the heat is not sufficient to decarboxylate THCA completely[36,67–69]. Bioavailability after oral uptake of THC via edibles is slightly worse compared to smoked or vaporized cannabis and hence appears to be a little less effective in pain-killing[17,63]. In contrast, sublingual administration in form of oral-mucosal sprays seems most effective in terms of bioavailability[70].

Disregarding all medicative benefits that cannabis (and THC) consumption provides, several studies imply that heavy recreational use goes along with mental health problems[71,72] Especially heavy consumption during adolescence can lead to neurodegenerative abnormalities, altered brain development, cognitive deficits, and can be a risk factor for the development of heavy psychosis[2,4,8,17,35]. In this regard, an increasing use among teens is problematic[52]. Though some studies argue that a recovery from these deficits is possible in case of long abstinence, other studies report about persisting impairments in cognitive abilities[73]. In addition, it is known that heavy cannabis consumers can develop a dependency with signs of addiction and withdrawal symptoms after termination of drug consumption[8,74].

Mura *et. al.* supposed that for heavy users the long-lasting effects of cannabis consumption can be explained by residual THC-concentrations in the brain, even during time of abstinence[75]. The authors compared blood and brain specimen in 12 post-mortem cases for THC and the metabolites 11-OH-THC and THC-COOH (**Figure 4**). No direct correlation could be found between detected blood- and brain concentrations. THC-concentrations were always higher in brain tissue than in blood and accumulation was especially found in brain areas with high CB_1-concentrations[75].

1.2 THC-induced problems concerning road safety

Increased supply of (legal) cannabis reduces the hurdles to get hold of the drug, which in turn might lead to an increasing number of consumers. This tendency can already be seen in some US-states where cannabis is legalized, even though the increase of consumers or consumption frequency is not dramatic[10–12,14]. Although the progression of cannabis consumption over the next couple of years cannot be foreseen, new problems and challenges related to it might soon appear in different aspects of life, like serious health effects, e.g., THC intoxication[14,76]. Another major challenge is already presented by drivers under the influence of THC.

After alcohol, cannabis is the most frequently detected drug in road users in western countries[77–80]. A great threat is the misconception of cannabis impaired people. Some negative effects of cannabis are often overestimated by the consumers, who attempt to compensate, e.g., by significant reduction of driving speed[64,81,82]. However, the assumption that driving under cannabis impairment is without risk is not true, as diverse studies demonstrated[83,84]. Several experimental studies have been performed to investigate acute effects of cannabis consumption on psychomotor skills and especially driving performances. The general outcome shows that cannabis impairs the performance on driving-related skills[82,85]. Across the board, people under the influence of THC showed reduced abilities to control the driving direction, had an increased reaction time and decreased attention[64,81,82,86,87]. Furthermore, alterations compared to sober people have been determined regarding maintenance of the speed and distances to other vehicles. All the mentioned effects typically lasts 3-4 hours following the drug intake. Interestingly, though dose dependent, the influence on the ability to drive does not increase exponentially with THC-concentrations in blood, as is the case for alcohol[88,89]. The mentioned results about impairment on the driving skills were mainly observed in experimental studies. These studies rely on results from driving simulators and hence do not represent scenarios on real streets. However, to gain more insights into the impact of psychoactive drugs as THC on road-safety, long-term epidemiological studies have been conducted.

Europe's largest research project for driving under the influence of drugs, alcohol and medicines (DRUID) summarised statistics of fatalities in five years (2006-2011). Samples of body fluids of around 50000 randomly selected drivers have been analysed within 18 European countries and after alcohol, THC has been the most frequently

detected drug. The estimated prevalence of THC was 1.32%[80]. In accordance with that, THC-impairment could be confirmed amongst seriously injured (0.5-7.6%) or killed drivers (0-6.1%)[78–80]. In general, the risk to be involved in fatalities was elevated 2 to 3-fold in comparison to non-impaired control groups[82,87].

In the USA, the effects of cannabis on driving performance is heavily debated, though similar tendencies can also be detected[77]. Among THC-induced drivers the risk to be involved into car crashes was slightly increased compared to sober people. The US National Highway Traffic Safety Administration (NHTSA) asserted that the prevalence of THC among weekend-night-time drivers increased from 5.6% (2007) to 12.6% (2013-2014). Since the legalisation of medical cannabis in Colorado, the number of impaired drivers participating in road traffic and the number of fatal car crashes with impaired drivers increased clearly, compared to states without legalisation[90,91]. Generally, the risk of driving after cannabis consumption should be better communicated in combination with explicit law enforcement, which could help to keep THC-impaired driving in check. The latter is quite difficult due to several reasons. On the one hand *per se* limits not always factor impairment, since especially for heavy users (or patients) an altered metabolism and distribution of THC is observed and thus the THC-blood concentration does not correlate to appraisable impairment[92]. Hence some countries have different policies to penalize drivers under the influence of THC. One approach is the “impairment-approach” (e.g., in Greece, Great Britain and Ireland) that considers obviously impaired driving behavior. Alternatively, in addition to a “zero tolerance policy” (e.g., in Switzerland, Italy, Poland, Portugal), a “two-tier” system is used where *per se* limits are combined with an obviously affected driving behavior (e.g., Germany, Belgium, France Finland)[81,85]. For moderate cannabis consumers, it is stated that at a THC blood concentration of about 3.7 ng/ml entails a similar impairment of driving skills as it is observed for a blood alcohol concentration (BAC) of 0.5‰[65,83], which is the actual legal cut-off limit for alcohol in several countries, and could therefore serve as a reasonable *per se* cut-off limit for THC. It has been shown that compared to sober drivers, a 2.7-fold increase of responsibility for road accidents is associated with drivers having a THC-blood concentration of > 1ng/ml. At concentrations ≥ 5 ng/ml, culpability even increases to 6.6-fold[88,93]. However, legal cut-off limits of THC-blood concentrations vary clearly between different western countries and range from 1 ng/ml to 9 ng/ml.

1.2.1 Drug detection

As mentioned above, an accurate determination of THC impairment for road safety remains difficult. The situation cannot be compared to alcohol, where a higher concentration in blood is equivalent to stronger impairment. For THC-blood concentrations, the level of intoxication depends on a number of variables, as for example daily cannabis consumers tolerate higher THC-concentrations and have an altered THC-metabolism compared to occasional users[94]. Available drug tests can verify recent cannabis consumption, but impairment remains difficult to verify[85,95,96].

Law enforcement officers are mostly authorized to collect samples of biological matrices such as urine and oral fluid. In case of blood sampling, the sample collection is an invasive procedure and a trained healthcare-practitioner has to do it. This issue provides a problem for routine roadside-tests by the police. Each mentioned biological matrix has its own advantage and disadvantage for the accurate detection of cannabis/THC consumption, as is explained below[97].

1.2.1.1 Blood/Plasma testing

The presence of THC or its main psychotropic metabolite 11-OH-THC in the brain is responsible for the negative behavioural effects. This “high-effect” which is almost equivalent to impairment of roadworthiness is temporally closely correlated with THC blood- and plasma-concentrations. This is true, independent of the way of consumption. For occasional smokers, symptoms of impairment are determined to last two to four hours following consumption. THC-concentrations in blood peak between 5 and 15 minutes after uptake, decrease rapidly thereafter, and generally remain detectable for three to six hours, dependent on the inhaled amount of THC[64,81,85,87]. However, for chronical cannabis smokers, THC can be detected for up to 30 days in blood and plasma[94,96,98,99]. If orally administered, a delayed onset in combination with a longer lasting duration of effects is reported. The delayed uptake into the blood (peak ca. 2h after consumption) leads to a “flattened” concentration curve, with a lower concentration maximum and a longer decline period[63,70,100]. Blood/plasma testing has been shown to be the most effective way for the detection of recent cannabis use and for Germany the determination of THC-plasma concentration is required for legal sentence[85].

1.2.1.2 Urine testing

A problem for roadside urine-sampling is the fact, that sample drawing is an intimate process. An appropriate facility is therefore needed. In addition, to guarantee that no sample manipulation is possible, police officers of the same sex have to observe the sample taking. Both may not always be present in police road side testing[97,101].

THC is quickly metabolized in the human body leading to several THC-metabolites, which can be used to detect recent cannabis consumption.[8592102] Predominantly in the liver, THC is enzymatically hydroxylated at C9 resulting in the psychoactive primary metabolite 11-hydroxy-Δ^9-tetrahydrocannabinol (11-OH-THC) (see **Figure 4**). Successive oxidation of 11-OH-THC results in the metabolite 11-Nor-9-carboxy-Δ^9-tetrahydrocannabinol (THC-COOH)[100]. Common urine tests rely on the detection of the non-psychoactive metabolite THC-COOH since it is the most abundant metabolite in urine[103]. In urine, THC-COOH is mostly conjugated with glucuronic acid for solubility reasons. Both, the free THC-COOH and the THC-COOH-glucuronide can be detected

via enzyme-linked immune assays. High specificity (91-89%) and little cross-reactivity (selectivity 92-94%) of these tests have been demonstrated. For confirmation and quantification of the immunoassay results, the glucuronide has to be hydrolysed for measurement via GC-MS or LC-MS-MS measurements[94,100,104].

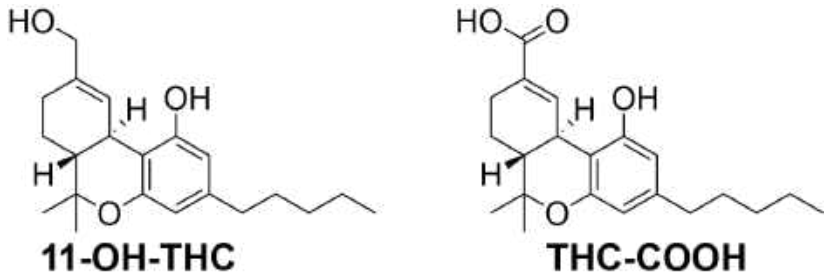

Fig. 4. Chemical structures of the two main metabolites of THC. 11-hydroxy-Δ^9-tetrahydrocannabinol (11-OH-THC) and 11-nor-9-carboxy-Δ^9-tetrahydrocannabinol (THC-COOH).

Though THC-COOH can be detected in blood quickly after administration (~30 min)[81,100,105] excretion into urine is slower. Therefore, detection of this metabolite in urine is possible only after the strongest impairment has passed[105–109]. Furthermore, once THC-COOH excretion into urine has started, the detection time for this metabolite can vary between 1-3 days for occasional users and even reach several weeks or month in case of heavy users[85,100,109,110]. Therefore, that detection of THC-COOH does not necessarily imply very recent cannabis consumption or impairment.

1.2.1.3 Oral fluid testing

Compared to blood or urine, the oral fluid (OF) is a relatively new biological matrix for drug testing. It clearly provides some advantages over the other two matrices, since it enables a non-invasive, gender-neutral sample collection and the detection time frame for THC and other cannabinoids is relatively small. Therefore, positive results in OF testing can be correlated to recent smoking and probable driving impairment[77,92,111].

The major route by which cannabinoids enter into OF is by contamination of the oral mucosa during administration of THC/cannabis. Passive diffusion of THC from blood to the OF does not play a relevant role. The oral mucosa is contaminated for some time after THC administration. Contamination is highest after smoking, and the drug can be detected in saliva until up to 15 h. For heavy daily smokers, positive samples could be collected up to two days of abstinence[109]. Furthermore, contamination of oral mucosa could also be detected after administration of an oromucosal spray (Sativex®), or consumption of cannabis-laced brownies[109–113].

Lipophilic THC forms a depot in the oral mucosa during smoking (or oral administration), from where it is released afterwards[109]. THC-concentrations in OF can reach extremely high values (> 1000 ng/ml) peaking directly after smoking (see **Figure 5 a**)[114–116]. Thereafter the concentrations decrease quickly within ca 2 h

post-smoking and then decline more gradually[113,117]. Furthermore, the elimination profile does not significantly alter between occasional and chronic cannabis smokers (compare **Figure 5 a, b**), implicating that THC detection time after the last smoking occasion is almost independent on smoking frequency and topography[116–118].

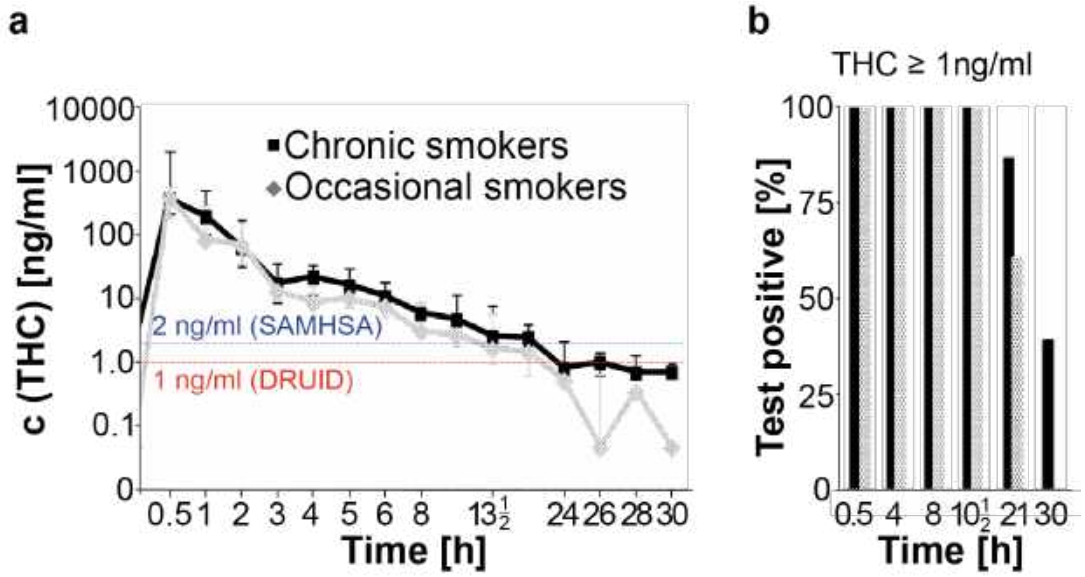

Fig. 5. Common cannabinoid detection times in OF via GC-MS. a) GC-MS detection of oral fluid (OF)-THC concentrations in daily chronic smokers and occasional smokers for 30 h, following smoking of a 6.8% THC-cigarette. The red dotted line represents the proposed cut-off concentration of 1 ng/ml as suggested in the *research project for driving under the influence of drugs, alcohol and medicines* (DRUID). The blue dotted line represents the 2 ng/ml cut-off proposed by the *Substance Abuse Mental Health Service Administration* (SAMHSA) b) Percentage of positive specimen for 30 h after smoking of a 6.8% THC cigarette, confirmed via GC-MS. Shown is the proposed cut-off concentration for THC ≥ 1 ng/ml (DRUID) All figures are modified after Anizan et. al. 2013[118].

If smoked, the concentration of THC in OF is higher than in blood and plasma samples[119,120]. In some cases, the elimination-profile of OF THC-concentrations has been found to mimic those of THC in blood[117,120]. However, since the contribution of blood-THC to OF-THC is only marginal and there is only little physical link between the two matrices, these findings appear to be hardly reliable[109,111,114,117,121]. Thus, there is no definite connection between the concentration of THC in blood and oral fluid, and calculations of blood/plasma concentrations[78,86,87] based on OF THC-concentrations is not possible. This is particularly important to know, since all legitimate cut-off concentrations, as well as all studies concerning driving capability were based on blood/plasma concentrations. Similar studies concerning OF-THC concentrations would therefore be important.

As subjective intoxication related with impaired driving performance is strongest for the first 2-4 h and can persist to almost 10 h post-smoking, it is important that reliable detection of THC in OF is possible in this time-span[122–126]. The detection-time frame varies between several studies, probably due to several reasons: A first challenge is the OF sampling. THC induces a dry mouth, making it hard to collect enough saliva to

accurately detect the actual concentrations[127]. Additionally, attachment of the highly hydrophobic THC to the collection device can provide a problem, which falsifies the readout. However, several new collection devices meanwhile ensure almost complete recovery levels[128,129].

With the highly sensitive GC-MS-MS method (cut-off 0.5 ng/ml) the mean post-smoking detection time for THC is around 13 h, but can vary strongly depending on the individual smoking habits. For chronical daily users, it even can be detected until up to 48 h after smoking. Similar results were obtained for THC detection via immunoassays with a cut-off of 1 ng/ml (mean detection time: 15 h, maximal detection time 30 h)[98,109,130]. Generally, the Substance Abuse Mental Health Service Administration (SAMHSA) propagates, that detection of ≥ 2 ng/ml THC in OF indicates cannabis/THC consumption within the last 24 h (compare to **Figure 5 a**)[130]. Contamination of oral mucosa by passive smoke also led to detectable THC concentration in OF, though the measured concentrations were significantly smaller than for active smokers[109,116,120]. Furthermore, the detection time frame is also clearly shortened and usually does not exceed 0.5-3 h. Worth mentioning is the fact, that the 3 h positive samples were obtained from subjects that have spent 3 hours in a heavily smoke-filled Dutch coffee shop[131]. Thus, the study most probably represents the upper time limit for contamination of the oral mucosa by passive THC-smoking.

Compared to test devices for urine, THC detection-time in OF is clearly shorter and linked more closely with recent THC consumption. To verify recent consumption, the detection of other cannabinoids as CBN or CBD could also be useful. Especially CBN and CBD are present in cannabis smoke, however in lower amount. For both, the elimination profiles in OF are comparable to that of THC, though with a reduced peak-concentration[113–115,118]. Therefore, a combined detection of THC and CBN (via GC-MS) could also be used to link a positive result to recent cannabis smoking[118]. Such a combined detection also would enable the discrimination of recreational smoking and medical administration, of Sativex®-spray as the ratio of THC to CBN is different in the latter[113].

A major problem has long been the specificity and sensitivity of OF-roadside testing-devices. A majority of these devices did not fulfil the criteria from the European Roadside Testing Assessment (ROSITA) project, which indicates that specificity and sensitivity have to be above 90%[119,132]. Recently Dräger developed the OF test-kit Drugtest 5000® that shows acceptable sensitivity (53%-93%) and specificity (71%-99%), and appears to be the most reliable OF roadside testing device at the moment[119,130,132,133].

Often, like for the Dräger drug test, the devices are based on the immunoassay principle of competitive inhibition[134]. For this purpose, antibodies are the applied biomolecules that detect the desired drugs in the samples. Besides antibodies, aptamers could be a promising class of biomolecules that can detect small molecule targets. Suitable aptamer candidates for THC that are capable to detect THC in the

desired concentration range in saliva could easily be incorporated into roadside test-devices.

1.3 Aptamers

In the last three decades, a tremendous development of aptamers has occurred. Besides antibodies, this class of functional biomolecules is becoming increasingly important as molecular tools used in chemical biology[135]. In general aptamers are short singe-stranded DNA or RNA oligonucleotides, capable of folding into defined three-dimensional structures and this binding to target molecules with high affinity and specificity. Aptamers are commonly identified via an iterative *in vitro* selection process, starting from a highly diverse library of 10^{15} different oligonucleotide sequences. The scope of aptamer-targets ranges from small organic molecules[136] and proteins[137], over ions[138] to even more complex structures as whole cell surfaces[139] or pathogenic microorganisms[140,141].

As aptamers can easily be achieved via solid phase synthesis, they have some clear advantages over antibodies. These include thermal stability and low/no immunogenicity[142–144]. Since aptamers can be chemically synthesized, a cheap and fast production is possible and there is no batch-to batch variation as it can sometimes be seen for antibodies[145,146]. In addition, aptamers can be chemically modified at defined positions, e.g., to increase their stability or affinity. Due to these advantages aptamers have found applications as tools for drug delivery[147,148], and diagnosis[149], can function as bio-sensors[150,151], and are a class of promising new therapeutics[144,152–154]. To date, only one aptamer (Macugen/Pegaptanib sodium) has found application as therapeutic agent, but around eleven more have entered clinical trials[144]. Pegaptanib is a heavily modified 27 nucleotide long RNA aptamer, which is therapeutically used to treat neovascular age-related macular degeneration (AMD). It is approved in the USA, Canada, Europe, Brazil, and Australia[155]. Besides the treatment of macular degeneration, aptamers could be promising therapeutics in fields as oncology[156,157] or coagulation[158–160]. Several candidates are in phase II or III in clinical trials.

1.3.1 SELEX

Aptamers are commonly selected in a process called systematic evolution of ligands by exponential enrichment (SELEX). Though there is a huge diversity of selection techniques, SELEX is mostly performed *in vitro*[161–163]. Chemically synthesised, single-stranded RNA- or DNA (starting-) libraries are incubated with the desired target molecule (I). Sequences not interacting with the target are subsequently removed (II) and target-binding sequences are recovered (III), (RT-)PCR amplified (IV), and converted into single-stranded sequences, respectively transcribed in case of RNA-libraries (V). The resultant, enriched library is then used for the subsequent SELEX

cycle. Ideally, several iterative cycles result in high affinity aptamers for the desired target molecule. **Figure 6** schematically depicts a DNA-SELEX cycle. In many cases, the target molecule has to be immobilized on a solid support, which enables the separation of binding and non-binding sequences. This immobilisation step always represents minor alterations regarding the chemical structure of the target. If the target molecule already carries suitable functional groups, it can be covalently coupled to a solid support via these groups. If no suitable functional groups are provided by target molecule, a manipulation of its chemical structure has to be done prior to the actual immobilisation step to introduce additional functional groups. These functional groups can then be used to covalently couple the target to the solid support. Hence the immobilised target differs chemically from its native form.

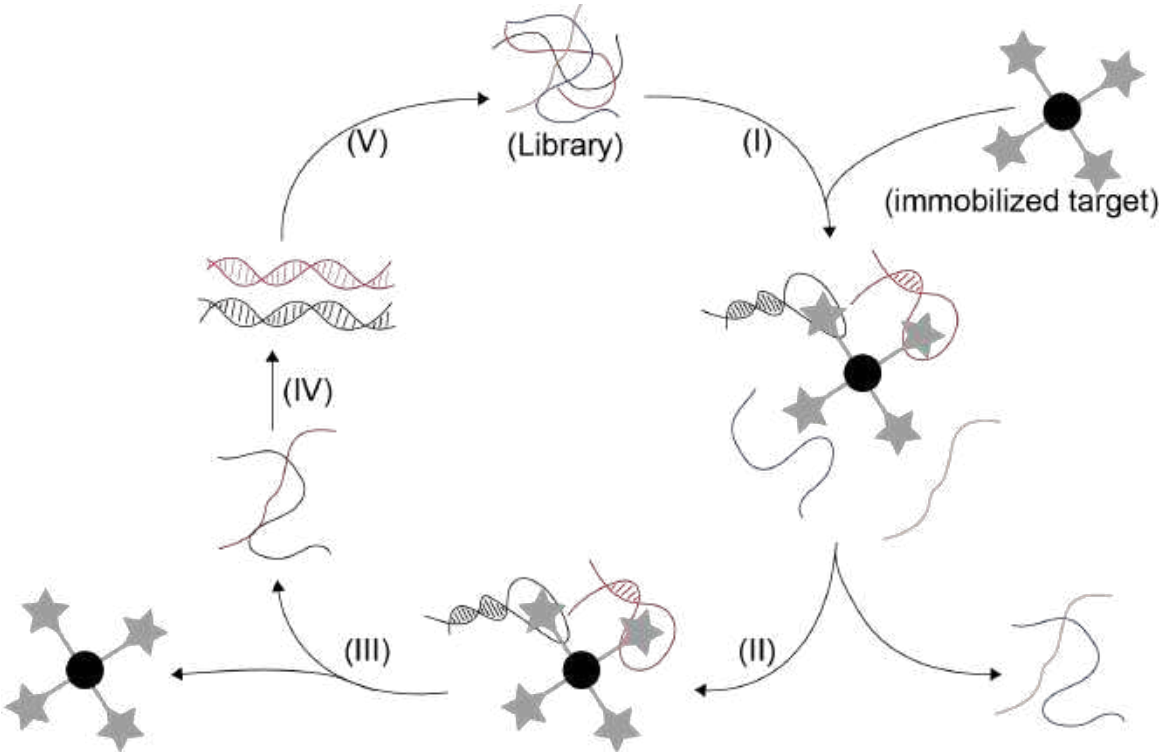

Fig. 6. Conventional (DNA) SELEX-cycle. Single-stranded starting library is incubated with the target (grey star) immobilized on a solid support (I). After removal of non-binding sequences (II) the binding sequences are recovered (III), subsequently PCR amplified (IV) and converted to single-stranded sequences (V) for the next cycle.

Meanwhile a large variety of different SELEX strategies with diverse advantages and disadvantages has been developed[161,164,165]. For example, capture-SELEX does not require immobilisation of the target molecule. This makes capture-SELEX especially promising for small molecule targets, since their immobilisation is often difficult due to a lack of functional groups. An illustration of the basic capture-SELEX concept is given in **Figure 7**. A specifically composed library is applied for this technique. This library contains a "docking sequence", which can hybridize to a complementary "capture-oligo". This "capture-oligo" contains a biotinylated linker and is immobilized on streptavidin coated magnetic particles. Thus, the library can be captured on the magnetic solid support, while the SELEX target can be titrated in solution. Upon binding of sequences to the target molecule a conformational change leads to elution

of those sequences from the solid support[166]. Since the library sequences are immobilised on sold support instead of the target molecule, this selection technique shows minimal non-specific binding. Other SELEX approaches rely on the difference in migration behaviour of target bound and non-bound sequences in an electric field, e.g., capillary electrophoresis (CE)-SELEX or electrophoretic mobility shift assay (EMSA)-SELEX[166,167]. Both methods are primarily applicable for protein targets, due to the following reason. Non-bound oligonucleotides of uniform length migrate through an electric field with the same velocity, independent of sequence. For target bound sequences, the size and charge of the complex is altered compared to free sequences, which results in a change of mobility. Differently migrating fractions can separately be collected and target-bound sequences can be recovered for the upcoming SELEX-cycle. However, the mentioned alteration in velocity is pronounced for huge targets like proteins, whereas for small molecules the effect on mobility is only marginal.

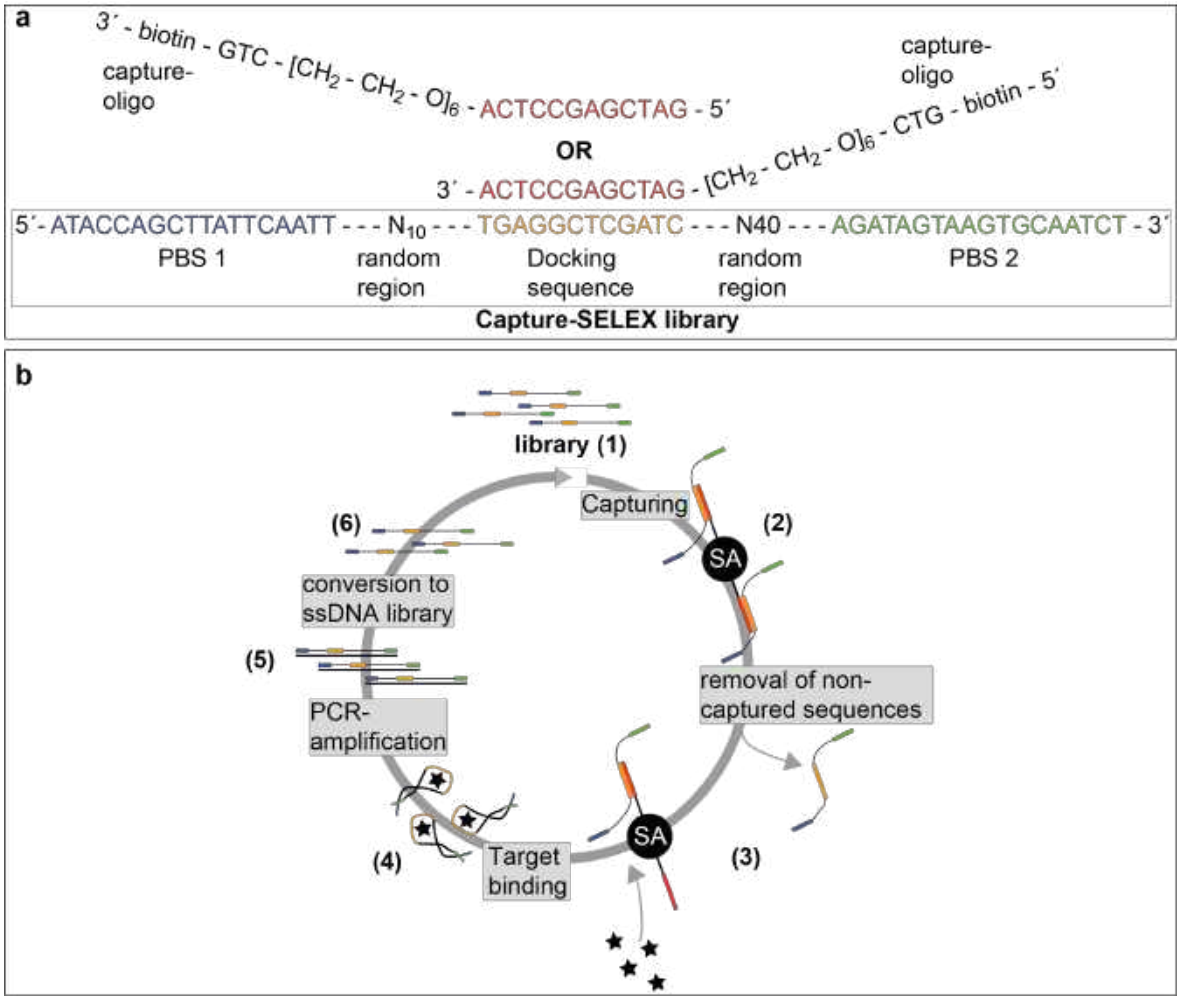

Fig.7. Explanation of Capture-SELEX. a) Design of the capture-oligo and the capture-SELEX library. The capture-oligo is immobilized to streptavidin beads. The library can be immobilized to the complementary capture-oligo (red) via the docking sequence (orange). b) The simplified capture-SELEX process is shown: The starting library and DNA pools of subsequent SELEX cycles (1) is immobilized via hybridisation to the capture-oligo, which is bound to streptavidin coated beads (2). Sequences that do not hybridise to the capture-oligo are removed via washing steps (3). During target binding (4) sequences with affinity to the target fold into a defined three-dimensional structure and are thereby released from the capture-oligo. These eluted sequences can subsequently be PCR amplified (5) and converted to single stranded pools for the next selection cycles (6). The figure is modified after Stoltenburg *et.al.* (2012) [168].

1.3.2 Modified aptamers

In order to improve pharmacological properties like the *in vivo* half-life time of aptamers (especially for nuclease-susceptible RNA-aptamers), to increase the binding affinity, or to enhance the selection success, several modifications can be incorporated to different positions of the biopolymers. Modifications concerning the sugar moiety, or the phosphate backbone are mostly introduced to increase *in vivo* stability of aptamers, whereas modifications of the nucleobases can rather increase the diversity and binding performances. Modifications can either be incorporated during the selection process or retroactively after completion of the SELEX process.

1.3.2.1 Sugar-phosphate-modifications

The most obvious difference between DNA and RNA aptamers is the sugar moiety. The 2´-OH of ribose makes RNA chemically less stable than DNA, which contains deoxyribose. RNA is more susceptible to auto-hydrolysis as well as enzymatic cleavage[169], which obviously is problematic for the stability of RNA aptamers. Thus, a package of aptamer modifications has been invented to increase RNA aptamer stability, ranging from substitutions of the 2-OH to alterations of the phosphodiester backbone. Various substitutions of the 2´-OH group ribose by 2´-fluoro-, 2´-amino-, or 2´-methoxy-ribose are common ways to improve nuclease resistance and thus also serum half-life time[170–172]. Capping of the 3´-end of RNA and DNA aptamers with 3´-biotin or 3´-inverted thymidine is also a common way to protect oligonucleotides from the attack of 3´- to 5´-exonucleases[144,173,174]. Furthermore, substitutions of conventional ribose by chemically altered structures help to improve the serum stability. Substitution of ribose by so called locked nucleic acids (LNAs)[175] or unlocked nucleic acids (UNAs) enhance serum stability and can alter biophysical properties like the melting temperature[176]. Spiegelmers are another group of RNA aptamers containing non-natural ribonucleotides. In this case they consist of L-ribonucleotides. Oligonucleotides containing L-ribonucleotides thus are mirror images of natural oligonucleotides and have a high resistance to nucleases. Spiegelmers therefore already have great biostability without further modifications of their chemical structure[177–179]. L-ribonucleotide containing oligonucleotides can be chemically synthesized, similar to natural oligonucleotides. However, selection of Spiegelmers is not possible via SELEX since L-ribonucleotides are not accessible for enzymatic procedures. They are obtained via SELEX with conventional oligonucleotides for mirror images of the target molecules. Mirroring of the resulting natural aptamers that were selected for the mirror image of the desired target molecule then leads to Spiegelmers[156,158,159,177].

Modification on the native phosphodiester linkage is another potential starting point for the introduction of modifications. Replacement of the phosphodiester group by several kinds of more hydrophobic triazoles can increases resistance to nuclease cleavage[180–

[182]. The same is true for the substitution of the phosphodiester by phosphorothioate, phosphorodithioate or methylphosphonate, which have been shown to reduce nuclease degradation[183,184].

One problem for aptamers with therapeutic purpose is, that DNA and RNA oligonucleotides show very short *in vivo* half-life times due to the fast renal filtration of such small molecules. The introduction of a high molecular weight modification like PEG-linker is a proven way to extend the *in vivo* half-life time. The total molecular weight is increased beyond the renal filtration threshold and thus the circulation time of aptamers is increased[148,185,186].

The most prominent example of a modified RNA aptamer is Macugen, the first Food and Drug administration (FDA)-approved aptamer based drug, carrying 2´-methoxy purines, 2´-fluoro pyrimidines and a 40 kDa PEG moiety at the 5´-end[187]. The mentioned Spiegelmers are another group of aptamers that have great potential as therapeutics and several of them are in phase II or III of clinical trials[156,158,160].

1.3.2.2 Introduction of artificial base-pairs: expanding the genetic alphabet

Despite the mentioned advantages of aptamers over antibodies, the success rate of SELEX is in need of improvement[188,189]. Besides the development of further selection strategies for the great variety of targets, chemical manipulation of the nucleobases helps to increase the success rate. The intrinsic restriction of chemical diversity of oligonucleotides compared to antibodies is thought to be one reason for the failure of a multiplicity of selections[190].Conventional nucleic acid libraries consist of four naturally occurring (deoxy)nucleosides carrying the nucleobases Adenine (A), Guanine (G), Cytosine (C) and Thymine (T) (Uracil for RNA) (**see Figure 8 a**). All mentioned nucleobases do have similar physical properties and chemical structures. Compared to this small repertoire of building blocks for oligonucleotides, proteins do have a broader collection of building blocks, as they consist of 21 amino acids. The chemical nature and physical properties of these amino acids can roughly be subdivided into hydrophobic, polar, acidic, and basic (**Figure 8 b**). Thus, the amount of potential interaction modes between proteins and their binding partners is increased compared to oligonucleotides. Especially hydrophobic contacts, which are frequently observed in protein–protein interactions[191,192] are rarely seen between conventional aptamers and their target molecules[193].

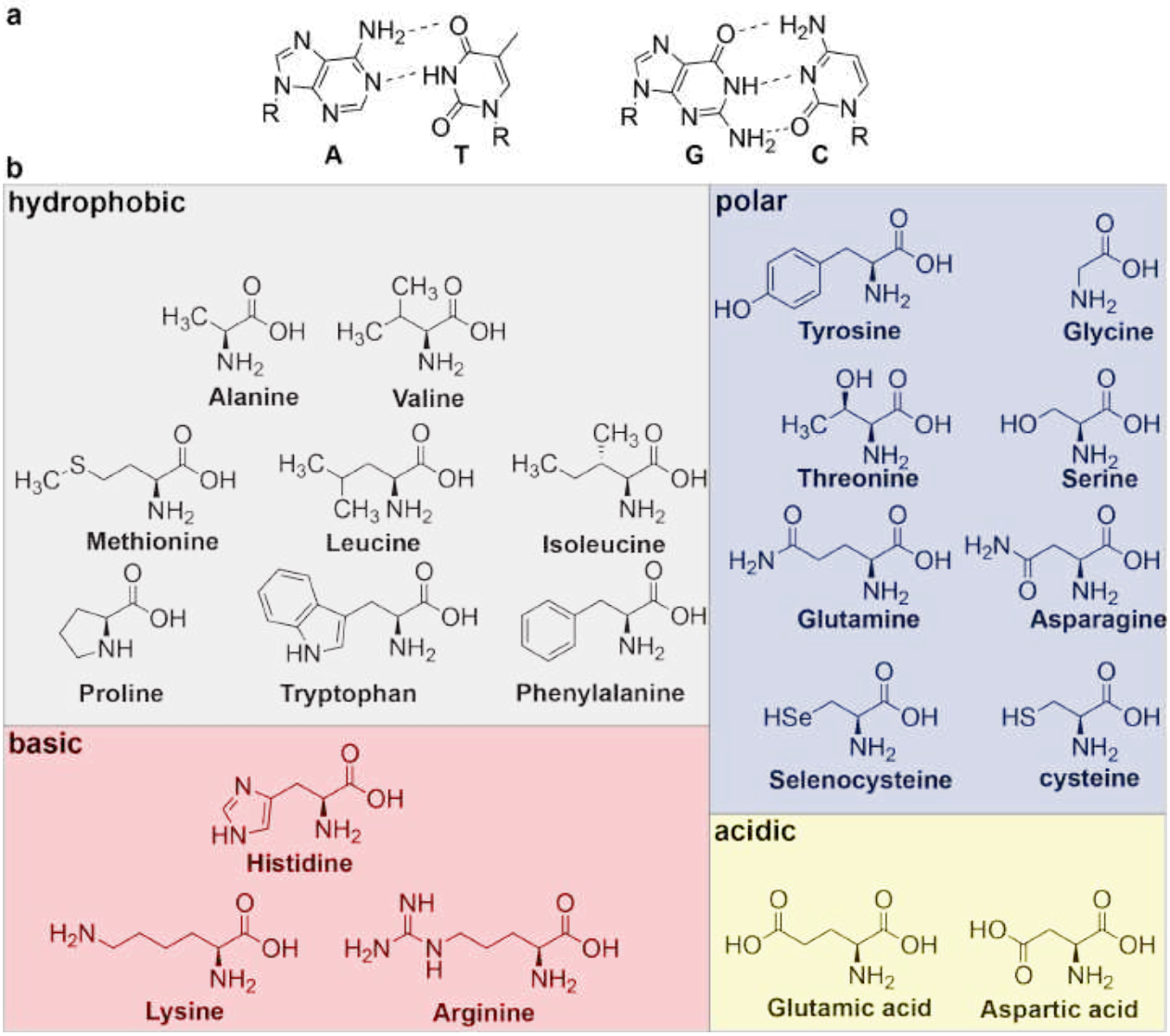

Fig. 8. Comparison between the chemical structure of nucleic acids and amino acids. a) Depiction of the pyrimidine nucleobases thymine (T) and cytosine (C) and the purine nucleobases Adenine (A) and Guanine (G) found in DNA oligonucleotides. b) Representation of the 21 amino acids. The side chains of the amino acids can be subdivided into hydrophobic, polar, basic and acidic.

Different attempts to increase the chemical diversity of aptamers have been published. Introduction of artificial additional base pairs into oligonucleotide sequences to increase the chemical repertoire for aptamers is one prominent possibility. Another popular approach is the modification of the chemical structure of existing nucleobases, which also increases the chemical repertoire. Newly introduced chemical groups facilitate additional types of interaction modes between the nucleic acids and the target structures, which helps to increase the affinity and specificity of resulting aptamers[194]. A variety of artificial base-pairs, either relying on shape-complementarity or H-bonding has been synthesized during the last years[195–197]. Two promising different artificial base pairs that have successfully been used for aptamer selection are detailed here (see **Figure 9**)[198,199].

The so called artificially expanded genetic information system (AEGIS)-SELEX makes use of an artificial third base pair consisting of the nucleotides 2-amino-8-(1′-β-D-2-deoxyribofuranosyl)-imidazo[1,2-a]-1,3,5-triazin-4(8H)one (**P**) and 6-amino-5-nitro- 3-(1′-β-D-2′-deoxyribofuranosyl)-2(1H)-pyridone (**Z**). Z-P base-pairing is based on H-bonding like in natural nucleotides (**Figure 9**). Randomized libraries containing six nucleotides (dG,dA,dT,dC,Z,P) can be created via solid-phase synthesis. Furthermore, the non-natural base–pair is recognized by Hot Start Taq polymerase, ensuring the applicability for SELEX. AEGIS-aptamers resulting from selections for breast cancer cells, an isolated protein target, and a protein overexpressed on a cell line showed binding properties that were greatly diminished in the absence of Z and/or P. That result indicates that those nucleotides strongly contributed to the binding event[198–200].

The second here described artificial base-pair consists of 7-(2-thienyl)imidazo[4,5-*b*]pyridine (**dDs)** and 2-nitro-4-propynylpyrrole **dPx** (see **Figure 9 b**). The **dDs-dPx** base-pair is worth mentioning, since its complementarity is based on size and shape, rather than H-bonding. The **dDs-dPx** base pair was successfully applied in genetic alphabet Expansion for Systematic Evolution of Ligands by EXponential enrichment (ExSELEX). In selections for VEGF-165 (k_D 0.65 pM) and IFN-γ (k_D 38 pM), as well as for cell-ExSELEX for three breast cancer cell lines (MCF7, MDA-MB-231, T-47D) only the hydrophobic **dDs** was introduced at fixed positions on the sense-strand of DNA-libraries[201]. The hydrophobic character of **dDx** and the resultant increased interaction properties might explain the >100-fold improved affinities of the thus selected aptamers, compared to conventional DNA aptamers[198]. Incorporation of the artificial base **dPx** into the sense-stand of DNA libraries was knowingly avoided. This was done to avoid **Px-Ds** pairing in the libraries, which accordingly increased the probability of interactions between the hydrophobic **Ds** with hydrophobic portions of the target proteins. The artificial **dPx** was just used as complementary base and only needed for the practicability of PCR-amplification.

ExSELEX libraries with the thus expanded genetic alphabet are incompatible with conventional sequencing techniques. Hence, sequencing of such libraries initially provided a big challenge. To circumvent the sequencing challenge Kimoto *et. al.* subdivided the applied SELEX library into more than 20 different sub-libraries. In each sub-library one to three dDs were present at defined fixed positions. A recognition tag consisting of two or three natural nucleotides was added to each sub-library as kind of “barcode”, to track the number and location of **dDs** in the sequences[193,198]. For the actual sequencing process, the **Ds** bases in the enriched sequences were replaced by natural bases (mainly adenine) by a replacement PCR amplification in the absence of **dDsTP** and **dPxTP**. Due to the high fidelity of the **dDs-dPx** pair, the replacement of the artificial **dDs** by a natural base is inefficient. Thus, for the replacement of the artificial to the natural base a mediator of the replacement PCR was introduced. This mediator again was an artificial nucleotide, the triphosphate of 4-propynylpyrrole-2-carbaldehyde (**dPa´**) (**Figure 9 b**). Since the fidelity of the **dDs-dPa´** pairing is lower than the **dDs-dPx** pairing, the misincorporation of natural bases into the sense strand of the enriched sequences during replacement PCR is increased. The replacement

PCR could be performed with AccuPrime*Pfx* DNA polymerase. After sequencing of the resulting natural DNA sequences, the original positions of dDs within the sequences could be identified with the “barcode-tag”[202].

The initial restrictions concerning the positions of dDs within the SELEX libraries were meanwhile conquered by an even more sophisticated way of sequencing[203]. In new versions of ExSELEX a completely randomized library containing dDs was applied in a selection of an aptamers for the von Willebrand factor A1-domain[203]. The Ds-containing aptamer showed significantly higher affinity to the target compared to a known aptamer consisting of natural nucleobases. The affinity of the resulting aptamer was even increased compared to aptamers resulting from the initial selection-strategy with predefined fixed positions of dDs. This result indicates that aptamers with artificial nucleobase have superior interaction capabilities compared to aptamers wit natural nucleobases[198,204].

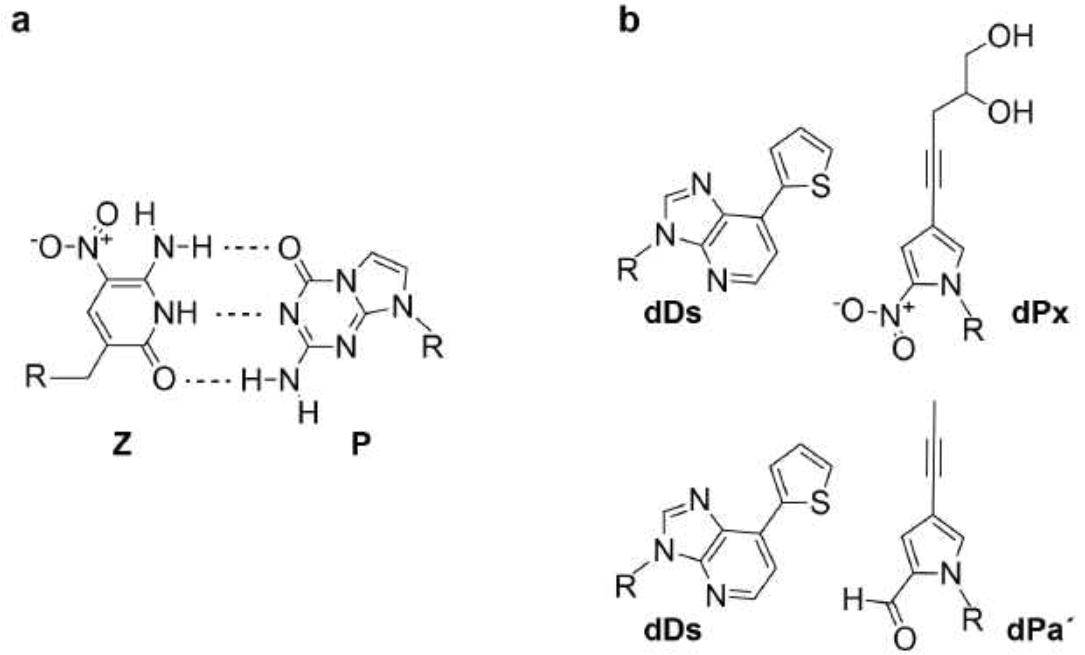

Fig. 9. Structures of some artificial base pairs. a) Recognition of the base pair 6-amino-5-nitro- 3-(1′-β-D-2′-deoxyribofuranosyl)-2(1H)-pyridone **(Z)** and 2-amino-8-(1′-β-D-2-deoxyribofuranosyl)-imidazo[1,2-a]-1,3,5-triazin-4(8H)one (**P**), which is used in AEGIS-SELEX is based on H-bonds. b) The basepair 2-nitro-4-propynylpyrrole (**dPx**) and 7-(2-thienyl)imidazo[4,5-*b*]pyridine (**dDs**), used in ExSLEX is based on size and shape complementary. The artificial nucleotide **dPa´** is used for the replacement PCR which is needed to replace the Dx bases into natural nucleotides for sequencing purposes.

1.3.2.3 Nucleobase modified oligonucleotides (SOMAmers)

Another approach to increase the chemical repertoire of oligonucleotides is the introduction of nucleobase-modified nucleotides into libraries for aptamer selection. The first nucleobase-modified aptamer was described by Latham et al. in 1994[205]. The thrombin-targeting modified aptamer harbored a 5-(1-pentynyl)-2’-deoxyuridine building block instead of dT and the target interaction depends on the pentinyl-modification[205,206]. Though it can be seen as a proof of applicability for this SELEX

approach, the resulting modified aptamer did not show superior binding behavior to thrombin compared to a previously discovered unmodified DNA aptamer[137]. Nucleobase-modified SELEX-libraries are still limited to four building blocks, in contrast to oligonucleotide-libraries with an expanded genetic alphabet. Nonetheless, introducing chemical modifications into the nucleobases clearly alters their biophysical properties. Libraries harboring these nucleotides therefore do have an increased chemical diversity, compared to conventional DNA-libraries.

The company SOMAlogic has commercialized the selection approach utilizing libraries with modified pyrimidines. Mainly inspired by the hydrophobic characters of amino acid side chains, a broad range of functionalized pyrimidine bases has been synthesized (see **Figure 10 a**). The C5-position on pyrimidines is the position of choice for the introduction of chemical modifications, since these modified nucleotides are still accessible for enzymatically catalyzed reactions as PCR[207].

The first selections were performed with just one modified pyrimidine, the deoxy uridine. The success-rate for those selections increased dramatically (to >80%) compared to selections with conventional oligonucleotides(<30%)[190,207]. By now, two differently modified pyrimidines (deoxy-uridine as well as deoxy-cytidine) can be incorporated into oligonucleotide libraries. Oligonucleotides bearing two distinct modifications have an even further increased chemical diversity, higher target-affinity, and nuclease resistance than those with one modification [208]. Libraries containing these modified nucleotides have been broadly applied in selections for thousands of protein targets resulting in high affinity aptamers, termed SOMAmers (Slow Off-rate Modified Aptamers)[209,210].

SOMAmers are mainly selected for diagnostic and biomarker discovery applications. Due to the multiplicity of existing SOMAmers, the so called SOMAscan approach permits the concurrent detection of thousands of proteins in a broad range of biological matrices[211–214]. A schematic representation of such a SOMAscan can be seen in **Figure 10 b**. SOMAmers (purple) for different proteins are equipped with individual fluorophores (F), as well as photo cleavable linkers (L) and a biotin-tag (B). The modified oligonucleotides are captured on streptavidin coated solid support and incubated with the matrix containing a diverse mixture of proteins. After the individual SOMAmers have bound their target proteins, the non-bound proteins are washed away. Captured proteins are successively biotinylated and the photo cleavable linker which attaches the SOMAmer-protein complex to the solid support is cleaved (**Figure 10 b (i)-(iii)**). Biotinylated proteins are captured on new streptavidin coated matrices and non-specific interactions to SOMAmers are disrupted by the addition of a polyanionic competitor (**iv**). Finally, the fluorescent tagged SOMAmers are released from their protein complex in a denaturating buffer (**v**) and hybridized to complementary sequences on a micro-array (**vi**). With the help of SOMAscan the concentration of several proteins in biological samples can directly be translated into SOMAmer based fluorescence intensities.

This multiplexed SOMAmer affinity assay is a novel tool in clinical diagnostics, as it helps to discover biomarkers for several diseases[207,210,215].

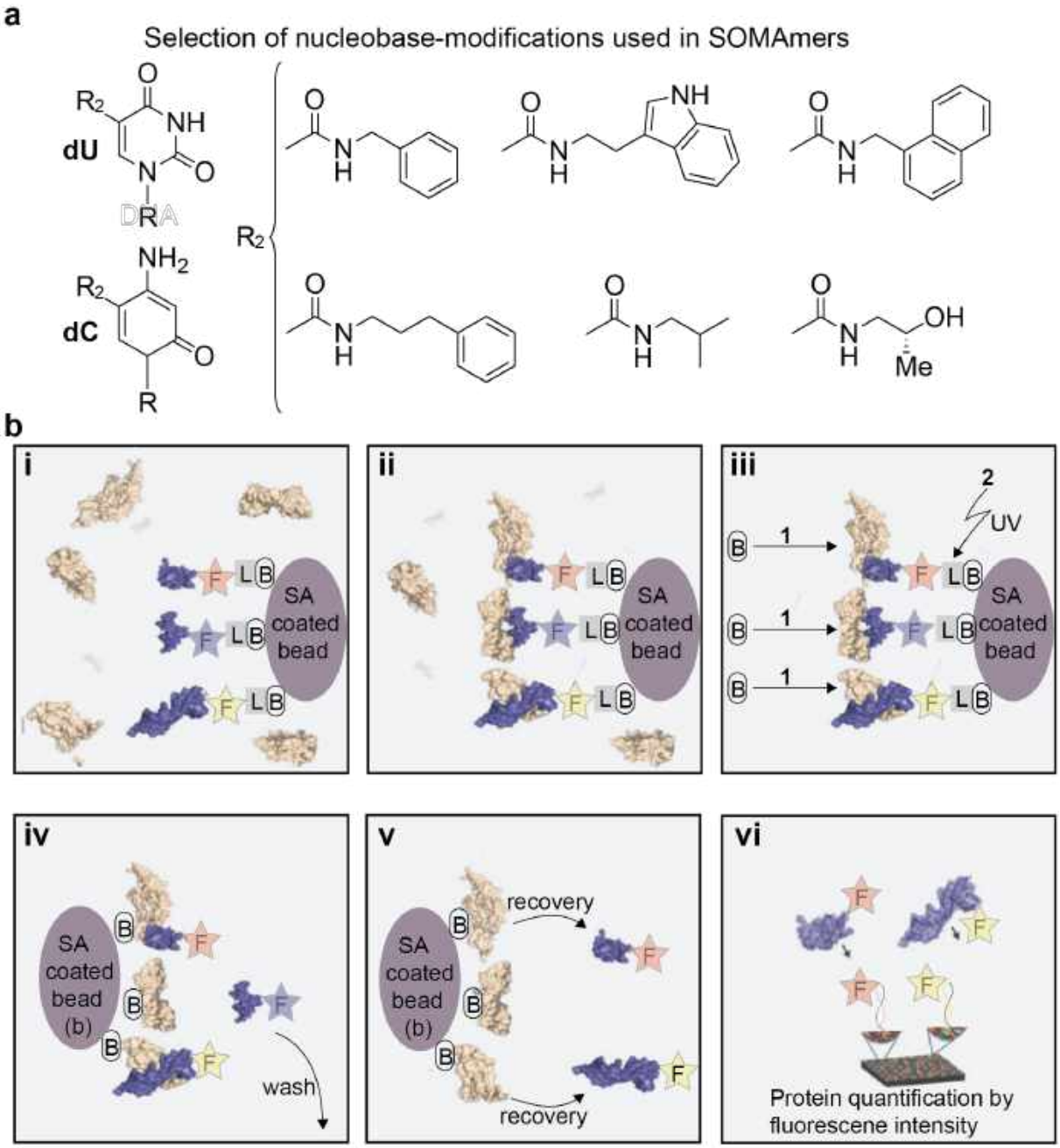

Fig. 10. Examples of utilized pyrimidine modifications during SOMAmer-selections and the scheme of a multiplexed SOMAmer affinity assay. a) A selection of chemical building blocks which can be introduced to the C5-position of both pyrimidine bases. b) Schematic mode of operation of a SOMAscan. Proteins of interest within a biological sample are bound by the corresponding SOMAmers (i)-(iii). This binding event is converted into fluorescent signals enabling the detection and quantification of proteins of interest (iv)-(vi). Figure 8 b was modified after Gold et. al[190].

For SOMAmers the amount of polar contacts with the protein targets are reduced compared to conventional DNA-aptamers[216]. Furthermore, the introduced protein-like side chains are often causative for target-interactions, as could be confirmed by diverse crystal structures[194,216–218]. Besides direct contact between nucleobase-modifications and protein-surfaces, several examples are known, wherein the modifications primarily help to stabilize the three-dimensional structures. Such three-dimensional structures have been previously unknown for aptamers. For example, SOMAmers containing hydrophobic modifications can fold into intramolecular zipper-like structures by π-π -stacking interactions with other modified pyrimidines (see **Figure 11**)[217,218]. The formation of those rigid 3-dimensional structures might also be supportive for the SOMAmer´s binding properties.

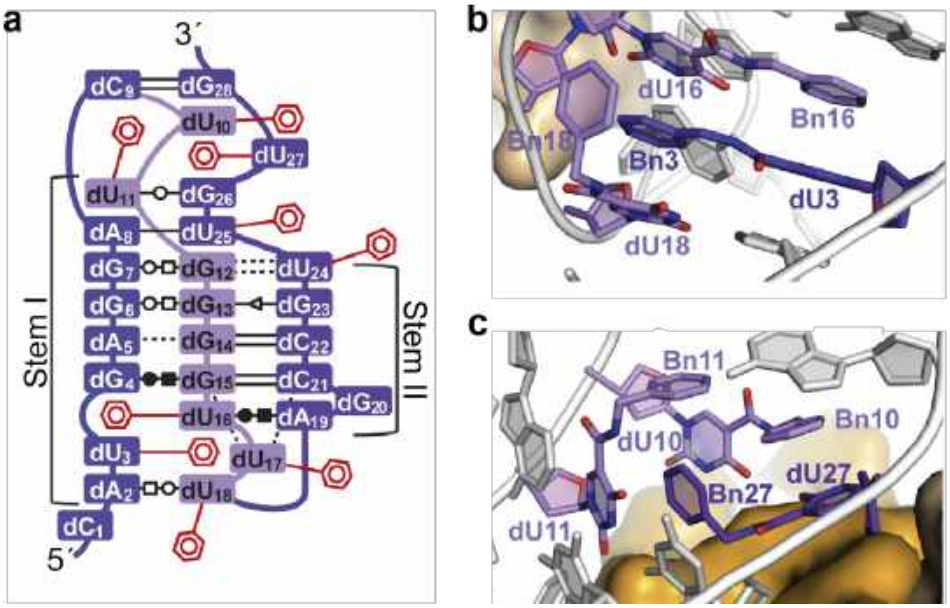

Fig. 11. Presentation of the NGF-SOMAmer forming zipper-like structures. The figure was modified after Jarvis *et. al.* [217] a) Cartoon illustration of the SOMAmer. Six out of nine benzyl-modified nucleotides are involved in structural stabilization of the SOMamer and do not directly interact with NGF. b, c) Within the two formed zipper-like structures, benzyl modifications show π-π -stacking interactions with adjacent modified pyrimidines. b) Bn-dU 16, Bn-dU 18 and Bn-dU 3, as well as c) Bn-dU 27, Bn-dU 11 and Bn-dU 10 form the zipper-like structures.

Disregarding the immense success of SOMAmer selections, this approach does pose some problems concerning the applicability in ordinary biochemistry labs. As can easily be envisioned, complex synthesis of the nucleoside-triphosphates and the phosphoramidites has to be performed previous to each selection-approach. The company SOMAlogic has automated the selection-process, resulting in SOMAmers for thousands of proteins. Naturally, that huge effort cannot be done in smaller laboratories. Another minor drawback of SOMAmer-selections is that a direct PCR-amplification of modified DNA-templates during SELEX is not possible. However, this problem can easily be circumvented by a two-step PCR-procedure. The modified templates are first PCR-amplified with the conventional set of nucleotides (dATP, dCTP, dTTP and dGTP). The resulting PCR-product can then be amplified with a dNTP-mixture containing modified nucleotides[219].

1.3.2.4 Click-chemistry modified oligonucleotides (Clickmers)

Clickmers can also be seen as a group of nucleobase modified oligonucleotides. The modification to nucleobases is done via click-chemistry. Clickmers are the result of a slightly modified SELEX procedure. This type of SELEX is also based on the introduction of chemical modifications to the C5-position of deoxy-uridine. It relies on the easily performed Cu(I)-catalyzed azide-alkyne 1,3-dipolar cycloaddition (CuAAC), which is also known as click-reaction[220–222]. Click-reaction does not interfere with natural occurring biochemical reactions and therefore is widely used to modify biomolecules with diverse modifications[223,224]. Carell *et al*. have shown that CuAAC is also feasible for DNA in aqueous solutions. Alkyne-bearing nucleoside triphosphates such as C5-ethynyl-2'-deoxyuridine (EdU) and C8-Alkyne-dUTP (C8-dU) can easily be incorporated into DNA oligonucleotides and are subsequently compatible with click-reaction in the presence of a Cu(I) chelating ligand, e.g., the Tris(3-hydroxypropyltriazolylmethyl)-amin (THPTA)[225–228]. THPTA protects the DNA from oxidative damage, induced by free Cu(I)-ions in aqueous solution[229].

Click-SELEX starts with a synthesized DNA library wherein each thymidine is substituted by the commercially available EdU. The alkyne-carrying deoxy uridines can be modified with a broad range of chemical building blocks, which are either commercially available or can easily be synthesized[230]. These azide-containing chemical entities can react with EdU-containing oligonucleotides via click-reaction[220–222]. Since click-reaction with EdU containing DNA-libraries is quickly performed, it offers a simple method to chemically modify these libraries. EdU containing, as well as click-modified oligonucleotide libraries are tolerated as templates for PCR amplification with *Pwo*-polymerase[225,231]. Since PCR can be done with a mixture of dATP, dGTP, dCTP and the triphosphate of the C5-ethiynyl-2´-deoxiuridine (EdUTP), the amplification products again contain EdU[225,232]. Of course, the desired chemical modification has to be re-introduced into the amplified oligonucleotide strands via click-reaction (see **Figure 12 a**)[232]. To date, click-SELEX has been performed for the target-protein C3-GFP. The resulting clickmer which binds to C3-GFP with a k_D of 18.4 ± 3.1 nM was modified with indol-azide[232]. One advantage of click-SELEX is its modularity. Similar to amino acid side chains, the chemical character of these azides can be either non-polar/hydrophobic, or polar. It is even possible to introduce charged entities into the DNA. Therefore, in the run-up of a SELEX, an azide can be chosen that is most promising to interact with the target molecule.

Implementation of click-SELEX is similar to that of a common DNA-SELEX (see **Figure 12 b**). Each cycle starts with the click-modification of the starting library with the azide of choice (I). Subsequent steps as the incubation of the modified library with the target molecule (II), separation of target-binding from non-binding sequences (III) and recovery of the binding sequences (IV) do not differ from the familiar procedure.

During PCR-amplification (V) with the d*NTP-mix (dA, dG, dC, EdU) the previously introduced chemical moiety is removed and replaced by EdU and the resulting double stranded library can be enzymatically digested to single–stranded sequences. Thus, the modification is only transiently present in each selection-cycle and therefore has to be re-introduced to the library before the subsequent cycle.

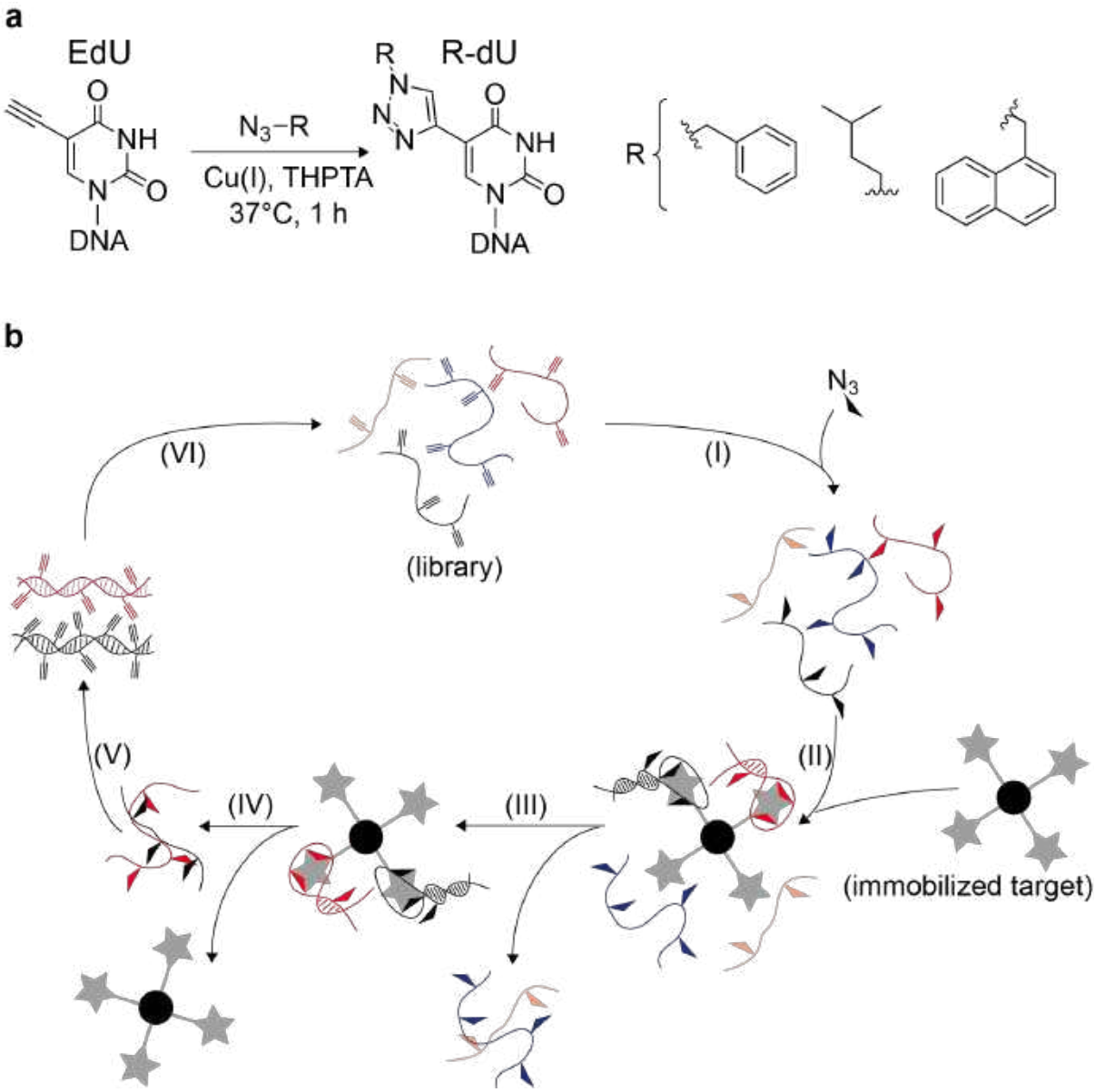

Fig. 12. Scheme of a Click-SELEX. a) EdU that has been incorporated into the oligonucleotide can be modified with an azide of choice via click-reaction. b) The click-SELEX cycle: The main difference to the conventional selection-cycle (**Figure 6**) is the modification of the library with CuAAC.

1.3.3 Aptamers as (live-cell) imaging tools

Aptamers as biosensors are not only restricted to the detection of drugs like THC[233–235], pollutants[236] or toxins[237,238] in numerous samples. They e.g. also find application in imaging approaches of RNA sequences in *in vitro* and living cells. Especially the role of non-coding RNA sequences (ncRNA) in cells is currently intensely studied. To investigate and understand the different functions, dynamics and the interactions of ncRNA with other biomolecules[239,240], imaging technologies have been developed. Those techniques enable spatiotemporal detection of single RNA molecules via fluorescence microscopy. However, technologies like fluorescence in situ hybridization (FISH)[241,242] or the MS2-green fluorescent protein (MS2-GFP)[243,244] system do have drawbacks regarding RNA imaging. For FISH, cumbersome probe design has to be done[245]. Furthermore, fixation of cells is usually required, meaning that only static measurements of RNA sequences are possible[241,245]. On the other hand, MS2-GFP is dependent on a large modification of the RNA sequence of interest, which might affect its biological functions[243,246].

To circumvent such drawbacks genetically encodable fluorescent reporters for RNA visualization in cells have been developed. Such fluorescent reporters consist of a cell-permeable fluorescent dye, and an RNA aptamer capable to specifically bind to it. The dye itself ideally shows only little auto fluorescence and exhibits a drastic increase in fluorescence intensity when bound by the aptamer. The RNA aptamer can be transcribed in living cells and thereafter bind and activate the fluorescence of its target. These genetically encodable fluorescent light-up aptamers (FLAPs)[247] can be fused to RNA sequences of interest to study their dynamics in cells. Furthermore, RNA-based allosteric sensors could be constructed that exhibit fluorescence upon binding to small molecules of interest in live cells[248–251].

One prominent example of such a genetically encodable FLAP mimics the green fluorescence of the enhanced green fluorescent protein (eGFP)[252]. The *in vitro* selected and discovered aptamer binds to the fluorophore 2,5-difluoro-4-hydroxybenzylidene imidazolinone (DFHBI). DFHBI is cell-permeable and does not show cytotoxicity, which are inevitable requirements for cell imaging purposes[252].The aptamer-DFHBI complex emits bright green fluorescence, when excited with an appropriate wavelength. Due to the green fluorescence the aptamer was called “Spinach”[252]. Spinach was one of the first successful approaches for the genetic encoding of fluorescent RNAs with the aim to track RNA sequences of interest in live cells.

In 2014 the reason for the distinct increase of fluorescence enhancement of DFHBI upon binding to Spinach was solved with help of x-ray crystallography[253,254]. The enhanced florescence of DFHBI can be explained by the unprecedented binding pocket provided by the Spinach aptamer[253,254]. The situation is comparable to that found for the chromophore (Z)-4-(4-hydroxybenzylidene)-1,2-dimethyl-1H-imidazolone (HBI) known from eGFP. The chemical structures of DFHBI and that of HBI clearly

resembles each other. Chemically synthesized HBI, as well as HBI in denatured eGFP is non fluorescent. Only in correctly folded eGFP green fluorescence is emitted upon photoexcitation. Both, photo excited DFHBI and HBI can dissipate the energy either in a nonradiative pathway involving intramolecular movements, or in a radiative pathway. In unfolded eGFP the HBI emits the energy mainly in the nonradiative way. In folded eGFP however HBI is captured in a defined binding pocket that prevents intramolecular movements and energy of photoexcited HBI is mainly dissipated via the radiative pathway[255,256].

In **Figure 13** a scheme of the binding pocket of the Spinach aptamer in presence of the ligand DFHBI is shown. The imidazolone and phenyl rings of the chromophore are orientated coplanarly and stack on top of a two-layered antiparallel G-quadruplex. A Hoogsteen base triplex “lid”, consisting of U50-A53-U29 (U29 not shown in **Figure 13** due to clarity reasons) seals the binding pocket from the top[254]. The aptamer thus sandwiches DFHBI in a hydrophobic pocked and largely shields it from the surrounding aqueous solution.

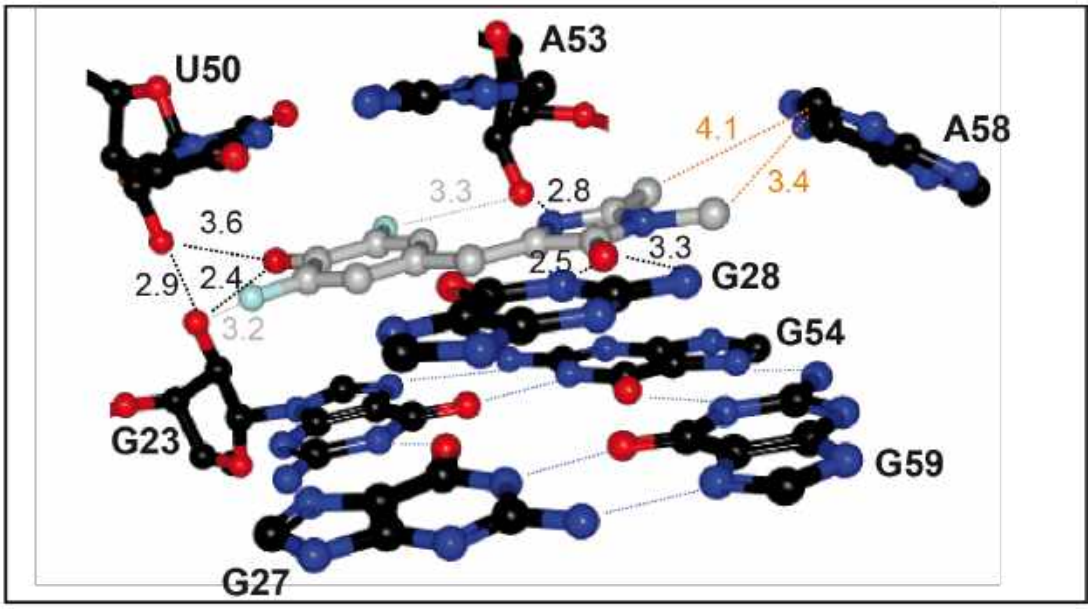

Fig. 13. Structure of the binding pocket of Spinach-RNA in the DFHBI-bound state. Carbon atoms of DFHBI are drawn in grey, those of nucleotides in black. Nitrogen atoms are drawn in blue, oxygen in red and fluorine in turquoise. Nucleotides G23, G27, G54, and G59 form a G-tetrad onto which DFHBI is coordinated. A base triplex “lid” consisting of U50-A53-U29 seals the binding pocket (U29 is omitted for clearity reasons). G28 is in the same plane as DFHBI. Black dashes (with the distances numbered in Å) represent hydrogen bonds from DFHBI to the G28 nucleobase and several 2´-hydroxyl groups. Potential hydrogen bonds from fluorine are represented with grey dashes. The imidazolone methyl groups of DFHBI may be engaged in hydrophobic interactions (orange dashes). The structure was handled with the free software protein workshop (PDB code 4kzd).

The fluorine, oxygen and nitrogen atoms of DFHBI participate in H-bonds with adjacent nucleotides. The combination of aromatic and polar interactions between DFHBI and the aptamer stabilizes the planar orientation of the chromophore and thereby restrict its vibrational or intramolecular movements. Hence, upon excitation of the chromophore, energy emission is mainly achieved by the radiative, fluorescent

pathway[254]. At neutral pH DFHBI is present in the anionic, phenolate state. The negatively charged phenolate is surrounded by seven adjacent RNA phosphates. This high concentration of negative charge attracts positively charged counter ions. Coordinated potassium ions (not shown in **Figure 13**) bridge functional groups of RNA, waters, and DFHBI and are thought to be responsible for the selectivity of Spinach to the anionic form of the fluorophore[253].

Due to poor folding of Spinach in living cells the obtained green fluorescence was dimmer than expected. Therefore several approaches have meanwhile been undertaken to improve Spinach´s overall performance *in vitro*[257] as well as in living cells. For all the later on developed aptamer derivatives the G-quadruplex containing core structure for DFHBI binding (**Figure 13**) remained largely unaltered. This DFHBI binding pocket is adjacent to two stem structures, which have been shown to be relevant for proper folding of the aptamer[247]. Manipulations on Spinach to improve its fluorescence performance mainly concern these stem structures. Some of the approaches to improve the overall performance of the Spinach aptamer are shortly described here. With help of systematic mutagenesis, a superior version of Spinach named Spinach2 was obtained[258]. It showed superior folding compared to Spinach resulting in higher fluorescence when used as fluorescent tags in living cells[258]. In another approach, shortening of one stem resulted in a truncated, more stable version of Spinach (Baby-Spinach). Baby-Spinach converts only half the length of the parental Spinach[259]. Still, Baby-Spinach showed even superior fluorescence intensities compared to Spinach2 in E.*coli* [259]. Random mutagenesis in combination with high throughput screening by microfluidic assisted in vitro compartmentalisation led to a less salt sensitive and thermally more stable aptamer variant called iSpinach. The iSpinach aptamer showed beneficial properties for *in vitro* applications[257,260]. Last named, a SELEX strategy coupled with fluorescence activated cell sorting (FACS) resulted in the Broccoli-aptamer. Broccoli showed even superior fluorescence intensity in living cells due to a reduced dependency on the magnesium ion concentration, and more robust folding than Spinach2[261].

Genetically encodable systems as the combinations of DFHBI and its diverse aptamers can be used for several *in vitro* and *ex vivo* applications. Besides live cell RNA imaging in prokaryotic and eukaryotic cells[258,262,263] those systems can also be used as live cell imaging tools for proteins and metabolites. Allosteric spinach based sensors for the intracellular detection of metabolites as S-adenosylmethionine (SAM)[249], cyclic adenosine monophosphate (cAMP)[264], or thiamine pyrophosphate (TPP)[248], as well as for protein expression[265] have been developed. Upon binding of these sensors to the individual target structures, conformational changes of the constructs lead to formation of initially inactive Spinach aptamers. Thus, fluorescence is only monitored, when proteins or metabolites of interest ae present. On the other hand a possible in vitro application of Spinach is the real-time transcription of RNA constructs of interest[266]. For this purpose Spinach is inserted into the sequence of the investigated RNA[267].

1.3.3.1 RNA aptamer-fluorophore complexes for super resolution techniques

Though fluorescence microscopy enables visualisation of small structures in living cells, the technique is restricted by the diffraction limit of light[268,269]. Since this diffraction limit is hampering the resolution of smaller subcellular structures, new techniques have been invented to overcome this diffraction barrier[268,270,271].

Super resolution imaging techniques that circumvent the diffraction-limited resolution barrier of conventional light microscopy have been developed. Examples of techniques enabling super resolution microscopy (SRM) are Photoactivated Localization Microscopy (PALM)[272273], Stimulated Emission Depletion (STED) microscopy[274,275], and Reversible Saturable Optical Linear Fluorescence Transition (RESOLFT)[276]. With help of SRM the resolution limit can be improved from around 200 nm to < 10 nm, and biological processes occurring in subcellular structures can be visualized[277,278]. Besides organic dyes (e.g., rhodamines, cyanines)[273] that can be used to label antibodies, tools for super resolution in live cell microscopy are often photo controllable fluorescent proteins[279]. With help of light of specific wavelengths, the fluorescence of these proteins can be regulated. Fluorescence of so-called photoactivatable fluorescent proteins (PAFPs) can be irreversibly turned on, that of reversibly switchable fluorescent proteins (rsFPs) can even be reversibly turned on and off[280]. Well-known PAFPs are amongst others the photoactivatable green fluorescent protein (PAGFP)[281], and the photoactivatable mCherry (PAmCherry1)[282,283]. PAFPs can be fused to proteins of interest and information about their localisation at high resolution can be gained[284].

Since aptamers are considerably smaller than proteins, they are advantageous over FPAFs or fluorescently labelled antibodies for super resolution microscopy[285]. It has been shown that large affinity tags as antibodies are not accurate enough for these imaging techniques. The large size of proteins displaces the fluorophore from the target structure and thus brings a linkage error from 10 to 20 nm[286,287]. Due to the smaller size of aptamers this linkage error is minimized and thus more detailed images can be gained[287]. Indeed, several fluorescently labelled DNA and RNA aptamers have already successfully been applied in super resolution microscopy. In 2016 Xiao *et. al.* primarily used a photoactivatable DNA aptamer for cancer diagnosis[288]. The nucleolin binding aptamer (AS1411)[289] carried a caged fluorescein derivative, whose fluorescence could be photoactivated with light of 488 nm. The photoactivatable aptamer could accurately detect nucleolin overexpressing MCF-7 breast cancer cells and can be used for highly selective cancer cell screening. It was reasoned that the photoactivation technique showed progress in more accurate and persistent imaging compared to traditional fluorophores[288]. De Castro *et. al.* compared the staining of an extracellular domain of the transferrin receptor (TfnR) with the fluorescently labelled receptor ligand transferrin, monoclonal antibodies and an aptamers in living human A431 cells[271]. In STED microscopy the aptamer showed superiority over antibodies, punctuating the usefulness of aptamers in super resolution microscopy[271].

The superiority of aptamers over antibodies in super resolution microscopy became also apparent in additional studies. Fluorescently labelled, nucleobase modified SOMAmers (compare to **section 1.3.2.3**)[194,290,291] targeting three membrane receptors relevant for human health were compared with antibodies in STED microscopy[286]. Staining of the receptors with SOMAmers revealed more epitopes and offered denser labelling of the target structures, thus enhancing the quality of information that are given by the images[285,286].

Hitherto mentioned aptamers that found application in super resolution imaging all carried a (caged) fluorescent label that was chemically attached to the oligonucleotides. However, since genetically encodable FLAPs as the Spinach- DFHBI complex exist, photoactivatable RNA-fluorophore systems for application in techniques as PALM or RESOLFT can be generated. With the synthesis of a DFHBI derivative that carries a photolabile protective group (PPG), RNA fluorophore complexes with photoactivation abilities could easily be developed[292]. In fact, due to the fast light induced *cis-trans* isomerisation of DFHBI, which is responsible for the fast fluorescence decay of the Spinach-DFHBI complex[293,294], such systems could not only be seen as photoactivatable but also reversibly photoactivatable[292].

A hint that such photoactivatable RNA-fluorophore complexes might work can be found in a photoactivatable version of GFP. With help of unnatural amino acid mutagenesis[295], a GFP-variant was generated containing a photocaged tyrosine analogue. The GFP66ONBY-called protein contained an *o*-nitrobenzyl-O-tyrosine (ONBY) substituting the natural tyrosine 66[296]. The caged protein exhibited no fluorescence. Only after removal of the photolabile protective group (PPG) with 365 nm, typical GFP fluorescence could be observed again. With help of x-ray crystallography it was confirmed, that GFP66ONBY was capable to form a mature fluorophore carrying the o-nitrobenzyl group[296]. The introduced o-nirobenzyl group quenches the excited fluorophore through a photo-induced electron-transfer from the excited S^1 excited fluorophore to the o-nitrobenzyl group[296]. Since fluorescence of GFP was successfully quenched in GFP66ONBY due to the caged fluorophore (Z)-4-(4-hydroxybenzylidene)-1,2-dimethyl-1H-imidazol-5(4H)-one (HBI), an analogous version of an *o*-nitrobenzyl caged DFHBI might be useful for the construction of a photoactivatable RNA-fluorophore complex.

1.3.3.2 DFHBI derivatives for the development of a red-shifted FLAP

FLAPs are emerging tools for microscopy that find comparable applications as fluorescent proteins (FPs)[297]. Meanwhile several FPs emitting light of different colors are available to study the functions of living systems[297]. Up to now the amount color diversity of FLAPs is not as sophisticated as for fluorescent proteins[298,299]. However, a couple of RNA aptamers have recently been selected that bind and activate the fluorescence of exogenous dyes. Besides the already mentioned optimized versions

of Spinach[257–260] and Broccoli[261], further aptamer-fluorophore complexes have been selected that broaden the color palette of fluorescent RNAs. As Spinach and its derivatives these further fluorescent RNAs find applications for *in vitro*- and cell imaging applications[262,300,301].

A few examples of FLAPs with red-shifted fluorescence are named here. Mentioned fluorophores are shown in **Figure 14**. Spectral characteristics of these fluorophores in complex with some of their aptamers are listed in **Table 1**. Well-functioning examples are the aptamers Mango, Mango II, and Mango III, all binding to biotin-tagged thiazole orange derivatives with nanomolar affinity[300]. Upon binding of the Mango aptamers to the thiazole orange derivates TO1-biotin or TO1-biotin, their fluorescence is significantly increased[302–304]. As DFHBI, the thiazole orange derivatives are also cell membrane permeable and lack cytotoxicity. Interestingly since Mango binds both thiazole orange derivatives TO1-biotin and TO3-biotin, also two complexes result that show individual excitation and emission spectra (**Table 1**). While Mango in complex with TO1 shows yellow fluorescence (535 nm) upon excitation at 510 nm, the Mango-TO3 complex shows a strongly red-shifted fluorescence (excitation: 637 nm; emission: 658 nm). Another aptamer that enhances the fluorescent of its target 3,5-difluoro-4-hydroxybenzylidene-imidazolinone-2-oxime (DFHO) by >1000 fold is Corn. A quasi-symmetric homodimer of the 28-nt long RNA aptamer specifically binds the fluorophore, resulting in yellow fluorescence emission at 543 nm[305]. Like for Spinach and Broccoli, live-cell RNA imaging with Mango and Corn have successfully been performed[262,300,301].

As shown by these few examples, several organic dyes in combination with aptamers that increase their fluorescence are useful to broaden the fluorescence color palette of FLAPs. As becomes obvious, selected aptamers are often capable to bind several organic dyes with similar chemical structures. For instance, the already mentioned Mango aptamers built fluorescent complexes with the thiazole orange derivatives TO1-biotin and TO3-biotin. Furthermore, Spinach2 and Broccoli not only bind and enhance the fluorescence of DFHBI, they also built fluorescent complexes with DFHBI-1T an DFHBI-2T (**Figure 14 a**, **Table 1**). The aptamers tolerate the trifluoroethyl-substituent at the N-1-position, as well as a trifluoromethyl substituent on the C-2 position of the imidazolinone ring. These alterations slightly decrease the affinity of the aptamer to the fluorophore (in case of Spinach2) but also lead to red-shifted fluorescence emission[306].

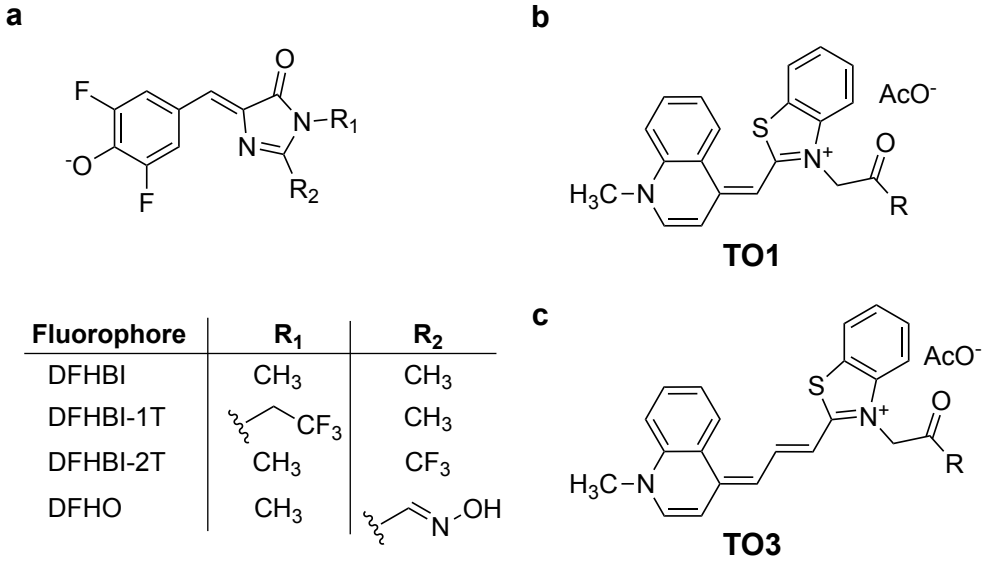

Fluorophore	R_1	R_2
DFHBI	CH_3	CH_3
DFHBI-1T	CF_3	CH_3
DFHBI-2T	CH_3	CF_3
DFHO	CH_3	N OH

Fig 14. A selection of fluorophores bound by RNA aptamers. a) HBI-derived fluorophores DFHBI, DFHBI-1T, DFHBI-2T (bound by Spinach derivatives) and DFHO (bound by Corn). b,c) Thiazol orange derivatives TO1 (b) and TO3 (c) bound by Mango aptamers. R = Biotin-tag.

Table 1. Selection of spectral characteristics of aptamer-fluorophore complexes

Aptamer	Fluorophore	k_D [nM]	λ_{ex} [nm]	λ_{em} [nm]	Ref.
Spinach2	DFHBI	530	447	501	258
	DFHBI-1T	560	482	505	306
	DFHBI-2T	1300	500	523	306
Broccoli	DFHBI	not specified	450	501	261
	DFHBI-1T	360	427	507	261
Mango	TO1-biotin	3.9	510	535	302
	TO3-biotin	8	637	658	303
Mango II	TO1-biotin	1.1	510	535	303
	TO3-biotin	1.4	635	660	303
Mango III	TO1-biotin	2.3	510	535	304
	TO3-biotin	8.7	635	660	304
Corn	DFHO	70	505	545	262

Giving this result, further alterations on DFHBI could lead to additional red-shifted emission properties of aptamer-fluorophore complexes. Besides introduction of electron-withdrawing groups[306], an increase of the aromatic system could also lead to such an effect. Naturally for such cases the chemical alterations on DFHBI must not disturb binding to the aptamer. Complexes of already existing aptamers as Spinach with such DFHBI derivatives potentially might show red-shifted emission, hence help to increase the color palette of FLAPs.

2. Aim of the study

The aim of this study was to utilize the concept of click-SELEX to identify a clickmer for the small molecule THC. THC is the psychoactive constituent of the plant *cannabis sativa*. A clickmer could be an appropriate biomolecule capable to detect small amounts of THC in biological matrices as oral fluid. Based on a clickmer as a sensor molecule a THC-test-device similar to already existing lateral flow devices was set out to be constructed. Therefore, the aim of this thesis was the identification of a clickmer which binds to THC with appropriate affinity and selectivity.

Being the main psychotropic ingredient in cannabis, THC negatively affects psychomotor skills of consumers. In times of worldwide increasing acceptance and decreasing criminalisation of cannabis consumption, traffic accidents under influence of THC are getting an ever-expanding issue in terms of road safety. Though some antibody –based test devices that can detect THC in oral fluid of road users already exist, the accuracy for many of those devices is unsatisfactory. Generally, those devices rely on antibody-based detection.

Alternative biomolecules capable to detect low amounts of THC in small volumes could be aptamers. Being similarly capable of binding to specific target molecules with high affinity, aptamers also have some advantages compared to antibodies as, e.g., low-priced production, no batch to batch variation and higher thermostability. However, identifying non-modified DNA, or RNA-aptamers with conventional SELEX is challenging for small molecule targets as THC. The terpeno-phenolic scaffold of THC is extremely nonpolar and hydrophobic. Hence, it is quite unlikely for THC to undergo polar, or H-bonding interactions with potential binding ligands. On the other hand, the amount of polar interactions for conventional DNA-or RNA-aptamers to the individual targets is commonly quite high. Canonical nucleobases are prone to undergo polar modes of interaction, thus the chance for a successful selection with non-modified libraries for THC seems to be limited.

A convenient alternative to common DNA/RNA-SELEX could be the modular click-SELEX approach. The utilized libraries for click-SELEX carry Ethynyldeoxyuridine (EdU) instead of dT, which is susceptible for chemical modification via CuAAC. Hence, the biophysical properties of click-SELEX libraries are clearly altered compared to common DNA-SELEX libraries, due to the additionally introduced chemical entities. In case of click-SELEX for THC, the modification of SELEX-libraries with more hydrophobic chemical entities seemed quite promising for a successful selection. The introduction of hydrophobic building blocks with an aromatic system in the selection was regarded as a promising starting point.

The aim of another project was the synthesis of new DFHBI derivatives to develop new fluorescent light-up aptamer (FLAP) systems. Synthesis of a photoactivatable DFHBI derivative was intended, to develop a photoactivatable FLAP. Such systems could be applied for super resolution microscopy techniques. Similar to existing HBI-based

photoactivatable fluorescent proteins (PAFPs)[296], complexes of aptamers with the photoactivatable DFHBI with comparable photoactivation properties should result.

Furthermore, synthesis of a DFHBI derivative with an increased aromatic system was planned, to develop a FLAP with red-shifted fluorescence. Since slight modifications on the DFHBI structure do not disturb the binding of Spinach2 or Broccoli[306], a FLAP system of existing aptamers with such a DFHBI derivative seemed possible. Alternatively, an RNA SELEX for such a new DFHBI derivative could result in a completely new aptamer-fluorophore complex with red-shifted fluorescence emission.

3. Results

In this chapter, the results of the click-SELEX for THC immobilized on magnetic particles is summarised. Aspects concerning the choice of the applied library, the chemical modification during SELEX and the investigation and characterisation of THC binding clickmers are abstracted.

Furthermore, the synthesis and photometric characteristics of a photoactivatable DFHBI derivative (PA-DFHBI) in complex with Spinach and Broccoli aptamers are summarized. In addition, the results of live cell applications of PA-DFHBI in bacteria and mammalian cells is shown.

Finally, the synthesis of a DFHBI derivative with an enlarged aromatic system (eDFHBI) is summarized. Photometric properties of that compound in complex with Baby-Spinach are depicted and the result of an RNA SELEX for eDFHBI is presented.

3.1 Preparation of a THC-modified solid support for SELEX

To perform a selection for small molecule targets, most commonly the target is immobilized to a solid phase (e.g., magnetic particles), which facilitates the incubation of SELEX-libraries with the target, the separation of non-binding sequences, and the recovery of binding sequences (see **section 1.3.1**). In case of small molecules this immobilisation is commonly performed via covalent coupling of functional groups located on the target structure to suitable functional groups on the solid support. In order to perform the covalent coupling, the target-scaffold sometimes has to be chemically manipulated. In case of THC, the only functional group available for covalent coupling is a phenolic group (**Figure 15**). However, if the phenolic oxygen is used for covalent attachment to a solid support, the only existing functional polar group of THC would be amended. Since that functional group could potentially be involved in possible interactions to oligonucleotide-ligands, it was decided to use another way off immobilisation.

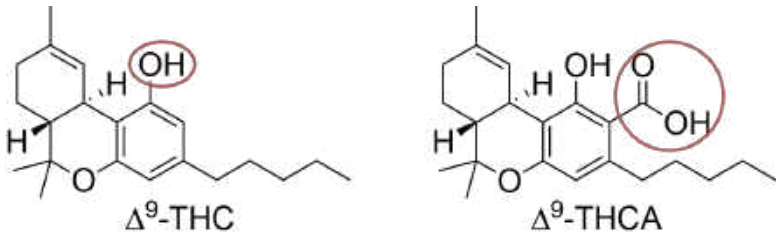

Fig. 15. Comparison of Δ^9-THCand Δ^9-THCA with respect to the functional groups that can be used for immobilisation on solid support. The red cycles mark these functional groups. Δ^9-THC just contains the phenolic group. In contrast to that Δ^9-THCA additionally carries a carboxylic group which simplifies the immobilisation of this compound.

Therefore, THCA, the natural precursor of THC was used for the immobilisation process. As can be seen in **Figure 15**, THCA carries an additional carboxylic group at the C2-position of the tricyclic ring-system (dibenzopyran numbering). This carboxylic acid could easily be used for functionalisation and coupling of the target to magnetic beads for click-SELEX purposes. To couple THCA to M280-tosylactivated magnetic Dynabeads™ (Thermo Fisher), THCA had to be chemically modified beforehand. The carboxylic acid of THCA was activated with 1-Ethyl-3-(3-dimethylaminopropyl) carbodiimid (EDC) and reacted with the primary amine of BOC-Ethylenedioxy bis-ethylamine. After completion of the reaction, the terminal Boc-group was removed under acidic conditions. Each reaction step was purified via HPLC and the purified product was in turn analyzed by HPLC-MS. In **Figure 16** the reaction steps are illustrated.

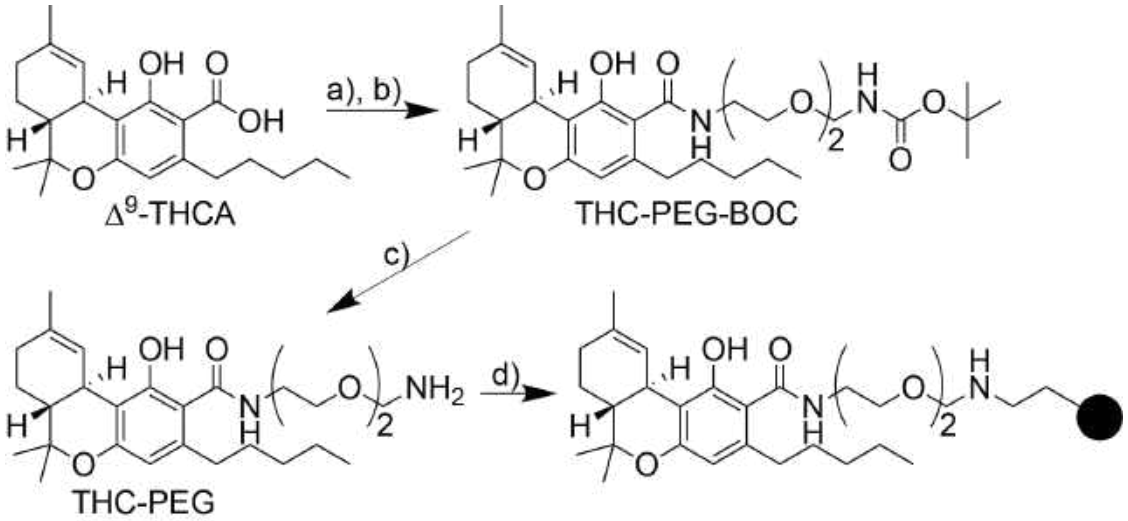

Figure 16. Immobilization of Δ^9-THCA to M280 tosyl-activated Dynabeads. Δ^9-THCA was dissolved in CH_2Cl_3 and stirred with a) EDC and b) *N*-Boc- 2,2′-(ethylenedioxy)diethylamine for 2 days at room temperature. After purification of the reaction product (THCA-PEG-BOC) via HPLC, c) 4N HCl in dioxane was added and the solution stirred for 2 h. The product was purified via HPLC. The resulting compound (THC-PEG) was dissolved in borate buffer (pH 9.5) and reacted with d) M280 tosyl-activated Dynabeads™ for 2 days.

Table 2 shows the detected masses of the starting compound THCA and the reaction products THC-PEG-BOC and THC-PEG. The actual chromatograms of the reaction products are shown in the **Appendix** (**Figure A1**).

Table 2. LC-gradient and detected masses for THCA, THC-PEG-BOC, and THC-PEG via HPLC-MS.

Compound	LC-gradient ACN [%]	calculated mass [m/z]	detected mass [m/z] positive mode	detected mass [m/z] negative mode
THCA	60-80 0.4 ml/min	358.48	359.2 $[M+H]^+$; 381.2 $[M+Na]^+$	357.11 $[M-H]^-$
THC-PEG-BOC	60-80 0.4 ml/min	588.38	589.5 $[M+H]^+$; 611.4 $[M+Na]^+$	587.22 $[M-H]^-$
THC-PEG	5-100 0.4 ml/min	488.33	489.3 $[M+H]^+$; 511.2 $[M+Na]^+$	487.28 $[M-H]^-$

The HPLC-purified compound could be coupled to M280 tosyl-activated Dynabeads™ at pH 9.5. Potentially remaining tosyl-groups that did not react with the target, were blocked with an aqueous solution of an excess of methylamine. The same was done with beads whereon the target was not immobilized and that are hereafter referred to as “non-modified beads”. The latter was used as control for follow-up experiments.
To ensure successful immobilisation, bead coupled THCA was detected via fluorescence labelled antibodies. Both, THCA-coupled and non-modified beads were successively incubated with a primary THC-antibody and subsequently with a fluorescently labelled secondary antibody. Fluorescence of the secondary antibody could be detected with a fluorescence imaging system. Therefore, the same volume of THCA-coupled and non-modified beads was pipetted onto the glass plate of the imaging system and the fluorescence intensities of both samples at (700 nm) was recorded. **Figure 17** shows the difference of fluorescence intensities between THCA-coupled and non-modified beads. The clearly observable difference in fluorescence intensities was taken as an evidence for successful THCA immobilization. By the way, though THCA was used for chemical modification and coupling to magnetic beads, those beads are subsequently called “THC-modified”. This is done, though the chemical structure of the immobilized compound resembles more that of THCA than THC.

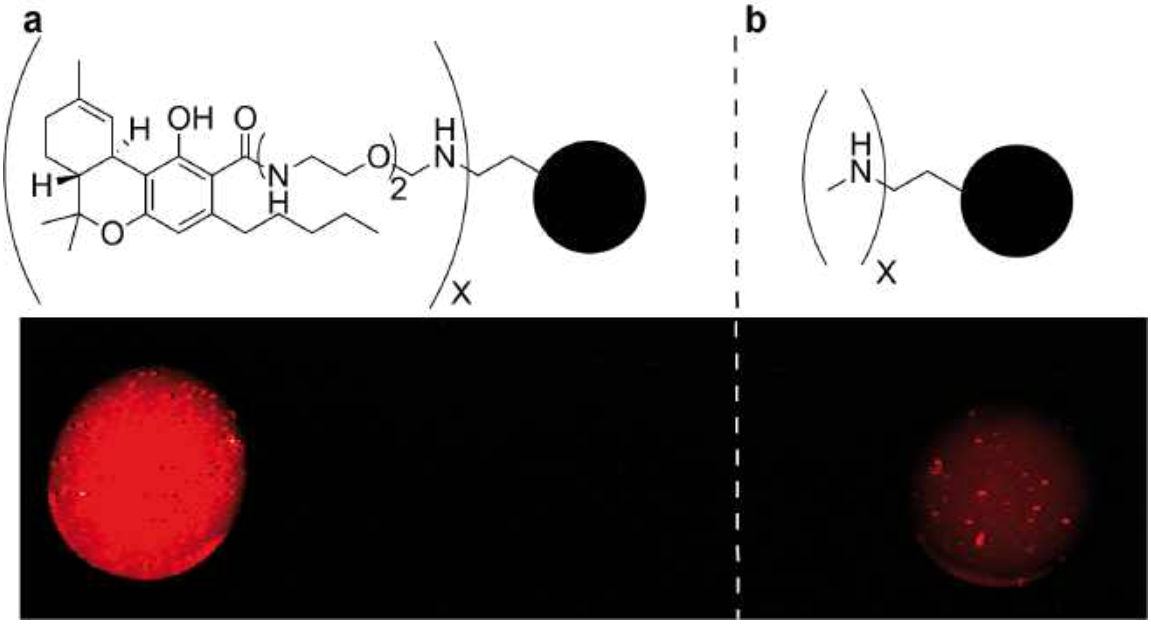

Fig. 17. Antibody-staining of successful THCA immobilisation to magnetic particles. a) The fluorescence of “THC-modified” beads. b) In comparison the fluorescence of “non-modified beads” that where blocked with methylamine is shown. In both cases an antibody conjugated to a fluorescent dye was used to visualize the coupled THCA (at 700 nm).

3.2 Click-SELEX for THC

Click-SELEX was performed with the FT-2 library which had previously been shown to be suitable for the selection of clickmers (**Figure 18**)[232].

5'-Cy5-CACGACGCAAGGGACCACAGG-N42-CAGCACGACACCGCAGAGGCA-3'

within N42: dA:dG:dC:EdU = 1:1:1:1

Fig 18. Representation of the N42-library. The random region consists of an equimolar ratio of dA, dG, dC and EdU. It is flanked by two 21 nt long primer binding sites. Primer binding sites lack EdU nucleotides. This was done to avoid potential problems in PCR that are associated with the alkyne-modification[232].

Nucleotides are equally distributed within the random region of this library. Accordingly, in average 10.5 EdU are present in the 42 nt long randomised region. These EdU functionalities are susceptible for quantitative click-modification during the iterative cyclic selection process. The randomised region is flanked by two 21 nt long primers. Since it is not known, if EdU-dA base pairing disturbs the PCR-amplification of the library, primers were designed in a way that this base pairing is prohibited in the primer-binding region. Furthermore, this way the incorporation of EdU at pre-defined positions within the library was avoided. The starting library as well as the forward-primer were Cy5-labelled, which enabled a facile detection of binding to THC-modified or non-modified magnetic beads via flow cytometry.

To suppress non-specific binding of the modified oligonucleotides to target-coupled and empty beads a so-called click-competitor was created. The competitor consists of a 42 nt long randomized sequence with an equimolar ratio of all four nucleotides (dA, dG, dC, and EdU)[232]. Since the click-competitor is lacking the primer binding sites, it could not be PCR-amplified during SELEX and had to be re-introduced into the binding-mixture for every selection cycle. Analogous to the FT-2-library, the click-competitor was click-modified with the same azide.

3.2.1 Characterisation of the FT-2-library for selection

The Cy5-labelled starting library was click-modified with different azide and binding of these modified libraries to THC-modified or non-modified beads was monitored via flow cytometry. Cy5-fluorescence on beads of the gated population P2 was recorded (green population in **Figure 19 a)**. The utilized azides were either commercially available or synthesized by different members of our group. These are benzyl-azide (Bn-), 1-(2-azidomethyl) naphthalene (Nap-), Azido-benzenepropanoic acid (Phen-), 2-azidopropan-1-ol (Prop), and 1-azido-2-methylpropane (iBu-). Analytical data of the used azides can be seen in **Appendix**, **Figures A7-A11**. Binding of the differently modified starting libraries (each 500 nM) to the THC-coupled M280 dynabeads and to non-coupled beads was investigated. Additionally, the click-competitor individually modified with the appropriate azide, was added in equimolar concentrations into the

binding solutions of starting library and beads. This way, the nonspecific interaction of the library with the beads based on the sole click-modification should be reduced.

As can be seen in **Figure 19 b**, libraries modified with aromatic azides showed slightly higher binding to THC-modified beads than to the non-modified beads. However, this tendency could not be observed for libraries that were click-modified with aliphatic azides. In all cases, fluorescence intensities-values were normalized to the value of the benzyl-azide modified library. **Figure 19 c** depicts the fold-change of binding between THC-modified and non-modified beads. Bn- and Nap- modified libraries roughly bound twice as good to THC-coupled beads than to empty beads. A similar tendency, yet less pronounced could be observed for the Phen-modified library (1.9-fold). Since the non-specific background-binding to empty beads was less distinct for the Bn- modified library than for the Nap- modified one, the actual implementation of click-SELEX was done with the benzyl-modification.

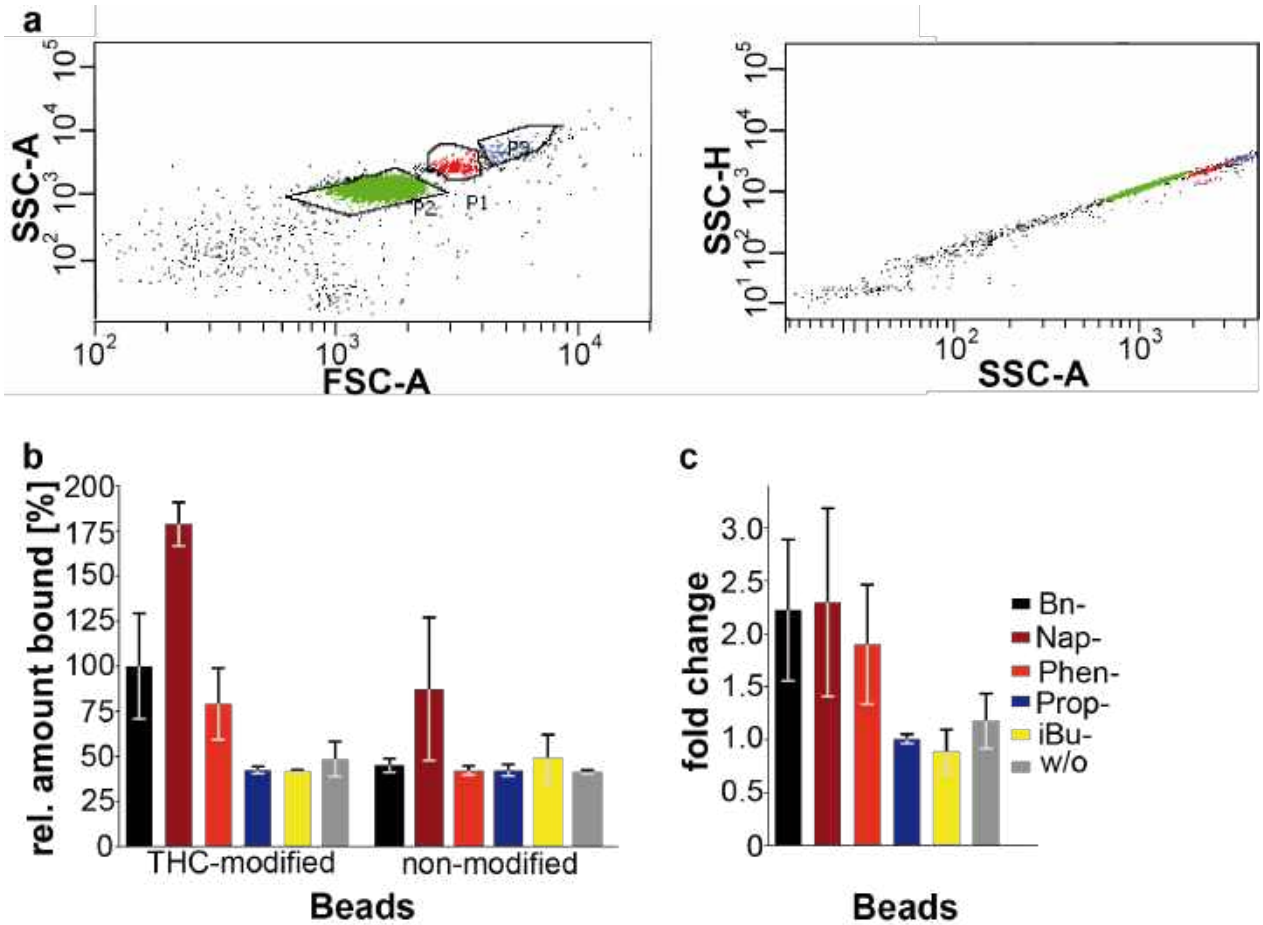

Fig. 19. Binding of FT-2 library click-modified with different azides to Dynabeads™. Flow cytometry was used to monitor binding of the starting library to THC-modified and non-modiied beads. a) Gated population from flow cytometry is shown. Fluorescence from population P2 were recorded for all samples. b) Juxtaposition of binding behaviour of differently clicked starting libraries to THC-modified and non-modified beads. c) Calculated fold change of binding of the libraries to THC-modified and empty beads. Abbreviations of the applied azides were Bn- (benzyl), Nap- (1-(2-azidomethyl) naphthalene), Phen- (Azido-benzenepropanoic acid), Prop- (2-azidopropan-1-ol), iBu (1-azido-2-methylpropane) (mean ± SD; n=3).

For a convenient click-SELEX procedure each individual EdU within the library should ideally be successfully click-modified with the desired azide. However, during SELEX it is hard to guarantee a quantitative click-reaction for every SELEX-cycle. Quantification of click-reaction via HPLC/HPLC-MS was not possible, since the PCR-amplification yield was not sufficient for this purpose. However, a quantitative click-reaction could be shown for the starting library. For this purpose, equal amounts of FT 2 library were either click-modified with benzyl-azide or stayed non-modified. Subsequently both samples were enzymatically digested to nucleosides. Resulting nucleosides from both digests were finally separated by HPLC. The separation profile of the non-clicked library showed, that the EdU is eluted from the HPLC-column at about 12 min (see **Figure 20 a**). By comparing that chromatogram with the one of the benzyl-clicked library, it became obvious that the click reaction proceeded quantitatively, at least within the detection limits (**Figure 20 b**). The nucleosides dC, dG and dA retained the previously shown retention time, whereas the EdU-peak at 12 min vanished completely. Instead a new peak appeared at a retention time of 27 min, representing the benzyl-clicked EdU (Bn-dU).

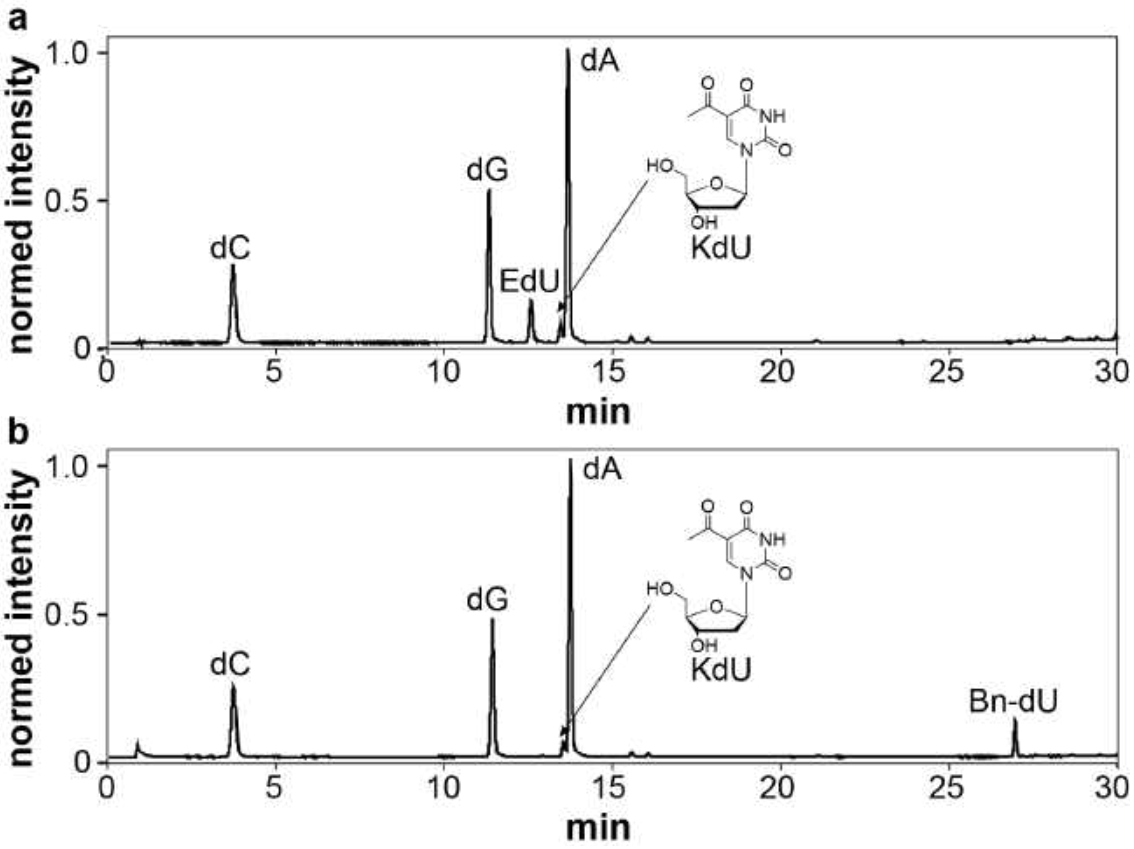

Fig. 20. FT2- starting library digested into nucleosides, which are subsequently separated via HPLC. The tiny peak in both chromatograms that is accentuated with an arrow corresponds to the oxidized EdU, named KdU. a) Starting library without click modification was digested. b) Digestion of a sample of the same library which was click-modified with benzyl-azide before the digest to nucleosides is shown.

The tiny peak between dG and dA in both chromatograms (at about 13.2 min, **Figure 20 a, b,** accentuated with an arrow) corresponded to a partially damaged EdU, where the ethinyl-moiety is oxidized. During solid phase synthesis and subsequent DNA workup of libraries containing unprotected alkyne-bearing EdU, roughly 20% of the alkyne is oxidized to a ketone[307]. The resulting ketone containing C5-acetyl residue was named KdU. Naturally, KdU is not available for functionalisation via click-chemistry any longer. The problem of KdU production only occurs for chemically synthesized DNA containing EdU, however. EdU-containing DNA that has been enzymatically amplified does not contain this oxidation product. The FT-2 library that was applied for this SELEX was synthesized on solid phase and accordingly did contain a small fraction of KdU. Therefore, this undesired side-product reduced the total amount of EdU that could be click-modified during the first SELEX-cycle. The problem of KdU formation during solid phase synthesis and workup potentially can be bypassed by using TIPS-protected EdU phosphoramidites. This approach can easily be done for oligonucleotides with defined sequences. For SELEX starting-libraries with an enormous number of different sequences however, the incorporation of TIPS-protected EdU phosphoramidites provided some problems which reduced the total yield.

3.2.2 Library enrichment studies

Initially nine cycles of click-SELEX were performed for enriching THC-binding sequences. Since no significant enrichment of binding sequences could be seen, seven additional SELEX cycles with harsher selection conditions were added for further enrichment of THC-binding sequences. Binding investigations were initially performed with only one concentration (500 nM) of the DNA of the 9th and the 16th selection-cycle, as well as with the starting library. Both, clicked and non-clicked DNA was incubated with either THC-modified or non-modified beads in 1x SELEX buffer for 30 min. After some washing-steps of the beads with SELEX-buffer flow cytometry was performed to quantify the remaining DNA on the beads.

As shown in **Figure 21 a**, an enrichment of binding sequences to THC-modified beads had taken place during the 16 SELEX cycles, since more DNA of cycle 9 remained on the beads compared to starting library. This trend was even more pronounced for SELEX cycle 16. DNA of the 16th SELEX-cycle bound roughly 4.5 times better to THC-modified beads than the starting-library. Additionally, the binding was clearly dependent on the click-modification. Roughly 90% of binding were lost if the click-modification was omitted (see **Figure 21 b**). The non-modified beads were rarely bound by the compared DNA-libraries, independent on the presence of click-modification.

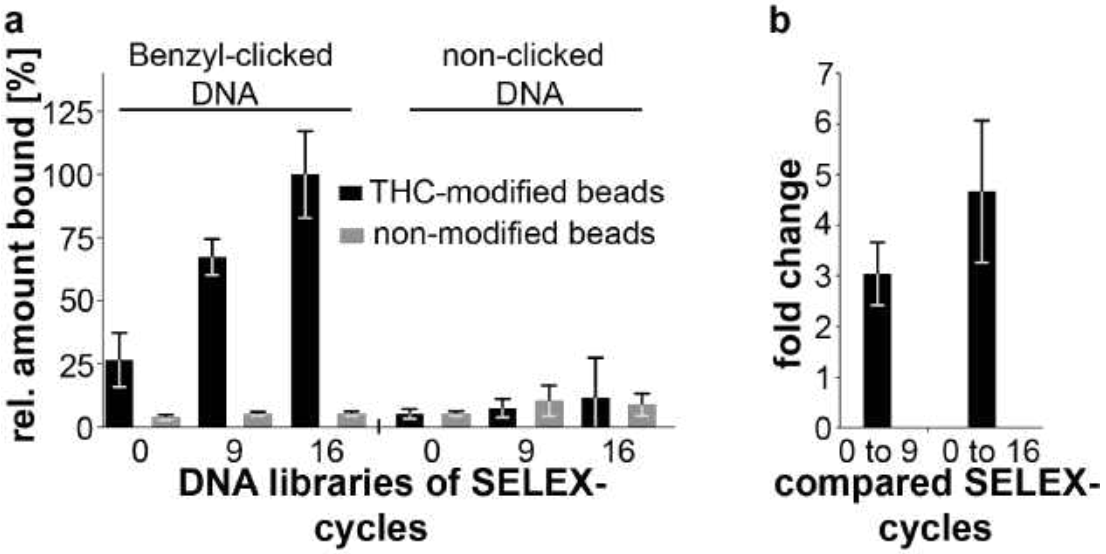

Fig. 21. Library enrichment during 16 cycles of selection. a) Binding investigations of 500 nM benzyl-clicked and non-clicked libraries of starting library (0), the library after 9 cycles, and 16 cycles of selection to THC-modified beads (black bars) and non-modified beads (grey bars). b) A 3-fold respectively a 4.5-fold enrichment compared to that of the starting library can be seen for the libraries of cycle 9 and 16 (mean + SD; n=5).

3.2.3 Sanger sequencing & NGS analysis

Sanger sequencing has been performed for the library of the 9th SELEX cycle. 48 individual sequences were sent for sequencing (see **Appendix, Table A1**). However, among the group of obtained sequences, no obvious enrichment of individual sequences could be seen, though some of the obtained sequences seemed to share a motif at the beginning of the random region. In general, the amount of EdU seemed to be slightly reduced among the obtained sequences from Sanger sequencing compared to the starting library (dA=24.3%; dC=23.1%; dG=32.5%; EdU=19.9%).

As mentioned before, click-SELEX was continued for seven additional cycles due to insufficient enrichment of single sequences. An illustration of the performed click-SELEX-cycles is shown in **Table 3**. The used amount of non-modified and THC-modified beads is given in microliter of bead-suspension. It has to be mentioned, that in both cases 30 µg of beads are suspended in one microliter of buffer. Negative-SELEX steps were started from cycle 10 onwards. With progressing SELEX-cycles, the number of washing steps was dramatically increased to reduce the amount of non-specifically binding sequences. Moreover, for the last few selection-cycles the recovery method of binding sequences was switched from heat-denaturation to affinity-elution (with THCA). For this purpose, 10% DMSO were titrated into the SELEX buffer to assure better solubility of the used amount of THCA.

Table 3. Procedure of the click-SELEX for THC-modified beads.

SELEX-cycle	Non-modified beads	THC-modified beads	Washing	Recovery
1	—	50 µl	3x 200 µl; 5 min	Heat 5 min; 90°C
2				
3				
4			4x 200 µl; 5mi	
5				
6		40 µl	5x 200 µl; 5min	
7				
8		30 µl		
9				
10	30 µl	20 µl	15x 200 µl; 5 min	
11	2x 30 µl			
12		10 µl		Affinity 100 µM THCA (10%DMSO)
13			10 x 1 ml; 5 min	
14	3x 30 µl		15x 1ml; 5 min	Affinity 10 µM THCA (10%DMSO)
15				Affinity 100 nM THCA (10% DMSO)
16				Affinity 10 nM THCA (10% DMSO)

After completion of 16 SELEX cycles, next-generation sequencing (NGS)-analysis has been performed with libraries of different SELEX cycles. For sequencing purposes, the EdU-bearing click-DNA libraries were first converted into conventional DNA-libraries via PCR with the triphosphates of dA, dT, dC and dG. Since canonical DNA was used for sequencing, dT instead of EdU is depicted in **Figures 22 and 23**. Naturally in the original click-libraries the corresponding nucleotides were EdU. The composition of nucleotides among the different SELEX-cycles is shown in **Figure 22 a**. An obvious enrichment of G-residues among the libraries of later SELEX cycles is observable. At cycle 16 the total frequency of G´s was almost 50% (**Figure 22 a**), whereas the absolute number of EdU was depleted.

In agreement with this is the distribution of nucleotides among each position within the randomized region (**Figure 22 b**). The distribution started to change at rather high selection cycles. A dramatic alteration of the nucleotide distribution has taken place between SELEX-cycles 12 and 13 as can be seen in **Figure 22 b**. Apart from a depletion of EdU in cycle 12, the ratio of the remaining three nucleotides was still

similar to that observable for the starting library (SL). In SELEX-cycle 13 however, a significant enrichment of the G-residues is apparent, especially within the first 20 positions of the randomized region. This alteration of the nucleotide distribution went along with higher selection stringency for the last selection cycles (**Table 3**).

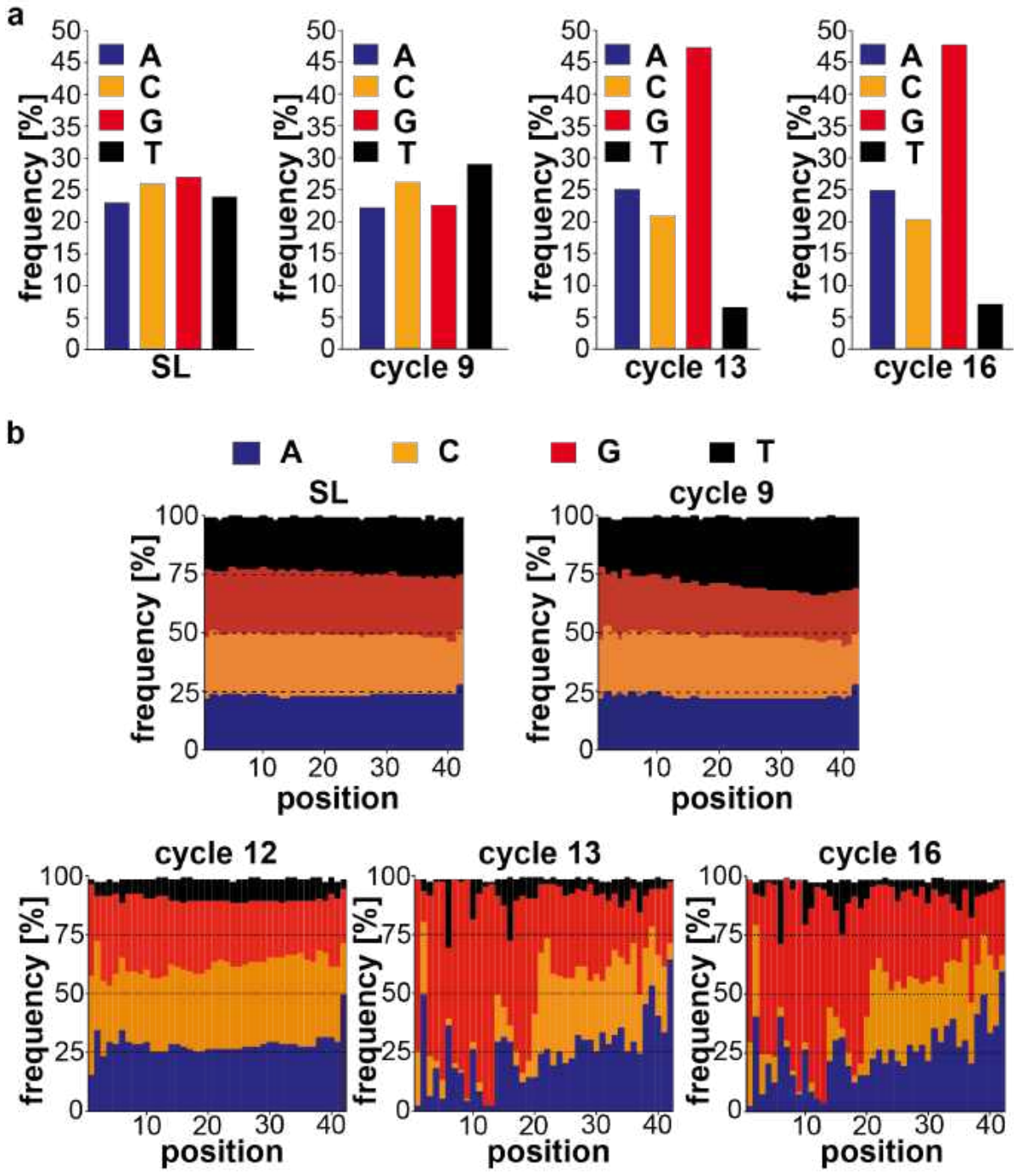

Fig.22. Frequency of nucleotides in libraries of consecutive SELEX cycles. NGS was done with libraries of different SELEX cycles. a) The development of nucleotide composition within the complete randomized region of different SELEX cycles is shown. The starting library (SL) consisted of an almost equimolar distribution of the four nucleotides dA, dG, dC and EdU. b) Nucleotide distribution for each position within the randomized region of different SELEX cycles.

Figure 23 also reveals the effect of a higher selection stringency onwards. The amount of unique sequences among the DNA libraries of every SELEX cycles is depicted in **Figure 23 a**. During the first 12 SELEX-cycles the number of unique sequences remained close to 100%, meaning that no strong enrichment of defined THC-binding sequences occurred so far. Only for the last four SELEX cycles the number of unique sequences is strongly reduced (to 25% for SELEX- cycle 16). This indicates an enrichment of sequences, that potentially bind to THC-modified beads. At the same time a motif arose that consisted of a highly conserved G-rich region. In consistency with the finding that the total number of EdU-residues was reduced among the remaining sequences of cycle 16, only one EdU could be found within the 19 nt long mentioned motif. Starting from position three, the motif showed four consecutive G-triads, separated only by interrupting short nucleotide sequences. The high presence of G-residues led to the assumption of a G-quadruplex as a possible three-dimensional architecture (see **section 3.3.4**). The enrichment of G-rich sequences with increased SELEX cycles can also be seen in **Appendix Figure A2**.

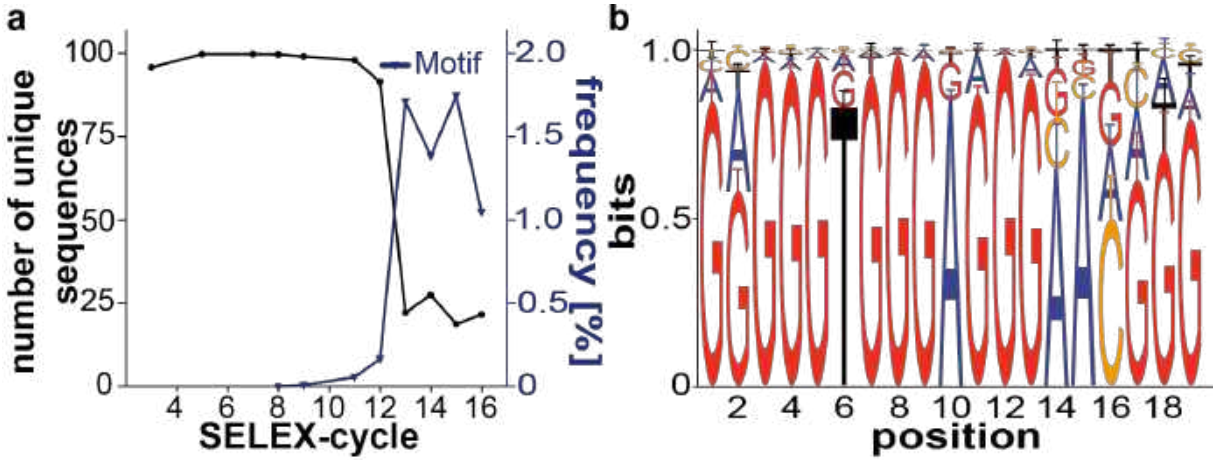

Fig. 23. Enrichment of SELEX libraries during selection. a) progression of unique sequences during SELEX cycles and appearance of a found G-rich motif. b) Nucleotide allocation within the emerged motif.

3.3 Binding studies of selected sequences to THC-modified beads

3.3.1 Affinity determination of different sequences

The sequences C11, C14, C18 and C33 all contained a 21 nt long G-rich region with high similarity to the motif depicted in **Figure 23 b**. All four sequences have already been found among the library of SELEX-cycle 9 with Sanger-sequencing. The found motif spans roughly half of the total sequence length (see **Figure 24 a**). The motif region is represented with coloured letters. While the similarity within this motif-region of the sequences is apparent, no similarity could be found within the rest of the oligonucleotides. The highest similarity in the motif-region could be seen for C11 and C33. Both sequences shared a highly similar motif-region, differing only in four nucleotides. In both sequences, the location of a benzyl-modified EdU was exactly at

the same position. Though the similarity to the motif was reduced for the sequences C14 and C18, the G-rich region clearly can be seen (**Figure 24 a**). Main differences to the motif are the location of benzy-modified EdU. C14 did not have any EdU in the motif-region and generally only contained one EdU at all. For C18 the location of EdU within the motif-region was shifted.

All four oligonucleotides were analysed concerning their binding properties to THC modified beads. Sequences were PCR-amplified, digested into the single strand and click-modified with benzyl-azide. In **Figure 24 b** a juxtaposition of binding-behaviour to THC-modified beads of C11, C14, C18 and C33 can be seen. Another sequence, resulting from another click-SELEX for THC (B10) and likewise click-modified with benzyl azide was applied as a non-binding control[308]. The sequence of that control can be seen in the **section 7.1**. Sequence C11 and C33 showed comparable concentration-dependent binding to THC-modified beads. Though C14 and C18 also did show concentration dependent binding, the affinities were obviously reduced compared to those of C11 and C33. This result indicated that a benzyl modified EdU at position “four” supports binding of the sequences C11 and C18. However, the assumption arose, that the G-rich region also contributes in a significant way to the binding to THC-modified beads of all the tested sequence. Both questions are addressed in the subsequent chapter.

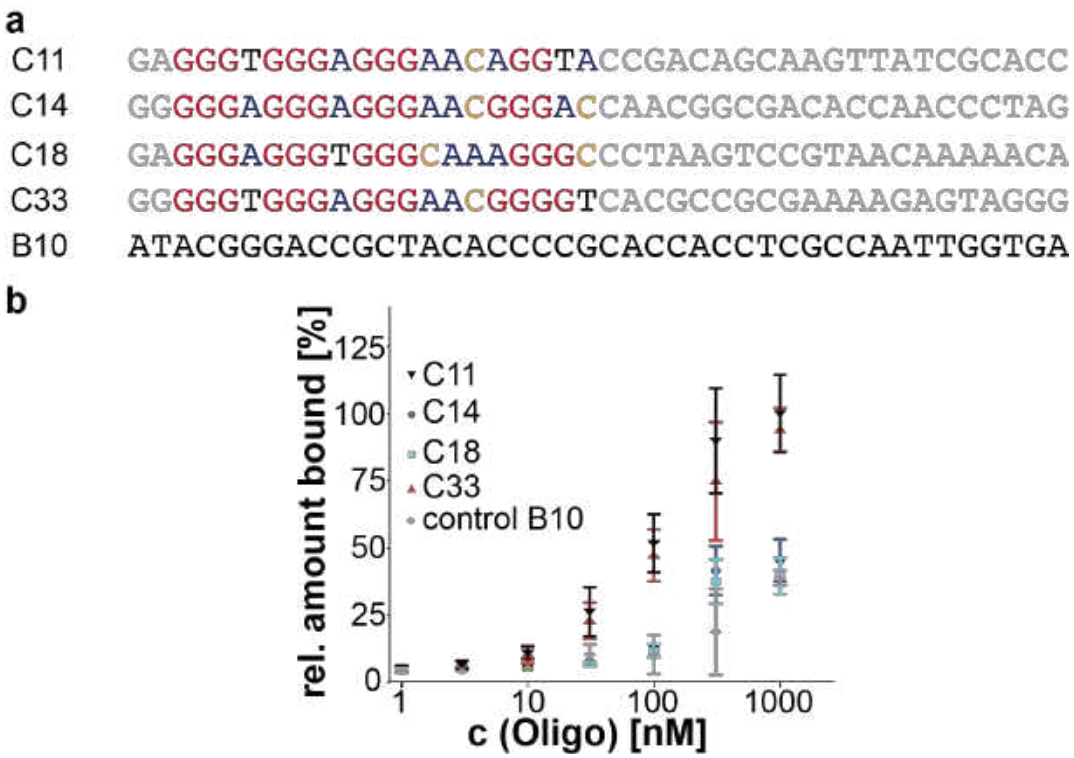

Fig. 24. Affinity determination of different sequences. The sequences C11, C14, C18, C33, and the control-sequence B10 were investigated. Each Thymidine represented in the sequences of course is a benzyl-modified EdU for the binding investigations. a) Sequences of C11, C14, C18, C33, and B10 are shown without the primer binding-sites. Regions with similarity to the identified motif (compare to Figure 18 b) are coloured. b) Concentration dependent binding to THC modified beads. Grey curves represent the binding of a non-binding control (mean ± SD; n=3).

3.3.2 kD-determination of the identified sequence C11 and a truncated version.

Due to the results displayed in **Figure 24 b,** which show concentration dependent binding of C11 and C33 to THC-modified beads, it was decided to investigate the sequence C11 more deeply. Compared to the libraries of the last SELEX-cycles, the nucleotide distribution in the random region is similar (G=38%; C=21.4; T=11.9; A=28.6). To get a first proposal about a possible secondary structure of C11, mfold prediction was applied[309]. The resulting predicted secondary structure is shown in **Figure 25 a**. The sequences are depicted in a colour-code. Benzyl-clicked EdU are displayed in black. As can clearly be seen, the regions of the primer binding sites are not involved in any predicted secondary structures, what led to the hypothesis that they are not necessary for binding of C11 to THC-modified beads. To confirm this hypothesis, a truncated version of C11 was synthesised (C11.41) and its binding was analysed via flow cytometry in parallel to the full-length sequence. The total length of the truncated version was 41 nucleotides. As shown in **Figure 25 b** and **Figure 25 c** the determined dissociation constants of the full-length and the truncated sequence did indeed not differ relevantly.

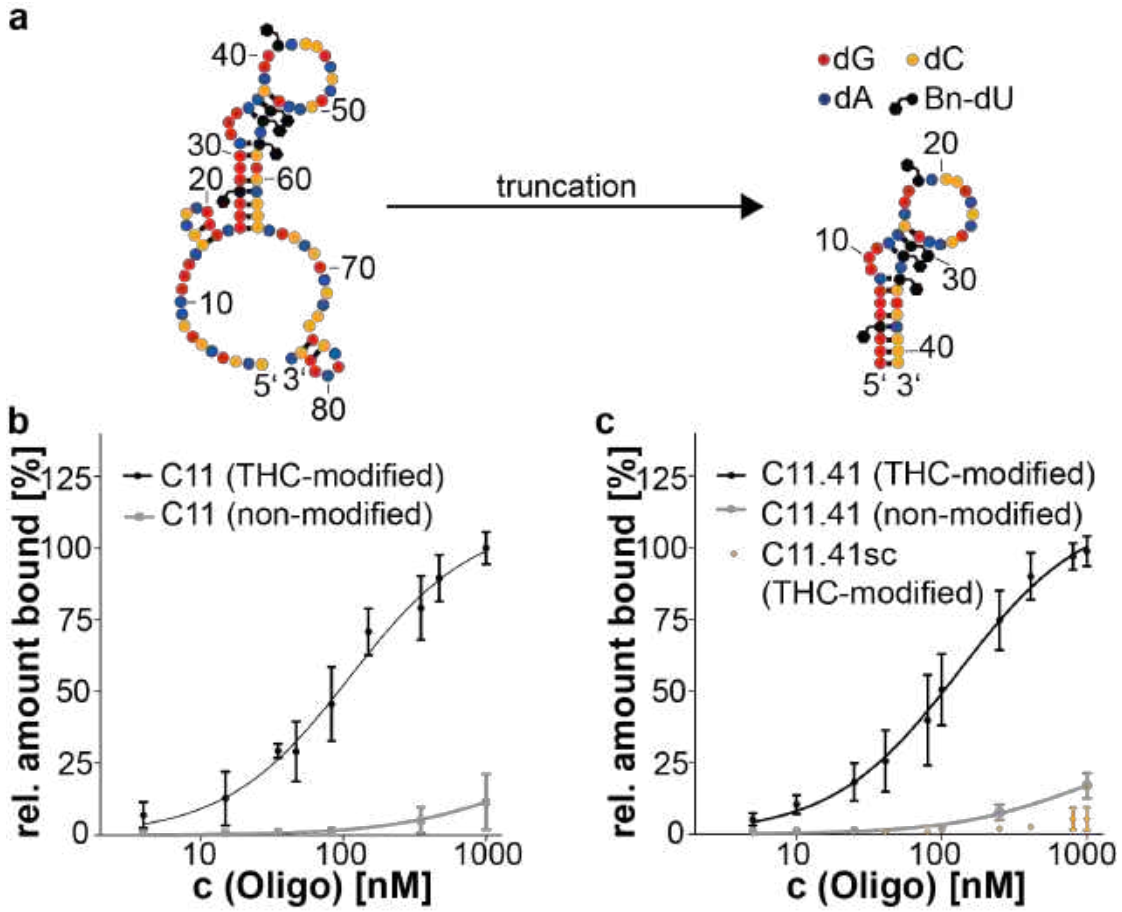

Fig. 25. Sequences and k_D-determination of C11 and the truncated version C11.41. a) mfold predicted secondary structures of the full-length C11 and a 41 nt long truncated sequence (C11.41) b) Affinity of the benzyl-clicked sequence C11 for THC-modified and non-modified beads. c) Affinity of C11.41 to THC-modified and non-modified beads. A scrambled version of C11.41 also does not bind to the THC-modified beads (mean ± SD, n=3).

Even more important, C11.41sc, a sequence with the same nucleotide distribution but a scrambled nucleotide order, does not show such a concentration dependent binding to the target coupled beads (**Figure 25 c**). Hence the observed binding is dependent on the oligonucleotide sequence. **Table 4** summarizes the determined k_D-values of C11, C11.41, as well as C11.41sc.

Table 4. k_D-values of C11, C11.41, C11.41sc to THC-modified beads.

Sequence name	k_D [nM]
C11	111.0 ± 20.2
C11.41	131.1 ± 10.2
C11.41sc	n.d.

Since the G-rich sequences C11 (and C33) did show concentration dependent binding to THC-modified beads (compare to **Figure 24 b**), it was speculated that this G-rich motif alone could already be sufficient for binding to the THC-modified beads. To clarify this question, sequences only consisting of this G-rich motif were investigated concerning their binding behaviour. Therefore, even further truncated versions of C11 and C33 only comprising the coloured region in **Figure 24 a** were tested. In parallel an equally truncated versions of C14 was tested. All sequences consisted of only 19 nucleotides and therefore were named C11_19, C14_19, and C33_19. In contrast to C11_19 and C33_19 that contained one EdU at exactly the same position of their sequences, C14_19 did not contain any EdU at all. This way it was tried to find out, if the benzyl-modified EdU within C11_19 and C33_19 does have a contribution for the binding to THC-modified beads.

Again, flow cytometry was applied to compare the binding performance of the newly ordered truncated oligonucleotides. The sequence C11.41 and the scrambled non-binding version C11.41sc were used as reference sequences. The result is shown in **Figure 26**.

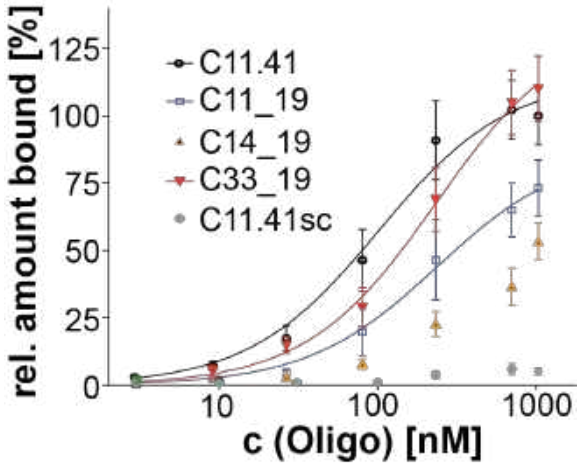

Fig.26. Affinity determination of the 19-mer sequences C11_19, C14_19 and C33_19. Concentration dependent binding is compared to that of C11.41 and the non-binding control C11.41sc. (mean ± SD; n=3).

Compared to the full-length versions of C11, C14 and C33 (**Figure 24 b**) the truncated sequences showed reduced affinities to THC-modified beads. While the affinity of C11_19 and C33_19 (**Figure 26, Table 5**) are alleviated compared to the corresponding full-length versions, affinity of C14_19 was even more weakened and a distinct k_D-value could not be calculated (**Figure 26, Table 5**).

Table 5. k_D-values of C11.41, C11.41sc and the 19-mers to THC-modified beads.

Sequence name	k_D [nM]
C11.41	128.4 ± 15.5
C11_19	317.2 ± 43.1
C14_19	n.d.
C33_19	311.0 ± 30.2
C11.41sc	n.d.

This result demonstrates that the G-rich motif-region apparently plays an elementary role in the binding properties to THC-modified beads. Nonetheless, it is not solely responsible for the binding. The benzyl modified EdU located at the defined position within the sequences C11_19 and C33_19 seems to contribute to a better affinity. C14_19 is lacking that modification, resulting in an obviously reduced affinity of that sequence. In summary it is assumed, that the combination of the G-rich region together with the benzyl-clicked EdU localized therein is largely responsible for the determined affinities. Still, the affinities of the 19-mers is weakened compared to the full-length versions, the remaining part of the oligonucleotides probably support the binding.

The oligonucleotides that were applied in flow cytometry assays (**Figure 25** and **Figure 26**) were synthesized by Ella-Biotech (Martnsried). To ascertain the integrity of the sequences HPLC-MS analysis was done. All mentioned sequence can be seen in in **section 7.1**. **Table 6** summarises the calculated and detected masses for the benzyl-clicked and the non-clicked oligonucleotides. HPLC-chromatograms can be seen in **Appendix Figures A3 -A4.**

Table 6. Detected masses of C11.41 and C11.41sc and of the 19 nucleotide long C11_19, C14_19 and C33_19 in non-clicked and benzyl-clicked state.

Oligonucleotide	calculated mass non-clicked [m/z]	detected mass non-clicked [m/z]	calculated mass benzyl-clicked [m/z]	detected mass benzyl-clicked [m/z|
C11.41	13428.00	13428.06	14093.75	14093.20
C11.41sc	13428.00	13428.29	14093.75	14093.50
C11_19	6687.00	6687.14	6953.3	6953.05
C14_19	6567.00	6565.94	-	-
C33_19	6719.00	6719.20	6985.3	6984.70

3.3.3 Identification of crucial, click-modified positions within C11.41

Since the affinity of C11.41 to THC-modified beads is higher than that of C11_19 and almost identical to that of the full-length C11, most of the following assays were performed with C11.41. First, the effect of the click-modifications on the binding performances was further investigated.

Binding of the not click-modified C11.41 to THC-modified beads was highly reduced compared to the benzyl-clicked sequence. This fact supports the possibility that C11.41 is a true clickmer, whose binding is at least improved by the click-in modification. Since C11.41 does have 5 EdU-positions that can be modified via click-reaction, it was analysed, which of these positions are important for the binding to THC-modified beads. For that purpose, five different 41 nt long sequences were synthesised. In each of them one EdU was substituted by dT. The sequences and their detected masses can be seen in **Table 7** and **Table 8**. For **Table 7**, bold **X** represents EdU that can be modified via click-reaction, whereas italic *T* represents the EdU-substituting dT. The detected masses for the non-clicked as well as the benzyl-clicked sequences verified the integrity of the tested sequences (**Table 8**). HPLC-MS results of non-clicked and benzyl-clicked point mutants can also be seen in **Appendix, Figure A6**.

Table 7. Sequence of the five point-mutants U4T, U18T, U31T,U32T and U34T.

Name	Sequence
U4T	GGG *T*GG GAG GGA ACA GG**X** ACC GAC AGC AAG **XX**A **X**CG CAC CC
U18T	GGG **X**GG GAG GGA ACA GG*T* ACC GAC AGC AAG **XX**A **X**CG CAC CC
U31T	GGG **X**GG GAG GGA ACA GG**X** ACC GAC AGC AAG *T***X**A **X**CG CAC CC
U32T	GGG **X**GG GAG GGA ACA GG**X** ACC GAC AGC AAG **X***T*A **X**CG CAC CC
U34T	GGG **X**GG GAG GGA ACA GG**X** ACC GAC AGC AAG **XX**A *T*CG CAC CC

Table 8. Detected mass of the non-clicked and benzyl-clicked point mutants.

Oligonucleotide	calculated mass non-clicked [m/z]	detected mass non-clicked [m/z]	calculated mass benzyl-clicked [m/z]	detected mass benzyl-clicked [m/z|
U4T	13417	13417.38	13949.60	13949.80
U18T	13417	13417.25	13949.60	13950.05
U31T	13417	13417.38	13949.60	13949.85
U32T	13417	13417.25	13949.60	13949.81
U34T	13417	13417.34	13949.60	13949.65

The applied dilution series for binding-investigations were not performed until 1 µM concentrations in this case. Concentration dependent binding was compared to that of benzyl clicked C11.41 and C11.41sc, as well as the non-clicked C11.41. For this investigation, again the benzyl-clicked competitor (100 nM) was added for all concentrations. The results are shown in **Figure 27 a.** It became obvious that the benzyl-modified EdU at position "four" supports the binding of C11.41 to THC-modified beads, since binding of the point mutant U4T is significantly reduced compared to C11.41, especially for the concentrations of 50 nM and 100 nM. In contrast, all other point mutants showed binding to THC-modified beads comparable to that of C11.41. In **Figure 27 b** the binding of 100 nM of all the tested point-mutant sequences to THC-modified beads after subtraction of the observed values for the non-clicked C11.41 is highlighted. This way the effect of the binding dependency on the single click-modification becomes even more obvious. All observed relative fluorescence-intensity values were normalized to that of benzyl-clicked C11.41 at 100 nM (**Figure 27**).

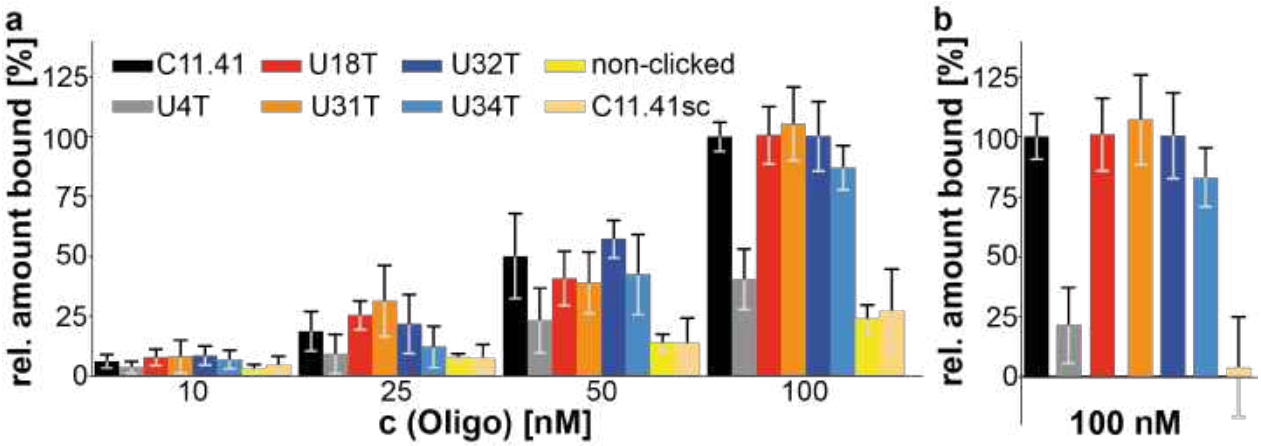

Fig. 27. Binding investigations of five pointmutants (see table 7 a). a) Binding of four different concentrations of benzyl-clicked pointmutants is compared to clicked and non-clicked C11.41 and clicked c11.41sc. b) The amount of non-clicked C11.41 is subtracted from the other values at 100 nM (mean + SD; n=6).

3.3.4 Secondary structure investigations of C11.41

As already mentioned, the percentage of G-residues among the libraries of later SELEX cycles was strongly elevated. The same is true for the investigated sequence C11.41. The thus far suggested secondary structure of the sequence was done by mfold prediction, which is based on thermodynamic calculations[309]. This prediction does not necessarily represent the actual folding and other ways of secondary structure formations are possible that cannot be predicted this way. Especially the high number of G-residues could be a hint that C11.41 does indeed fold into another secondary structure than suggested. In this chapter the formation of other secondary structures was investigated.

First, a hemin-peroxidase assay was performed with sequences of interest was performed. Hemin is a known co-factor of enzymes that catalyse peroxidase reactions. The cofactor alone is also capable to catalyse these reactions. However, its binding to the enzymes dramatically increases the catalytic activity. It has been found, that besides enzymes G-quadruplex (GQ) forming structures can also bind to Hemin and thus increase its catalytic activity. Hemin binds to external guanidines in GQ structures. Intramolecular parallel GQ´s lead to higher peroxidase activity than antiparallel ones[310–313].

Possible peroxidase activity is monitored in a colorimetric way in this assay. Herein the dye 2,2'-azino-bis(3-ethylbenzothiazoline-6-sulfonate) (ABTS) is used as a chromogen, which in the presence of H_2O_2 absorbs strongly at 414 nm upon one-electron oxidation to its radical anion $ABTS^{\bullet+}$. The increase of absorption at 414 nm over time can simply be detected. This oxidation reaction affords strictly stoichiometric ratios between ABTS and H_2O_2, which should ideally be at 1:0.5 as it can be seen in equation [1][314–316].

$$H_2O_2 + 2\ ABTS + 2\ H^+ \xrightarrow[Hemin]{G\text{-quadruplex,}} 2\ H_2O + 2\ ABTS^{\bullet+} \qquad [1]$$

$$4\ ABTS^{\bullet+} + 2\ H_2O \longrightarrow 4\ ABTS + O_2 + 4\ H^+ \qquad [2]$$

Potassium ions are known to stabilize GQs. Therefore, the assay was performed in a phosphate buffer (pH7.4) and in the absence or presence of potassium ions. Ideally a clear difference in peroxidase activity should be visible between both conditions, if GQs are indeed formed.

Figure 28 shows the result of the hemin-peroxidase assay, which was done with C11.41 and C11.41sc. As a positive control the aptamer C10.36, which forms a single stranded, three-layered parallel GQ together with a pointmutant of this (G24A, which is forming a two-layered GQ), was used. C10.36 is a known aptamer for Burkitt´s lymphoma cells[317]. In **Figure 28 a, d)**, the peroxidase-activity in presence of hemin in potassium containing THC-SELEX buffer is shown. An increase in absorption over time could be detected for C11.41(red) and C10.36 (blue), though in the latter case a decrease of absorption could be seen after a while. The slight increase for C11.41sc (black) can be explained with the low intrinsic activity of hemin alone. For G24A (grey) which is known to form a 2-layered GQ, only a comparatively slight absorption increase could be detected in relation to C10.36. **Figure 28 b, e)** shows the result of the assay performed in buffer lacking potassium ions. For C10.36 and C11.41 a similar, jet weaker effect compared to the scenario of K^+-containing buffer could be seen. In the absence of hemin (**Figure 28 c, f**), no peroxidase activity could be monitored, as expected.

A shortage of H_2O_2 as well as an excess easily affects the reaction and subsequently the readout of the assay. Thus, a H_2O_2 shortage can lead to a “back”-reaction of reduced ABTS (see equation [2]). On the other hand, peroxide excess leads to a further oxidation of $ABTS^{\bullet+}$ to $ABTS^{2+}$. Latter is quite unstable and decomposes into five different fragments. The absorption maximum of this compound mix shift within this process from 414 nm ($ABTS^{\bullet+}$) towards lower wavelength of 260-294 nm ($ABTS^{2+}$ and decomposition products)[314]. For the performed assay the fact, that absorption intensities at 414 nm unexpectedly started to decease again after a few minutes (especially for C10.36, **Figure 28 d**) could be explained by both scenarios, over-oxidation of $ABTS^{\bullet+}$ as well as the “back”-reaction. However, since the assay was performed at a pH of 7.4 the “back”-reaction is more likely in this scenario, as further oxidation to $ABTS^{2+}$ prefers quite acidic conditions[316]. In general, most references have performed oxidation assays at a pH of 6 or lower, since the kinetics are best under these slightly acidic conditions[314,316]. However, neither C10.36 nor C11.41 were selected at these pH-ranges and thus the assay was performed at pH 7.4. This should just slow down the reaction rates, which are not of prior interest in that case.

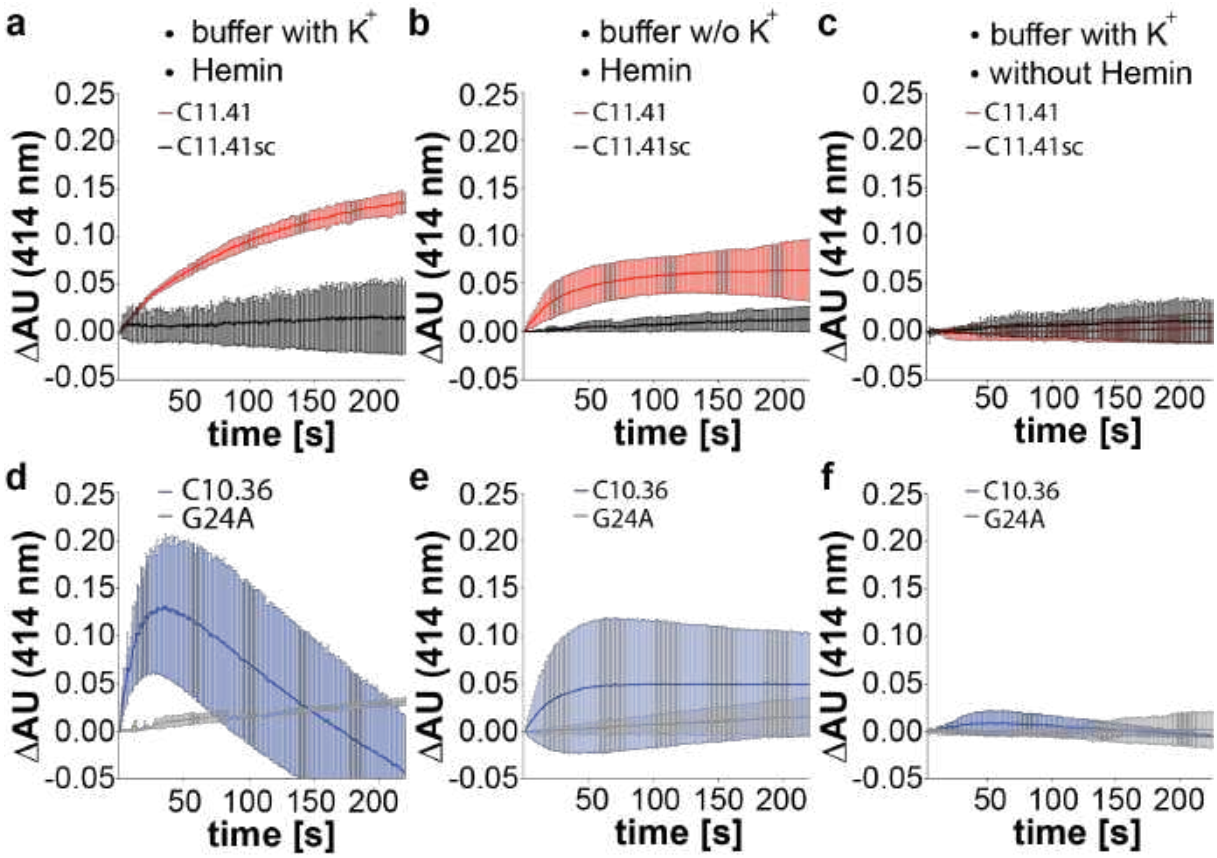

Fig. 28. Hemin-peroxidase assay. Time dependent increase of absorption at 414 nm**.** The assay was performed under differing buffer compositions (n=2). a, d) The result of the assay in the presence of hemin in potassium containing buffer is shown. b, d) The result in the presence of hemin, but in buffer without potassium ions is depicted. c, f) The assay was performed without hemin in potassium containing buffer. a-c) shows the increase of absorption at 414 nm over time for the tested sequences C11.41 (red) and C11.41sc (black). d-f) shows the result of the control sequences C10.36 (blue)and G24A (grey).

During the performed assay, the above-mentioned undesired side reactions going along with a decrease of absorption at 414 nm could easily have taken place due to miscalculations or pipetting errors of the individual compounds. This might explain the unexpected curve progression after one minute, in case of C10.36. However, the fact that the absorption intensities at 414 nm initially rise for DNA-samples C10.36 and C11.41 strongly hint the presence of GQ´s, whereas this increase in absorption could not be detected for scrambled versions of the DNA samples or just in the presence of hemin alone without DNA. Furthermore, the presence of K^+-ions increases the oxidation rate (for C11.41 and C10.36), which further supports the hypothesis of the formation of GQs for these sequences. Generally spoken, the assay seemed to be too prone for errors. The results of the readout are just sufficient to give hints about possible three-dimensional structures.

The hemin-peroxidase assay indicated a possible GQ-formation of C11.41 in potassium containing buffer. A two-layered G-quadruplex of the sequence seems possible, as a hypothetical illustration in **Figure 29 a** suggests. Since potassium ions are known to stabilize GQ structures, further assays with C11.41 were done via flow cytometry. First of all, it was tried to estimate if K^+-ions support binding of the sequences C11.41 to THC-modified beads. Binding in phosphate buffered solutions of 100 nM C11.41 and C11.41sc, both clicked with benzyl-azide, was analysed. **Figure 29 b** clearly shows, that binding-performance of C11.41 is negatively affected by the absence of K^+-ions. Together with the hemin-peroxidase assay this showed that potassium influenced the biophysical characteristics of C11.41 and the evidence for the formation of a GQ concretized.

Next, circular dichroism (CD)-spectroscopy was applied, which is a regularly used method to study GQ-formations and topologies[318,319]. GQ-geometries are polymorphous due to differences in types of connecting loops, the glycosidic bond angle orientation (*syn, anti*) and numerous other parameters as G-quartet stacking geometry. Therefore, each specific geometry shows specific CD-spectra[318,320]. In general, it can be said, that parallel topologies of GQ´s show a dominant positive peak at ~264 nm another one at 210 nm, and a negative one at ~245 nm. In contrast to that, for antiparallel structures sharp negative peaks occur at ~260 nm together with a positive peak at ~295 nm. So called “hybrids” can also occur with maxima at ~295 nm and ~260 nm and a minimum at ~245 nm[318–321].

CD-spectroscopy was performed in THC-SELEX buffer and water for C11.41 and C11.41sc, as well as for C10.36. C10.36 was used as a positive control. In **Figure 29 c** the CD-spectra of C11.41 and C11.41sc are shown. In potassium containing buffer the spectrum equals that of parallel GQ´s with a maximum at ~264 nm and a minimum at ~240 nm. In water, lacking the G-quartet stabilizing potassium ion, the peak intensity is significantly reduced, due to a probably less stable complex. The scrambled variant however shows a completely different spectrum, meaning that it does not fold into a GQ. The result for C10.36 greatly resembles that of 11.41, verifying its folding into a parallel conformation. Again, the spectrum in water is greatly weakened.

In summary it was shown, that the sequence C11.41 most probably folds into a parallel GQ. Furthermore, one click-modified EdU which is located in the middle of the GQ greatly supports the affinity of that sequence to THC-modified beads, whereas the other EdU could be substituted by dT without loss of affinity. Those results led to the assumption, that C11.41 could probably be even further varied.

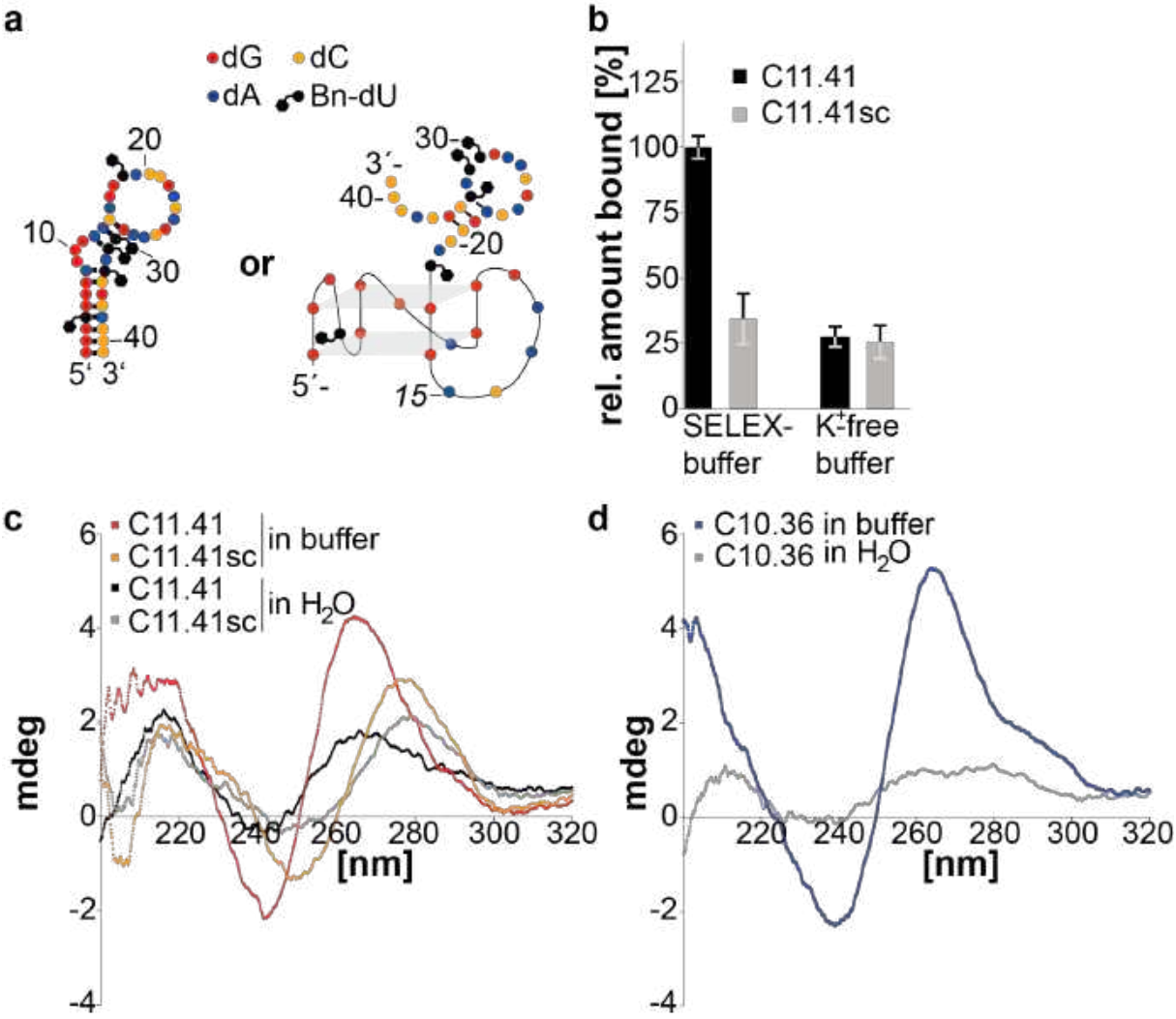

Fig. 29. Potassium-dependent binding and CD-spectra of C11.41. a) Two suggestions for secondary structure formation of C11.41 are shown. The mfold predicted structure that was already shown in Figure 20 is compared to another potential secondary structure, wherein the sequence folds into a parallel 2-layered G-quadruplex. b) Potassium dependency of C11.41 and C11.41sc (100 nM) on binding to THC-modified beads is shown. Values are normalized to that of C11.41 in SELEX-buffer. c) CD-spectroscopy of C11.41 and C11.41sc (5 µM) in SELEX buffer and water. d) CD-spectra of the positive control sequence C10.36 in buffer and water.

The observed indication that C11.41 presumably folds into a parallel G-quadruplex together with the fact that only one click-modified EdU within the sequence supports the binding to THC-modified beads led to the design of two further variants of C11.41. The first variant of C11.41, simply contained one EdU within the sequence at position four (C11.41_4), that could be click-modified.

The second variant wherein the dA at position 15 was substituted by a dG was called C11.41_A15G. In contrast to C11.41, which probably folds into a two layered-GQ (**Figure 29 a**), C11.41_A15G potentially could fold into a three-layered GQ. Furthermore, C11.41_A15G also just carries one EdU modification at position four. As for all the other oligonucleotides that were synthesized via solid phase synthesis, the correct mass of the two new sequences were verified in non-clicked, as well as in the benzyl-clicked state. The results are summarized in **Table 9**.

Table 9. Detected mass of non-clicked and benzyl-clicked C11.41_4 and C11.41_A15G.

Oligonucleotide	calculated mass non-clicked [m/z]	detected mass non-clicked [m/z]	calculated mass benzyl-clicked [m/z]	detected mass benzyl-clicked [m/z]
C11.41_4	13388	13389.03	13521.15	13522.51
C11.41_A15G	13404	13405.10	13537.15	13538.52

First of all, simple affinity-determination to THC-modified beads via flow cytometry were performed. The affinity of C11.41_4 and C11.41_A15G, click-functionalized with benzyl-azide were compared to that of C11.41. The result can be seen in **Figure 30**. The concentration-dependent binding to the THC-modified beads did not differ significantly between the three tested sequences (see **Table 10)**.

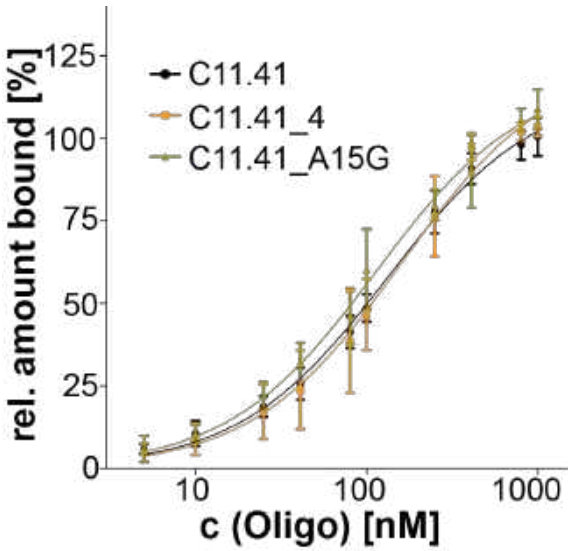

Figure 30. Affinity determination of the variant C11.41_4 and C11.41_A15G. Affinity-determination of the two variants C11.41_4 (orange) and C11.41_A15G (green) compared to C11.41 (black) is shown. The affinities to THC-modified beads do not differ significantly (mean + SD; n=5).

Table 10. k_D-values of benzyl-clicked C11.41, C11.41_4, and C11.41_A15G to THC-modified beads.

Sequence name	k_D [nM]
C11.41	132.8 ± 7.8
C11.41_4	159.3 ± 17.45
C11.41_A15G	113.4 ± 9.2

Based on these findings, C11.41_A15G was further investigated concerning its binding performance in dependence on the click-modification. 200 nM of differently click-modified oligo was tested. The result can be seen in **Figure 31 a**. Applied click-modifications can be divided into azides with an aromatic core (1-6) and aliphatic azides (7-11). The chemical structure of all tested azides is shown in **Figure 31 b**. A tendency is perceptible, of which DNA that has been modified with an aromatic azide shows a stronger binding to THC-modified beads than DNA modified with aliphatic azides. Binding values were normalized to the value obtained with the benzyl-modification (**1**). Further tested azides were 1-(2-azidomethyl) naphthalene (**2**), 4-(azidomethyl)-3,4-dihydro-benzooxazine (**3**), Azido-benzenepropanoic acid (**4**), 3-(2-azidoethyl)-indole (**5**), 4-(2-azidoethyl) imidazole (**6**), 1-azido-2-methylpropane (**7**), 3-azido-1-propanol (**8**), 4-(2-azidoethyl)morpholine (**9**), 2-azido-ethanamine (**10**), and 2-(azidoethyl)guanidine (**11**).

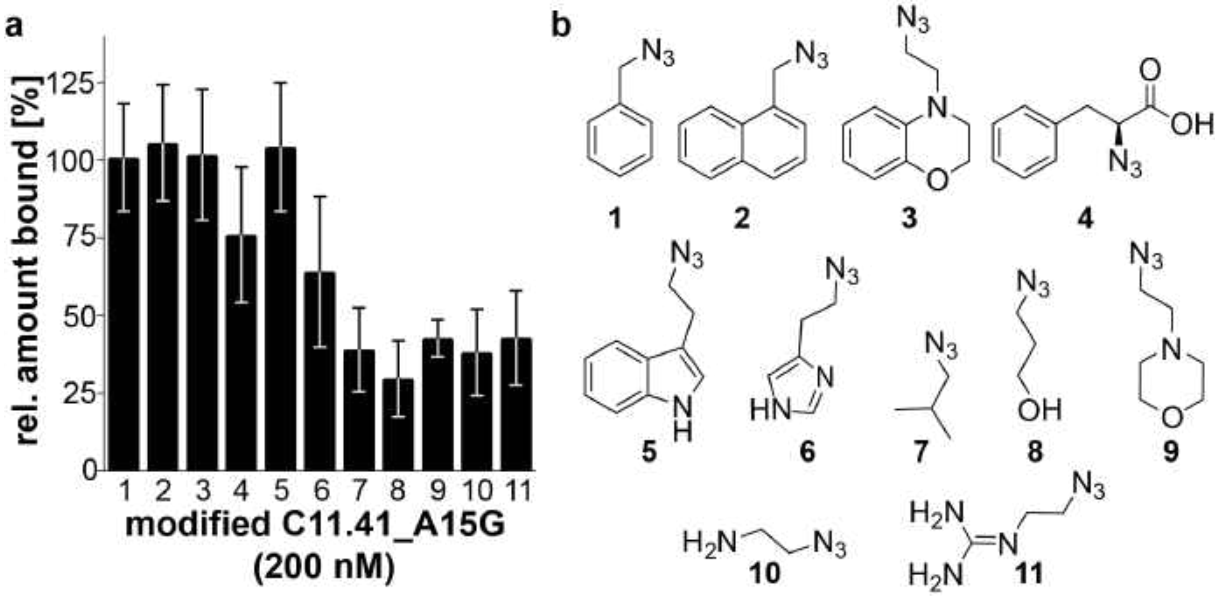

Fig. 31. Binding dependency on the applied click-modification for C11.41_A15G. a) Binding of C11.41_A15G (200 nM) that was click-modified with different azides to THC-modified beads. Values are normed to that of benzyl-modified oligo. b) Chemical structure of the different azides used to modify the sequence C11.41_A15G.

Since most of the applied azides seen in **Figure 31 b** were synthesized in our laboratory, it had to be guaranteed that they all are accessible to click-reaction with DNA. Therefore, a test click-reaction of all these azides has been performed with a 16-nucleotide long test-oligonucleotide that contained just one EdU. To verify the susceptibility of all the applied azides for click-reaction the click-modified 16-mer was investigated via HPLC-MS. The correct product mass for every click-reaction was used as proof, that those azides could all be used to modify the clickmer-sequences. All the detected masses can be seen in **Table 11**. NMR spectra of the applied azides are shown in **Appendix Figure A7-A15**. The problem with the 16-mer test-sequence was, that it had not been synthesized with a TIPS-protection group for the alkyne. Therefore, approximately 20% of the available alkyne-containing strands were oxidized to the ketone, which in turn was no longer susceptible for click-reaction.

For all analysed click-modified test-sequences, two UV-peaks in the chromatogram showed up. In most cases the masses of the ketone-containing sequence (K-dU), as well as the masses corresponding to the click-modified sequence could be observed (see **Appendix, Figure A5**).

An additional information must be given for the 4-(azidomethyl)-3,4-dihydro-benzooxazine (**Azide 3** in **Figure 31 b**). In contrast to all the other compounds, for this compound NMR data are missing. Since the DNA-sequences that were click-modified with this azide did have the desired mass however (see **Table 11** and **Appendix, Figure A5**), it was decided to include this azide in the binding investigations.

Table 11. Detected masses for the 16-mer test-sequence click-modified with the azides 1 – 11 that were used to modify C11.41_A15G (Figure 22 b).

Azide, used to modify the 16-mer test-sequence	Calculated mass [m/z]	Detected mass [m/z]
-	4858.00	4858.24
1	4991.15	4991.74
2	5055.10	5055.83
3	5034.07	5035.77
4	5049.07	5049.79
5	5044.09	5044.86
6	4995.07	4995.74
7	4957.08	4957.88
8	4959.11	4960.28
9	5014.19	5014.68
10	4944.06	4943.53
11	4986.08	4986,73

Figure 31 shows obvious differences in binding performance depending on the click-modification. Therefore, the most promising azides (column 1, 2, 3, and 5 in **Figure 31 a**) were chosen to be tested in a concentration dependent binding analysis. C11.41_A15G was therefore click-modified with benzyl-azide (**Bn-dU**), naphtalane-azide (**Nap-dU**), indole-azide (**Ind-dU**), and benzooxazine-azide (**Bo-dU**) and the affinity of these modified oligonucleotides were compared to THC-modified beads (**Figure 32**). The applied click-competitor, click-modified with the corresponding azide was used at a concentration of 1 µM. The result can be seen in **Figure 32**. Again, the k_D-value for the benzyl-modified oligo was in the range as measured before as was that of the benzooxazol-modified clickmer, and the indol-modified one (compare **Table 12**).

Table 12. k_D-values differently click-modified C11.41_A15G.

Modification	k_D [nM]
Bn-modified	128.1 ± 10.1
Nap-modified	88.3 ± 6.7
Ind-modified	117.3 ± 10.6
Bo-modified	128.2 ± 13.4

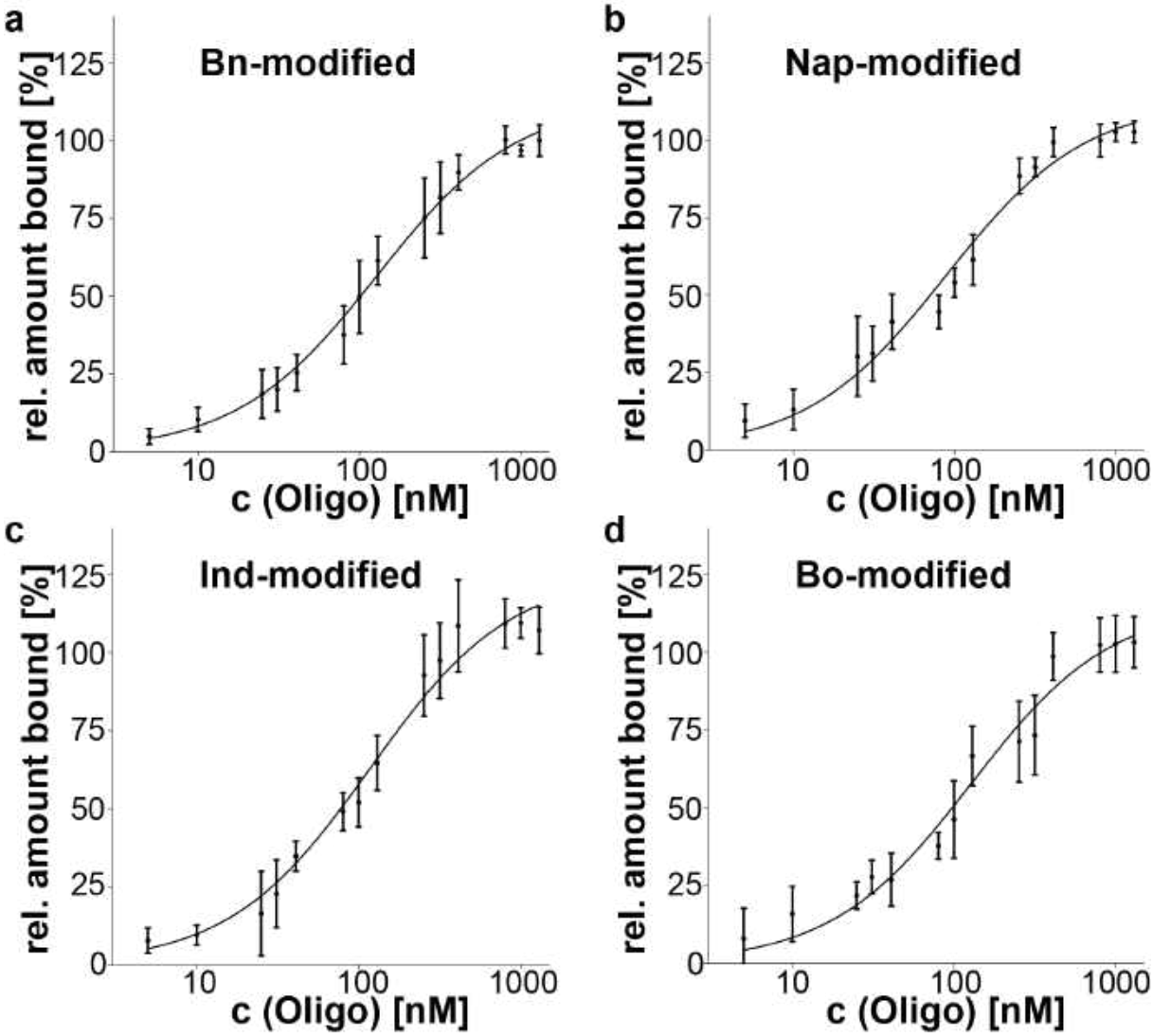

Fig. 32. Concentration dependent binding of differently click-modified C11.41_A15G. Binding of C11.41_A15G, modified with a) benzyl-azide, b) 1-(2-azidomethyl) naphthalene, c) 3-(2-azidoethyl)-indole, and d) 4-(azidomethyl)-3,4-dihydro-benzooxazine (mean + SD; n=5).

A slightly better affinity-value was calculated for the naphthalene-modified clickmer with a measured k_D of 88.3 ± 6.7 nM. In general, the result is in agreement with that of **Figure 31.** There is a strong evidence, that the aromatic modifications help to increase the affinity of the oligonucleotide towards THC-modified beads.

Though the probability that the altered sequences also fold into parallel GQs was high, CD-spectroscopy with the two new oligonucleotides C11.41_4 and C11.41_A15G was repeated. This was mainly done to demonstrate that the alterations do not affect the three-dimensional folding. Once more, spectra of C11.41 & C11.41sc were collected in SELEX-buffer and water as has already been done for **Figure 29 c**. These spectra were used as a comparison for the spectra of C11.41_4 and C11.41_A15G. The characteristic positive and negative bands for a parallel GQ again is present in the

case of C11.41 (red and black curve) and the destabilization of the structure in water can again be seen, whereas the scrambled version shows a completely different spectrum (**Figure 33 a**). The spectra of the alternated sequence C11.41_4 and C11.41_A15G in SELEX buffer greatly resemble that of C11.41 in (**Figure 33 b**).

Till now, CD-spectra of C11.41, C11.41sc as well as C11.41_4 and C11.41_A15G were always measured in a non-clicked condition. However, since the modification is located in the centre of the GQ, it potentially could alter the secondary structure of the investigated oligonucleotides. Therefore, it was examined if the click-modification disturbs the 3D-structure of C11.41_4 and C11.41_A15G in some way. Both sequences were clicked with benzyl-azide before CD-spectroscopy was started. In **Figure 33 b** the spectra of benzyl-clicked and non-clicked sequences was recorded. In both sequences, the benzyl-modifications led to a decrease of peak intensities (compare dark red vs. light red for C11.41_A15G and dark blue vs. light blue for C11.41_4). Probably the benzyl-modification does slightly destabilize the structures. Nonetheless, the important three-dimensional GQ-structure stays intact even if a chemical moiety is introduced into the G-rich region. Of course, it cannot be said with certainty, that all the other introduced azides do not destroy the GQ-structure, as well. However, it remains quite unlikely, that the introduction of any of the other utilized azides would destroy the secondary structure formation of the oligonucleotides.

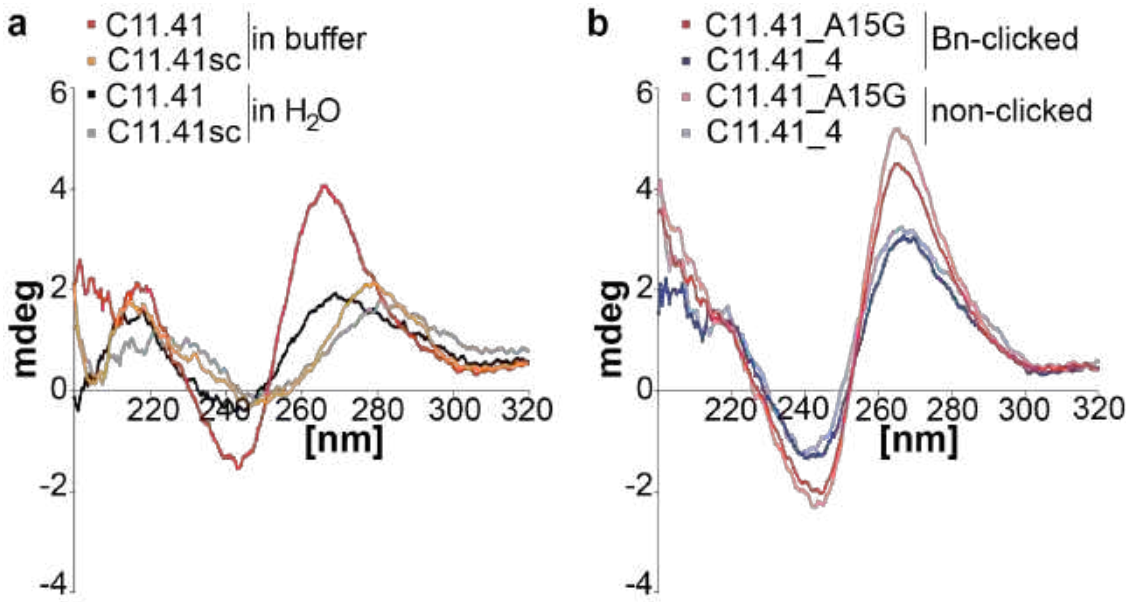

Fig. 33. CD-spectroscopy of C11.41 and the newly investigated sequences C11.41_4 and C11.41_A15G. a) CD-spectra of non-clicked C11.41 and C11.41sc in buffer and in water. The measurement was done with the same oligonucleotides and under the same conditions as already shown in Figure 24. b) CD-spectra of benzyl-clicked C11.41_A15G (light red) and non-clicked C11.41_A15G (dark red) as well as benzyl-clicked C11.41_4 (light blue) and non-clicked C11.41_4 (dark blue) in SELEX buffer.

3.3.5 Specificity determination of C11.41 C11.41_A15G

Till now it has been shown, that C11.41 and even the altered version C11.41_A15G, containing only one click-modifiable position within its sequence, do bind to THC-modified beads. However, if the clickmers are also capable to bind THC/THCA in solution has not been clarified jet. Though there are several methods that can be used to detect binding of aptamers to their target molecules, the choice of the assay has to fulfil specific criteria for each individual case. Different circumstances already excluded multiple assays for the desired situation. Radioactive binding investigations are only restricted to Cherenkov radiation analysis in this case, wherewith affinities cannot be determined. Filter retention assays, as often performed for affinity investigation between proteins and nucleic acids, are not possible in the case of small molecules. Surface plasmon resonance spectroscopy potentially could be used. However, this approach would afford comparatively high amounts of the molecules THCA, or THC and therefore was avoided. Nonetheless, a few different approaches have been done to get clarity if the clickmer is capable to bind to the target molecule in solution:

One approach to perform binding investigations of C11.41 to THCA in solution has been microscale thermophoresis (MST). The method relies on the movement of small molecules through a temperature gradient, called thermophoresis. Usually the temperature gradient (2-6 °C) is induced by an infra-red laser in a minuscule region (~50 µm) of the sample. Parameters influencing thermophoresis are charge, size and the hydration shell surrounding the molecule. When the molecule is bound by a binding partner, at least one of these factors, in most cases the hydration shell, is altered leading to an altered thermophoresis of the molecule. Thermophoresis can be monitored by recording the fluorescence signal of fluorescent labels on one of the binding partners, since upon induction of the temperature gradient a depletion or accumulation of fluorescent molecules in the field of elevated temperature takes place. This can be physically expressed by the soret coefficient (S_T), dependent on the amount of substance and temperature change: $C_{hot}/C_{cold}=\exp(-S_T\Delta T)$.

The method is known to be suitable for measurements of binding events between oligonucleotides to small molecule targets[322,323]. For the assay, several capillaries with constant concentrations of Cy5- labeled C11.41 or C11.41sc were incubated with increasing conentrations of THCA and thermophoresis for each sample was recorded. Since THCA is highly hydrophobic and hardly soluble in buffered aqueous solutions, it was previously dissolvedin DMSO. The amount of DMSO that has been used in the final aqueous solution has been 10% for all tested samples. Benzyl-clicked sequence C11.41 and C11.41sc were pre-incubated with increasing amounts of THCA in SELEX buffer at 37°C. Subsequently the samples were transferred into the MST-capillaries and the measurement was started. The change of fluorescence intensities in cold vs hot equilibrium ($\Delta F=F(T_{hot})/F(T_{cold})$ for all samples was plotted against the increased concentrations of THCA. In theory, dissociation constants can be calculated, if this assay was appropriate to monitor the interaction of the clickmer to THCA[324,325]. For this precise case, MST would be a nice way to confirm the dissociation constant

between the clickmer and THCA in solution, that has previously been determined via flow cytometry. In addition, it would be an easy method to get information about the specificity of the clickmers, since other compounds that are related to THCA could be measured in the same way.

Unluckily, titration of increasing concentrations of THCA into the solution of benzyl-modified oligonucleotides in SELEX- buffer did not change the MST-signal, compared to the signal of the sequences alone in solution (**Figure 34**), which hints that this method probably is not appropriate to confirm the binding event in solution.

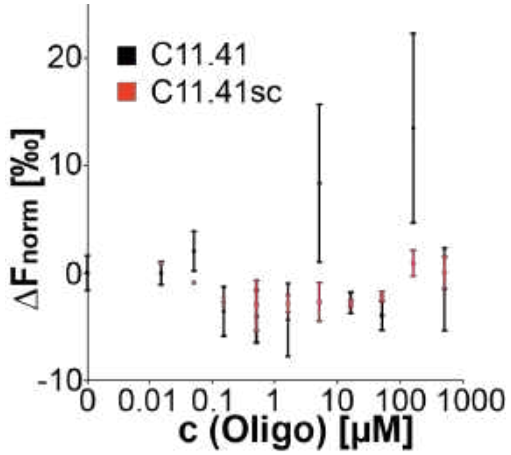

Fig. 34. Microscale thermophoresis of C11.41 and C11.41sc with THCA. Increasing concentrations of THCA were incubated with constant concentrations of C11.41 and C11.41sc. ΔFnorm [‰] was monitored as function of the added THCA-concentration (mean ± SD; n = 2).

As already explained, thermophoresis is dependent on size, charge and conformation of the molecule with corresponding hydration shell[326]. Since charge and size of the oligonucleotide will most probably not be influenced upon binding to THCA, the only parameter responsible on thermophoresis change is the hydration shell. Structure and size of that shell can be reorganized, upon a secondary structure change of the aptamer during the binding event. For C11.41 and C11.41sc however, it is possible, that the secondary structure of the oligonucleotides in this specific case do not change upon binding to THCA.

As a second approach to determine specificity and affinity of the clickmer fluorescence polarization (FP) has been tested. As for MST, this method also has the advantage, that none of the binding partners has to be immobilized on solid support and affinities in free solutions can be measured. If fluorescent molecules in solution are excited with linear polarised light, they will also emit linear polarised light in the same plane as long as they stay stationary and do not move. In reality however, solubilised molecules do tumble via diffusion and rotation in solution throughout the excited state of the fluorophore. Thus, the emitted light is no longer polarised in the same plane as the exciting light. The depolarisation of emitted light can be quantified as fluorescence anisotropy. Anisotropy results from the fact, that the rate of rotational diffusion

generally is higher than the fluorescence lifetime of excited fluorophores (in ns range), synonymous to emission rate. The rotational velocity of molecules in solution is dependent on the viscosity of the solvent as well as the molecular size of the molecule itself[327]. Small molecules do rotate faster than large molecules. Hence, fluorescently labelled ligands alone do rotate faster than they do after a binding event to the corresponding binding-partner. Changes in fluorescence polarisation therefore can be used to study molecular binding-interactions in solution. Fluorescence polarization and –anisotropy can be experimentally measured by recording the emission intensity perpendicular (I_+) and parallel (I_{II}) to the plane of excitation. The difference between I_+ and I_{II} is taken as degree of polarization[327]. Both, fluorescence anisotropy (equation [3]) and polarization (equation [4]) contain the same information and are unit-less, though polarization is often expressed in milliP (mP).

$$FA = \frac{I_{II} - I_+}{I_{II} + 2I_+} \qquad [3]$$

$$FP = \frac{I_{II} - I_+}{I_{II} + I_+} \qquad [4]$$

$$FA = \frac{2FP}{3 - P} \quad ; \quad FP = \frac{3FA}{2 + FA} \qquad [5]$$

Anisotropy and fluorescence polarisation can be interchanged with equations [5]. Though the assay can be used to detect interaction between any binding partners, the molecular weight of the non-labelled partner should be clearly exceeding that of the fluorescently labelled molecule, since the observed effect then is more pronounced[328,329].

For this assay, Δ^9-tetrahydrocannabinol (THC) was fluorescently labelled (**Figure 35 a**), since it has a smaller molecular weight than the oligonucleotides and changes in FP to the heavy ligands can be better detected. The applied label was fluorescein isothiocyanate (FITC). The FITC- labelled THC was kindly provided by Franziska Pfeiffer. In contrast to the previously performed MST-measurement the target molecule therefore was a chemically altered THC instead of THCA. Therefore, the chemical structure of the target also differed slightly from the molecule that was used during the SELEX. FITC was attached to the oxygen of the former phenolic group of THC via a linker (THC-L-FITC). For THC-L-FITC the linker was introduced to spatially separate the THC and the chromophore. This was done to rule out that interaction of the clickmer-sequence with THC is sterically hindered by the bulky FITC-moiety (**Figure 35 c**). For the binding investigation, the full length C11 was used due to higher molecular weight compared to the truncated sequences. Hence a potential change in fluorescence polarisation upon binding to FITC-THC would be better detectable. As a negative control the sequence B10 that resulted from another click-SELEX for THC was taken in this case. Here, 0.5 µM and 1 µM of C11 and B10 were titrated into the solution of constant concentrations of THC-L-FITC in SELEX-buffer.

As a positive control a THC antibody was titrated into the SELEX buffer. A second used control-protein within this assay was BSA.

The results of the FP-assay are shown in **Figure 35 c**. It can be seen, that the presence of the THC antibody leads to a change of fluorescence polarisation. Naturally this was expected since the antibody is known to bind to the THC structure. A quite similar result was observed with the protein BSA. This probably could be explained by non-specific adhesion of the hydrophobic FITC-THC to the similarly hydrophobic surface of that protein. For the investigated oligonucleotides however, there is no difference in fluorescence polarisation. For C11, neither a 0.5 µM nor a 1 µM concentration led to a change in fluorescence polarisation. The same is true for the sequence B10. Of course, the concentrations of the oligonucleotides could have been further increased. Yet, the absence of any signal for the applied concentrations (0.5 µM and 1 µM) disadvised from continuous trials with altered binding-conditions. The missing difference in fluorescence polarisation could indicate, that no binding event between THC-L-FITC and the oligonucleotide takes place and thus no difference in rotational diffusion occurs.

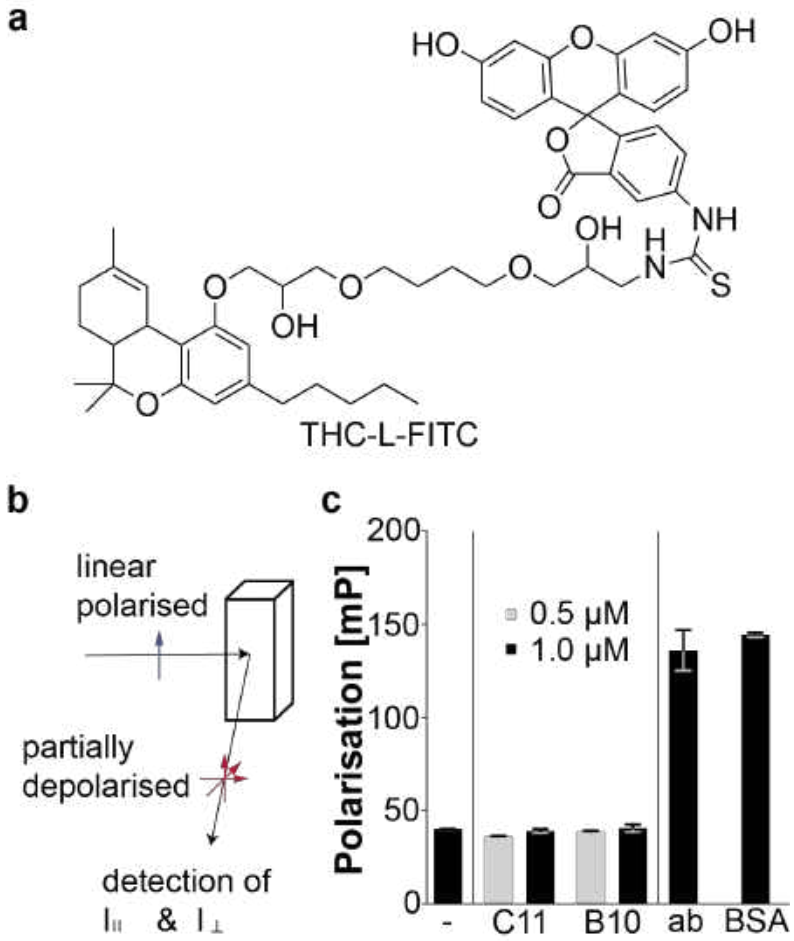

Fig. 35. FP-assay to measure interaction of C11 to FITC-THC. a) The chemical structure of THC-L-FITC, synthesized by Franziska Pfeiffer is shown. b) Scheme of fluorescence polarisation measurement. The sample is excited with linear polarised light. The ration between polarised and partially depolarised emitted fluorescence can be calculated. c) C11 and a non-binding control (B10) were incubated in 0.5 µM (grey bar) and 1 µM (black bar) concentrations with THC-L-FITC. As control, the same has been done with an antibody for THC and BSA (mean± SD; n=2).

Since thus far none of the tested assays was successful to confirm binding of C11 (C11.41 respectively) to the target molecule THC/THCA in free solution, a rather indirect approach to proof this binding event was used. Again, flow cytometry was applied in a competition assay. Constant concentrations (200 nM) of benzyl-modified C11.41 (or C11.41_A15G) were pre-incubated with increasing amounts of THCA for 30 min at 37 °C. Subsequently these solutions were incubated with THC-modified beads for 30 min. After three washing steps of the beads in SELEX-buffer, the flow cytometry measurement was started. The fluorescence-intensities on the THC-modified beads were monitored and the result represented in the graph of **Figure 36 a.** Decreasing fluorescence on the beads implied binding of the tested clickmer to the THCA in solution. Thus, the clickmer could not bind to the target immobilized to the beads anymore. As can be seen, both benzyl-clicked sequences C11.41 and C11.41_A15G showed affinity to solubilized THCA. Calculated IC_{50}-values of 16.8 µM with a 95% confidence interval between 11.774 to 24.192 µM (C11.41), and 54.261 µM with a 95% confidence interval between 37.000 to 79.574 µM resulted.

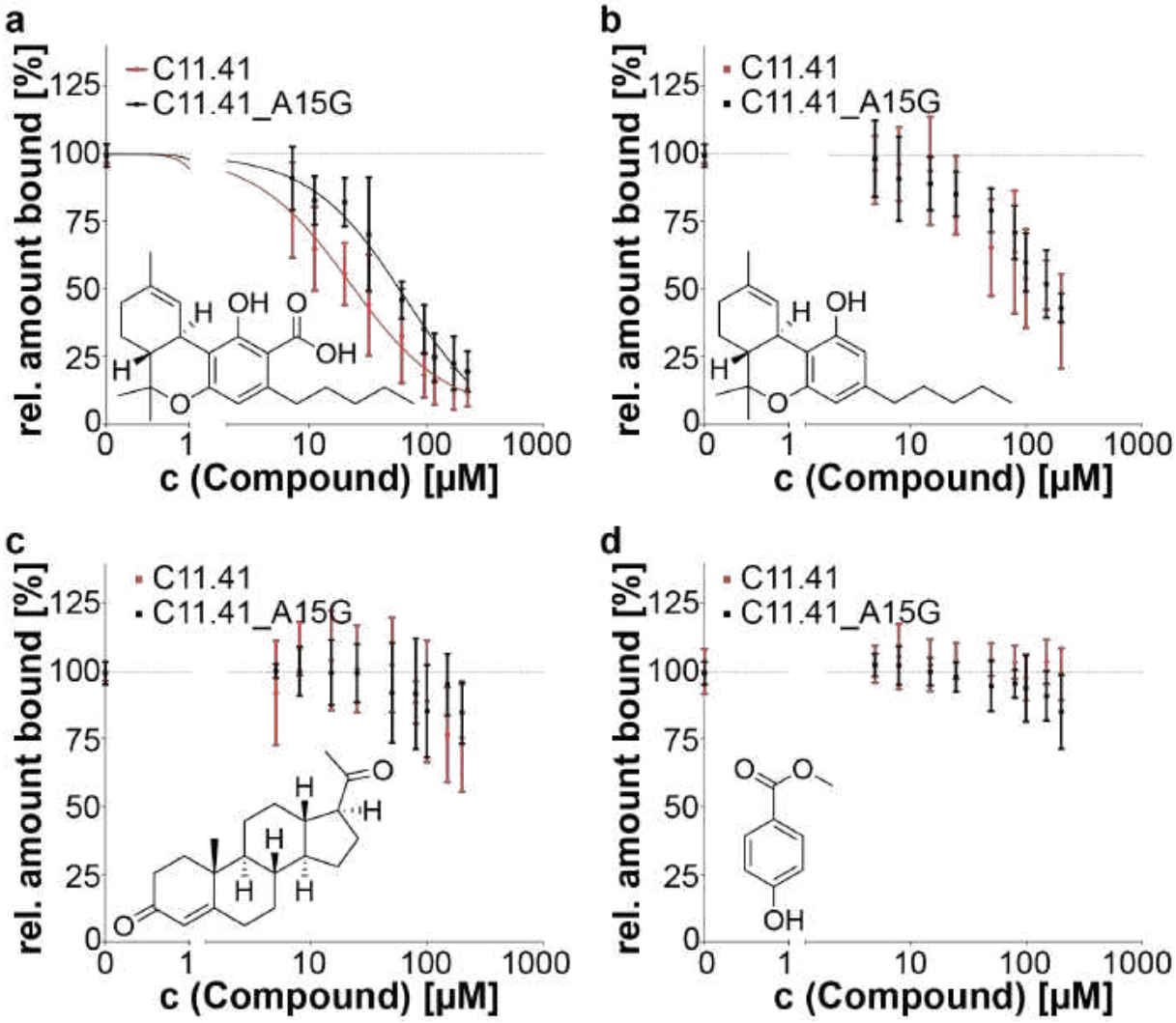

Fig. 36. Competition assay with the compounds THCA, THC, progesterone and 4-hydroxy benzoic acid methyl ester (HBM). Increasing concentrations of THCA (a), THC (b), progesterone (c), and HBM (d) were titrated to 200 nM of C11.41 (red curves) or C11.41_A15G (black curves) and binding to THC-modified beads was measured via flow cytometry. Calculated IC_{50}-values for THCA were 16.8 µM (C11.41) and 54.2 µM (C11.41_A15G) respectively (mean + SD; n=6).

Due to solubility reasons of THCA, it again was pre-diluted in DMSO. These dilutions were then titrated into the solution of the clickmer in SELEX buffer. For all the tested THCA-concentrations, the final portion of DMSO in solution was 10%. Obviously, the presence of that amount of DMSO did not affect binding of the clickmers to the THC-modified beads.

This assay has not only been performed with THCA, but also with the highly-related THC and the compounds progesterone and 4-hydroxy benzoic acid methyl-ester (HBM) (**Figure 36 b-d**). Progesterone was chosen because it has a polycyclic framework similar to that of THC. Furthermore, it also is a highly hydrophobic molecule and its estimated solubility in aqueous solution is in the same range as that of THC and THCA. The second chosen compound tested in the competition assay was 4-hydroxy benzoic acid methyl ester. This compound mimics the aromatic core region of THC and contains a phenolic oxygen.

For all tested compounds the assay was performed in the same way. Binding of the tested clickmers to THC could be demonstrated, though to a reduced extend than to THCA. Again, benzyl-clicked C11.41_A15G with only one modifiable EdU position left showed a very similar behaviour compared to the original C11.41. Progesterone and HBM however, were not bound by either of the tested sequences, at least within the tested concentration range. It might be that progesterone could be bound at even higher concentrations, as the course of the curve in **Figure 36 c** indicates. However, potential affinity to that compound would be significantly lower than to THCA or THC.

3.3.6 Binding studies of C11 to THC(A) via Cherenkov radiation and lateral flow test

Hitherto performed assays were performed to confirm the binding of C11.41 to THCA rather than to THC. To confirm recognition of THC by the clickmer, further investigations have been done. Therefore, a Cherenkov assay with THC immobilized to a sepharose matrix has been done. THC-modified sepharose was prepared by Franziska Pfeiffer. Therein the actual compound THC was used for immobilisation purposes. THC is covalently coupled via the phenolic oxygen to the sepharose matrix. Hence, the molecule again structurally differs from the SELEX-target. In parallel the Cherenkov assay has been performed with sepharose that does not contain THC. For the assay itself, a mimic of a SELEX-cycle consisting of incubation and several washing steps has been done. Applied oligonucleotides were the radioactively labelled full-length C11 and the non-binding control sequence B10.The total amount of radioactivity found in the incubation-, washing- and sepharose containing fractions was set to 100% and the amount of radioactively labelled DNA remaining on the sepharose then can be expressed as values in per cent. The assay relies on the Cherenkov radiation, which appears if a charged particle as an electron moves through a dielectric medium with a speed that exceeds the phase velocity of light in that medium[330,331]. Molecules of the medium are polarized by the passing electron and upon relaxation of

the molecules a bluish glow is emitted that can be detected with specialized instruments like the liquid scintillation counter[331]. Since ^{32}P which is used to label the oligonucleotides is a β^-emitter, the released electron can induce Cherenkov radiation, which is proportional to the amount of ^{32}P per sample[332].

Detected Cherenkov-radiation is directly proportional to the amount of radioactivity, hence to the amount of DNA within a sample[330,332]. As it can be seen in **Figure 37 a**, radioactively labelled C11 binds to THC-sepharose (~16%) to a higher extend than to empty sepharose matrix (~3%). Though the non-binding control B10 also binds to a higher extend to THC-sepharose (~6%) than to empty sepharose matrix (~3%) the observed effect is much less pronounced. indicating that the affinity of benzyl-modified C11 to the THC-sepharose indeed is higher than that of B10.

Although a distinct affinity for THC could not be determined for benzyl-clicked C11.41 or C11.41_A15G, a test-approach was started to investigate, if the clickmer recognizes THC in a simple lateral-flow device. This was done with the radioactively labelled full-length version C11, as well as with the Cy5-labelled C11.41. As non-binding control-sequences the radioactively labelled B10 as well as the Cy5-labelled C11.41sc were used. **Figure 37 b** shows a schematic build-up of this device. It consists of a sample pad, whereon an aqueous sample containing a clickmer or an antibody can be trickled. Due to capillary forces the liquid then will move up the nitrocellulose membrane. In the middle of the membrane two BSA-small-molecule conjugates are dotted. The test-line consists of a THC-BSA conjugate, control line is an ampicillin (AMP)-BSA conjugate dotted on the membrane. As the liquid passes these lines, the included THC-antibody or clickmer ideally binds to the test-line, whereas the control line is not bound. Binding can be detected, if the ligands are labelled in some way. Finally, the liquid will reach the absorption pad.

To demonstrate the operational reliability of the explained device, it was initially run with a primary THC-antibody. As soon as the membrane was dried again, a labelled secondary antibody in PBS-buffer followed. After several washing steps of the membrane with PBS buffer, fluorescence-intensity and location of the labelled secondary antibody was investigated on an imaging system. Two different stripes were tested, equipped with either 0.05 µg THC-BSA (1) or 0.2 µg THC-BSA (2) on the test line (**Figure 37 c)**. Independent of the BSA-THC-amount on the stripes, the antibodies recognised the THC test line (overexposed white line). For stripe (2) a tiny amount of secondary antibody obviously stuck non-specifically to the control-line, and accumulation of this antibody can also be seen on the sample- and absorption pad. However, the THC test-line was clearly favoured for binding and non-specific binding to the control line probably could have been further lowered by additional washing steps.

In **Figure 37 d**, radioactively labelled and benzyl-modified C11 and B10 in SELEX-buffer were added onto the test-stipes. After several washing steps of the membrane with SELEX-buffer, the remaining radioactivity was quantified. However, neither for

C11 nor for B10 an accumulation of radioactively labelled oligonucleotides could be seen on the THC-BSA or the AMP-BSA test-line (higher amounts of radioactively labelled DNA are represented by darker colour).

Finally, the Cy5-labelled, truncated and benzyl-modified oligonucleotides C11.41 and C11.41sc were also applied to the mentioned test-devices (see **Figure 37 d**). In this case, the Cy5-fluorescence on the stripes was recorded with the phosphoimager. The oligonucleotides were applied in two different concentrations, 0.2 µM and 0.5 µM. Again, no binding of both oligonucleotides to the THC-BSA nor AMP-BSA could be recorded (**Figure 37 e**). These results indicated, that binding between THC-BSA and the used oligonucleotides cannot be demonstrated with the help of these test devices. Probably the presence of BSA on the nitrocellulose membrane or the way, THC is conjugated to BSA could negatively affect a potential binding event.

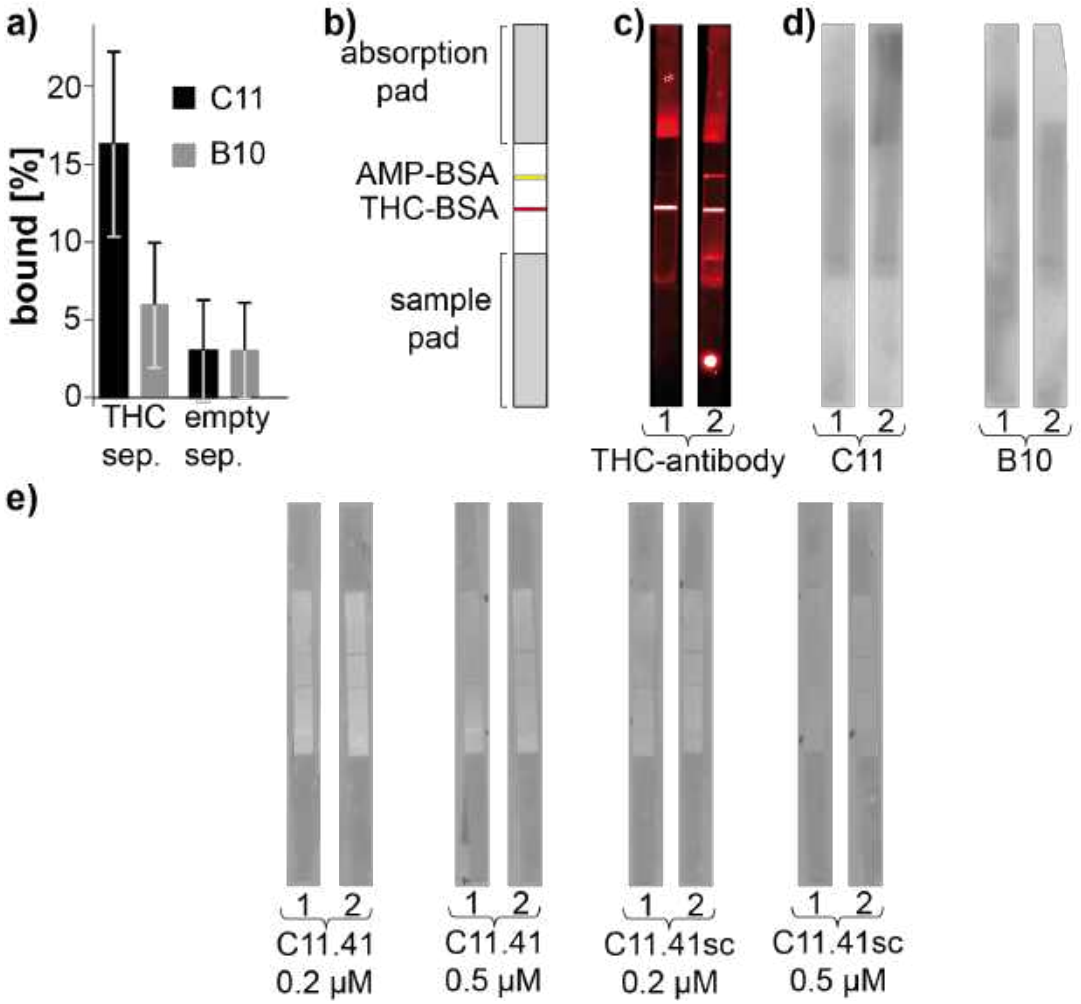

Fig. 37. Cherenkov assay and lateral flow test. a) Cherenkov assay of radioactively labelled C11 (black bars) and B10 (grey bars) to THC-sepharose and empty sepharose. (mean + SD; n = 3). b) schematic principle for lateral flow test. c) Primary THC-antibody and successively a labelled secondary antibody are run on lateral flow devices with 0.05 µg THC-BSA construct (1) and 0.2 µg THC-BSA construct (2) on the test-line. d) lateral flow devices (1) and (2) are run with radioactively labelled C11 andB10. e) lateral flow devices (1) and (2) are run with Cy5-labeled 0.2 µM and 0.5 µM C11.41 and C11.41sc.

3.4 Development of a photoactivatable DFHBI derivative (PA-DFHBI)

In this chapter the synthesis of a photoactivatable DFHBI derivative is described. In combination with already existing aptamers binding to DFHBI, a photo controllable light up aptamer (FLAP) would be developed. Fluorescently labelled aptamers are known to have superior properties over antibodies in the field of super resolution microscopy[285,286]. These labelled aptamers have found applications in techniques as STED. With the development of photoactivatable FLAPs, these systems could find applications in further techniques of super resolution microscopy as RESOLFT or PALM. Since HBI derived photoactivatable proteins already have proven to be useful for these purposes, a DFHBI based system seemed to be promising for the development of a photoactivatable FLAP with comparable photoactivation properties.

The synthesis of a photoactivatable DFHBI-variant, knowledge of the mechanism responsible for the strong fluorescence increase of DFHBI in complex with its aptamer was important. Since interactions of the phenolate oxygen with counterions and nucleotides of Spinach are responsible for the efficient fluorescence increase[253], it was planned to synthesize a caged DFHBI variant. An *ortho*-nitrobenzyl group should be introduced with the aim to quench the fluorescence of the Spinach-DFHBI complex. Thus, an DFHBI derivative would result, analogue to the *o*-nitrobenzyl caged HBI found in the photoactivatable GFP (GFP66ONBY) would be gained[296]. For the synthesis of a caged DFHBI derivative, DFHBI was stirred with an excess of 2-nitrobenzyl chloride in DMF overnight (**Figure 38**). The resulting compound was chromatographically purified. The caged compound was called photoactivatable DFHBI (PA-DFHBI). HPLC-MS chromatograms as well as ^{1}H-NMR are shown in **Appendix Figure A18** and confirm the successful synthesis of PA-DFHBI.

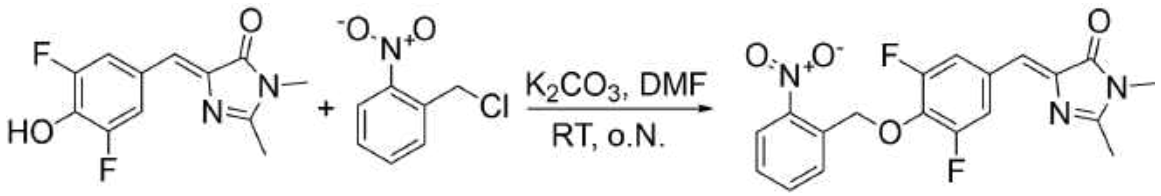

Fig. 38. Synthesis of PA-DFHBI. DFHBI was stirred with an equimolar amount of 2-Nitrobenzylchloride in presence of K_2CO_3 in DMF overnight.

3.4.1 *In vitro* characterization of PA-DFHBI

To analyse whether the photolabile protective group (PPG) of AP-DFHBI indeed quenches the fluorescence, Spinach2 was incubated with AP-DFHBI. As illustrated in **Figure 39**, the PPG leads to suppression of the fluorescence at 505 nm (orange curve), which could be observed for the complex of Spinach2 with DFHBI (dark green curve). Upon removal of the PPG on AP-DFHBI however, functional DFHBI is rebuilt and green fluorescence could again be seen (light green curve).

The PPG could be photolytically cleaved via irradiation of the compound with 385 nm for 1 min. A mutated version of Spinach (Mut) which does not induce fluorescence of DFHBI was used as a negative control. Mut RNA did not induce green fluorescence of DFHBI (blue, and yellow curve).

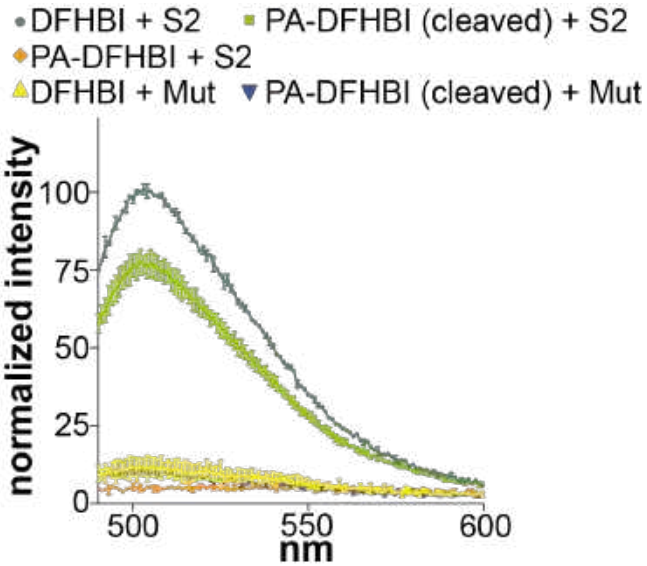

Fig. 39. Fluorescence of Spinach2 and a mutant RNA in combination with DFHBI and PA-DFHBI. 300 nM Spinach2 RNA or Mut-RNA were incubated with 10 µM PA-DFHBI or DFHBI. PA-DFHBI with Spinach2 did not show fluorescence at 505 nm (orange curve). Only after cleavage of the photocleavable group on PA-DFHBI (light green curve), the typical fluorescence of DFHBI with Spinach2 (dark green curve) was observed. Mut-RNA did not induce fluorescence with any of the tested compounds (n=2).

Following the above-mentioned results, the photometric properties of PA-DFHBI were further investigated. Paige *et. al*. had shown that the absorbance spectrum of DFHBI changes in dependence on the pH-value[252]. Again, the situation is comparable to that found for GFP. In GFP, HBI is predominantly present in the protonated phenol form, whereas in eGFP the deprotonated phenolate form predominates[333]. The phenol form of HBI shows an absorption maximum of around 390 nm, whereas the phenolate form shows a maximum of 475 nm. The phenolate form has a significantly higher extinction coefficient than the phenol form and thus eGFP exhibits higher green fluorescence than GFP[255,333]. Dependent on the pH-value, DFHBI is also either present in the phenol form (pH 5) or the phenolate form (pH 8). Thus, the absorption maximum shifts from 350 nm (pH 5) to 405 nm (pH 8) (see **Figure 40 a**)[252]. Moreover it was observed that the phenolate form of DFHBI was crucial for Spinach-induced fluorescence, since at low pH-values the total fluorescence intensity was dramatically reduced (not shown in Figure)[252].

Figure 40 b shows an absorption spectrum of the caged PA-DFHBI at pH 7.4. An absorption maximum at around 355 nm could be seen, which resembles more the spectrum known from DFHBI at pH 5. However, the typical absorption maximum of the common DFHBI at 405 nm could not be detected for AP-DFHBI. Next, it was checked

if PA-DFHBI indeed remains non-fluorescent in presence of the Spinach2 aptamer. In **Figure 40 c** the excitation spectra of DFHBI and PA-DFHBI in absence and presence of Spinach2 RNA is shown.

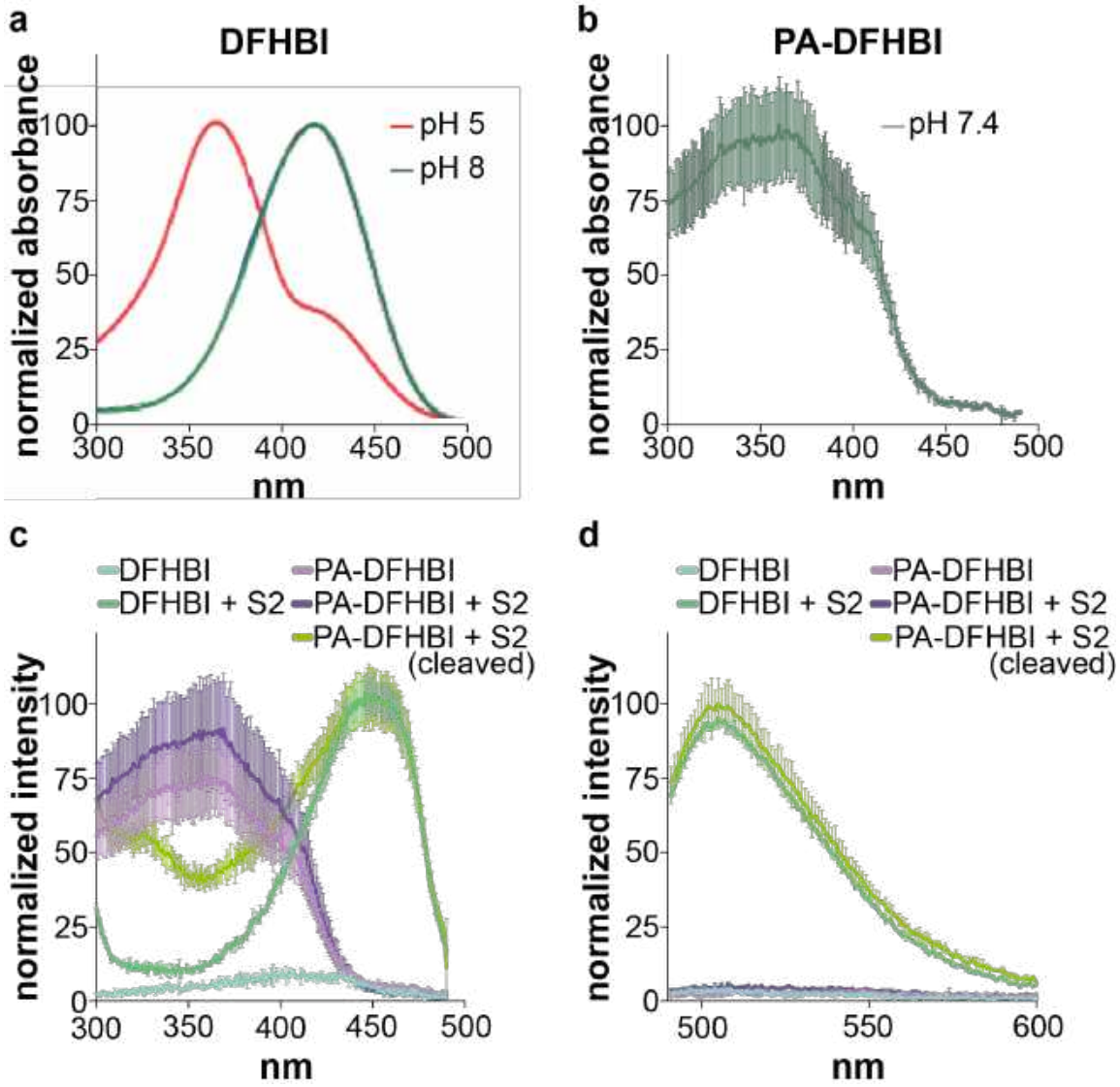

Fig. 40. Photometric properties of PA-DFHBI in comparison to DFHBI. a) Absorbance spectrum of DFHBI at pH 5 and pH 8, modified after Paige *et. al.*[252] b) Absorbance scan of 10 µM PA-DFHBI at pH 7.4. c) Excitation scan of the different DFHBI variants in combination with Spinach2 RNA in HEPES buffer pH 7.4. Spectra of 10 µM DFHBI in presence and absence of 300 nM Spinach22 RNA was compared to that of 10 µM PA-DFHBI in presence and absence of 10 nM Spinach-2 RNA. Furthermore, the excitation spectrum of PA-DFHBI that in presence of 300 nM Spinach-2 RNA is shown that has previously been irradiated at 385 nm. d) Emission scan of the same samples that were already used for Figure 36 c. All samples were excited at 460 nm while the emission at 505 nm was monitored. For Figure 37 c, d intensities were normalized to the maximal intensity for DFHBI with Spinach2. (n=2)

For DFHBI a significant excitation maximum at 460 nm was only detectable in presence of Spinach2, while in absence of the aptamer no distinct excitation maximum could be seen. In contrast to that, for PA-DFHBI neither in presence nor absence of the Spinach2-aptamer excitation could be monitored at 460 nm. Yet, an excitation maximum at 355 nm in absence as well as in presence of Spinach2 was observed.

However, if the PPG of PA-DFHBI is photolytically removed (irradiation at 385 nm for 1 min), an excitation maximum at 460 nm could also be observed, indicating that the original DFHBI was rebuilt. Corresponding emission spectra for DFHBI and PA-DFHBI in presence and absence of Spinach2 were also recorded (**Figure 40 d**). Samples were excited at 460 nm for that purpose. For DFHBI the expectable strong increase of fluorescence intensity at 505 nm could be seen in the presence of Spinach2. However, neither in absence nor in presence of Spinach2 the fluorescence-intensity of PA-DFHBI did exceed the fluorescence intensity of pure DFHBI-solution. Only if the complex of PA-DFHBI and Spinach2 was irradiated for 1 min at 385 nm, fluorescence at 505 nm could be detected (**Figure 40 d**). Taken together, the *ortho*-nitrobenzyl-group successfully supresses green fluorescence of PA-DFHBI Spinach2 complex, when excited at 460 nm. Only after irradiation of PA-DFHBI at 385 nm the PPG is removed. DFHBI is rebuilt and in complex with Spinach2 the typical green fluorescence can be observed again.

The result shown in **Figure 40 c, d** proved that upon cleavage of the photocleavable ortho-Nitrobenzyl group, DFHBI is built again. However, it was not proven yet if the caged compound PA-DFHBI is also bound by Spinach2. It might be possible that PA-DFHBI is not recognized by Spinach2 at all and only after conversion to DFHBI the aptamer binds the target molecule. On the other hand, it is also possible that PA-DFHBI is bound by Spinach2 but due to the PPG the fluorescence is not induced. To investigate if PA-DFHBI is bound by Spinach2 a competition assay was done. In Constant concentrations of DFHBI and Spinach2 were incubated with increasing concentrations of PA-DFHBI. The ssamples were excited at 460 nm and the fluorescence intensities at 505 nm were recorded. A decrease in fluorescence intensity at 505 nm could be observed with increasing PA-DFHBI-concentrations, which indicates binding of Spinach2 to PA-DFHBI (**Figure 41 a**). Cognate data were used to take a closer look on the concentration dependent binding of Spinach2 to PA-DFHBI. The resulting curve displayed in **Figure 41 b** allowed for a calculation of an IC_{50}-value of 8.5 µM. In **Figure 41 c** increasing concentrations of PA-DFHBI were incubated with Spinach2. The mixture was then irradiated at 385 nm for 1 min to remove the PPG and to form DFHBI. Subsequently, the solutions were excited at 460 nm and fluorescence intensities were again measured at 505 nm. In **Figure 41 d** the resulting fluorescence intensities were plotted against the concentrations of PA-DFHBI that were initially titrated into the solutions. Upon irradiation at 385 nm the original DFHBI was formed again and a sigmoidal binding-curve resulted. The calculated k_D-value of 453.8 ± 57.27 nM is almost identical of the reported k_D-value of 430 ± 15 nM for Spinach2 to DFHBI[258]. Due to that result it can be assumed, that an irradiation time of 1 min at 385 nm is sufficient to quantitatively remove all of the photocleavable groups from PA-DFHBI. Taken together, PA-DFHBI is bound by Spinach2. This complex remains non-fluorescent until the PPG is removed via irradiation with 385 nm, whereupon DFHBI is rebuilt and green fluorescence is seen.

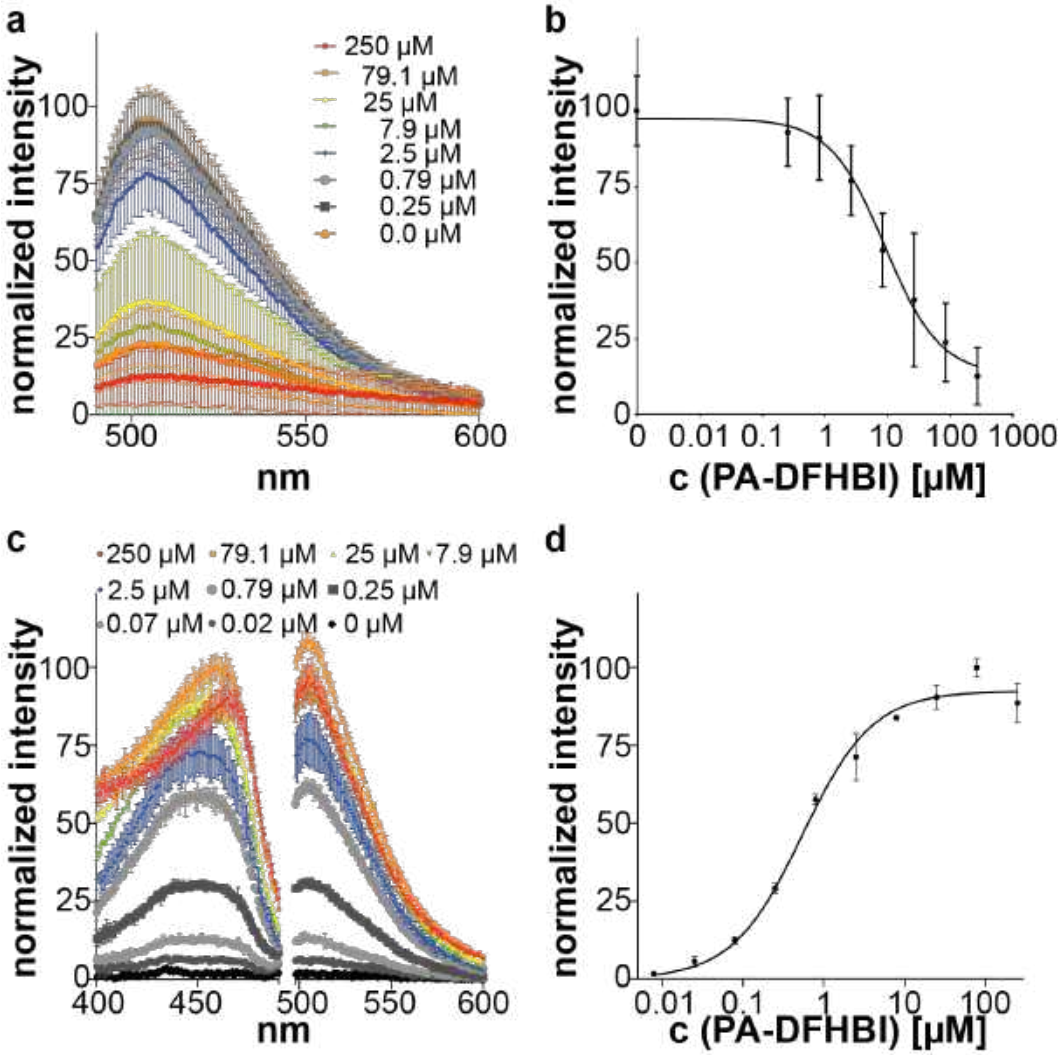

Fig. 41. Fluorescent binding investigations of Spinach2 to PA-DFHBI. a) 300 nM Spinach2 RNA were incubated with 10 µM DFHBI and increasing concentrations (specified in figure) of PA-DFHBI. b) The decrease of DFHBI fluorescence at 405 nm was plotted against the increasing concentrations of PA-DFHBI. The calculated IC_{50}-value was 8.5 ± 1.4 µM. c) 300 nM Spinach2 RNA were incubated with increasing concentrations of PA-DFHBI (specified in figure). The samples were irradiated at 385 nm to remove the PPG. Subsequently an excitation-emission scan was done. d) Fluorescence at 505 nm was measured for each sample after excitation at 460 nm. The calculated k_D-value was 453.8 ± 57.27 nM (n=2).

3.4.2 PA-DFHBI in bacterial cells

Since PA-DFHBI did quench Spinach2 induced fluorescence in vitro it now was investigated if this compound also is functional in living cells. E. *coli* cells were used to confirm that PA-DFHBI also works in bacteria. Broccoli- and Spinach2 plasmids for expression in bacterial cells were ordered. Spinach2 and Broccoli had been inserted into pET28c based plasmid[258,334]. To prove whether the used Broccoli and Spinach2 plasmids are functional, an *in* vitro transcription was done. Plasmids were used as template for PCR and subsequent transcription. Fluorescence spectra of the resulting RNA in presence of DFHBI were recorded (**Figure 42**).

The observed spectra confirmed the functionality of the plasmids as the fluorescence intensity of DFHBI is significantly increased in presence of *in* vitro transcribed Spinach2 (dark green curve) and Broccoli RNA (light green curve).

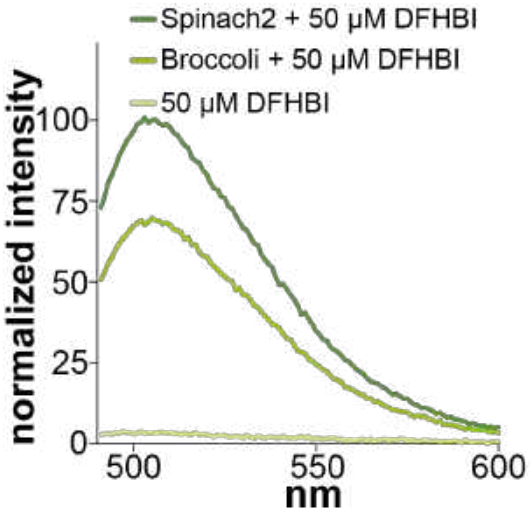

Fig 42. In vitro testing of the functionality of pET28c Spinach2 and pET28c Broccoli plasmids DNA for *in vitro* transcription of Spinach2 and Broccoli was obtained via PCR with pAV-5S based plasmids as template. 100 nM of Spinach2- or Broccoli RNA resulting from *in vitro* transcription were mixed with 50 µM DFHBI and the fluorescence was measured. Fluorescence intensity of DFHBI alone was used as control.

Since in vitro testing of Spinach2 and Broccoli fluorescence was successful, the ordered plasmids were now used for expression of the RNA in bacterial cells. For expression in bacteria the pET28c-Broccoli plasmid as well as the pET28c-Spinach2 plasmids were used. The expressed aptamers are embedded in a tRNA scaffold, which is known to facilitate correct folding of Spiach2 and Broccoli *in vivo.* This in turn leads to improved fluorescence of DFHBI[258,261]. Visualization of both DFHBI recognizing aptamers was done in BL21 (DE3) cells. Transcription of the desired RNA in bacteria was enhanced by addition of the inductor Isopropyl β-d-1-thiogalactopyranoside (IPTG). For measurement of fluorescence in *E.coli*, bacteria were suspended in M9 minimal media in presence or absence of DFHBI. **Figure 43 a** illustrates fluorescence of Spinach2 and Broccoli expressing bacteria. While DFHBI in M9 media showed only slight autofluorescence (black curve), fluorescence of Spinach2 (light green curve) and Broccoli (dark green curve) was significantly increased. Since the binding of Broccoli to DFHBI in E.*coli* is less dependent on high magnesium concentrations than that of Spinach2, it has been shown that the observed fluorescence brightness was around twice as high for Broccoli expressing bacteria than for Spinach2 expressing bacteria[261]. That tendency was also confirmed with the performed assay (**Figure 43 b**). Fluorescence brightness was more than 1.5-fold higher for the expressed Broccoli-RNA than for Spinach2-RNA.

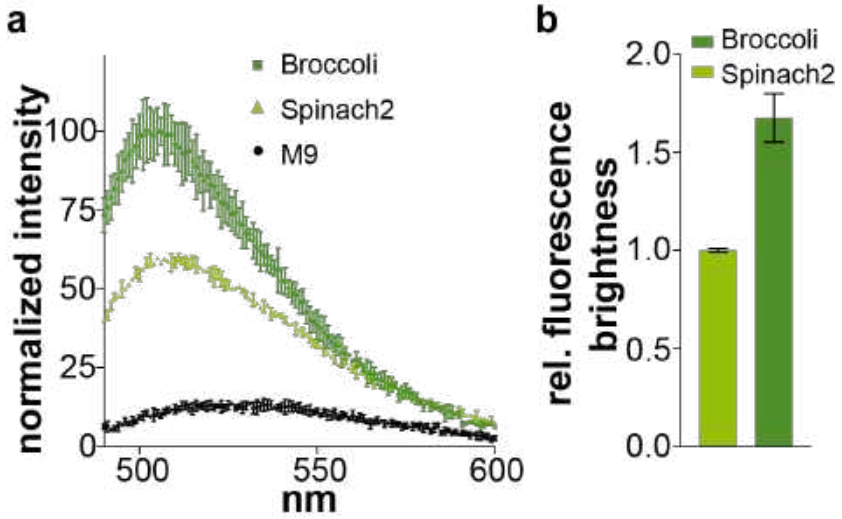

Fig. 43. Comparison of fluorescence intensities of Spinach2 and Broccoli in presence of DFHBI expressed in E. *coli*,. a) Fluorescence spectra of Broccoli and Spinach2 aptamers in presence of 50 µM DFHBI. The negative control (black curve) only contained DFHBI in M9 medium. Bacteria expressing Broccoli-RNA (dark green curve) showed highest fluorescence values. Total intensity for bacteria expressing Spinach2-RNA (slight green curve) was clearly reduced. b) The relative fluorescence brightness of Broccoli and Spinach2 expressing bacteria is shown. For Broccoli-RNA the brightness was around 1.7-fold higher than for Spinach2. Fluorescence values were normalized to those of Broccoli expressing bacteria. (n=2).

Next it was investigated if PA-DFHBI is functional in E. *coli* expressing Broccoli- and Spinach2-RNA. It was tested if bacteria remain non-fluorescent in presence of PA-DFHBI as it was shown for *in vitro* experiments (compare to **Figure 39**), and if the expected fluorescence could be retained upon removal of the PPG. Spinach2 and Broccoli expressing bacteria were incubated with DFHBI or PA-DFHBI in M9 minimal medium. Bacteria suspensions were exited at 460 nm and fluorescence at 505 nm was recorded. Observed fluorescence intensity values were normalized to those for bacteria that were incubated with DFHBI (100%). Autofluorescence of DFHBI in M9 medium was used as a control. As illustrated in **Figure 44 a, c,** Spinach2 and Broccoli expressing E. *coli* showed significantly higher fluorescence intensity values in presence of DFHBI, compared to DFHBI in M9 medium. The same is true, for cells that were incubated with PA-DFHBI and subsequently irradiated at 385 nm to remove the PPG. In contrast to that, cells that were incubated with PA-DFHBI without removal of the photocleavable group did not show that obvious fluorescent signal. The fluorescence intensities for these samples did not markedly exceed these of DFHBI in M9 minimal medium. This result illustrates that Spinach2 and Broccoli aptamers that are expressed in bacteria are responsible for the observed fluorescence. In addition, it could be shown that the observed fluorescence was indeed induced by the RNA aptamers that were expressed in bacteria. Expression of Broccoli and Spinach2 RNA in E. *coli* was induced via addition of IPTG (see **section 6.3.2**). The addition of the inductor IPTG to the cells led to an increased translation of the desired RNA. **Figure 44 b, d** illustrates this effect. Fluorescence intensity values for cells that were treated with IPTG prior to incubation with DFHBI or PA-DFHBI are shown in grey bars. Corresponding values for cells that were not treated with IPTG are shown in black bars. As illustrated, cells treated with IPTG show remarkably higher fluorescence intensities

with DFHBI compared to non-treated cells. The same result could be observed for cells that were incubated with AP-DFHBI whereof the PPG was photolytically cleaved. Taken together, in E. *coli* the fluorescence of PA-DFHBI could be activated via photolytic cleavage of the ether bond.

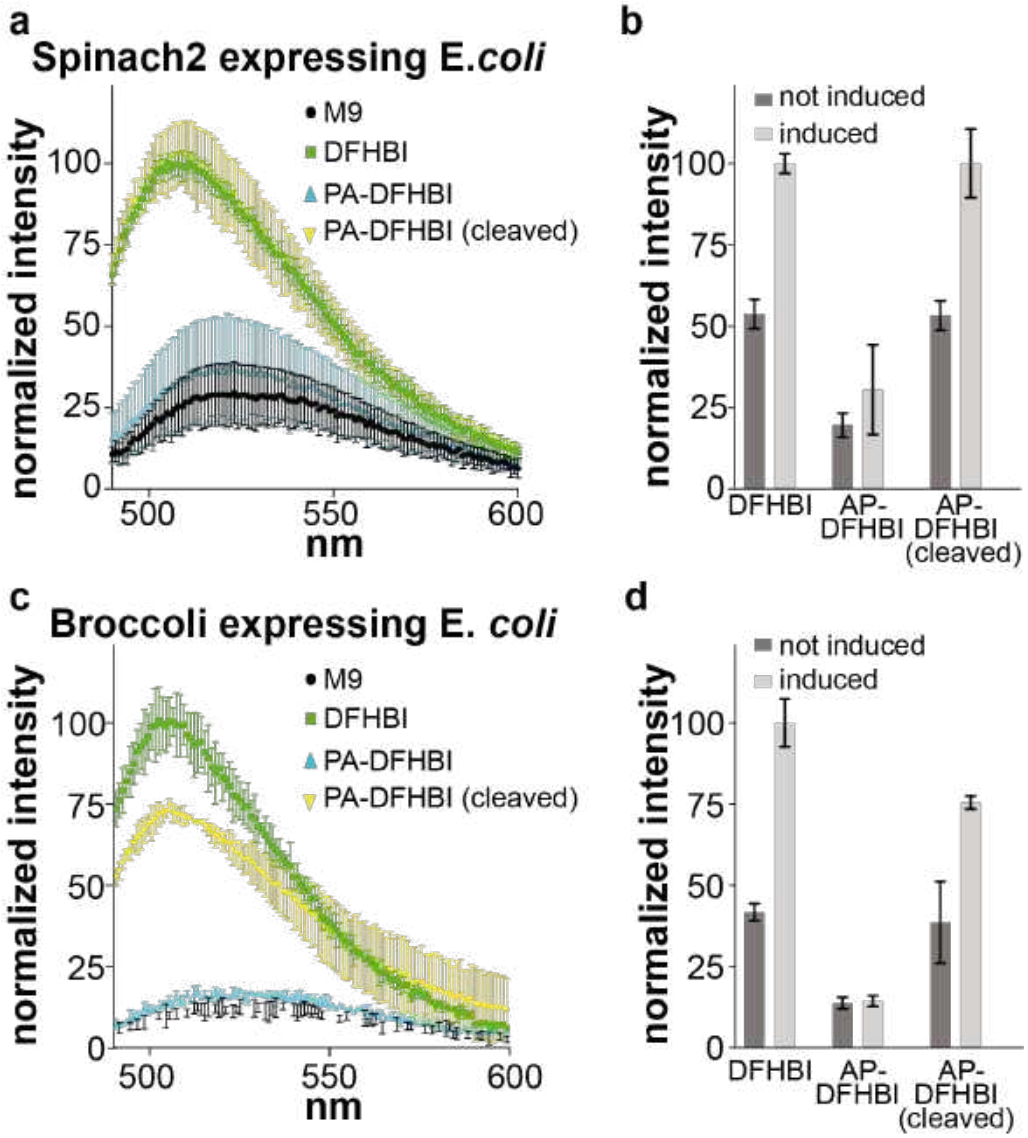

Fig. 44. Visualization of Broccoli and Spinach2 RNA in E. coli in presence of DFHBI and PA-DFHBI. a, c) Fluorescence scan of Spinach2 (a) and Broccoli (c) expressing bacteria. BL21 cells were incubated with 50 µM DFHBI (green curve) or PA-DFHBI blue and yellow curve). Half of the samples containing PA-DFHBI were irradiated at 385 nm to remove the PPG (yellow curve). Upon excitation of the cells at 460 nm fluorescence intensity was measured. b,d) Bacteria were incubated with DFHBI, AP-DFHBI and AP-DFHBI whereof the PPG was photolytically removed. Spinach2 (b) and Broccoli (d) expression was either induced (grey bars) or not induced (black bars) by addition of 1 mM IPTG. Fluorescence intensities were compared. (n=2).

3.4.3 PA-DFHBI in mammalian cells

Since PA-DFHBI was thought to find application in fluorescence microscopy, it had to be shown that this compound also is functional in mammalian cells. For expression in mammalian cells Spinach2 and Broccoli had been inserted into pAV5S based plasmids. Like it was done with the pET82c based plasmids (**section 3.4.2**) it was proved whether ordered Broccoli and Spinach2 plasmids are functional. Again an *in* vitro transcription was done. Plasmids were used as template for PCR and subsequent transcription and fluorescence spectra of the resulting RNA in presence of DFHBI were recorded (**Figure 45**). Again, the observed spectra confirmed the functionality of the plasmids as the fluorescence intensity of DFHBI is significantly increased in presence of *in* vitro transcribed Spinach2 (dark green curve) and Broccoli RNA (light green curve).

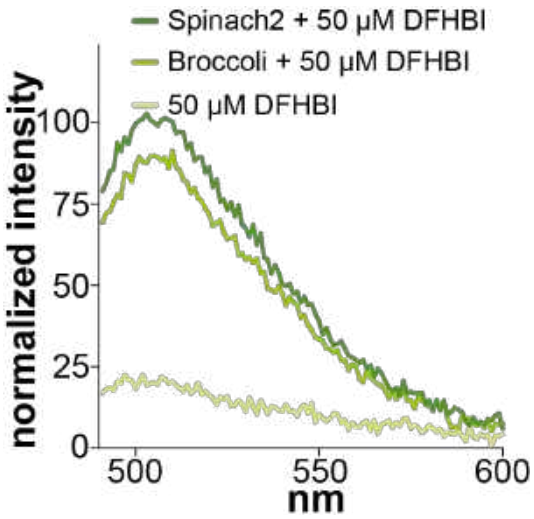

Fig 45. In vitro testing of the functionality of pET28c Spinach2 and pET28c Broccoli plasmids. DNA for *in vitro* transcription of Spinach2 and Broccoli was obtained via PCR with pAV-5S based plasmids as template. 100 nM of Spinach2- or Broccoli RNA resulting from *in vitro* transcription were mixed with 50 µM DFHBI and the fluorescence was measured. Fluorescence intensity of DFHBI alone was used as control.

Jaffrey et. al recommended to use human embryonic kidney (HEK 293) cells for expression of Spinach2 or Broccoli RNA in mammalian cells[335]. First transfections were done with the pAV Spinach2 plasmid. HEK 293 cells were co-transfected with pAV5S Spinach2 plasmid together with an mCherry plasmid. The mCherry plasmid was used as a control to see if transfection was successful. As a negative control, HEK cells that were not transfected with any of these plasmids were used. As can be seen in **Figure 46 a** HEK cells that were not transfected and incubated with DFHBI 2 hours prior to microscopy did neither show a red nor a green fluorescent signal. Given that result, it could be said that DFHBI in HEK cells did not emit its green fluorescence if no DFHBI binding aptamer is expressed in the cells. Furthermore, no non-specific background fluorescence of DFHBI could be observed. In contrast to that, HEK cells that were co-transfected with pAV5S Spinach2 and an mCherry plasmid are shown in **Figure 46 b**. After cells were incubated in presence of DFHBI prior to microscopy both,

red fluorescent as well as green fluorescent cells could be observed. This could be taken as a proof that co-transfection did work and HEK cells expressed mCherry as well a Spinach2-RNA. Cells that were co-transfected as those shown in **Figure 46 b** have also been incubated in presence of PA-DFHBI prior to microscopy. As can be seen in **Figure 46 c** cells did show red and green fluorescence, though the photocleavable group on PA-DFHBI had not been removed so far. In principal it was expected that the green fluorescence would be suppressed by the PPG on PA-DFHBI. The same phenomenon was observed after repeating the experiment.

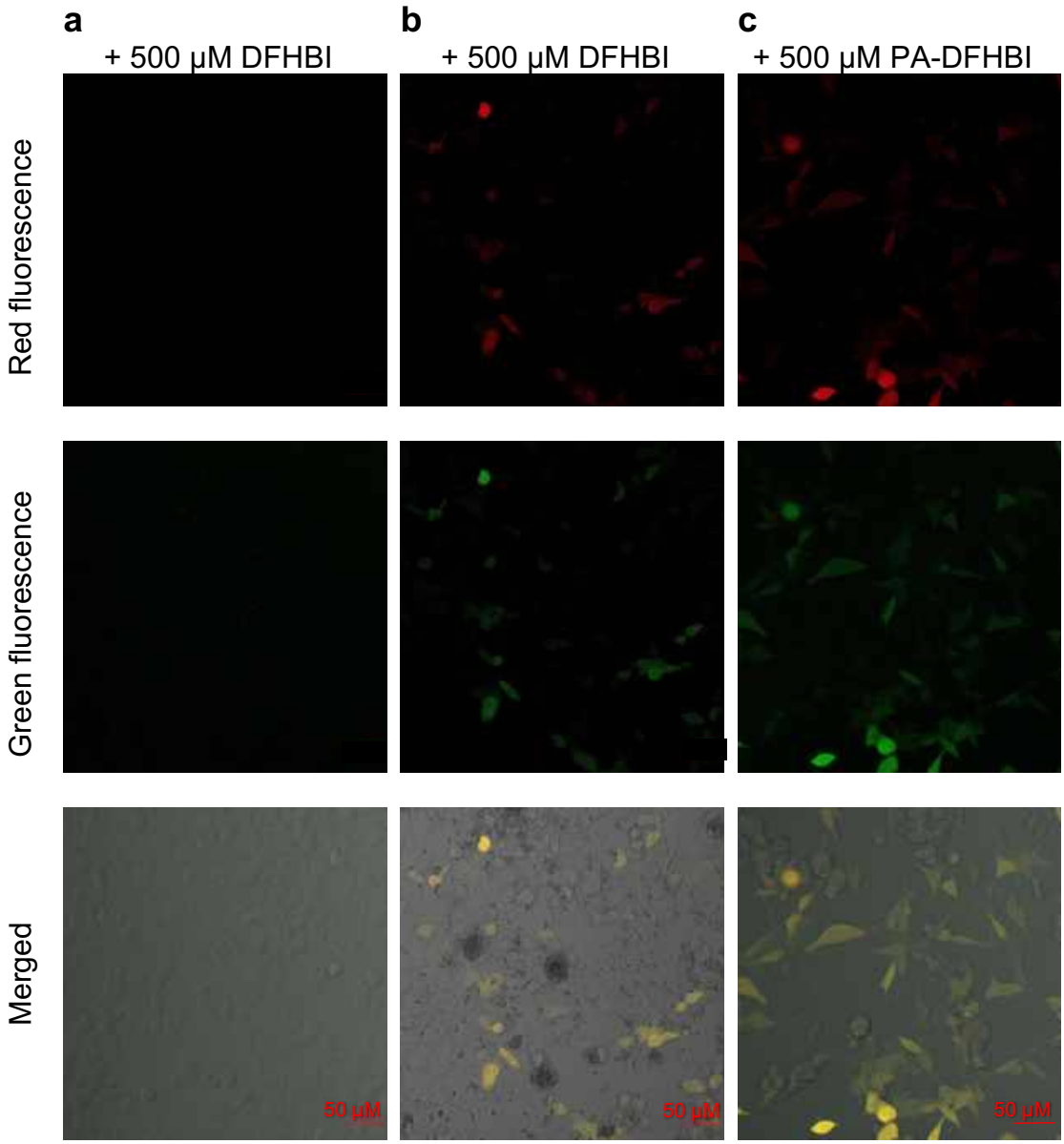

Fig 46. Microscopy images of HEK cells. a) Cells were incubated at 37°C for 48 h. Subsequently 500 µM DFHBI solution was added to the cells and incubated for 1 h. b) HEK cells were co-transfected with mCherry and pAV5S Spinach2 plasmid. Cells were incubated at 37°C for 48 h. Subsequently 500 µM DFHBI solution was added to the cells and incubated for two additional hours. Red fluorescence of mCherry (excitation: 543 nm, emission: 596-696 nm) as well as green fluorescence of Spinach2 (excitation: 488 nm, emission 500-540 nm) was recorded. c) HEK cells were co-transfected with mCherry and pAV5S Spinach2 plasmid. Cells were incubated at 37°C for 48 h. Subsequently 500 µM PA-DFHBI solution was added to the cells and incubated for two additional hours. Red fluorescence of mCherry (excitation: 543 nm, emission: 596-696 nm) as well as green fluorescence of Spinach2 (excitation: 488 nm, emission 500-540 nm) was recorded. (n=2).

The reason for the undesired green fluorescence of HEK cells in presence of DFHBI could not be clarified. One possibility could have been a contamination of the PA-DFHBI solution with normal DFHBI. To rule out that a contaminated PA-DFHBI solution was responsible for that unexpected result, HPLC-MS measurements have been performed. The HPLC chromatogram as well as the detected masses is shown in **Figure 47**. HPLC-MS was done with untreated PA-DFHBI solution, as well as with PA-DFHBI solution that was irradiated at 385 nm for 1 min. As can be seen, HPLC-chromatogram for the solution of PA-DFHBI only shows one UV-signal (retention time 13.2 min) and the detected masses correspond to that of PA-DFHBI (**Figure 47 a**). Since no UV-peak could be found at a retention time of 7.5 min similar to the result in **Figure 47 b**, it could be assumed that the compound was pure and did not contain any contamination of DFHBI. **Figure 47 b** shows the chromatogram of the same solution that had previously been irradiated with 385 nm for 1 min. A UV-signal can be seen at a retention time of 7.5 min. The detected masses correspond to the original DFHBI. Removal of the PPG seemed to be quantitative since the UV-signal corresponding to PA-DFHBI at a retention time of 13.2 min vanished completely.

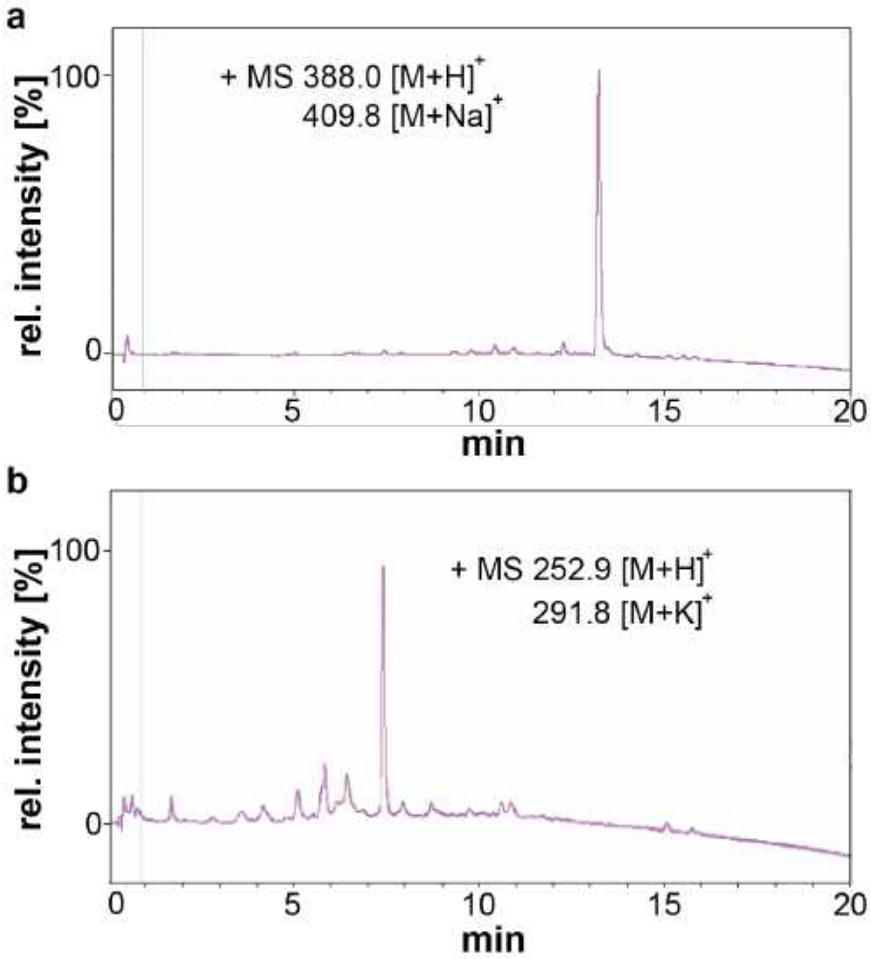

Fig. 47. HPLC-MS results of PA-DFHBI before and after photolytic removal of the PPG. A gradient of 5-100% ACN in 0.1% FA was applied in 30 min. a) HPLC-chromatogram of PA-DFHBI is shown. The detected masses corresponding to the depicted UV-signal match the mass of PA-DFHBI (exact mass: 387.1). b) HPLC-chromatogram of PA-DFHBI that has previously been irradiated with 385 nm to remove the PPG. The detected masses corresponding to the depicted UV-signal match the mass of the built DFHBI (exact mass: 252.07)

3.5 Development of red-shifted DFHBI variants

The colour palette of FLAPs so far encompasses green (Spinach and Spinach-derivatives, Broccoli)[252,257–259,261], yellow (Corn)[262,305], and orang/red (Mango I – Mango III)[302–304] fluorescent systems. Alterations on the chemical structure of the applied dyes could lead to red-shifted emission properties in complex with already existing RNA aptamers. Here it was tried to develop a new DFHBI variant with a red-shifted emission-wavelength compared to the Spinach-DFHBI complex. The Mango aptamers that bind two different derivates of thiazole orange and thereby enhancing fluorescence of different wavelengths, were taken as an example. The chemical structures of TO1 and TO3 are similar. TO3 only contains two additional carbon atoms in the methine bridge of TO1 that connects the benzothiazole ring and the quinoline ring of the chromophore (see **Figure 48 a**). The two thiazole orange derivatives TO1 and TO3 were used as inspiration for the synthesis of a new DFHBI derivative. For DFHBI, also a methine bridge is connecting the imidazolinone ring with 2,6-difluorophenole ring. Thus, it was planned to enlarge the aromatic system of DFHBI by inserting two additional carbon atoms to that methine bridge. The resulting compound (Z)-4-((E)-3-(3,5-difluoro-4-hydroxyphenyl)allylidene)-1,2-dimethyl-1H-imidazol-5(4H)-on was shortly named “enlarged DFHBI” (eDFHBI) (see **Figure 48 b**).

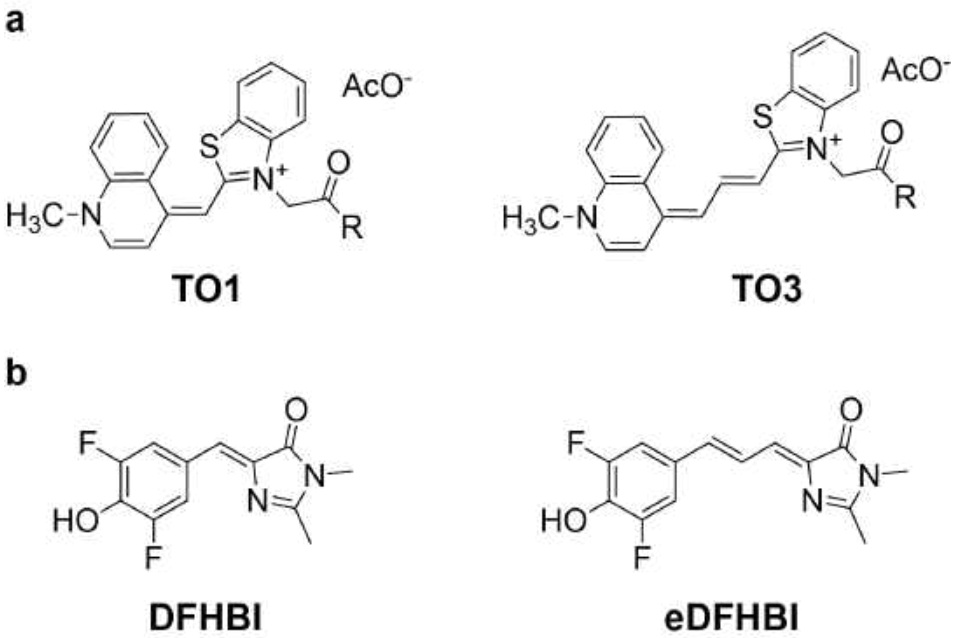

Fig. 48. The chemical structure of the thiazole orange fluorophores TO1 and TO3, as well as that of DFHBI and eDFHBI. a) The thiazole orange derivatives TO1 and TO3 are shown. TO3 contains two additional carbon atoms in the bridge connecting the benzothiazole ring and the quinoline ring. Both derivatives are bound by the same aptamers and yellow (TO1) respectivey red (TO3) fluorescenct complexes result[300]. b) Comparison of the chemical structures of DFHBI and the compound with an enlarged aromatic system, called eDFHBI.

The crystal structure of the Spinach-DFHBI complex did not reveal any kind of interaction between that methine bridge with adjacent nucleotides[252]. Thus, there was hope that eDFHBI might still be bound by spinach. Ideally the spinach-eDFHBI complex then would show a red-shifted fluorescence. If the combination of Spinach with eDFHBI did not lead to a new fluorescent complex, a new RNA aptamer selection for this target might be an option.

3.5.1 Synthesis of eDFHBI

For the synthesis of eDFHBI two different approaches were done (see **Figure 49**). The first approach (**Figure 49 a**) performed by Julia Hahn consisted of Heck-reaction between 4-bromo-2,6-difluorophenol and N-methoxy-N-methylacrylamide (**1**, in **Figure 49 a**), followed by a reduction of the resulting amide (**2**). The subsequent steps (**3**, **4**) were performed analogue to those for the synthesis of the original DFHBI. The synthesis is described in the bachelor thesis[336]. The resulting compound was purified via chromatography.
The second approach (**Figure 49 b**) performed by Sandra Trapp during her bachelor thesis[337] started with formylation of 2,6-difluorophenol via a Duff-reaction to result the 3,5-difluoro-4-hydroxybenzaldehyde (**1**, in **Figure 49 b**). After MOM-protection (**2)** a Wittig-reaction between the 3,5-difluoro-4-(methoxymethoxy)-benzaldehyde and Tributyl (1,3-dioxolan-2-ylmethyl) phosphonium bromide resulted in the (E)-3-(3,5-difluoro-4-hydroxyphenyl)-acrylaldehyde (**3)**. The final reaction steps (**4, 5**) matched the described steps for the synthesis of DFHBI. The last reaction step was performed with methylamine to result the eDFHBI, as well as with N-Boc-1,6-hexanediamine to result in a compound containing a linker that could be immobilised to a solid support (eDFHBI-NH_2). The latter was needed for a SELEX approach. This synthesis approach led to much better yields of eDFHBI and eDFHBI. Therefore, below shown results were all obtained with eDFHBI from that approach (**Figure 49 b**). ^{1}H-, ^{13}C-NMR as well as HPLC-MS of the resulting products are shown in **Appendix, Figure 19, Figure A20 and Figure A21**. In case of eDFHBI that was carrying the linker, NMR-spectra were recorded of the compound that still carried a Boc-protection group.

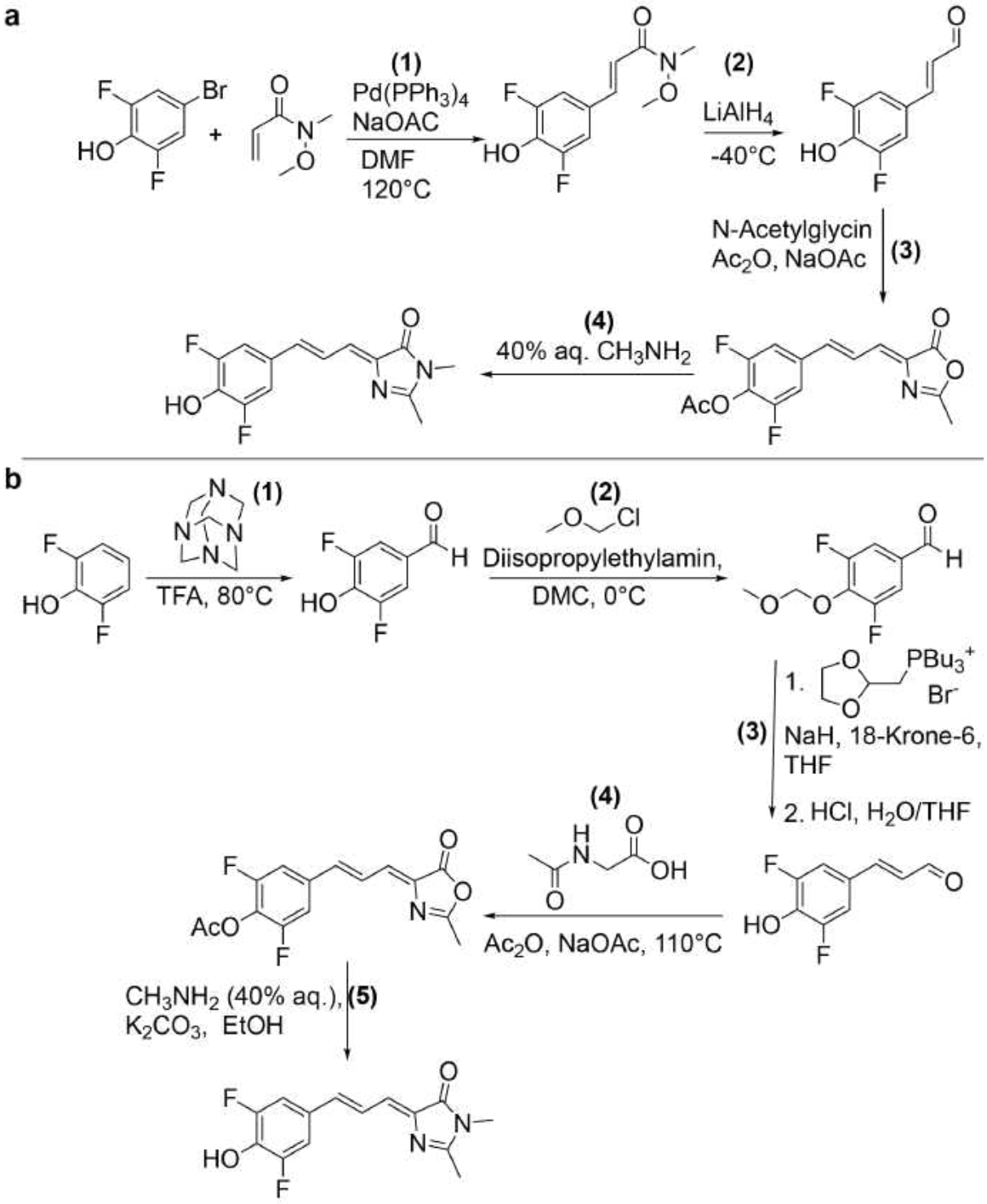

Fig. 49. Two alternative synthetic routes for eDFHBI performed by Julia Hahn and Sandra Trapp. a) The synthesis performed by Julia Hahn started with a Heck-reaction (1) and subsequent reduction (2) to an aldehyde. Following reaction steps (3, 4) were analogous to those for the synthesis of the original DFHBI[252]. b) Synthesis performed by Sandra Trapp started with a Duff reaction (1) followed by a Wittig reaction (3). Again, the remaining steps (4, 5) were analogous to those for the DFHBI synthesis.

3.5.2 Photometric properties of eDFHBI

First the resulting eDFHBI was characterized concerning its photometric properties. **Figure 50 a** shows the absorbance of the original DFHBI in dependence on the pH of the used HEPES buffer. The absorbance maximum shifts from around 360 nm at pH 5 to 430 nm for pH 7. In more acidic solutions DFHBI is predominantly present in its protonated form whereas at pH 7 and pH 8, the deprotonated for predominates, which explains the shift in absorbance. Only the deprotonated form of DFHBI is bound by Spinach resulting in the increase in fluorescence intensity at 505 nm[252]. A similar tendency in absorbance characteristics could be observed for eDFHBI (**Figure 50 b**). While absorbance maximum at pH 5 and pH 6 remained at 380 nm (protonated form), it shifted to 450 nm at pH 7 and pH 8 (deprotonated form).

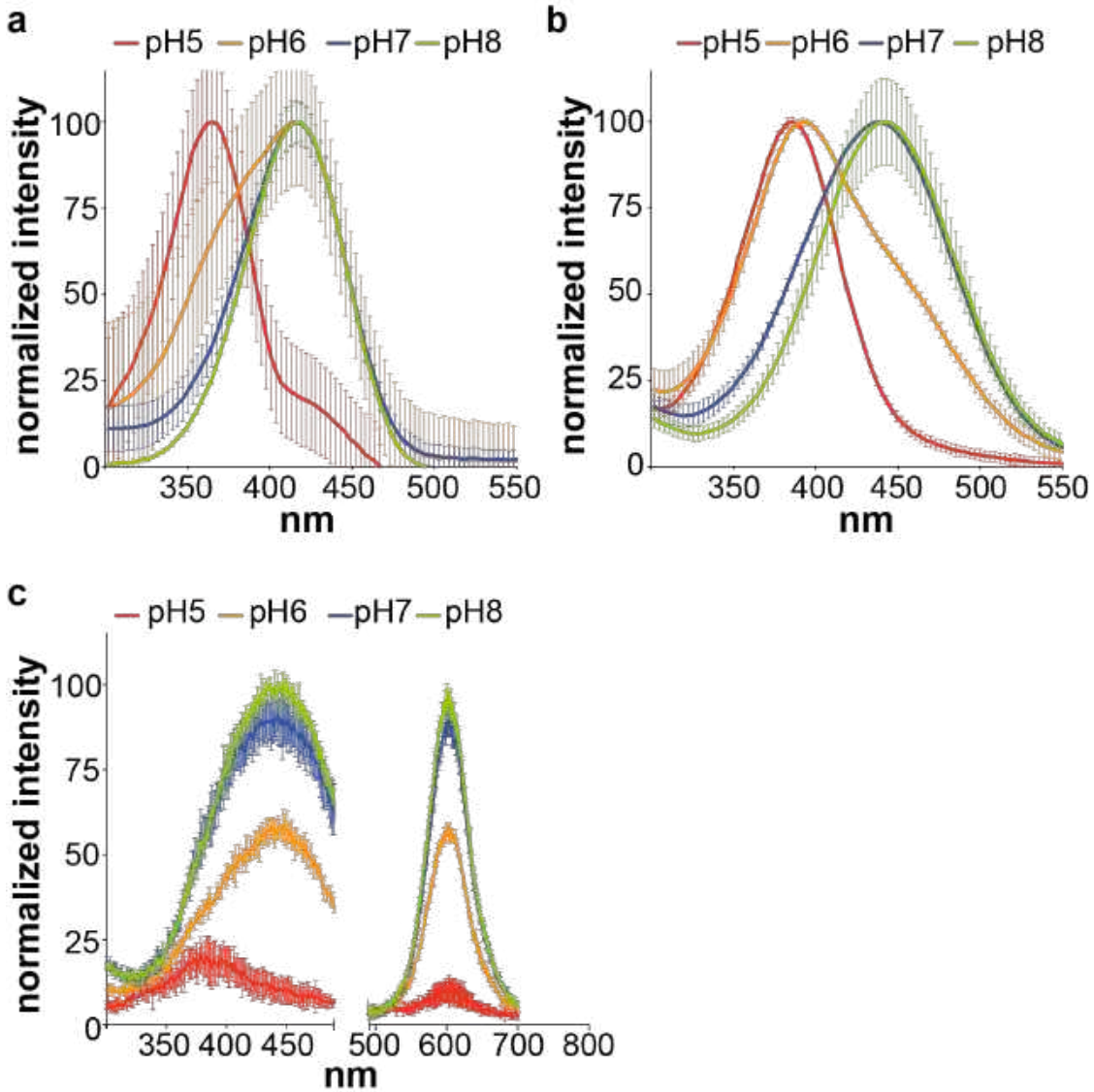

Fig. 50. **Photometric properties of DFHBI and eDFHBI**. a) Normalized absorbance spectra of 20 µM DFHBI in HEPES buffer of pH 5, pH 6, pH 7 and pH 8. b) Normalized absorbance spectra of 20 µM eDFHBI in HEPES buffer of pH 5, pH 6, pH 7 and pH 8. c) Normalized excitation-emission scan of 20 µM eDFHBI in HEPES buffer of pH 5, pH 6, pH 7 and pH 8.

In contrast to DFHBI, which is only slightly fluorescent at 505 nm in the absence of the Spinach aptamer, a strong autofluorescence of eDFHBI could be observed. **Figure 50 c** shows an excitation-emission scan of a 20 µM eDFHBI solution in HEPES buffer of different pH -values without the presence of any aptamer. Similar to DFHBI, the excitation maximum was at 460 nm. However, the emission maximum was shifted to 600 nm, which is clearly higher than the emission of DFHBI (together with Spinach aptamer). Again, a pH-dependency could be observed for the excitation-emission scan of eDFHBI. The protonated form of eDFHBI (pH 5 and pH 6) showed only little excitation- and emission intensities compared to those observed for the deprotonated form (pH 7 and pH 8).

Since there is an obvious similarity between the structures of DFHBI and eDFHBI (compare to **Figure 48 b**) it was investigated if the Spinach aptamer is also capable to bind eDFHBI. To check for binding of the aptamer to eDFHBI, a competition assay was performed. In this case Baby-Spinach was used. In presence of a 300 nM solution of Baby-Spinach and 10 µM DFHBI in HEPES of PH 7.4, increasing concentrations of eDFHBI were added. While the solutions were excited at 460 nm, an emission scan from 490 to 700 nm was performed. As shown in **Figure 51 a**, the fluorescence intensities at 505 nm that correspond to the emission maximum for the Spinach-DFHBI complex are decreasing with increasing concentrations of eDFHBI. In addition, emission-intensities of the solutions at 600 nm were increasing with increasing concentrations of eDFHBI. In **Figure 51 b** the fluorescence-intensities at 505 nm were plotted against the increased concentrations of eDFHBI. From the resulting curve an IC_{50}-value of 41.3 µM was calculated.

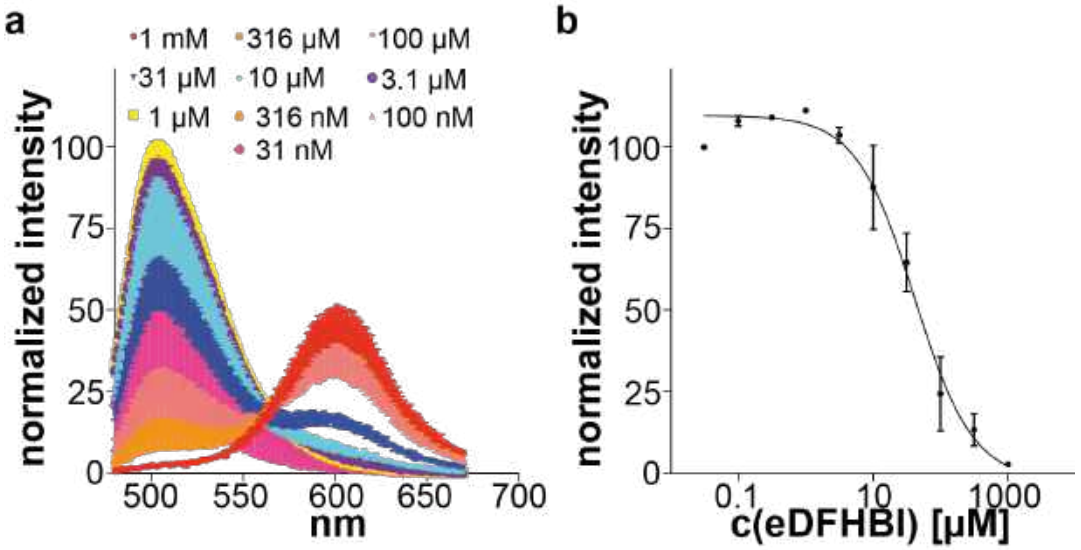

Fig.51. IC-50 determination of eDFHBI. a) 10 µM of DFHBI together with 500 nM Baby-Spinach are incubated with increasing amounts of eDFHBI in HEPES pH 7.4. An emission scan from 490 nm to 700 nM was performed while excitation was done at 450 nm. b) The decrease of baby-Spinach induced fluorescence at 505 nm is plotted against the increasing concentrations of eDFHBI. The calculated IC-50 value is at 41.3 µM (n=3).

This result indicates that eDFHBI indeed is competing DFHBI for binding to (Baby)-Spinach aptamer. Though eDFHBI most likeky is bound by Baby-spiach, it remained unclear if its fluorescence was also increased upon binding. Though an increasing emission at 600 nm can be observed in **Figure 51 a** with increasing concentrations of eDFHBI, this result can simple be caused by a high autofluorescence of eDFHBI and is not necessarily the result of a Baby-Spinach eDFHBI complex formation.

To analyze, if the fluorescence of eDFHBI is increased upon binding to Baby-Spinach, the aptamer and the chromophore were mixed in different ratios in HEPES of pH 7.4. The mixtures were excited at 460 nm and emission intensities at 600 nm were recorded. In **Figure 52 a** the fluorescence intensities at 600 nm of increasing concentrations of eDFHBI were recorded in absence (black dots) and presence (red dots) of Baby-Spinach. A strong autofluorescence of eDFHBI again became obvious, since the fluorescence intensity increase with the increasing concentrations even in absence of Baby-Spinach. The addition of Baby Spinach to the eDFHBI solutions did slightly increase the fluorescence intensities. Compared to the increase of fluorescence intensity for DFHBI in complex with the aptamer, the increase in case of eDFHBI remains poor. In **Figure 52 b** solutions of 10 µM eDFHBI were incubated with increasing concentrations of Baby-Spinach and the fluorescence intensities were monitored at 600 nm. For RNA concentrations above 1 µM an obvious increase of fluorescence intensity could be detected. Obviously, the aptamer is not only capable to bind eDFHBI but also increases the fluorescence of that compound. However, the affinity of the aptamer to eDFHBI seems poor compared to that to DFHBI.

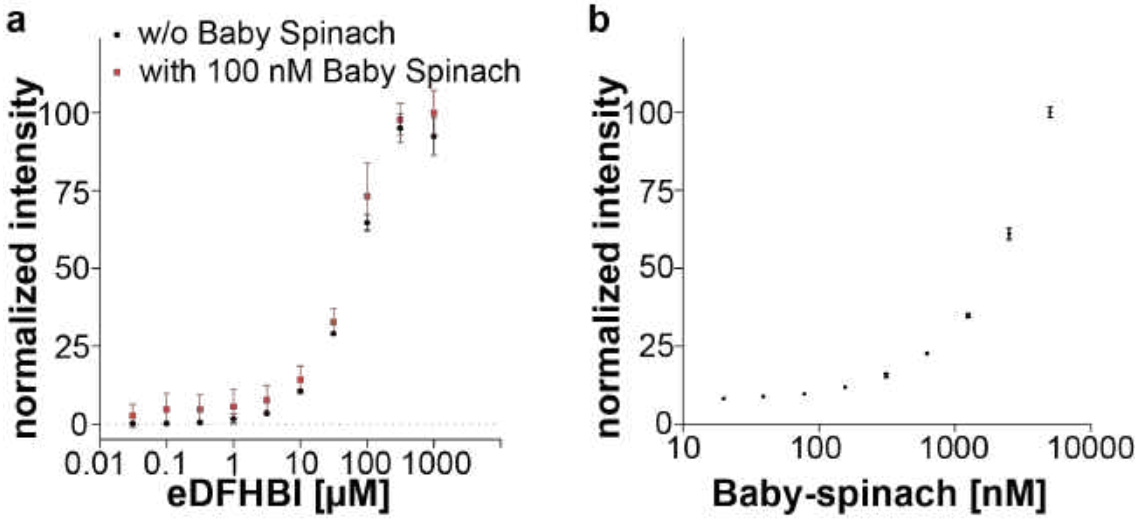

Fig. 52. Autofluorescence of eDFHBI and affinity determination of Baby-Spinach to eDFHBI. a) The fluorescence at 600 nm of increasing eDFHBI concentrations in HEPES pH7.4 was recorded in absence (black) and presence (red) of 100 nM Baby-Spinach. b) affinity determination of eDFHBI to Spinach baby. 10 µM eDFHBI in HEPES pH 7.4 was incubated wit increasing concentrations of Spinach baby. Excitation was done at 460 nm, whereas emission was measured at 600 nm (n=2).

3.5.3 RNA SELEX for eDFHBI

Since the affinity of Baby-Spinach to eDFHBI probably is in the high micromolar range, the combination of this aptamer and the chromophore is not useful for applications that are known for the Spinach-DFHBI complex. Hence, to get an aptamer with higher affinity to eDFHBI a new SELEX would be needed. For this purpose, altered versions of eDFHBI were synthesized that contained a primary amine group which could be used to covalently couple the compound to magnetic beads or a sepharose matrix NMR and HPLC-MS analysis can be seen in **Appendix, Figure A20,** and **Figure A21**). The resulting compound was used for immobilisation to M280-tosylactivated Dynabeads, as well as to epoxy-activated sepharose. To check, if the immobilisation of the chromophore was successful, fluorescence measurements of the magnetic beads as well as sepharose were undertaken. **Figure 53** shows the result of that fluorescence measurement. In **Figure 53 a,** an excitation-emission scan verifying the fluorescence properties of eDFHBI-modified as well as non-modified Dynabeads was performed. **Figure 53 b** shows the corresponding emission scan for eDFHBI-modified as well as non-modified sepharose. In case of non-modified magnetic Dynabeads there was already a strong signal for excitation at 460 nm and for emission at 550 nm. However, for eDFHBI-modified magnetic beads, the signal intensity for excitation at 460 nm was more pronounced. In addition, the emission intensity was increased compared to non-modified beads and moreover, the emission maximum was shifted to 590 nm. This shift in emission maximum is close to the cognate emission maximum of solubilized eDFHBI (600 nm). This result was taken as a proof that the compound indeed wsa covalently coupled to the magnetic beads. In case of sepharose the result looked more distinct. An obvious fluorescence at 600 nm could be observed for eDFHBI-modified seharose, while for the non-modified sepharose no fluorescence signal was detectable

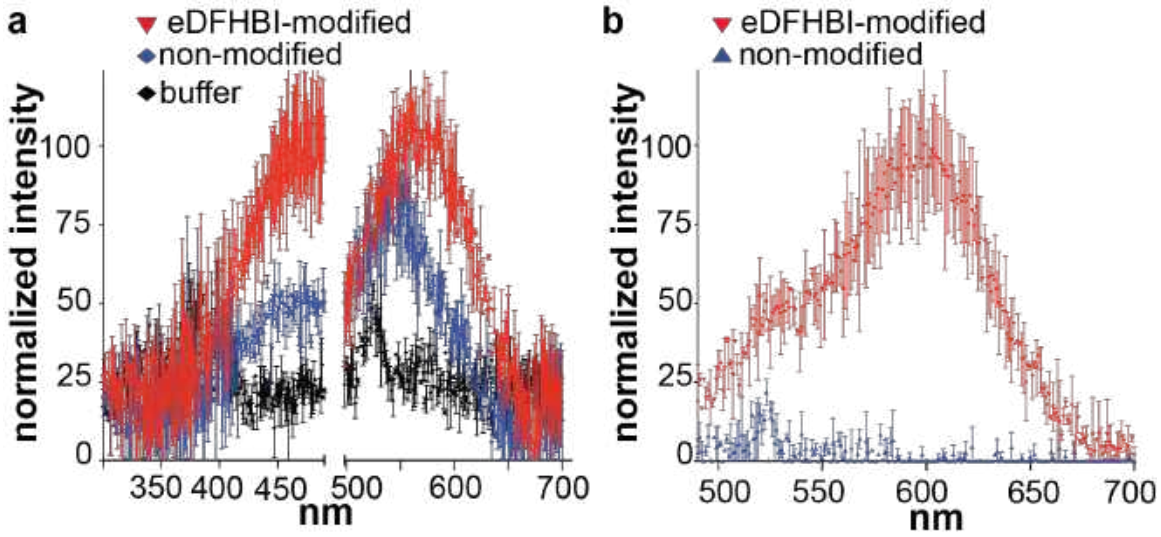

Fig. 53. Fluorescence scan of eDFHBI coupled magnetic beads and sepharose. a) Normalized excitation-emission scan of eDFHBI-modified and non-modified M280 tosylactivated beads. HEPES buffer was used as negative control to reflect the background signal. b) Normalized emission scan of eDFHBI-modified and non-modified sepharose. Prior to the scan, the sepharose was irradiated with 460 nm.

In a next attempt a SELEX targeting eDFHBI was performed. For the SELEX it was decided to use the Sul I RNA library containing a 40 nt long randomized region. Both, the eDFHBI-modified sepharose as well as the eDFHBI-modified magnetic beads described above were used for the selection. Nine cycles of SELEX were performed. The procedure of the SELEX is shown in **Table 13**.

Table 13. SELEX for eDFHBI.

Cycle	Pre-SELEX Matrix	Amount of matrix	SELEX Matrix	Amount of matrix	Wash	Elution	PCR-cycles
1	-	-	Sepharose	50 µl; ca.1µmol	300 µl; 5 mi	Heat	6
2	Sepharose	50 µl	Sepharose	50 µl; ca.1µmol	2x 300 µl; 5 min	Heat	7
3	M280-beads	50 µl	M280-beads	20 µl; ca 90 nmol	2x 500 µl; 5 min	Heat	15
4	M280-beads	50 µl	M280-beads	20 µl; ca 90 nmol	2x 500 µl; 5 min	Heat	12
5	Sepharose	50 µl	Sepharose	10 µl; ca. 200 nmol	8x 1 ml; 5 min	Heat	8
6	Sepharose	3x 50 µl	M280-beads	10 µl; ca 45 nmol	8x 1 ml; 5 min	Heat	15
7	M280-beads	3x 50 µl	M280-beads	5 µl; ca 23 nmol	8x 1ml; 5 min	Affinity; 100 nM eDFHBI	10
8	M280-beads	3x 50 µl	M280-beads	5 µl; ca 23 nmol	11x 1ml; 5 min	Affinity; 50 nM eDFHBI	12
9	M280-beads	3x 50 µl	M280-beads	5 µl; ca 23 nmol	11x 1ml; 5 min	Affinity; 50 nM eDFHBI	9

Two different approaches were done to verify an enrichment of eDFHBI binding sequences. First large amounts of RNA of SELEX cycle 1, 6, and 9 were prepared. Equal amounts of RNA (800 nM) from these SELEX cycles were then incubated with 10 µM eDFHBI in HEPES of pH 7.4. The mixtures were excited at 460 nm and fluorescence intensities at 600 nm were recorded (**Figure 54 a)** It becomes obvious that eDFHBI alone already shows the same fluorescence intensity at 600 nm as the mixtures of 800 nM RNA from all SELEX-cycles together with eDFHBI. Thus, with this assay no enrichment of eDFHBI binding sequences could be verified. Naturally it could be, that RNA sequences bind eDFHBI but do not show an increase in fluorescence upon binding to eDFHBI were enriched during the selection. To rule this out, a radioactive binding assay was performed. In **Figure 54 b** the result of the Cherenkov assay can be seen. Unfortunately, no enrichment of RNA binding to eDFHBI-modified sepharose could be observed. On the contrary, RNA of the first SELEX cycle seemed to bind even slightly better to the eDFHBI-modified matrix.

Taken the results of **Figure 54 a, b** together, it must be said that the SELEX approach obviously was not successful. Probably an RNA-library similar to that used for the DFHBI-SELEX would be more promising for a successful selection (see **discussion**).

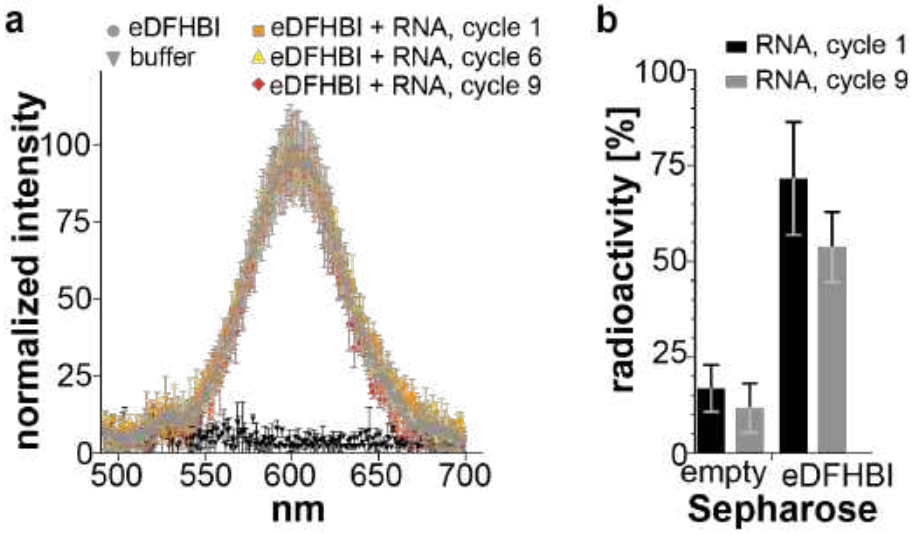

Fig. 54. Evaluation of eDFHBI-SELEX. a) 800 nM of RNA from SELEX cycle 1, 6, and cycle 9 are mixed with 10 µM eDFHBI in HEPES pH7.4. The samples are irradiated at 460 nm and emission is recorded at 600 nm. For comparison reasons the fluorescence of 10 µM eDFHBI alone is recorded. b) A Cherenkov assay was performed with RNA of SELEX-cycle 1 and cycle 9. Radioactively labelled DNA was incubated with empty sepharose and eDFHBI.coupled sepharose. A SELEX cycle was mimicked and the remaining radioactivity sticking to the matrix was recorded.

4. Discussion

Being potential alternatives for antibodies, chemical modified aptamers (clickmers) could be useful for a broad range of applications. In this case it was intended to identify clickmers, binding to THC with high affinity and specificity. Such clickmer for THC could possibly serve as a sensor-molecule in roadside drug-tests devices. In this thesis, the application of the newly developed click-SELEX[232,235] (see **section 1.3.2.4**) for the small molecule THC(A) was described.

4.1 Rational choice for click-SELEX for THC

THC is a tricyclic, extremely hydrophobic and almost planar small molecule. Due to the poverty on functional groups it is very nonpolar and therefore limited in its ability to undergo ionic or polar interactions with potential binding partners. Binding to the cannabinoid receptors CB_1 and CB_2 is enabled through a multiplicity of hydrophobic interactions, with nonpolar and aromatic amino acids. In particular, several phenylalanine residues are in close proximity to THC, probably interacting via π-π-stacking with their aromatic core (see **Figure 2**)[32–34].

Taken together, THC is an extraordinary hard to address target molecule for conventional DNA or RNA aptamers, since aptamer binding interaction with targets is mostly characterised by H-bond-, and charge-charge-interactions, as well as shape complementarity and polar contacts, whereas hydrophobic contacts or stacking interactions are rare[194,338,339]. Therefore, the click-SELEX approach which is inspired by the base-modified SOMAmers was the method of choice for this selection. Especially for protein targets the success rate increased dramatically for selections with libraries containing non-natural nucleobases compared to those with conventional oligonucleotides. In addition, quite often functional groups with hydrophobic characters increased the affinities best[190,219].

Click-SELEX represents an elegant method to chemically modify DNA. Click-reaction can be smoothly performed in every laboratory without the need of complex synthesis of artificial bases or chemically altered nucleobases. It offers a great variety of moieties that can be incorporated into DNA. As previously described, different alkyne-containing deoxy uridines are commercially available. For SELEX purposes, the long flexible linker of C8-dU is unfavorable for the purpose of aptamer selections, as an exact positioning of the modification relative to the rest of the DNA is impossible[232]. Therefore, for click-SELEX the EdU is used, which does not have such a flexible linker, meaning that after click-reaction with an azide bearing entity, the modification is located at a defined position. For click-SELEX, benzyl azide was chosen, since the benzyl-residue mimics the side chain of phenylalanine and resulting clickmers after successful selection hypothetically could bear characteristics, that resemble that of the receptors. As phenylalanine residues within the cannabinoid receptors CB_1 and CB_2,

benzyl-residues located on the clickmer might interact with THC via hydrophobic π-π-stacking interactions

4.2 Click-SELEX to increase the success of selections for small molecules

Click-SELEX already has been shown to be a simple method to generate nucleobase-modified aptamers for the protein target C3-GFP. The via click-chemistry introduced modifications play an essential role in the high affinity of the clickmer to the target-protein[232]. Similar to SOMAmers, amino-acid like side-chains that are attached to the C5-position of EdU expand the chemical repertoire of the oligonucleotides and support the interaction to proteins[207]. However, selections for small molecules often provide big challenges, too. Apart from the frequent need of chemical manipulation of their structure for immobilisation purposes, there is a big size difference between the small molecules an aptamers, which makes SELEX challenging[136]. Furthermore, there might be a shortage of functional groups on the small molecule with which the aptamer could interact. Increasing the chemical diversity of the nucleic acids by introducing further modifications to the nucleobases therefore might also increase the success rate of SELEX for small molecules.
In this thesis it has been shown, that click-SELEX is indeed a possible approach to generate nucleobase-modified aptamers for small molecules. The hydrophobic modification greatly contributes to the affinity of C11.41 to the small molecule THC. There is a reason to believe, that the tricyclic ring system of THC is interacting with the planar plane of a G-Quadruplex and the benzyl-modification via π-π -interactions.

Most aptamer selections with nucleobase modifications have been performed for protein targets. However, besides the here described clickmer C11.41, Soh *et. al.* meanwhile also showed that SELEX with nucleobase-modifications introduced via click-chemistry lead to high affinity aptamers for small molecules[340]. Although they used an altered selection strategy, the chemical modifications introduced at the C5-position of deoxy-uracil are fundamental for the aptamer affinities to the target molecule. They used a so-called click-particle display (click-PD) strategy to select a boronic acid modified aptamer for epinephrine with an affinity of about 1 µM. Thus far, no conventional aptamer for this target molecule has been reported. The particle display was already developed in the same group[341,342]. For this technique the library is incubated with forward primer-coated beads and an emulsion PCR is performed resulting in particles that carry many copies of one sequence. After single strand generation, the ssDNA carrying beads are incubated with fluorescently labelled target molecules and subjected to FACS screening. This way, particles that carry target-binding sequences can be differentiated from particles carrying non-binding sequences. The DNA is subsequently amplified and subjected to the next PD-SELEX step. For click-PD the only difference is, that the DNA contains either C8-alkyne-dUTP, or dibenzocyclooctyl-dUTP (DBCO-dUTP) instead of dT. Libraries containing DBCO-dUTP can be used for strain-promoted alkyne-azide cycloaddition (SPAAC), while C8-

alkyne-dUTP containing libraries are accessible to CuAAC. In contrast to our click-SELEX approach, for click-PD the click-reaction is performed with the double-stranded emulsion-PCR product and the conversion into single stranded library is performed subsequently. Obviously, this does not impair the quantitative yield of click-reaction. This is understandable, since the alkyne- as well as the dibenzocyclooctyl- side chain point away from the major groove of the double helix[227]. The remaining cycle for the click-PD resembles that of the described particle display cycle.

For the small molecule epinephrine, a DBCO-dUTP containing library was subjected to a SPAAC with a boronic acid azide, since the boronic acid modification is incompatible with the CuAAC conditions[340]. However, Soh *et. al.* also demonstrated that the click-PD method itself is compatible with CuAAC as they have shown with a selection for the lectin concanavalin A (Con A)[340]. For epinephrine an aptamer resulted that contained 4 boronic acid modifications within the random region. The FACS-determined k_D was 0.3 ± 0.18 µM. Similar to our click-SELEX for THC the modification for the click-PD SELEX was wisely chosen. We have decided to use an aromatic azide (benzyl-azide) to modify our SELEX-libraries since the aromatic core is able to interact with the tricyclic, hydrophobic framework of THC. For the click-PD boronic acid was chosen, since it was found to form reversible covalent bonds with the diol found in epinephrine[343–345].
Both the clickmer for THC and the boronic acid modified aptamer for epinephrine are good examples that nucleobase modifications indeed increase the success rate of selections for small molecules. The modularity of click-reaction was useful in both cases, since the utilized modifications could be chosen in advance of the SELEX procedures and have been shown to have a significant impact of binding performance to the corresponding targets. Both approaches might be useful for selections of further small molecule aptamers.

4.3 Click-SELEX for THC-modified beads

Initially, nine cycles of click-SELEX for THC were performed and the library of the 9th cyle was sequenced with sanger sequencing. A table with all the observed sequences is shown in the **Appendix, Table A1**. Since the library of the 9th SELEX cycle did not seem to be highly enriched for THC-binding sequences, 7 more click-SELEX cycles with more stringent selection conditions were added. The libraries of several SELEX cycles were subsequently investigated with NGS to analyse the enrichment of THC-binding sequences. An observable enrichment of individual sequences among the libraries obviously started at quite late SELEX-cycles. This is most likely due to more harsh washing steps during the SELEX. The progression of unique sequences with consecutive SELEX cycles (**Figure 22**) as well as the changes in the nucleotide distribution within the randomised sequences (**Figure 23**) was taken as an indicator for the enrichment of individual sequences among the libraries. In general, NGS

revealed an enrichment of sequences, rich in G-residues especially right at the start of the random region. Overall, a high percentage of G-residues was found for the library of SELEX cycle 16, whereas benzyl-modified EdU clearly have been depleted compared to the starting library (**Figure 22**).

The depletion of benzyl-modified EdU-residues within the libraries of proceeding SELEX-cycles is somewhat in contradiction to the basic idea of click-SELEX. Concerning the selection strategy, benzyl-modified sequences should be better capable to bind to the hydrophobic THC. Similar to the interaction of CB_1 to THC[32], wherein the drug is surrounded by several phenylalanine-residues in a hydrophobic binding pocket, it could be assumed that a multiplicity of benzyl-modification within the clickmer would lead to better binders. Accordingly, a decrease of the amount of benzyl-modifications was not expected. One possible explanation for this depletion of Bn-dU could be the formation of highly stable globular structures, driven by the hydrophobic effect. This entropy-driven effect also is known to be the cause for the formation of many globular proteins[346,347]. The number of non-polar surfaces exposed to water molecules is minimised by the interaction of non-polar groups with one another. Hydrophobic clusters are formed, wherein solvating water molecules are supplanted[348,349]. Of course, the hydrophobic effect already contributes to the tertiary folding of conventional oligonucleotides.
However, for DNA-sequences that were click-modified with hydrophobic building blocks as, e.g., benzyl, this effect could intensely contribute to the formation of very stable, hitherto unknown tertiary structures of the oligonucleotides. This in turn could decrease the susceptibility of those sequences for PCR-amplification. Naturally this effect would be more pronounced for sequences with ≥ 25% Bn-dU, than for sequences with a depleted amount of Bn-dU. As a result, mainly sequences with a depleted amount of Bn-dU remain at the end of a click-SELEX process. Of course, this is just a theoretical explanation for the phenomenon observed in the click-SELEX for THC. To strengthen that theory, more experiments would be needed. First and foremost, this effect should not be notable for click-SELEX that are performed with less hydrophobic, more polar click-in modifications.

Another explanation for the Bn-dU depletion could be caused by an increased error-rate in PCR-amplification for heavily click-modified sequences. Of course, it has been confirmed, that the click-SELEX cycle can be performed and that click-modified DNA sequences as well as EdU containing sequences are tolerated by *Pwo*-polymerase as template. However, the fidelity of the polymerase has been shown to be tremendously decreased compared to non-modified DNA-samples, as Pfeiffer *et. al.* showed[350]. It was demonstrated, that predominantly the EdU-positions within the template sequence were mutated during PCR-amplification. Naturally this effect also leads to a depletion of the Bn-dU amount within the libraries of progressed SELEX-cycles. Potentially click-SELEX could be further optimized to circumvent the increased error-rate in PCR amplification of (clicked) EdU containing template. Though the *Pwo*-polymerase already has been reported to have broad substrate acceptance[231] it still might not be the optimal polymerase for click-SELEX. Other polymerases like KOD XL, or Deep

vent *exo*$^{-}$ [227] are also known to readily incorporate alkyne-bearing building blocks. Eventually one of these polymerases does not reveal such a high error-rate, as the *Pwo*-polymerase does.

A third reason for the observed depletion of Bn-dU could simply be, that SELEX was performed for a small molecule in this case. In contrast to protein targets that offer huge surfaces for possible interactions, THC just provides the tricyclic ring system. The small size of THC might restrict the number of the bulky aromatic modifications on the clickmer that can interact with the target. For SOMAmers that are always selected for protein targets, the amount of nucleobase modifications is mostly relatively high and the majority of modifications is relevant for the SOMAmers[190,194,216,351]. Another tendency can be seen for the click-PD approach performed by Soh *et. al*[340]*.* Nucleobase-modified aptamers are published for the small molecule epinephrine, as well as for the lectin Con A. In both cases the SELEX was started with a library containing a 40 nt long random region with an equivalent distribution of the nucleotides dA, dC, dG and DBCO-dUTP (in case of epinephrine-SELEX) or C8-alkyne-dUTP (Con A SELEX). A selection of aptamer candidates with sufficient affinities is given for epinephrine, as well as for Con A.

The total amount of nucleobase-modifications is around 22% for the selection of Con A aptamers (8-9 modified nucelotides in 40 nucleotide long sequences), which is similar to the distribution within the starting library. In contrast to that the given aptamer-candidates for epinephrine only contained roughly 8% of modified nucleobases (3-4 modified nucleotides in 40 nucleotide long sequences), meaning that the modified nucleobases are also depleted during SELEX for this small molecule[340]. Both, the epinephrine aptamer as well as the clickmer for THC belong to the first nucleobase modified aptamers for small molecule targets. In both cases the depletion of modified nucleotides could be seen. For further selected small molecule aptamers with nucleobase-modifications it has to be seen if depletion of modified nucleotides can also be detected.

4.3.1 Secondary structure adaption of THC binding C11 derivatives.

The predominantly investigated sequence in this thesis is C11.41 and slightly varied versions of it. As explained in the result part, this 41-nucleotide long sequence is a result of a truncation of the sequence C11, which was one candidate from sequencing results. The truncation was based on secondary structure predictions from mfold[309]. Due to that prediction the primer binding sites of the initially 82 nucleotide long sequence were cut off, since they did not seem to participate in any secondary structure formation (**Figure 25**). As could be observed by flow cytometry binding analysis, cutting of the primer binding sites of C11 did not affect the affinity of the sequence to THC-modified beads.

Predicted G-scores for full-length C11 and the truncated C11.41 (and especially C11.41_4 & C11.41_A15G) are quite comparable. Those scores represent the likelihood for oligonucleotide sequences to fold into stable GQ´s. Tools that can be used to predict such scores, use special algorithmic rules that consider several aspects, especially the length of G-tetrads and the length of the loops connecting those tetrads[352–354]. It can be assumed, that the same G-residues of C11 and C11.41 participate in GQ-formation independent on the presence or absence of the primer binding sites. Further investigations via CD-spectroscopy indeed indicated that the formation of a parallel G-quadruplex within the sequence is extremely likely (**Figure 29**). This in turn means that the decision of cutting of the primer binding sites of C11 was initially based on wrong assumptions. Still, the fact that this truncation did not destroy the binding capability to THC-modified beads is not completely surprising. Actually, it is not seldom, that the primer binding sites of aptamers do not participate in secondary structures. Ellington and Cowperthwaite analysed more than 2000 known aptamers from the aptamer data base and concluded that for the majority of those aptamers, the secondary structure was independent of the primer binding sites[355]. This observation could probably be explained by the SELEX procedure itself. Sequences, wherein the primer binding sites are strongly contributing to secondary structures might disturb their own amplification during the PCR-process, since annealing to the primers is hindered. This means that in the SELEX starting library there already is a selective advantage for sequences wherein the random region does not interact with the primer binding sites. Those sequences are more readily amplified during proceeding SELEX and are likely to dominate the oligonucleotide pools of later SELEX cycles[356]. Click-SELEX probably could further pronounce this bias. While modifications are introduced in the random region of the library, the primer binding sites were constructed that way that no modification could be introduced. So far it is not known for click-SELEX, to which extend the modifications in the random region participate in secondary structure formation. In theory they could lead to completely new structures that are unknown for conventional DNA or RNA sequences. Similar to some cases of known SOMAmers, it might be possible that modifications within the random region interact with one another leading to hitherto unknown structures of the DNA. For SOMAmers, crystal structures revealed such cases, where modified nucleobases interact with each other and thereby unwind the helical DNA structure. In case of the NGF-SOMAmer, the IL-1-SOMAmer and further SOMAmers, zipper-like structures could be found resulting from π-π-stacking of the aromatic modifications with adjacent uridine[207–209,194] . For clickmers, as well as for click-SELEX libraries a similar phenomenon could be conceivable. Since the primer binding sites do not carry modifications, they cannot participate in structures similar to the mentioned ones. Hence, the primer binding sites presumably are excluded from complex structure formation.

As already mentioned, it is assumed that C11.41 folds into a parallel G-quadruplex. Some crystal sturctures of nucleobase modified SOMAmers are known that also form such secondary structures. One crystal structure of an Interleukin-6 (IL-6) binding SOMAmer revealed the formation of an antiparallel G-quadruplex that contributes to the affinity of the sequence called SL1025[216,357]. SL1025 binds to IL-6 with an k_D of

270 nM and inhibits the biologic activity of that cytokine. The sequence that originally resulted from a SELEX with a Bn-dU modified library actually consists of two distinct domains, the GQ domain and a stem-loop domain. Post SELEX modifications of the resulting sequence led to the highly modified SL1025. The 23-nucleotide long sequence contained besides eight Bn-dU modifications, six 2´-O-methyl substitutions as well as one Nap-dU and one Pe-dU substitution. Similar to the C11.41 clickmer for THC, it could be confirmed for SL1025 that the GQ-domain maintained an appreciable, yet reduced binding affinity to IL-6, alongside an inhibitory effect of IL-6 *in vitro*[216]. In this particular case, the GQ provides a rigid scaffold that helps to orientate the five modified nucleotides adjacent to the domain in the right way. That way, four of the five aromatic nucleobase-modifications are in direct contact with the protein surface. Observed interactions of the nucleobase modifications were mainly edge-to-face stacking interactions with aromatic amino acids like phenylalanine and tyrosine. Since the GQ-core of the clickmer C11.41 also maintained slight binding affinity to the small molecule THC, a similar explanation is possible in this case. The GQ might help to position the one benzyl-modification in a defined way, that supports stacking-interactions between the modification and the target.

4.3.2 Contribution of the click-modification on the affinity of C11.41 to THC-modified beads

For C11.41 it could be shown that the affinity to THC-modified beads can be tuned by varying the click-in modification (**Figure 31** and **Figure 32**). Naturally, it cannot be guaranteed that the different modifications do not change the secondary folding of the sequence. CD-spectra where mostly performed with C11.41, C11.41_4 and C11.41_A15G in the non-clicked state of the sequences. Only the benzyl-clicked C11.41_A15G was once checked vie CD-spectroscopy (**Figure 33**). Since the benzyl-modification did not relevantly change the spectra, which still showed the characteristic peaks for a parallel GQ, it can be speculated that all the other tested click-modifications also do not change the general secondary structure of the clickmer.

To get more detailed information about the stability of the GQ in the non-clicked and benzyl-clicked condition, melting curve analysis in combination with CD-spectroscopy would have to be performed with all the used modifications. However, **Figures 31** and **32** indicate that aromatic modifications support the affinity to THC-modified beads, whereas aliphatic modifications do not show this result. Again, this result can be compared to that of the already mentioned IL-6 SOMAmer SL1025. In this case adjacent to the GQ-core there are five nucleobase-modifications. For four of these five modifications it could be shown, that substitutions of the modifications did lead to obvious changes in affinity to IL-6. Particularly position 7 was sensitive for alterations of the nucleobase modifications. Replacement of the original benzyl-modification with non-aromatic residues always resulted in >100-fold reduced affinities. Substituting benzyl with larger aromatic functional groups however improved the affinity to IL-6. Especially the Bn-dU substitution by 5-[N-(3, 4-methylenedioxybenzyl)carboxamide]-

2´-deoxyuridine (MBn-dU) resulted in a 37-fold increased affinity in combination with a 13-fold better inhibitory activity of IL-6 *in vitro*[216]. The given explanation in this case is, that the benzyl-modification fills a deep cleft on the IL-6 surface and that double-ring substituents can even better fill this cleft. Of course, the small molecule THC does not have the complex surface as the cytokine. Still, also in this case the larger aromatic double-ring modifications possess a larger surface compared to the benzyl-modification, which might enhance the interaction with THC.

Like for Rohrbach *et. al*. a direct involvement and supportive contribution of the introduced modification to the GQ-stability can also be speculated[338]. This observation was found in case of the thrombin aptamer HD1-22[338]. Introduction of several polycyclic aromatic hydrocarbons (PAHs) to a preferred position located at the GQ-region within the aptamer resulted in improved stabilities, affinities, and anticoagulant activities of the PAH-modified aptamer, compared to the non-modified aptamer. Stabilisation of the GQ-domain and increased affinity to thrombin was in addition dependent on the actual PAH-structure. NMR-data of the best PAH-modified aptamer revealed that the polyaromatic system interacting with the upper layer of the GQ, which probably results in the mentioned improved properties[338]. For C11.41_A15G a comparable scenario could be possible.
The introduced aromatic system could potentially stick on top of the GQ-structure of C11.41_A15G, thereby stabilizing that structure. Like for the PAH-modified HD1-22, the nature of the introduced aromatic system could have slight influences on the resulting stability of the GQ. This in turn could explain the small alterations in the observed affinities of differently modified C11.41_A15G to THC-modified beads. Thus, modification of C11.41 in the region of the GQ with aromatic residues could lead to a stabilisation of the GQ- structure, which in turn could be responsible to improved affinities to the target molecule.

4.3.3 Contribution of the stem-loop part on the affinity of C11.41 to THC-modified beads

Due to the arrangement of G-residues in C11.41, a 2-layered parallel G-quadruplex is likely for this sequence, as it is schematically depicted in **Figure 29**. The slightly varied C11.41_A15G potentially should be capable of forming an even more stable 3-layered parallel GQ, as is shown in **Figure 55**. In both cases however, it remains unsolved in which way the remaining part of the 41-nucleotide long sequence contributes to the binding affinity for THC-modified beads. In any case, the remaining nucleotide sequence is involved in binding to the target, since the affinity is markedly reduced for the GQ-part alone (see **Figure 26**).

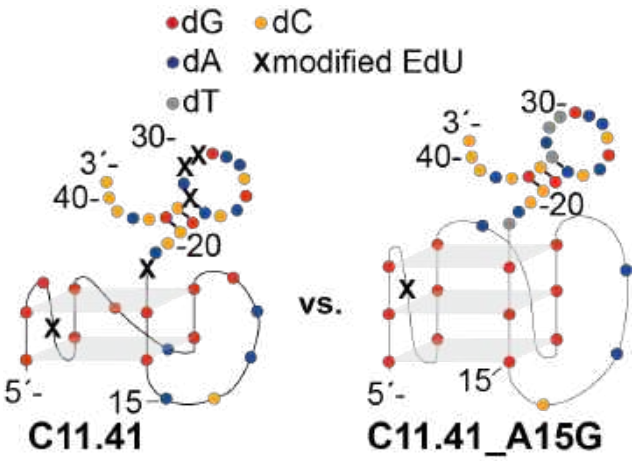

Fig. 55. Suggested secondary structures of C11.41 and C11.41_A15G. The slightly modified C11.41_A15G might fold into a 3-layered parallel GQ, in contrast to C11.41. Additionally, C11.41_A15G only contains the one benzyl-clicked EdU, which is important for the affinity to THC-modified beads.

Naturally, it has to be checked, if the GQ-structure remains intact upon binding of THC to the clickmer. However, it can be assumed that the GQ-motif is intact in the THC-bound, as well as in the non-bound state, since it is unlikely that the binding event disrupts this stable structure. Correct secondary structure of the remaining part of the clickmer cannot be predicted with certainty. However, mfold prediction of the sequence of the remaining 23 nucleotides suggested a stem loop structure (see **Figure 55**)[309]. Possibly that remaining stem-loop part could stabilizes the orientation of THC in the binding pocket.

This would explain the observed effect of this part on the clicker´s affinity to THC-modified beads (**Figure 26**). The binding event eventually could be similar to that of the RNA aptamer “Spinach” to its ligand 3,5-difluoro-4-hydroxybenzylidene imidazolinone (DFHBI)[254,302]. The Spinach aptamer folds into a rigid two-layered antiparallel G-quadruplex in the presence as well as in the absence of the chromophore DFHBI. The GQ in combination with adjacent nucleotides provides a partially pre-formed binding pocket for the chromophore. The GQ serves as a planar hydrophobic stacking platform onto which DFHBI is bound in a planar configuration. Binding of DFHBI locally induces structural changes, mainly concerning five nucleosides from a helical stem structure called P2 that is flanking the GQ. In the DFHBI-bound state, these nucleotides together with the GQ form a hydrophobic binding site, which stabilizes DFHBI´s planar conformation and restricts its motion. Upon binding of DFHBI to Spinach, the chromophores fluorescence is strongly increased[252,254,258]. For C11.41 and C11.41_A15G a similar scenario is thinkable. The GQ could serve as a platform onto which the tricyclic, hydrophobic and almost planar small molecule THC could stick. Adjacent nucleotides could interact with the hydroxy-group and the carboxylic acid (in case of THCA) via H-bonds. The benzyl-modification could also participate in stabilizing the THC orientation on top of the GQ by π-π -stacking. Naturally this hypothesis would have to be confirmed via crystal structures of the clickmer with THC and THCA.

Another explanation for the function of the hypothetical stem-loop might be possible interactions with the matrix onto which THCA was immobilized. The introduction of the linker naturally altered the chemical structure of THCA, which was used for immobilization purposes (**Figure 16**). The immobilized compound offers several polar functional groups that are not present in case of solubilized THC or THCA. In the immobilized state there are two amide-bonds as well as two further oxygens containing to the attached linker, wherewith the oligonucleotide could interact. Furthermore, the magnetic particles of the dynabeads are caught in a functionalized polystyrene cage coated with a polyurethane layer[358]. Potential interactions between the clickmer and this scaffold also cannot be excluded. Therefore, the stem-loop part of C11.41 could potentially interact with the linker and the adjacent bead-surface and thus increase the affinity of the sequence to THC-modified beads. This would mean that this part of the sequence does not participate at all in interactions with the THC-core. As already discussed, the GQ-domain of C11.41 alone, which consists of 19 nucleotides already shows detectable, though reduced affinity to THC-modified beads (**Figure 26**). On the other hand, the 41 nucleotide long sequences C11.41 and C11.41_A15G show reduced affinities to THCA and THC in solution, compared to the THC-modified beads (see below, **section 4.3.4**). Eventually the reason for the reduced affinity of the 19-mers to THC-modified beads, as well as the reduced affinity of C11.41 (C11.41_A15G) to solubilized THCA and THC is the same. In both cases a relevant part of one binding partner is missing. The 19-mer lacks the stem-loop that interacts with the linker and bead-surface.

In case of solubilized THCA and THC the linker and bead-surface of the THC-modified beads are missing. Therefore, interaction with the nucleotides of the hypothetical stem-loop of C11.41 cannot occur. Thus, in both cases the total affinity is significantly weakened.

4.3.4 Applicability of C11.41 for THC detection in aqueous solutions

The determined IC_{50}-values in the competition assay (**Figure 36**) are just a mathematical approach to quantify binding. Comparing the dissociation constant of C11.41 (C11.41_A15G) to THC-modified beads and the IC_{50} value for free THCA is difficult in this case. First of all, the term IC_{50} is not really correct in this context, since it originates from enzyme kinetics and determines the inhibitor-concentration needed to halve the reaction rate of a given enzyme, thus leading to half-maximal inhibition. Usually, IC_{50} is not equivalent to the k_i-value, which is the dissociation constant of enzyme and its inhibitor. For competitive inhibition however, the IC_{50} and k_i- value become roughly equal, when the substrate concentration [S] is infinitesimal[359,360]. For the competition scenario that was performed via flow cytometry, the substrate can be said to be the THC-modified beads and its concentration indeed is very small. Therefore, the calculated IC_{50}-value is equal to the k_i-value, which in this case is the dissociation constant between the clickmer and free THCA in solution. Since the IC_{50}

was calculated to be roughly 16 µM (**Figure 36**), the affinity of C11.41 to THCA in solution can be estimated to be around 16 µM.

As mentioned, it could be demonstrated that C11.41 (C11.41_A15G) besides THCA also recognizes THC in free solution. Of course, this result was quite pleasing. Still, recognition of THC was not self-evident, since the chemical discrepancy between the THC-modified beads and the free THC is even higher than the difference between the immobilized THC and THCA. THC is lacking the carboxylic acid known from THCA, and of course also does not carry the amide group known from the THC-modified beads. Still with the competition assay an IC_{50}-value (equivalent to k_i-value) of ~ 100 – 230 µM for both oligonucleotides could be estimated, meaning that also this compound is bound in solution by the clickmer. It is a delightful result that THC is also bound in solution, since this is the psychoactive compound of *cannabis sativa* and SELEX was initially started to get clickmers for THC.

Of course, the observed affinity to THCA and THC in solution must be seen with caution, since the way it has obtained is quite “indirect”. An additional assay would be of great help to confirm that result, however another way to visualize binding in solution has not been found so far, for this specific case. However, if the clickmer should be applied within an oral fluid (OF) roadside test for THC, the affinity of that clickmer should somehow be ascertainable.

MST and FP-assays did not show binding of the clickmer to either THCA or THC. Since the rigid GQ-structure of C11.41 probably does not significantly change upon binding to THCA. Therefore, probably no structural reorganization of the oligonucleotide takes place and no thermophoretic alterations occur, which explains the failure of MST (**Figure 34**). The FP-assay might not have worked due to the fluorescently labeled THC that was applied in this case (**Figure 35 a**). The THC-L-FITC obviously differs from THCA and THC. The applied THC-L-FITC lacks the carboxylic acid respectively the chemical linker at the C2-position of the tricyclic ring system (compare to **Figure 1 a**), which is present in free THCA or the compound which was immobilised for SELEX purposes (concerning to the dibenzopyran numbering of THC). Therefore, it might be that this compound is not interacting with the clickmer at all. Another explanation for the failure of the assay could be, that the difference in molecular weight of free THC-L-FITC and the complex of the clickmer together with THC-L-FITC is not big enough, meaning that the rotational diffusion is not altered enough to see an effect in this assay.

Surface plasmon resonance (SPR) might be a further method to determine affinity of the clickmer to THC[361,362]. The clickmer would have to be immobilized on a chip surface and solubilized THC in increasing concentrations would be titrated into the binding solution. SPR has not been performed for this case, yet. Large amounts of the oligonucleotides are necessary for this assay. Furthermore, if that kind of measurement is suitable to determine binding of C11.41 to THC is not guaranteed.

If clickmers should be useful biosensors in saliva-based roadside test devices for THC they should be capable to detect the drug in the lower nanomalar range, as it is proposed by DRUID[65] (1ng/ml = 3.18 nM) and SAMSHA (2 ng/ml = 6.36 nM)[130]. Hitherto performed affinity determination of the clickmer C11.41 and C11.41_A15G resulted in k_D-values of about 120 nM to THC-modified beads, respectively 16 µM for solubilized THCA. Affinity to solubilized THC was even further reduced. Hence, the found sequences will not be applicable in such roadside test devices. The affinity of clickmers for solubilized THC should be significantly lower than that found for C11.41, since it should be capable to specifically and selectively recognize nanomolar quantities of THC in saliva samples.

In **Figure 37** a simplified lateral flow test was run with the full-length sequence C11, as well as C11.41 and C11.41sc. Neither of these oligonucleotides specifically bound to the BSA-THC conjugates that were spotted onto the nitrocellulose membrane of the lateral flow stripe. Naturally, one explanation for the failure of this test might be, that the affinity of the clickmer is not high enough to detect the THC. The amount of THC-BSA conjugates that were spotted onto the membrane were 0.05 µg and 0.2 µg in this case. It is not exactly known how many molecules THC are conjugated per BSA. Another explanation of course might be that THC conjugated to BSA is not recognized by the clickmer sequence, since the chemical structure of THC is again differing from the SELEX-target. Furthermore, it might be, that THC is strongly interacting with the surface of BSA via hydrophobic interactions, hence the interaction of THC with the clickmer is blocked by the bulky protein.
It can indeed be assumed that THC strongly sticks to BSA, since an obvious change in fluorescence-polarisation was observable when BSA was added into the solution of THC-L-FITC (**Figure 35**). This change in fluorescence-polarisation can probably be explained by sticking of THC-L-FITC to the protein. If this is mainly caused by the THC-core or the conjugated FITC cannot be further specified. Still it can be assumed that there is an unspecific interaction of BSA to THC.

The utilized lateral flow test is just a model (**Figure 37 b**) that was used to verify binding of THC by the discovered clickmer. The build-up of an actual clickmer-based lateral flow device which can be used in road-side testing will different from the explained one. Like for aptamer-target interactions, the binding of THC by a clickmer could be transduced to a detectable colorimetric signal. One possibility to visualize interactions of aptamers to proteins[363], whole cells[364], as well as small molecules like toxins, or drugs[238,365] could be the use of gold nanoparticles (AuPNs). Several formats are possible to construct aptamer-based lateral flow devices. Though similar approaches are not known for clickmers yet, it is likely, that the functional principle is also compatible with those base-modified oligonucleotides.

4.4 DFHBI derivatives for live cell imaging purposes

4.4.1 Applicability of PA-DFHBI for live-cell imaging.

The synthesized PA-DFHBI that carried *o*-nitrobenzyl as a PPG did show expectable results *in vitro*. The compound was bound by Spinach2 and Broccoli (see **Figure 40**, and **Figure 41**). Fluorescence of these complexes was quenched as long as the *o*-nitrobenzyl group was not photolytically cleaved off. Upon removal of the PPG however, typical green fluorescence of DFHBI o-nitrobenzyl group could be seen (**Figure 39**). Functionality of the photoactivatable PA-DFHBI in bacteria was also confirmed (**Figure 44**). Fluorescence of Spinach2 and Broccoli expressing E. *coli* incubated with PA-DFHBI could be activated via photolytic removal of the PPG. In HEK cells however the same tendency could not be seen. Cells expressing Spinach2 directly showed green fluorescence when incubated with PA-DFHBI. In this thesis only the pAV5S Spinach2 plasmid was used for the transfection of HEK cells, though a plasmid for the expression of Broccoli was also available. But since PA-DFHBI did not perform in cells as expected, the same experiments with Broccoli expressing cells were omitted. Malfunctioning of PA-DFHBI in HEK cells must be a reason for this unexpected result and therefore is independent on the expressed aptamer.

The most likely explanation for that scenario is, that the PA-DFHBI solution was contaminated with normal DFHBI. However, HPLC-chromatogram of PA-DFHBI only showed one UV-absorbance peak. Possible contaminations with DFHBI could not be detected with this method. Still that result does not rule out contamination of the PA-DFHBI solution with tiny amounts of DFHBI.
In fact, contaminations remain the most logical reason for the observed result. It is extremely unlikely that the *o*-nitrobenzyl group is cleaved off in a nonradiative way. The *o*-nitrobenzyl group has already been applied for fluorescence quenching of other fluorophores[366–369]. The PPG usually is photolytically released from the caged compounds[370,371]. In 2014 Han *et. at.* has shown that o-nitrobenzyl ethers can also be chemically cleaved[372]. However, 20% aqueous NaOH in methanol at 75°C is required for that cleavage and the PA-DFHBI has not been exposed to such conditions. Therefore, the o-nitrobenzyl group should not be cleaved off chemically. Furthermore, it can be ruled out that the *o*-nitrobenzyl ether bond is somehow cleaved of by unknown processes inside the mammalian cells, since *o*-NB caged compounds already have been shown to work intracellular[373,374]. Though oxidoreductases like the human cytochrome P450 enzymes are known to be capable to cleave some ether bonds, *o*-nitrobenzyl ethers do not belong to these substrates[375].

Theoretically the PPG could be accidentally cleaved during careless handling of the compound. However, this was tried to be avoided as far as possible. During treatment of HEK cells the PA-DFHBI solution was shortly exposed to (white light). However light intensity and the short period of time should not be sufficient to remove the PPG. This is particularly true, since for experiments with bacteria the PA-DFHBI solution was also temporarily exposed to white light and varying temperatures and in that case undesired

removal of the PPG did not occur. Therefore, it would be worthwhile to redo the synthesis of PA-DFHBI and the experiments with HEK cells. Instead of the *o*-nitrobenzyl group, derivatives of it like 1-(2´-nitrophenyl)ethyl (NPE) could also be applied.

4.4.2 Applicability of eDFHBI as chromophore for fluorescent RNA aptamers.

The synthesized enlarged DFHBI (eDFHBI) theoretically could be an alternative fluorophore that is bound and whose fluorescence is enhanced by Spinach, or Broccoli aptamers. Besides the Mango aptamers that also recognize two derivates of thiazole orange (TO1 and TO3), further RNA aptamers exist that bind and activate two different cyanine dyes[376]. Thus the fluorescent color of the aptamer DIR2s-Apt can be switched by simply exchanging the cyanine dye in the medium[376]. If the affinity of Spinach or Broccoli aptamers to eDFHBI would be in the same range as to DFHBI, the fluorescent color would be arbitrary by the choice of the fluorophore, comparable to the situation for DIR2s-Apt.

Compared to DFHBI, eDFHBI showed a significantly red-shifted fluorescence. In addition, the stokes-shift was tremendously increased for eDFHBI. While both fluorophores could be excited at 460 nm, DFHBI-fluorescence in complex with Spinach was observed at 505 nm. For eDFHBI however emission at 600 nm was seen. Fluorescene of eDFHBI could be slightly increased upon binding to the Baby-Spinach aptamer. It can therefore be assumed that eDFHBI does occupy the same binding pocket provided by Baby-Spinach as DFHBI does[252]. However, eDFHBI presumably is too large to perfectly fit into this pocket, which is most likely the reason for the poor affinity of Baby-spinach to that compound (**Figure 51**), as well as the poor enhancement in fluorescence intensity (**Figure 52**). Assuming the difluorophenol-part of eDFHBI and DFHBI both occupy exactly the same position within the Baby-Spinach binding pocket (compare to **Figure 13**), then the imidazolinone ring would not occupy its ideal location within that binding pocket in case of eDFHBI. Thus, the imidazolinone ring of eDFHBI does not properly interact with the nucleotide G28 and the 2´-OH of A53 of the aptamer (compare to **Figure 13**). However, these interactions are known to be important for an optimal fluorescence intensity of DFHBI[252]. It is therefore likely that fluorescence of eDFHBI is not effectively enhanced by Baby-Spinach due to the loss of the mentioned interactions. In this thesis only Baby-Spinach has been tested to increase the fluorescence intensity of eDFHBI. It might be that Broccoli or dimeric Broccoli are better capable to enhance that fluorescence. However this remains unlikely since Baby-Spinach and Broccoli share an almost identical binding core for DFHBI[377].

To obtain an aptamer that effectively increases the fluorescence of eDFHBI, an RNA SELEX for that target has been done with a SUL I library. SELEX did not seem to be successful as radioactive and fluorescent binding experiments with libraries of different

SELEX cycles implied (**Figure 54**). Probably in SELEX for eDFHBI a starting library containing an universal pre-formed stem-loop should be used, as has been done for the SELEX of Spinach or DIR2s-Apt[252,376]. Since Baby-Spinach already led to slight fluorescence increase of eDFHBI, it might be possible to perform a SELEX similar to that performed for the discovery of iSpinach[257]. It might be that alterations within the G-quadruplex containing binding pocket of Spinach lead to higher affinities of the RNA to eDFHBI as well as an improved fluorescence enhancement of the compound. Thus random mutagenesis SELEX with Spinach based sequences in combination with a high throughput screening technique might be useful. Sequences capable to bind eDFHBI with high affinity and that efficiently enhance its fluorescence could easily be isolated[257].

Unfortunately, eDFHBI alone already showed remarkable autofluorescence. For live cell imaging applications this characteristic is disadvantageous, since it would imply extremely high background fluorescence in cells. Therefore, another selection for eDFHBI would not be advisable due to the already mentioned high autofluorescence of that compound. A probably more reasonable approach to get to a red fluorescent Spinach-chromophore system would be the synthesis of other DFHBI-like compounds. Potentially promising compounds could be the chromophore analogues of the red fluorescent protein (RFP) synthesized by Yao *et. a*l. that were named, e.g., DFHBSI, DFHBNI[378]. G-quadruplex containing DNA aptamers induced red fluorescence of these compounds[378]. The core structure of DFHBI is preserved within these compounds which increases the possibility that they fit into the binding pocket of Spinach and Broccoli aptamers. However, if Spinach binds these chromophores, it is again likely that its affinity to these compounds is reduced, compared to the affinity to DFHBI. This can be said since bulky CF_3-substituents that are substituting the methyl group at the C2 position on the imidazolinone ring of the compound DFHBI-2T already reduces the affinity. The DFHBSI and DFHBNI chromophores also carry bulky substituents at this position. However, since DFHBSI and DFHBNI do not show autofluorescence, these chromophores are more convenient for the development of a red fluorescent RNA system.

5. Outlook

5.1 Further SELEX strategies for THC-binding clickmers

Click-SELEX for THC-modified magnetic beads resulted in clickmers capable to bind the immobilized target with nanomolar affinity. The in advance chosen benzyl-modification showed a significant contribution to the determined affinity. However, recognition of the clickmer to THC and its chemically closely related compound THCA in solution seemed largely lost. It is hypnotised that the clickmer also interacts with parts of the bead surface, whereon THCA was immobilized for the SELEX. Recognition of solubilized THC by the clickmer with high affinity and specificity however is an essential requirement, if the clicker should find application as a sensor molecule in roadside OF test devices. Thus, the found clickmer cannot be used for that intended purpose.

Especially in case of SELEX for small molecules as THC, the immobilisation of the target molecule is likely to cause complications. There is a high probability that not only the target molecule itself, but also the linkage to a solid support as well as the solid support itself are contributing to binding interactions with oligonucleotides. It is very difficult to avoid such undesired interactions. One promising way to prohibit interactions of oligonucleotides with a solid support is Capture-SELEX. As described in the introduction (section 1.3.1), for this type of SELEX there is no need for immobilisation of the target molecule. Instead the SELEX library containing a short docking sequence is annealed to a complementary capture-oligonucleotide, which in turn is immobilised on magnetic beads. If oligonucleotides interact with the solubilized target molecule, a conformational change within the sequence might occur which disrupts basepairing to the capture-oligo. Thus, the sequences that bind to the target are eluted from the magnetic particles and can be amplified for further SELEX cycles[166,168].

For prospective SELEX approaches, it might be possible to combine the techniques of click-SELEX with that of capture-SELEX[167]. The need to alter the chemical structure of THC for the purpose of immobilization would be circumvented in this case. This in turn could lead to potential clickmers with higher sensitivity for THC, since the actual, non-modified compound can be used in this case. In addition, capture-SELEX relies on an induced conformational change of the oligonucleotide upon binding to the target molecule. This in turn might be beneficial for the purpose to develop a road-side test based on the resulting clickmer. Oligonucleotides undergoing a strong conformational change upon binding to the target can easily be utilized *, e.g.,* in a competitive lateral-flow clickmer assay[380].

It has to be seen however, if devices that detect THC in saliva are the best way to proof recent marijuana consumption in road users. Meanwhile a breathalyser, comparable to that for alcohol is being developed[381]. With the help of semiconductor-enriched single-walled carbon nanotubes (s-SWCNTs), THC can be detected in breath of suspects. A breathalyser-prototype using nanotechnology and machine learning can

detect tiny amounts of THC in breath. If THC is present in breath, it adsorbs to the nanotubes, which changes their electrical properties. Using machine learning THC can specifically be detected by the way the nanotubes react to electrical current. Accordingly, this method provides more accurate results than mass spectrometry[381].

5.2 Photoactivatable DFHBI derivatives

The herein synthesized photoactivatable PA-DFHBI showed functionality *in vitro* as well as in bacteria with Spinach2 and Broccoli. However, in mammalian cells the system did not work. The observed spontaneous fluorescence emission in HEK cells without previous photolytic removal of the PPG on PA-DFHBI is most likely caused by tiny contaminations of the PA-DFHBI solution with DFHBI. In theory the system should also work in HEK cells. Therefore, a new synthesis of PA-DFHBI could be done. Contaminations of the compound with original DFHBI should be persnicketily avoided. Alternatively, instead of *o*-nitrobenzyl-, other caging groups as, e.g., 2-(4-nitrophenyl)ethyl (NPE) could be used as PPG.

5.3 DFHBI derivatives for the development of re-shifted FLAPs

The herein synthesized eDFHBI indeed did show a red-shifted emission wavelength compared to the original DFHBI. It could be shown that the aptamer Baby-Spinach was capable to bind the newly synthesized DFHBI derivative. Furthermore, binding of the fluorophore by the aptamer also further enhanced the intrinsically high fluorescence of eDFHBI. Though no assay was done to determine the actual k_D-value of Baby-Spinach to eDFHBI, it can be assumed that the affinity of the aptamer to the fluorophore is distinctly weaker than that to the original DFHBI.
RNA SELEX with a library containing a completely randomized region did not result in aptamers that bind and increase the fluorescence of eDFHBI. Potentially further performed SELEX should be done with libraries containing pre-formed stem-loop structures. Alternatively using random mutagenesis hypothetically aptamers could be discovered, that bind eDFHBI with high affinity and furthermore enhance te red fluorescence of tat compound.
However, in contrast to DFHBI, eDFHBI already showed a strong autofluorescence. This strong fluorescence even in absence of binding RNA aptamers is disadvantageous in context of intracellular imaging purposes, since it presumable would show high background fluorescence. Therefore it might be advisable to use other DFHBI derived fluorophores that do not show such a strong autofluorescence to develop a FLAP emitting red-shifted fluorescence.

6. Methods

6.1 Synthesis of used THC and DFHBI derivatives

6.1.1 Synthesis of THC-PEG for immobilization on solid support

As a first step, N-Boc- 2,2′-(ethylenedioxy)diethylamine was synthesized. 2,2′ (Ethylenedioxy)bis(ethylamine) was dissolved in dioxane. To that solution 0.1 eq. of Di-*tert*-butyl dicarbonate dissolved in dioxane was slowly added. Subsequently, the solvent was evaporated the crude residue dissolved in CH_2Cl_2. The solution was washed 2x with water and 2x with saline. Finally, the CH_2Cl_2 was evaporated. A slightly yellow oil (*N*-Boc- 2,2′-(ethylenedioxy)diethylamine) resulted.

Next the so-called THC-PEG was synthesized. The resulting compound was used for immobilisation on solid support. The carboxylic acid of THCA was starting point for chemical modification of that compound. The carboxylic acid was first converted into an acid amide. Therefore, THCA was dissolved in $CHCl_3$ and a 2-fold excess of EDC was added to the solution. After 2h of incubation, 1.5 eq. of *N*-Boc- 2,2′-(ethylenedioxy)diethylamine were added. The mixture was shaken for 2 days at room-temperature and the reaction procedure monitored via HPLC-MS (**section 6.6.1**). After completion of the reaction the BOC-protected compound was purified over HPLC. Subsequently, the solvent was evaporated and the compound was dissolved in 4N HCl in dioxane for 2h, to remove the BOC protection group. After removal of the acidic solution, HPLC-purification was again conducted. Formation of the desired product was again confirmed via HPLC-MS and the final product was dissolved in borate buffer of pH 9.5 with 30% DMSO in a final concentration of 5 mM.

6.1.3 Synthesis of PA-DFHBI

For the synthesis of DFHBI the procedure described by Paige *et. al.* was used[252]. DFHBI was stirred with an equimolar amount of 2-nitrobenzylchloride and a 2-fold molar excess of K_2CO_3 in DMF overnight. The resulting product was purified via flash chromatography.

6.1.4 Synthesis of eDFHBI

Two different strategies were used for the synthesis of eDFHBI. The synthesis performed by Julia Hahn[336] started with a Heck-reaction. N-methoxy-N-methylacrylamide was stirred with a 2-fold excess of 4-bromo-2,6-difluorophenole and sodium acetate in presence of catalytic amounts of Tetrakis(triphenylphosphine)palladium(0) in DMF at 120°C overnight. The organic phase was washed with saturated NaCl and NH_4Cl solutions. The aqueous phases were extracted with ethyl acetate solution.

Solvent was evaporated and the product purified via flash chromatography. Resulting 3,5-difluoro-4-hydroxy-N-N-methyl cinnamide was reduced with 1.3-fold molar excess of $LiAlH_4$ in THF at -40°C for 5 minutes. A 1 M solution of NaCl was added to quench the reaction. THF was evaporated and the reaction product purified via flash chromatography. With the resulting aldehyde ((2E)-3-(3,5-difluoro-4-hydroxyphenyl)prop-2-enal) the following steps were analogous to those for the synthesis of the original eDFHBI[252].

Synthesis performed by Sandra Trapp[337] started with a Duff-reaction to yield 3,5-difluoro-4-hydroxy-benzaldehyde. 2,6-difluorophenole was stirred with equimolar amount of hexamethylenetetramine in TFA at 80°C overnight. Saturated $NaHCO_3$ solution was added. The aqueous phase was extracted with CH_2Cl_2 and the resulting organic phase acidified to pH 1 with HCl solution. The solvent was subsequently evaporated. The resulting 3,5-difluoro-4-hydroxy-benzaldehyde was a 2-fold excess of diisopropylethylamine and methoxymethyl chloride at room temperature in CH_2Cl_2 overnight. Reaction was quenched with NH_4Cl solution and the organic solvent evaporated. The product was purified via flash chromatography.

For the Wittig-reaction equimolar amounts of NaOH and Tributyl (1,3-dioxolan-2-ylmethyl)phosphonium bromide together with 18-crown-6 was stirred in THF for four hours. Then an equimolar amount of 3,5-difluoro-4-(methoxymethoxy)benzaldehyde was added and the solution was stirred overnight. Water was added to quench the reaction. The aqueous phase was extracted with CH_2Cl_2 and the combined organic fractions evaporated. Resulting solid was dissolved in THC and 1N HCl solution was added. The organic fraction was separated and evaporated. The product was purified via flash chromatography. Again, with the resulting aldehyde the subsequent steps were analogous to those for the synthesis of the original DFHBI[252]. Additionally, the last reaction step was also performed with N-Boc-1,6-hexanediamine instead of methylamine, to obtain eDFHBI carrying a free amine. Thereof, the last reaction step that is shown in was performed with N-Boc-1,6-hexanediamine instead of methylamine. The BOC-group was subsequently removed with 4N HCl in dioxane. The resulting compound was used for immobilisation to M280-tosylactivated Dynabeads, as well as to epoxy-activated sepharose.

6.2 Preparation of solid support for SELEX

6.2.1 Immobilisation of THC-PEG on magnetic beads

M280 tosyl-activated Dynabeads resided at a concentration of 30 mg/ml in a storage buffer. The calculated loading capacity of the beads was 4.5 µmmol/l of bead-suspension. 500 µl of beads, needed for the upcoming coupling step, were removed from the storage container and the storage buffer was removed. The same was done with 200 µl beads which were subsequently not coupled to PEG-THC. Beads were washed 5x for 2 min with 1 ml of borate buffer pH 9.5. For the coupling reaction, the beads were suspended in the 5 mM solution of PEG-THC in borate buffer (with 30% DMSO) and shaken for 2 days at room temperature. Afterwards, the buffer was removed, and the beads washed 3x with 1 ml borate buffer. For blocking of unreacted tosyl-groups, beads were shaken for 10h in borate buffer containing 5% Methyl-amine. This step was also performed for the beads that were not coupled to the target molecule. At the end, the buffer was removed from both beads-suspensions, beads were washed 3x with 1 ml borate buffer for 3 min and 5x with SELEX buffer for 2 min, and then dissolved in a volume to obtain a 30 mg/ml bead suspension again. Beads were stored at 4 °C.

6.2.2 Detection of THC on magnetic Dynabeads and lateral flow stripes

To verify a successful coupling of PEG-THC to the magnetic Dynabeads, THC antibodies were used. For this purpose, the initially prepared bead-suspensions (**section 6.1.3**) were diluted 1:10 in PBS buffer, resulting in a 3 mg/ml suspension. 30 µl of these suspensions were washed 2x with 1 ml PBS + 0.1% BSA for 15 min at 37°C. In 148.5 µl PBS, 1.5 µl of a monoclonal mouse THC-antibody (Fitzgerald) was added and incubated with the beads for 1 h at 37 °C and 400 rpm. Liquid was removed again and the beads were again washed 3x with 500 µl PBS + 0.1% BSA for 5 min at 400 rpm. The liquid was removed,149 µl PBS and 1µl of (1:1000 diluted) goat anti mouse antibody (GAM 647) were added and incubated for 30 min at 37 °C and 400 rpm. The liquid was removed again, beads were washed 5x with 500 µl PBS + 0.1% BSA, and finally the beads were suspended in 50 µl PBS. 30 µl of that suspension was pipetted onto the glass surface of the Odyssey reader. The fluorescence of the secondary antibody was recorded at 700 nm.

A quite similar approach was done with the lateral-flow stripes equipped with the BSA-THC conjugates. Stripes were incubated 20 in ml PBS + 0.1% BSA. Stripes were shaken for 20 min at room-temperature. After the membrane was dried completely the stripes were incubated in a mixture of 6.71 µl of the monoclonal mouse THC-antibody in 1 ml PBS buffer for 30 min at 37 °C. Afterwards the stripes were washed 3x with 10 ml PBS + 0.1% BSA for 15 min. Then 6.71 µl of the GAM 647 in 1 ml PBS were added to the stripes.

The samples were incubation for 30 min at 37 °C was followed by 5 additional washing steps of the stripes in PBS + 0.1% BSA. The membranes were dried and the fluorescence on the stripes was recorded with the Odyssey reader.

6.2.3 Immobilisation of eDFHBI-NH_2 on magnetic beads

Again, M280 tosyl-activated Dynabeads were used. 500 µl of beads were removed from the stock solution for the subsequent coupling reaction of eDFHBI-NH_2. Additionally, 200 µl of beads were removed, whereon no target was coupled. Beads were suspended in a 5 mM solution of eDFHBI-NH_2 in borate buffer pH 9.5 (with 10% DMSO) and shaken overnight at room temperature. The buffer was removed and beads washed 3x with 1 ml borate buffer. For blocking of unreacted tosyl-groups, beads were shaken for 10h in borate buffer containing 5% Methyl-amine. This step was also performed for the beads that were not coupled to the target molecule. Finally, beads were washed 3x with 1 ml SELEX buffer and a suspension of 30 mg/ml was stored at 4°C in SELEX buffer.

6.2.4 Immobilisation of eDFHBI-NH_2 on epoxy activated sepharose

A 30 mM eDFHBI-NH_2 solution in HEPES pH 8 (with 10% DMSO) was prepared. 2x 100 mg sepharose was removed and swollen in water. The waer was removed and the sepharose washed with 300 ml H_2O. Swollen beads were incubated with the eDFHBI-NH_2 solution on a shaker overnight. To block remaining epoxy-groups a 5% methylamine solution in HEPES pH 8. This was also done with sepharose that was not coupled to the target. The solutions were removed and beads stored in HEPES pH7.4 at 4°C

6.2 Working with nucleic acids

6.2.1 Polymerarse chain reaction (PCR)

6.2.1.1 PCR for click-SELEX

To amplify EdU-containing DNA, *Pwo*-polymerase (Genaxxon) was used. The protocol is depicted in **Table 14**. The forward-primer was 5´-Cy5-labeled, the reverse primer had a phosphate group at the 5´-end. For each SELEX-cycle the volume of all components was scaled-up to achieve a total volume of 800 µl. Samples were prepared on ice. The PCR was performed in a Biometra T3-Master cycler. The thermocycler was pre-heated to 95 °C. The performed program was as follows: 2 min 95°C, 30 s 95°C, 30 sec. 62 °C, 1 min 72°C, ∞ min 4°C. PCR performance was checked with agarose-gel electrophoresis (**see section 6.2.7**)

Table 14. 100 µl PCR-mix for click-SELEX.

Compound	Volume [µl]	Stock concentration	Final concentration
PWO DNA polymerase buffer (with 2 mM Mg^{2+})	10	10x	1x
5´-primer	1	50 µM	0.5 µM
3´-primer	1	50 µM	0.5 µM
d*NTP-mix (1:1:1:1; dATP, dCTP, dGTP,EdUTP)	1	25 mM	250 µM
PWO DNA polymerase	1	2.5 U/µl	0.025 U/µl
template	X		0.5 pmol
ddH_2O	Fill up to 100 µl		

6.2.1.2 PCR for Spinach, and Broccoli constructs and RNA libraries.

To amplify Spinach2, Baby-Spinach, Broccoli, and a mutant RNA (Mut) the following mixtures (**Table 15**) was used. The following program on a thermo cycler was applied: 1 min 95 °C, 1 min 95°C, 1 min 55°C, 1 min 72°C, storage 4°C. PCR performance was checked with agarose-gel electrophoresis (**section 6.2.6**). During SELEX for eDFHBI with the Sul I library the mixture of **Table 15** was also used. For amplification of the Sul I library the following program on a thermocycler was used: 1 min 95°C, 30 sec 95°C, 30 sec 60°C, 30 sec 72°C, storage 4°C.

Table 15. 100 µl PCR-mix for Spinach and Broccoli constructs, and Sul I library.

Compound	Volume [µl]	Stock concentration	Final concentration
Pfu-Polymerase buffer	10	10x	1x
$MgCl_2$-solution	8	25 mM	2 mM
5´-Primer	1	100 µM	1 µM
3´-Primer	1	100 µM	1 µM
dNTP-mix	1	25 mM	250 µM
Template	x		
Pfu-Polymerase	1	2.5 U/µl	0.025 U/µl
ddH_2O	Fill up to 100 µl		

6.2.1.3 Reverse transcription PCR of Sul I library

During RNA SELEX for eDFHBI the RNA of different SELEX cycles had to be reverse transcribed for amplification purposes. **Table 16** summarizes the mixture needed for the reverse transcription. The mixture was incubated at 60°C for 5 min and was subsequently cooled to 4°C.

Table 16. Mixture for reverse transcription PCR.

Compound	Volume	Final concentration
5x Gotaq Flexi Buffer (Promega)	20	1x
5x 1st strand buffer (Invitrogen)	4	0.2x
100 mM DTT	2	2 mM
50 µM For-primer	1	0.5 µM
50 µM Rev-primer	1	0.5µM
25 mM $MgCl_2$	6	1.5 mM
25 mM dNTPs	1.2	300 µM
RNA	62.8	

Finally, 1 µl of superscript reverse transcriptase as well as 1 µl of Gotaq Flexi DNA polymerase (5 U/µl) was added and the PCR program mentioned in **section 6.2.1.2** was applied.

6.2.2 λ-Exonuclease digestion to single stranded DNA

dsDNA obtained via PCR was purified using spin-columns (see **section 6.2.10.1**) and subsequently degraded to single stranded DNA. 5 µl λ-Exonuclease (5000 U/ml; Thermo Scientific) together with 20 µl of the corresponding 10x nuclease buffer were added to 200 µl dsDNA solution in water and incubated for 60 min at 37°C. The 5´→3´-exodeoxyribonuclease selectively digests the 5´-phosphorylated strand of the dsDNA. Successful exonuclease digestion was confirmed by agarose-gel electrophoresis (**section 6.2.6**).

6.2.3 Click-reaction with single stranded DNA

For click-reaction, a click-catalyst solution was prepared. First, a 100 mM ascorbate solution was prepared by the addition of 500 µl ddH_2O to 10 mg sodium-ascorbate. To avoid oxidation of ascorbate in water, this solution had to be prepared freshly for each click-approach.

Ingredients for 100 µl of click-catalyst solution are listed in **Table 17 a.** For each click-reaction that solution was freshly prepared, to preclude the presence of Cu(II) ions. Cu(II)SO_4 is *in situ* reduced to Cu(I) with ascorbate. Tris(3-hydroxypropyltriazolylmethyl) amin (THPTA) is water-soluble ligad for Cu(I) ions, which stabilizes the Cu(I) oxidation state and thereby protects DNA from oxidative damage[229].

Table 17 a. Catalyst solution for click-reaction of DNA with azides.

Compound	Volume [µl]	Stock concentration	Final concentration [nM]
Sodium ascorbate	25	100 mM	25
THPTA	4	100 mM	4
$CuSO_4$	1	100 mM	1
H_2O	70		

Preparation of a 100 µl click-reaction was done as described in **Table 17 b**. Reaction was incubated for 1h at 37 °C and 650 rpm. Subsequently, the clicked DNA was purified using spin columns (**section 6.2.10.1**).

Table 17 b. Mixture for click-reaction of single-stranded DNA.

Compound	Volume [µl]	Stock concentration	Final concentration
ssDNA	70		
10x PBS buffer	10	10x	1x PBS
Azide (dissolved in DMSO)	10	10 mM	1 mM
Click-catalyst solution	10		

6.2.4 Transcription of Spinach2 and Broccoli-constructs as well as Sul I library

PCR products of the Spinach and Broccoli constructs as well as the Sul I library were done with forward primers containing a T7-promotor. Thus, transcription could be done to result in the desired RNA. **Table 18** summarizes the transcription mixture. The mixtures were incubated at 37°C overnight.

Table 18. 100 µl transcription mixture.

Compound	Volume [µl]	Stock concentration	Final concentration
Tris-HCl pH 7.9	20	200 mM	40 mM
$MgCl_2$	1.7	1500 mM	25 mM
DTT	5	100 mM	5 mM
NTP-mix	10	25 mM	2,5 mM
RNAsin (Promega)	1.24	40 U/µl	0.5 U/µl
IPP (Roche)	0.2 µl	2 U/µl	0.02 U/µl
dsDNA template	10		
T7 RNA-Polmerase	10	50 U/µl	0.5 U/µl
ddH_2O	41.86		

6.2.5 Polyacrylamid-gel electrophoresis

The transcription yield was checked via agarose-gel electrophoresis. RNA was precipitated. To the transcription volume 1/10 volume of 3 M NaOAc solution pH 5.4 as well as 3 volumes EtOH were added. The solution was spun at 20817 g for 30 min at 4°C. The supernatant was removed, and the pellets washed 2x with 70% EtOH solution. Finally, the pellets were suspended in polyacrylamide loading buffer.

Table 19. Mixture for the preparation of a 10% PAA gel.

Compound	Volume
30% Acrylamid,0,8%BisAA in 8.3 M Urea	28 ml
8.3 M Urea	35 ml
8.3 M Urea in 10x TBE	7 ml
10 % APS	560 µl
TEMED	28 µl

A 10% polyacrylamide-gel was prepared as summarized in **Table 19**. The gels were run for 2 h at 350 V; 20 W. After completion of the run, RNA was visualized via UV-shadowing and sliced out. RNA was eluted from the polyacrylamide gels via electroelution in 1M NaOAc solution.

6.2.6 Agarose-gel electrophoresis

To validate the correct length and purity of dsDNA, ssDNA, and RNA, 4% agarose gels were used. For this purpose, 12 g agarose were suspended in 300 ml TBE-buffer the suspension boiled in the microwave until a colorless viscous solution resulted. Before pouring into corresponding forms, ethidium bromide was added in a 1:10000 dilution. Poured gels could be stored at 4 °C for several weeks.

5 µl of dsDNA or ssDNA samples were mixed with 1 µl of 6x DNA loading-buffer and samples were loaded onto the gel. The gels were run for 15 min at 250 V in 0.5x TBE-buffer. Afterwards they were examined in a UV illumination chamber. The size of the DNA products was compared to a DNA ultra low range ladder (Life technologies).

6.2.7 Concentration determination

Oligonucleotide concentrations in solution were determined in two ways. The first method of determination was via UV-absorption. Absorbance maximum of DNA is around 260 nm. Concentration of oligonucleotides can be calculated with the Lambert-Beer equation. With the molar extinction extinction coefficient of the given DNA strand, the concentration could be calculated.

$$A\lambda = -\lg\left(\frac{I}{I0}\right) = \varepsilon\lambda * c * d$$

A_λ = Absorption at the measured wavelength
I = Intensity of transmitted light
I_0 = Intensity of incident light
ε_λ = Extinction coefficient at the measured wavelength [l/(mol*cm)]
c = concentration [mol/l]
d = pathlength [cm]

Since most of the used DNA-sequences contained a Cy5-label at the 5´-end, quantification via the Cy5- extinction coefficient (250 l/(mol*cm) at 651 nm) was also possible. Calculated values for Cy5-concentration and DNA-concentration often differed, especially for DNA-sequences that have previously been click-modified. Since binding investigations of the DNA-seqeunces was mostly done via flow cytometry, the calculated values for Cy5-concentrations were usually taken.

6.2.8 Digestion to nucleotides

Quantification of click-reaction with diverse synthesized oligonucleotide libraries, as well as with PCR-amplified single oligonucleotide sequences or –libraries was not possible via HPLC-MS. This might be due to slight impurities within the samples resulting from the click-reaction itself which could not be removed with the applied purification steps. Hence observed masses could not clearly be assigned to the fully click-modified libraries/ single sequences. Therefore, the click-modified strands were first enzymatically digested to nucleosides that could in turn be analyzed with HPLC-MS.

To get smooth HPLC chromatograms, around 300 pmol of DNA were used per digestion approach. The single stranded oligonucleotides were initially cleaved into 5´-phosphomononucleotides with the help of S1 endonuclease[184]. The total volume of the first part of the enzymatic digestion was 27 µl (see **Table 20 a**). The DNA was incubated together with S1 endonuclease in the corresponding 1x S1 nuclease reaction buffer (Life Technologies).

Table 20 a. First part of the enzymatic digestion of oligonucleotides to nucleosides.

Compound	Volume [µl]	Stock concentration	Final concentration
S1 nuclease reaction buffer	3	5x	0.5 x
S1 nuclease	0.5	100 U/µl	1.66 U/µl
ssDNA in water	27		~ 300 pmol

Incubation was done for 1h at 800 rpm and 37 °C. Following the first incubation step, Alkaline phosphatase I (Promega), Snake venom phosphodiesterase I, and Benzonase (Merck) together with 10x phosphatase buffer were added in the amount shown in **Table 20 b**. That enzymatic mixture completes the break of the phosphodiester backbone and the digestion into nucleosides by hydrolysis of 5´-phosphate groups.

Table 20 b. Second part of the enzymatic digestion of oligonucleotides to nucleosides.

Compound	Volume [µl]	Stock concentration	Final concentration
Phosphatase buffer	3.5	10x	1x
Alkaline phosphatase I (CIAP)	0.5	1U/µl	0.01 U/µl
Snake venom phosphodiesterase I	0.5	1U/µl	0.01 U/µl
0.5 µl Benzonase nuclease	0.5	250 U/µl	3.57 U/µl

The mixture was incubated for 2h at 37°C and 800 rpm. After completion, the enzyme was removed from the nucleoside solution. So the samples were heated to 95 °C for 5 minutes and centrifuged at 12000 g. Finally, 20 µl of the solutions were used for HPLC/HPLC-MS investigations, respectively (**section 6.8.3**).

6.2.9 Radioactive labelling of oligonucleotides

For radioactive labelling, around 50 pmol of non-clicked, single stranded and purified DNA was used. Briefly, the DNA was mixed with T4-Polynucleotide kinase (T4-PNK; 0.4 U/µl in final volume), the corresponding 10x T4-PNK-buffer (1x buffer in final volume), and γ-^{32}P-ATP in 50 µl. T4-PNK catalyses the transfer of the radioactive phosphate of ATP to the 5´-hydroxygroup on the oligonucleotide. The mixture was incubated at 37 °C for 1 h. Labelled DNA was subsequently purified via gel-filtration columns, click-modified (**section 6.2.3**) and finally purified over silica spin columns (**section 6.2.10.1**)

6.2.10 Oligonucleotide-purification

6.2.10.1 Silica spin columns

PCR-products, single-stranded DNA after exonuclease digestion and single-stranded click-modified DNA were typically purified with the NucleoSpin Gel- and PCR cleanup kit from Macherey-Nagel. Purification of dsDNA and ssDNA was done according to the manufacturer's recommendations. Briefly, 200 µl of PCR-products were generally applied to one NucleoSpin column.

Purified DNA was eluted in a volume of 50 µl ddH_2O and the yield of different NucleoSpin columns pooled. During click-SELEX 20 µl backups were taken per selection cycle. 200 µl of exonuclease-digestion products were applied to one NucleoSpin column and ssDNA was eluted in 80 µl ddH_2O. After click-reaction with the ssDNA, 100 µl of DNA were applied per NucleoSpin column. Products were eluted in 40 µl ddH_2O

6.2.10.2 Plasmid purification

For sequencing purposes, plasmid purification was done utilizing the plasmid DNA purification kit from Macherey-Nagel. Purification was done according to the manufacturer's recommendations

6.2.10.3 Gel filtration

Radioactively labelled ssDNA was purified using G25 gel-filtration spin columns from GE Healthcare were used according to the manufacturers recommendation.

6.3 Expression of Spinach2 and Broccoli in bacterial and mammalian cells.

Before Broccoli- and Spinach2-RNA was expressed in cells, fluorescence properties of the RNAs were first tested *in vitro*. This was done to confirm that plasmids were indeed encoding for the desired RNA aptamers. For this purpose, an *in vitro* transcription was performed. Plasmids were first used as template for PCR amplification (**section 6.2.1.2, Table 15**). In **section 7.1** the sequence of the Spinach2 forward- and reverse primers is shown that were applied for PCR amplification of Spinach2 and Broccoli DNA templates. Since the primer-binding sites of Broccoli and Spinach2 are identical (**see section 7.1**) these primers could be used for amplification of both templates. The resulting PCR products encoding for either Broccoli-, or Spinach2 RNA contained a T7 promotor which was necessary for *in vitro* transcription. After completion of transcription, the resulting RNA was purified and incubated with DFHBI to generate the expected fluorescent signal. Upon excitation of the samples at 460 nm, fluorescence was recorded at 505 nm. As negative control, the autofluorescence of DFHBI alone was recorded.

To amplify the Broccoli and Spinach2 plasmids XL10 cells were transformed with 20 ng of pET28c or pAV5S plasmids. Cells were thawed on ice before plasmids were added. After heating to 42°C for 90 s, cells were again stored on ice. LB medium was added and cells shaken at 37°C for 1 h.

Finally, 300 µl of the suspensions were plated on agar plates containing either ampicillin (for pAV5S plasmids) or kanamycin. Next morning single colonies were picked for inoculation in 100 ml LB-media containing the appropriate antibiotic. Cultures were shaken overnight at 37°C. Finally the volumes were devided to 2x 50 ml with were spun down for 30 min at 4200 rpm. Pellets were dried and a plasmid preparation was started. The plasmid preparation was done as explained in the manufacturer´s protocol (M&N)[382].

6.3.1 Expression and of Spinach2 and Broccoli in E.coli.

BL21 E.*coli* cells were used to express Broccoli and Spinach2. Cells were transformed with 40 ng of pET28c plamsids. Cells were plated on agar plates containing kanamycin and incubated over night at 37°C. Next morning single colonies were picked for inoculation in LB-medium containing kanamycin. To enhance Broccoli and Spinach2 transcription, the inductor IPTG (1 mM) was added at an OD_{600}=0.4 and cells were incubated for additional 2 h at 37°C. 100 µl aliquots of the culture were removed and spun down to pellet the culture. Pellets were subsequently dissolved in M9 minimal medium. The M9 medium contained either 50 µM DFHBI or PA-DFHBI. Cells were again shaken at 37°C for 30 min. Bacteria cultures that were incubated with PA-DFHBI were previously split into two separate cultures. One of these resulting cultures was irradiated with 385 nm for 1 min to remove the *o*-nitrobenzyl group. Finally, the suspensions were investigated for fluorescence. Aliquots of the bacteria cultures were excited at 460 nm and fluorescence emission at 505 nm was recorded.

6.3.2 Visualization of Spinach2 and Broccoli in vitro and in E. coli

DNA templates for Spinach2, Baby-Spinach and Broccoli could be amplified via PCR (**see section 6.2.1.2, Table 15**). Applied templates and primers are named in **section 7.1.2**. The ordered pET28c based and pAV5S based plasmids could also be used as template for PCR amplification. Since the applied forward-primers contained a T7-promotor, *in vitro* transcription was possible (**see section 6.2.4, Table 18**). Resulting RNA was purified as described in **section 6.2.5, Table 19.**

Mostly, 300 nM RNA constructs were incubated with 10 µM DFHBI or 10 µM PA-DFHBI in HEPES pH7.4 at 37°C for 30 min. In case of PA-DFHBI, 10% DMSO were present in the final solutions due to solubility problems of PA-DFHBI. The PPG on PA-DFHBI could photolytically be removed. Solutions containing RNA together with PA-DFHBI, as well as bacteria suspensions in M9 media containing DFHBI were irradiated at 385 nm for 1 min.Samples were pipetted onto 96-well plates. Each well was excited at 460 nm and fluorescence emission was recorded with an Enspire plate-reader (Perkin Elmer).

6.3.3 Expression and visualization of Spinach2 and Broccoli in HEK 293 cells

HEK cells grew to 80% confluency in Dulbecco´s modified Eagle medium (DMEM) + 10% fetal calf serum (FCS). 35000 HEK 293 cells in 500 µl DMEM + 10% FCS were seeded in different wells of a 24-well dish. Cells were allowed to adhere and grew for 24 h at 37°C. To co-transfect cells with mCherry and pAV5S Spinach2 a 1:4 ratio of DNA to Fugene. Therefore, 43 µl H_2O together with 600 ng of mCherry and 600 ng of pAV5s Spinach2 were mixed and 4.4 µl Fugene was added to the mixtures. As negative control, water was mixed with Fugene without the plasmids. The mixtures were shortly mixed by flicking the tubes. Of these transfection mixtures 25 µl were added to wells with grown HEK cells and the medium was gently pipetted up and down 5 times. 24 hours after transfection the medium was replaced with 500 µl of fresh, pre-warmed DMEM + 10%FCS. Again 24 hours later (48 h after transfection) the medium was again replaced by a mixture of DMEM containing either 500 µM DFHBI or 500 µMPA-DFHBI. Cells were incubated at 37°C for 30 min and subsequently analyzed by confocal laser scanning microscopy (LSM 710, Zeiss). Fluorescence of mCherry (ex: 543 nm; em: 596-696 nm) and DFHBI (ex: 488 nm; 500-540 nm) was recorded.

6.4 SELEX

6.4.1 Click-SELEX for THC-modified Dynabeads

The utilized click-SELEX library has been developed and characterised in the click-SELEX for C3-GFP by Fabian Tolle[232]. Click-SELEX for THC-modified beads was started with the click-modification of 500 pmol FT-2 starting library with benzyl-azide. The library was purified, mixed with 500 pmol of the benzyl-clicked “click-competitor” (panacea) and incubated with THC-modified beads in 1x SELEX buffer. Incubation was done for 30 min at 37 °C and 900 rpm. Later the DNA-mixture was removed from the beads and they were washed with SELEX-buffer remove non-binding sequences. In later SELEX cycles, the volume and number of washing steps was increased, whereas the number of THC-modified beads was decreased. Additionally, in later selection cycles some negative-selection steps with non-modified beads were included, before the DNA mixture was incubated with the THC-modified beads. Furthermore, the method to recover THC binding sequences changed from denaturation conditions (80 °C, 5 min) in early cycles, to affinity elution in the last few cycles (see **Table 2**). The amount of the supplied click-competitor remained constant at 500 pmol per cycle.

6.4.2 RNA SELEX for eDFHBI with Sul I library

SELEX for eDFHBI immobilized to magnetic beads and sepharose was started with 500 nmol of Sul I library. SELEX was performed in 40 mM HEPES pH 7.4 with 125 mM KCl and 5 mM $MgCl_2$. For every SELEX cycle, RNA was heated to 75°C prior to incubation with the eDFHBI carrying matrix. With progressing SELEX cycles, the number of washing steps to remove nonspecific binding RNA sequences was increased (**see Table 9**)

Beginning with cycle two, pre-SELEX was performed with either non-modified sepharose or non-modified magnetic beads. During SELEX the amount of eDFHBI that was immobilized to sepharose or magnetic beads was reduced within consecutive selection-cycles. Additionally, the matrix was washed several times with SELEX buffer (HEPES, pH7.4). For the first six SELEX cycles, binding RNA was recovered via heat (80°C, 5 min). For the last three SELEX cycles bound RNA was recovered via affinity elution.

6.5 Sequencing

6.5.1 Sanger-Sequencing

The DNA-library obtained after 9 cycles of click-SELEX was used for Sanger-sequencing. A 300 µl PCR-master mix was prepared as shown in **Table 21**. The same PCR-program was used as explained in **section 6.2.1.1**, however primers without the Cy5- and phosphate modification were used. Instead of the d*NTP-mix a conventional dNTP-mix with equal amounts of dTTP, dGTP, dATP, and dCTP was used. Here, *Taq*-polymerase instead of *Pwo*-polymerase was utilized to attach 3´-overhang deoxyadenosines that are essential for the subsequent cloning approach. Of the PCR master-mix 100 µl were removed for a no-template control. To the remaining 200 µl PCR-mix, 1 µl of the DNA resulting from the 9th SELEX-cycle was added. The PCR-performance was analysed on agarose-gel.

Table 21. PCR-amplification master-mix for the library of the 9th click-SELEX cycle for Sanger Sequencing purposes.

Compound	Volume [µl]	Stock concentration	Final concentration
$MgCl_2$	24	25 mM	2.0 µM
5´-primer	3	50 µM	0.5 µM
3´-primer	3	50 µM	0.5 µM
dNTP-mix	3	25 mM	250 µM
Taq-polymerase	3	5 U/µl	0.05 U/µl
Taq-polymerase buffer	60	5x	1x
template	x		
ddH_2O	Fill up to 300 µl		

Cloning of the non-purified PCR (and no template-control) product into TOPO®-vector and transformation of the recombinant vector into electro-competent One-shot® TOP10 cells was performed as described in the TOPO® TA Cloning® Kit user guide[383]. After plasmid-purification, 30 ng/µl plasmid DNA were sent to GATC-Biotech for Sanger-sequencing.

6.5.2 Next-Generation sequencing (NGS)

With NGS the entire number of sequences among the libraries of each SELEX-cycle is encompassed, whereby the enrichment of individual sequences or sequence-families during the complete SELEX process can be tracked. For NGS the libraries of SELEX-cycles 3, 5, 7, 8, 9 and 11-16 were sequenced. Samples for each cycle were amplified with primers bearing a different set of index-sequences at the 5´-end. 24 primer pairs with 12 different index-sequences existed. Those indices are needed to bundle the parallel sequencing of several cycles in one run. **Table 22** summarizes the twelve available index sequences.

Table 22. Available Index-sequences for NGS.

Index No	Sequence	Index No	Sequence	Index No	Sequence
1	ATCACG	2	CGATGT	3	TTAGGC
4	TGACCA	5	ACAGTG	6	GCCAAT
7	CAGATC	8	ACTTGA	9	GATCAG
10	TAGCTT	11	GGCTAG	12	CTTGTA

Cycles 3, 5, 7, 8, and 9 were sequenced in another NGS-run than the cycles 11-16. For cycles 3, 5, 7, 8, and 9 were amplified with Index-primers 1-5, whereas the cycles 11-16 were amplified with index 1-6, for the individual NGS-runs. PCR-product formation was verified with agarose gel electrophoresis. The PCR-products were purified with silica spin columns (**section 6.2.7.1**) and equal amounts of PCR-products were pooled, leading to a V_{total} of 60 µl with 1-2 µg DNA from the pooled samples. Finally, adapter ligation was performed with the TruSeq DNA PCR-Free sample preparation kit (Ref.15037063, Illumina). 40 µl End Repair Mix 2 was added and the end-repair protocol run (30 min, 30 °C, hold 4 °C). After silica spin column purification and recovery of DNA in 40 µl resuspension buffer, adenylation of the 3´-end was done by addition of 20 µl A-tailing mix and run of the ATAIL70 protocol (30 min 37 °C, 5 min 70 °C, 5 min 4 °C). Adapter ligation was performed by addition of 5 µl Ligation-Mix 2 and 5 µl of the desired adapter. The LIG-protocol (10 min 30 °C, 5 min 4 °C) was run. Products were loaded on 2% agarose gel and after electrophoresis, the desired bands were cut out of the gel (ca. 210 bp long) and DNA was eluted with silica spin columns. Recovery of DNA was done in 40 µl resuspension buffer. Sequencing itself was performed on an Illumina HighSeq 1500.

6.6 Binding-investigations

Binding investigations were mostly performed by flow cytometry. The fluorescence of Cy5-labelled oligonucleotide libraries or single sequences sticking to THC-modified or empty beads was monitored. All flow cytometry binding assays were performed with the same conditions.

6.6.1 Flow cytometry

Dynabeads™ (THCA-, or non-coupled) were diluted 1:100 in 1x SELEX buffer resulting in a suspension of 3 mg/ml beads. Directly before incubation with the DNA samples, 10 µl of the prepared bead-suspension were transferred into a new 1.5 ml Eppendorf-tube on a magnet, and the supernatant was removed from the beads.

The desired concentrations of the DNA-samples were mixed in a volume of 20 µl 1x SELEX buffer. The click-competitor, click-modified with the corresponding azides was added into the solutions at a concentration of containing 1 µM. Samples were added to the Dynabeads and the suspensions were pipetted up- and down several times. All samples were incubated at 37°C for 30 min 800 rpm. Afterwards, the suspensions were put on a magnet, where the supernatant is removed. Beads were in turn washed with 200 µl 1x SELEX buffer for 5 min at 37°C, 800 rpm. This washing step was repeated two times. Finally, the beads were suspended 200 µl 1x SELEX buffer and directly transferred into tubes for flow cytometry.

In case of competition assays performed with flow cytometry, increasing concentrations of different chemical compounds were titrated into the solution of the DNA samples and click-competitor in 1x SELEX buffer. In all samples, the resulting solutions contained 10% DMSO. After 30 min of incubation at 37°C, the solutions were added to the beads. Incubation of the bead-suspensions and following washing steps were performed as previously described.

Binding interactions of tested oligonucleotides with THC-modified or empty magnetic beads were measured on a FACSCanto II (BD Biosciences). The mean Cy5 fluorescence intensities (APC-A-channel) were recorded for all samples. 30000 events were measured per sample. All recorded values were normalized to the value of the applied highest oligonucleotide concentration of best binding samples. Replicates of independently performed measurements were evaluated with Prism 5.0 (GraphPad).

6.6.2 Microscale Thermophoresis (MST)

10 nM of Cy5-labelled oligonucleotides (C11.41 and C11.41sc) click-modified with benzyl-azide were mixed with increasing concentrations of THCA in 15 µl SELEX buffer (containing 10% DMSO). Samples were incubated for 30 min at 37°C and then transferred into utilized glass capillaries by dipping the capillary ends into the solutions.

The MST measurement was performed on a Monolith NT.115 instrument (NanoTemper). Baseline was subtracted from raw data. Applied THCA concentrations were plotted against the observed MST-signal.

6.6.3 Fluorescence polarization (FP)

For this assay, a THC-variant was used containing a FITC-label. This FITC-THC was synthesized by Franziska Pfeiffer. 0.24 µM solutions of FITC-THC were prepared in PBS buffer as well as in 1 x SELEX buffer with final amounts of 7 % ACN due to solubility reasons. The oligonucleotide sequences C11 and B10 as non-binding control were PCR-amplified, digested to single stranded DNA and click-modified with benzyl-azide (**section 6.1.3.1 to 6.1.3.3**). After purification, the oligonucleotides were dissolved in 1x SELEX buffer. A 1:250 dilution of the monoclonal mouse THC-antibody was prepared in PBS buffer. Furthermore a 1 mg/ml BSA solution in PBS-buffer was prepared.

For the assay itself, 5 µl of the PBS-diluted FITC-THC solutions were mixed with 10 µl of the antibody-, or BSA-dilution in PBS. In parallel, 5 µl of the FITC-THC solutions in SELEX buffer were mixed with 10 µl of the prepared oligonucleotide- solutions in 1x SELEX buffer. Similar solutions of all the tested compounds were prepared without the FITC-THC. All 15 µl samples were incubated in a 96 well plate at 37°C for 30 min. Afterwards the plate was shortly centrifuged and placed into the Tecan Ultra plate reader. The temperature during the FP-measurement within the reader was set to 37°C. Results of 2x duplicates were evaluated with Prism 5.0.

6.6.4 Cherenkov assay

This method was used as a further test to verify binding of click-modified oligonucleotide sequences to the target THC. The immobilization of THC to a solid support has been different compared to the way, the target was immobilized for the SELEX process. Herein the phenolic oxygen of THC was used to nucleophilic attack epoxy-group on Epoxy-activated sepharose (Merck). The preparation of the THC-sepharose was done by Franziska Pfeiffer. After completion of the coupling, remaining active groups were blocked with 1 M ethanolamine at pH 8.0 for 4h at 50°C. Afterwards blocking solutions were removed and the sepharose matrix was stored at 4°C in buffer.

Defined amounts of sepharose matrix could be transferred into columns. The storage buffer could easily be removed from the matrix by centrifugation at 400 rpm for 1 min. Matrix was then washed 3x with SELEX buffer for 1 min at 37°C at 800 rpm. Buffer could again be discarded.

A common click-SELEX cycle was imitated with the ^{32}P-radioactively labelled and benzyl-clicked C11 and B10 (non-binding control). Oligonucleotides were incubated with THC-sepharose as well as empty sepharose matrix in a volume of 100 µl at 37°C for 30 min at 800 rpm. The benzyl-clicked competitor was used at a concentration of 0.5 µM. Afterwards the incubation solutions were removed from the sepharose matrix by centrifugation at 400 rpm for 1 min. The flow-through fractions of the incubation step, as well as subsequent washing steps (3 x) were collected in a new 1.5 ml tubes. Finally the sepharose matrix was suspended in 100 µl SELEX buffer again and also transferred into a new 1.5 ml tube. The volume of all collected fractions was filled up to 1 ml with ddH_2O. All tubes were positioned into the liquid scintillation counter. The Cherenkov radiation of all the collected fractions was recorded by the liquid scintillation counter. The result of three independently performed assays was evaluated with the software Prism 5.0 (GraphPad).

As for click-SELEX the same assay was also performed with radioactively labelled RNA resulting from the SELEX for eDFHBI. RNA of SELEX cycle 1, and 9 were incubated with non-modified and eDFHBI-modified sepharose. The matrix was washed 5 times with 500 µl SELEX buffer for 5 minutes. The relative amount of radioactivela labelled RNA that remained on the sepharose matrix was then detected via the liquid scintillation counter.

6.6.5 Fluorescence scan of DFHBI derivatives

Fluorescence spectra of DFHBI and PA-DFHBI in combination with diverse RNA-constructs was recorded as explained in **section 6.3.2.**
In case of eDFHBI excitation and emission scans of that compound were also performed with an Enspire plate reader. Varying concentrations of eDFHBI were incubated with 300 nM Baby-Spinach, or 300 nM RNA libraries of different SELEX cycles for 30 min at 37°C. Samples were subsequently pipetted into a 96-well plate. Excitation was done at 460 nm while fluorescence emission at 600 nm was recorded.

6.7 CD-spectroscopy

CD-spectroscopy was performed to verify the formation of G-quadruplex (GQ) structure within the clickmer sequences C11.41, as well as C11.41_4 and C11.41_A15G. The spectrum of the scrambled version C11.41sc was recorded for comparison reasons. As a positive control, C10.36 was used, that demonstrably forms into a parallel GQ. For the measurement, 10 µM solutions of the mentioned DNA were

dissolved either in ddH_2O, or in 1x SELEX buffer. Samples were heated to 85°C for 3 min and then cooled to 37°C. After incubation time of 30 min at 37°C, the DNA-samples were transferred into the corresponding cuvette. The measurement itself was done on a Jasco J-810 Spectropolarimeter. Spectra were recorded between 200 nm and 320 nm. Evaluation of the curves was done with Prism 5.0 (GraphPad).

6.8 High-performance liquid chromatography – MS (HPLC/MS)

Reverse phase chromatography columns were used for the purification and analyzation of the chemically modified THCA, as well as the applied click-modified oligonucleotides, and nucleosides. The so-called reverse phase chromatography is based on diverging retention times of different chemical molecules on the lipophilic stationary phase of the column. Polar, hydrophobic compounds do hardly interact with the column material and are eluted prior to more hydrophobic compounds. For pure purification purposes, an analytical Agilent 1100 HPLC system was used. For HPLC in combination with ESI-mass spectrometry a 1100 HPLC system together with a HTC Esquire (Bruker) mass spectrometer was utilized.

6.8.1 HPLC-MS of small molecules

6.8.1.1 HPLC-MS of THC and THCA derivatives

All reaction steps within the synthesis of PEG-THC were purified with an Agilent 1100 HPLC system. The utilized column was a 5 µm SB-C18 2.1 x 50 mm Zorbax (Agilent). As mobile phases ddH_2O with 0.1% formic acid (FA, A) and acetonitrile (ACN, B) was applied. For purification purposes a gradient from 20% ACN to 100% ACN in 30 min with a flow of 0.8 ml/min was used. UV-absorption at 245 nm was monitored and the corresponding UV-absorption peaks of the desired products were collected. For HPLC with mass chromatography of THCA and THC-PEGBoc, a gradient of 60% - 80% ACN in 20 min with a flow of 0.4ml/min was used. For THC-PEG a gradient of 5% - 100% ACN in 20 min was applied. The UV-chromatogram at 245 nm was recorded. In parallel masses were measured using ultra scan in an alternating mode.

HPLC-chromatography without mass spectrometry was also performed, to estimate the solubility of increasing amounts of THC and THCA. Dilution series of both compounds were done in pure DMSO, as well as in a mixture of ddH_2O with 10% DMSO. The solutions were filtered through CHROMAFIL® Polyamid/Nylon (Macherey-Nagel) syringe-filter tips (Ø=0.45 µm), to remove potentially precipitated compounds. Equal amounts of DMSO- and ddH_2O-DMSO dilutions were injected into the HPLC system. The applied gradient was 40% - 100% ACN in 30 min with a flow of 0.8 ml/min. The applied reverse phase column for HPLC-MS purposes again was a 5 µm SB-C18 2.1 x 50 mm Zorbax.

6.8.1.2 HPLC-MS of DFHBI derivatives

Again, as mobile phases for HPLC, ddH_2O with 0.1% FA (A) and Acetonitrile (B) was used. Measurement of PA-DFHBI a gradient of 5% ACN to 100% ACN in either 30, or 50 min with a flow of 0.8 ml/min was applied. UV-absorption at 245 nm was monitored. The utilized column was the 5 µm SB-C18 2.1 x 50 mm Zorbax (Agilent).

For HPLC-MS of eDFHBI again the 5 µm SB-C18 2.1 x 50 mm Zorbax (Agilent) was used. A gradient of 20% to 100% ACN in 30 min with a flow of 0.8 ml/min was applied. UV absorption peaks at 245 nm were recrded.

6.8.2 HPLC-MS of click-modified oligonucleotides

To demonstrate the applicability of the click-reaction between alkyne-bearing DNA and a selection of different azides, a 16-mer “test-oligo” was used that contained only one EdU within the sequence. Click-reactions with different azides were performed and the resulting masses of the “test-oligo” were recorded. The result was taken as proof, that the applied azides are also accessible for the modification of oligonucleotides with more than one EdU.

In addition, EdU-containing single sequence oligonucleotides that were synthesized with a triisopropylsilyl (TIPS) protection group during solid phase synthesis by Ella Biotech (Martinsried) could be analyzed concerning their correct masses in a clicked, and non-clicked state. The negatively charged DNA does not interact good with reverse phase chromatography columns. Hence, for oligonucleotide analysis, ion-pairing reverse phase chromatography was used. Upon addition of triethylammonium hexafluoroisopropanol (1,1,1,3,3,3—hexafluoro-2-propanol adjusted to pH 7.0 with trimethylamine) a less polar counter ion for DNA is formed, which clearly increases retention time of DNA on the column and hence leads to a better HPLC separation. Additionally, it enables high sensitivity electrospray ionization[384].

A Hypersil OS (C18) column (Agilent) was utilized. Mobile phases were 10 mM TEA with 100 mM HFIP (A) and acetonitrile (B). Generally, 10 pmol of non-modified and click-modified DNA samples were injected. A gradient of 0% - 30% ACN in 20 min with a flow of 0.5 ml/min was used. The sample-masses were measured with an ultra scan in the negative mode with the following settings: nebulizer: 50 psi, dry gas: 10 l/min, dry temperature: 265 °C, SPS: 1000 m/z, ICC: 70000, scan: 500-1500 m/z.

6.8.3 HPLC-MS with nucleosides

Nucleosides resulting from the enzymatic digestion of clicked and non-clicked oligonucleotides (**section 5.1.3.9)** were analyzed the following way. The mobile phases for nucleoside analysis were 20 mM ammonium acetate acidified to pH 5.4 with acetic acid (A) and acetonitrile (B). The utilized HPLC column was a 5 µm SB-C18 2.1 x 50 mm Zorbax (Agilent). The following gradient for HPLC-seperation was used: 0% ACN for 3 min was followed by a gradient from 0% - 20% ACN in 17 min with a flow-rate of 0.3 ml/min. The samples were measured with the standard enhanced mode (alternating) with the following settings: nebulizer: 40 psi, dry gas: 9 l/min, dry temperature:365 °C, SPS: 400 m/z ICC_{neg}: 50000, ICC_{pos}: 100000, scan: 120-800 m/z.

7. Materials

7.1 Nucleic acids

7.1.1 Oligonucleotides used in click-SELEX for THC-modified beads

Most applied nucleic acids were synthesized and HPLC-purified by Ella Biotech. An exception is the sequence B10, which was PCR-amplified. Synthesis for nucleic acids containing EdU within the sequences was mostly performed with a TIPS-protection for the alkyne. Exceptions of this were the FT-2 starting library, the click-competitor (Panacea) and the 16-mer test-strand.

FT-2 library within the N42 region (dA, dG, dC, EdU; 1:1:1:1)
5´-Cy5- CACGACGCAAGGGACCACAGG-N42-CAGCACGACACCGCAGAGGCA-3´
FT2-Forward primer was synthesized with and without 5´-Cy5-lable.
5´-(Cy5)- CACGACGCAAGGGACCACAGG-3´
FT2-Reverse primer was synthesized with and without 5´-Phosphate.
5´-(Phosphate)-CAGCACGACACCGCAGAGGCA-3´
Click-competitor (Panacea) within the N42 region (dA, dG, dC, EdU; 1:1:1:1)
5´-N42-A-3´
Test-strand (X = EdU)
5´-GCACTGTXCATTCGCG-3´
C11.41 (**X** = EdU)
5´-Cy5-GGG**X**GGGAGGGAACAGG**X**ACCGACAGCAAG**XX**A**X**CGCACCC-3´
C11.41sc (**X** = EdU)
5´-Cy5- ACGGCAA**X**GCGCGCGACCGACGGGAAGGG**X**ACA**X**GAC**XX**AG-3´
U4T (**X** = EdU)
5´-Cy5-GGG*T*GGGAGGGAACAGG**X**ACCGACAGCAAG**XX**A**X**CGCACCC-3´
U18T (**X** = EdU)
5´-Cy5-GGG**X**GGGAGGGAACAGG*T*ACCGACAGCAAG**XX**A**X**CGCACCC-3´
U31T (**X** = EdU)
5´-Cy5-GGG**X**GGGAGGGAACAGG**X**ACCGACAGCAAG*T***X**A**X**CGCACCC-3´
U32T (**X** = EdU)
5´-Cy5-GGG**X**GGGAGGGAACAGG**X**ACCGACAGCAAG**X***T*A**X**CGCACCC-3´
U34T (**X** = EdU)
5´-Cy5-GGG**X**GGGAGGGAACAGG**X**ACCGACAGCAAG**XX**A*T*CGCACCC-3´
C11.41_4 (**X** = EdU)
5´-Cy5-GGG**X**GGGAGGGAACAGGTACCGACAGCAAGTTATCGCACCC-3´
C11.41_A15G (**X** = EdU)
5´-Cy5-GGG**X**GGGAGGGAACGGGTACCGACAGCAAGTTATCGCACCC-3´
B10 control (**X** = EdU)
5´-Cy5-CACGACGCAAGGGACCACAGGA**X**ACZGGACCGC**X**ACACCCCGCAC
CACC**X**CGCCAA**XX**GG**X**GACAGCACGACACCGCAGAGGCA-3´

7.1.2 DNA templates and primers for amplification of Spinach and Broccoli derivatives.

Spinach2, Baby-Spinach and Broccoli DNA templates are shown below. All these DNA templates could be amplified with the Spinach2.wt. primers. For amplification of a Spinach-Mutant that does not bind DFHBI (Mut) amplification was done with an additional set of primers.

Spinach2 RNA
5´-GAUGUAACUGAAUGAAAUGGUGAAGGACGGGUCCAGUAGGCUGCUUCGG
CAGCCUACUUGUUGAGUAGAGUGUGAGCUCCGUAACUAGUUACAUC-3´
Broccoli-RNA
5´-GAGACGCAACUGAAUGAAAUGGUGAAGGAGACGGUCGGGUCCAGGCACA
AAAAUGUUGCC UGUUGAGUAGAGUGUGGGCUCCGUAACUAGUCGCGUCAC-
3´

Spinach2.wt.Forward primer
5´-TAATACGACTCACTATAGATGTAACTGAATGAAATGGT-3´
Spinach2.wt.Reverse primer
5´-GATGTAACTAGTTACGGAGCT-3´
Non-binding Spinach mutant (Mut)
5´-
GACGCGACUGAAUGAAAUGGUGAAGGACGGGUCCAGAUGCUUCGGACGCUU
G
UUGAGUAGAGUGUGAGCUCCGUAACUAGUCGCGUC-3´
Mut Forward primer
5´-AATTCTAATACGACTCACTATAGACGCGACTGAATGAAATG-3´
Mut Reverse primer
5´-GACGCGACTAGTTACGGAGC-3´

7.1.3 Sul I library and primers used in SELEX for eDFHBI

The Sul I library and primers used during SELEX for eDFHBI is listed below.

Sul1 RNA library:
5´-GGGAGGACGAUGCGG-N40-CAGACGACUCGCUGAGGAUCCGAGA-3´
Sul1-Forward primer
5´-GGGGGAATTCTAATACGACTCACTATAGGGAGGACGATGCGG-3´
Sul1-Reverse primer
5´-TCTCGGATCCTCAGCGAGTCGTCTG-3´

7.2 Chemicals

Chemical	Provider	CAS
Acetic acid (MS-grade)	Sigma-Aldrich	64-19-7
Agarose	Roth	9012-36-6
Ammonium acetate (MS grade)	Sigma-Aldrich	631-61-8
Alkaline Phosphatase (CIAP) (M2825)	Promega	
2-azido-ethanamine	Synthesized by Jörg Ewers	
2-(azidoethyl)guanidine hydrochloride	Synthesized by Olga Wolters	
2,6-difluorophenol	Sigma-Aldrich	28177-48-2
3-(2-azidoethyl)-indole	Synthesized by Gerhard Brändle /Jörg Ewers	
4-(2-azidoethyl) imidazole	Synthesized by Gerhard Brändle	
4-(2-azidoethyl)morpholine	Synthesized by Gerhard Brändle	
4-(azidomethyl)-3,4-dihydro-benzooxazine	Synthesized by Gerhard Brändle	
1-(2-azidomethyl) naphthalene	Synthesized by Gerhard Brändle	
1-azido-2-methylpropane	Synthesized by Gerhard Brändle/Jörg Ewers	
3-azido-1-propanol	Synthesized by Gerhard Brändle	
Benzonase	Sigma-Aldrich	9025-64-4
Benzyl-azide solution 0.5 M	Sigma-Aldrich	622-79-7
γ -^{32}P-ATP (NEG502A)	Perkin Elmer	
Boric acid	Labochem International	10043-35-3
4-Bromo-2,6-difluorophenol	Alfa Aesar	104197-13-9
Copper sulphate		7758-98-7
Crown ether/18-crown-6	Sigma-Aldrich	17455-13-9
DNA-ladder (GeneRuler™ Ultra lowrange)	Fermentas	
Di-*tert*-butyl dicarbonate	Sigma-Aldrich	24424-99-5
Diisobutylaluminiumhydrid	Acros Organics	1191-15-7
Dipotassium phosphate	Sigma-Aldrich	7758-11-4
Dynabeads M280-tosylactivated	Invitrogen	
Epoxy-activated Sepharose™ 6B	GE Healthcare	
1-Ethyl-3-(3 dimethylaminopropyl)carbodiimid hydrochloride	Iris-Biotech	25952-53-8
Ethinyldeoxy uridine triphosphate (EdUTP) (BCT-08)	BaseClick	
Ethidiumbromide 1% solution	Roth	1239-45-8
Formic acid (MS grade)	Sigma-Aldrich	64-18-6
Hexafluoro-2-propanol (HFIP) (MS-grade)	Sigma-Aldrich	920-66-1

Chemical	Provider	CAS
λ-Exonuclease (EN0561)	Thermo Scientific	
L-Phenylalanine	Sigma-Aldrich	63-91-2
Monoclonal THC-antibody	Fitzgerald	
Monopotassium phosphate	Sigma-Aldrich	778-77-0
N-Acetylglycine	Sigma-Aldrich	543-24-8
N-Boc- 2,2′-(ethylenedioxy)diethylamine	Sigma-Aldrich	153086-78-3
N-Boc-1,6-hexandiamine	Alfa-Aesar	51857-17-1
N-Methoxy-N-methylacetamide	Sigma-Aldrich	78191-00-1
Nuclease S1	Life Technologies	18001-016
Pwo DNA Polymerase (M3002)	Genaxxon	
Phosphodiesterase I (PDE I)	Sigma-Aldrich	9025-82-5
Potassium chloride	Roth	7447-40-7
Sodium azide	Sigma-Aldrich	26628-22-8
Sodiumchloride	Fisher Scientific	7647-14-5
Sodiumhydroxide	VWR	1310-73-2
Sodium hydrogencarbonate	Sigma-Aldrich	144-55-8
Sodium Sulphate	Sigma-Aldrich	7757-82-6
(-)-trans-Δ^9THC carboxylic acid (THCA-A)	Lipomed	23978-85-0
T4 Polynucleotide kinase (T4-PNK) (M0201)	NEB	
Taq-DNA polymerase	New England Biolabs	
Monoclonal THC-antibody	Fitzgerald	
Tetrakis(triphenylphosphine)palladium(0)	Sigma-Aldrich	14221-01-3
Triflic acid	Sigma-Aldrich	1493-13-6
Triethylamine (MS grade)	Sigma-Aldrich	121-44-8
Tris(3-hydroxypropyltriazolylmethyl)amine (BCMI- 006)	BaseClick	

7.3 Commercial kits

Application	Kit	Provider
PCR-purification	NucleoSpin Gel and PCR Clean-up	Macherey-Nagel
Gel filtration	G25 spin columns	GE Healthcare
Plasmid purification	NucleoSpin Plasmid	Macherey-Nagel
Size exclusion	Amicon-Ultra	Merck Millipore
TOPO TA cloning	TOPO TA cloning kit for sequencing	Life Technologies
Adapter ligation	TruSeq DNA PCR-Free (LT) sample prep. kit	Illumina

7.4 Buffers & Solutions

Name	Ingredients	Final concentration
DNA loading buffer (6x)	Glycerol	60%
	Tris	10 mM
	EDTA-Na_2	60 mM
	Xylencyanol	0.03%
K^+-free buffer pH 7.4	Na_2HPO_4 x 2 H_2O	50.8 mM
	NaH_2PO_4 x 2 H_2O	15.0 mM
	NaCl	152.0 mM
	$MgCl_2$	3.0 mM
SELEX-buffer pH 7.4	K_2HPO_4	50.8 mM
	KH_2PO_4	14.7 mM
	NaCl	136.0 mM
	KCl	26.8 mM
	$MgCl_2$	3.0 mM
TBE-buffer pH 8.0	Tris	89 mM
	Biric acid	89 mM
	EDTA-Na_2	2 mM
HEPES buffer pH 7.4	HEPES	40 mM
	KCl	125 mM
	$MgCl_2$	3 mM

7.5 Equipment

Equipment		Provider
Agarose chamber		
Analytical balance		Sartorius
Balance		Sartorius
Flowcytometer	FACSCanto II	BD Biosciences
HPLC	1100	Agilent
HPLC	1200	Agilent
Hypersil OS		Agilent
Imaging System	Odyssey	Li-Cor
Magnetic rack		Life Technologies
Equipment		**Provider**
Microscale Thermophoresis	Monolith NT.115	Nano Temper
MS	Esquire HTC	Bruker
NMR Benchtop	Spinsolve Carbon	Magritek
PCR Thermocycler	Mastercycler Personal	Eppendorff
PCR Thermocycler		
Phosphoimager (PI)	FLA-3000	Fuji
PI Screens and Cassetts		Fuji
Pipets		Eppendorf
Plastic consumables		Sarstedt
Thermomixer		Eppendorf
UV Transilluminator		VWR
Spectrophotometer	Nanodrop 2000	Thermo Scientific
Zorbax		Agilent

8 Appendix

Table A1. Sequences resulting from Sanger sequencing after 9 cycles of click-SELEX for THC

	Sequence
Forward primer	CAC GAC GCA AGG GAC CAC AGG
Reverse primer binding-site	CAG CAC GAC ACC GCA GAG GCA
C 1	ACA CGG GCT TGA TTC GTA ACT ATC TCC CGG TTT TTT TAA AAT
C 4	ATG CCT GAG TCT CCC CTT TCT ATG GGA CTT GAA TGA TTC GAG
C 5	CCG AAA AGG GAG GGA GGG TGG GAA AAA ATG CCA ATG TGG GCA
C 8	ATG CCT GAG TCT CCC CTT TCT ATG GGA CTT GAA TGA TTC GAG
C 11	GAG GGT GGG AGG GAA CAG GTA CCG ACA GCA AGT TAT CGC ACC
C 12	GTG GGA GGG AGG GAA ATN NNG NCN CAN CNN ACA ACN NNA ACG
C 14	GGG GGA GGG AGG GAA CGG GAC CAA CGG CGA CAC CAA CCC TAG
C 18	GAG GGA GGG TGG GCA AAG GGC CCT AAG TCC GTA ACA AAA ACA
C 22	CGC TCG GAC ACC TCG TGC TTT TAC CCA CAG GAC TTT CAG GCC
C 23	TTA TTC CTT CCC CGC ATA CTT GCG GCA CGT CTG GGT TTC AAC
C 24	GCG GGA GGG GGG GAG TGG GAC CAA GTC CAA ATG CGG AAC GGA
C 26	GTA GGG CGG GCG GGA TGT GGG CCC GAC GTA ACA AGA CAA AGC
C 28	TTC TCC CCC GCA GTG TTC GAG CGG GAT CCG GGT ATC TAG GG
C 30	GCG GGA GGG GGG GGG AGA GTC CCG CGT AGA AAC AGG ACA AGA
C 32	AAT GTA GTG TTC CAT TAG GCT CTA AAG TCA GGC AGC TAA CA
C 33	GGG GGT GGG AGG GAA CGG GGT CAC GCC GCG AAA AGA GTA GGG
C 34	AGG CGA AGG GTC CCA TGT CAT ACC CCT GTT TCT TTT CCT TTC
C 35	AAG GCA GTG TGG CCA AGA CTT CCG CAT TTT TCT TAG TTT CTC

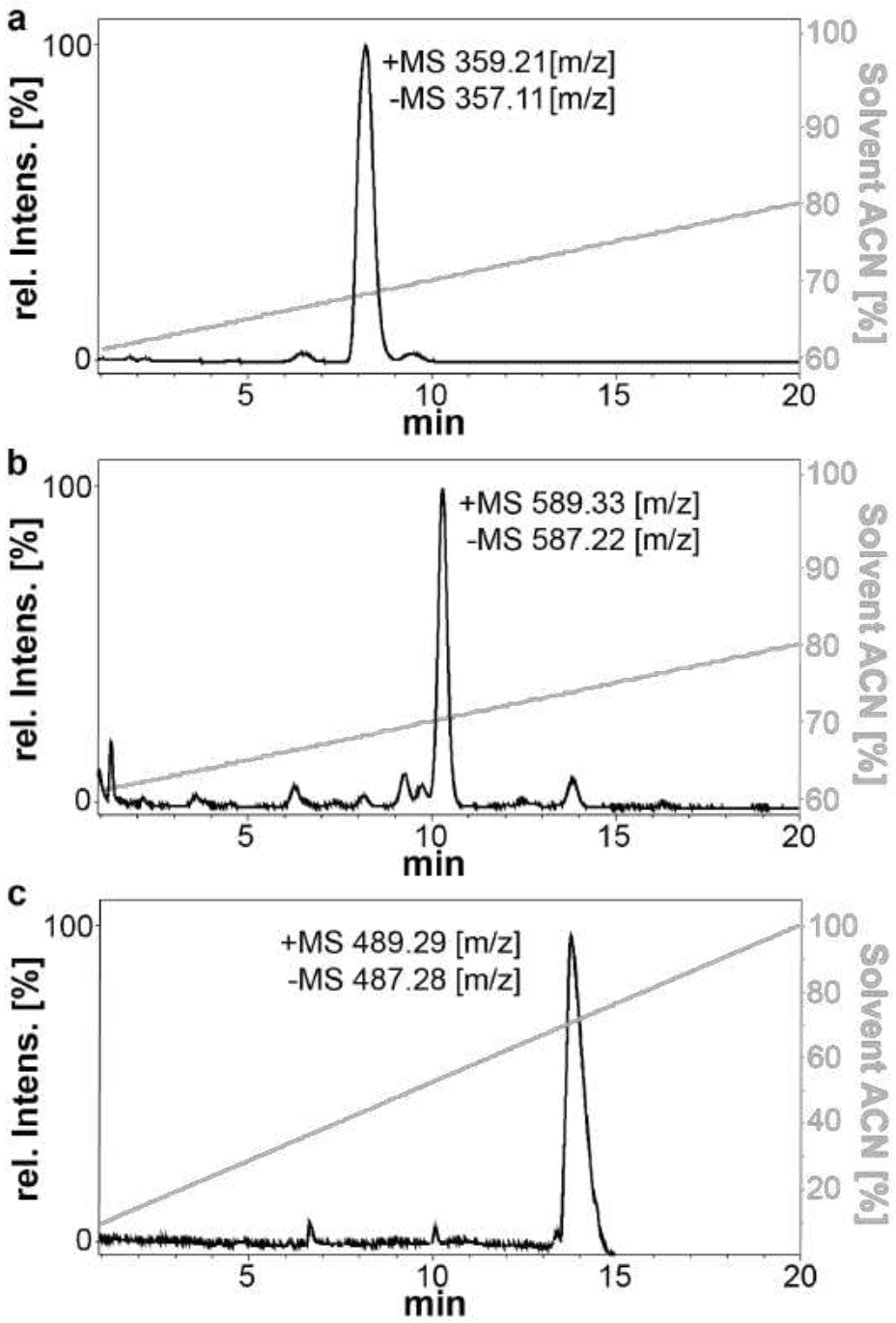

Fig. A1. HPLC-MS results for the synthesis of THC-PEG. The flow was 0.4ml/min for all samples.a) THCA. b) THC-PEG-Boc. c) THC-PEG.

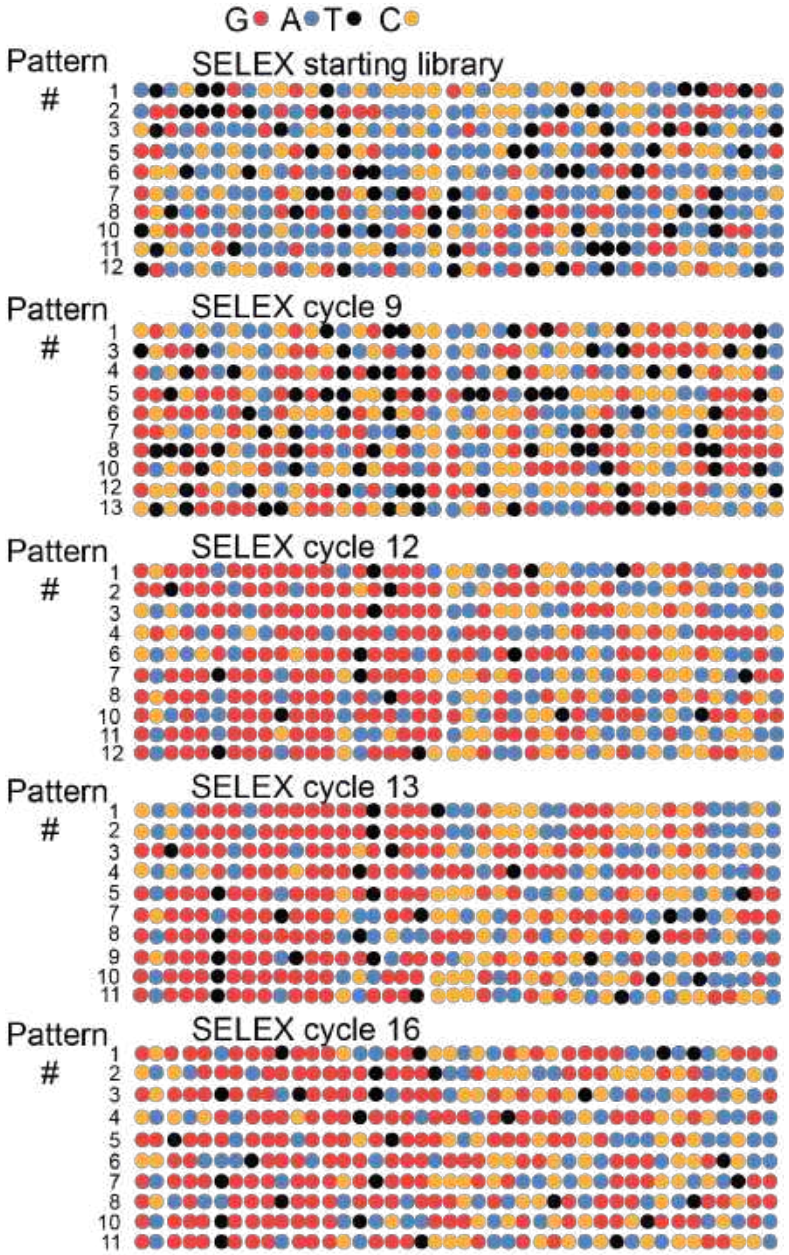

Fig. A2. NGS-result of click-SELEX. Depiction of the top ten full-length patterns of the startinglibrary, as well as from SELEX cycle 9, 12, 13, and 16. An enrichment of G´s in later SELEX cycles, can be Observed.

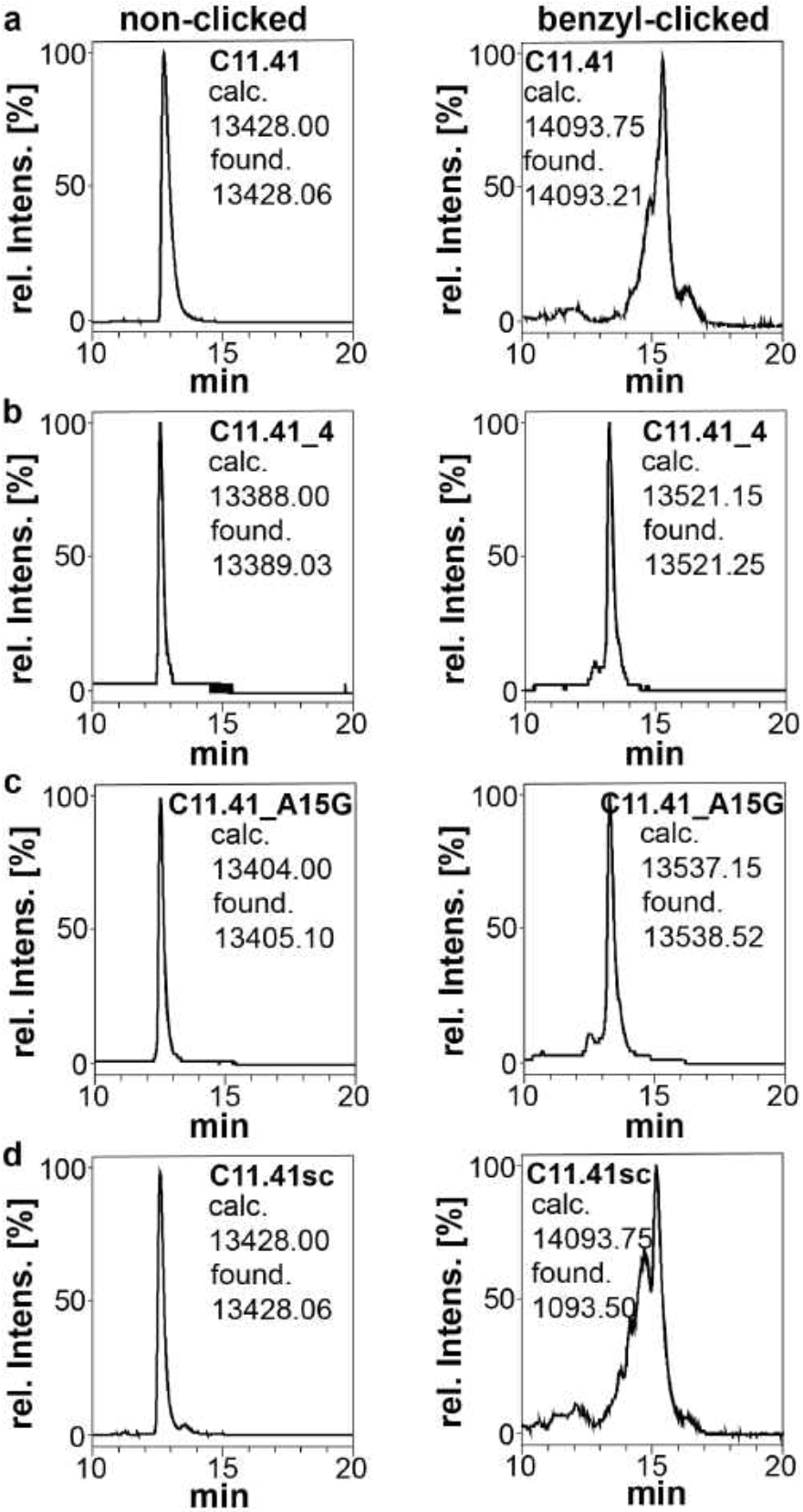

Fig. A3..Detected masses of the truncated variants of C11. Non-clicked and benzyl-clicked C11.41 (a), C11.41_4 (b), C11.41_A15G (c) and the scrambled variant (d) are shown.

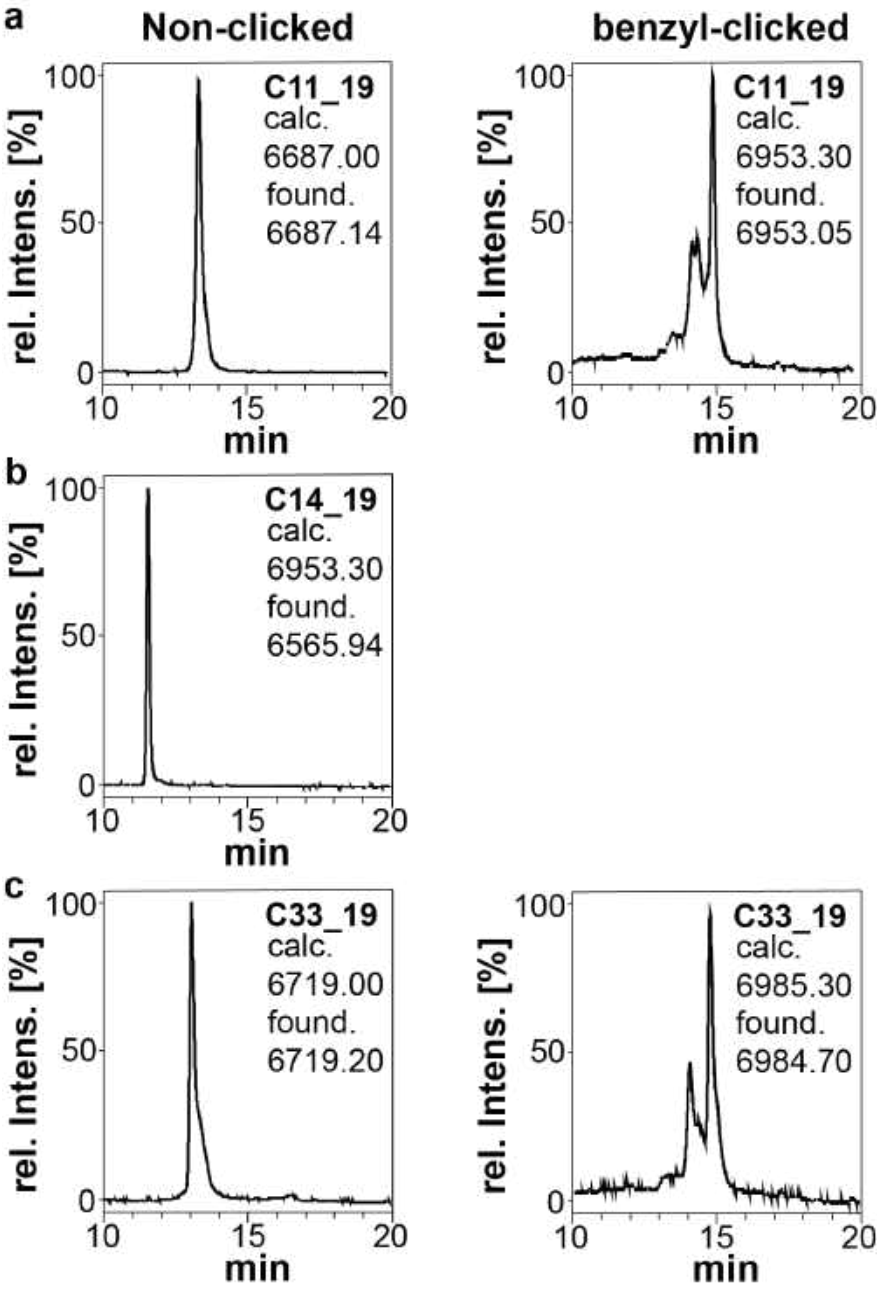

Fig. A4..Detected masses of the 19-mers. Non-clicked and benzyl-clicked C11_19 (a), C14_19 (b), C33_19 (c). C14_19 did not contain a EdU and thus could not be click-modified.

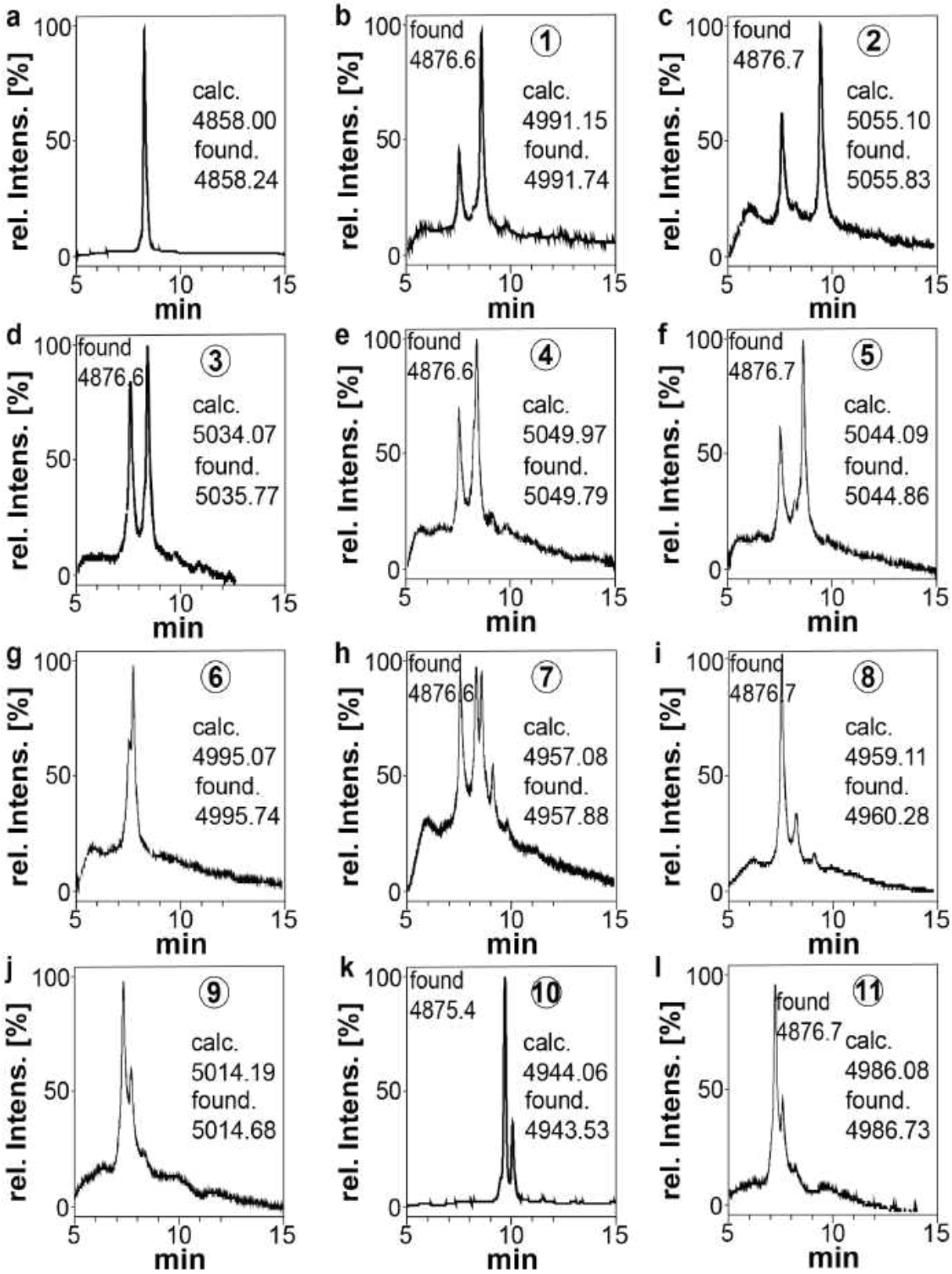

Fig. A5. Detected masses of the test strand click-modified with the azides described in section 3.1.4.3. Chromatogramm and detected masses of Non-clicked (a) and click-modified test-strands (b-l) corresponding to the applied azides 1-11.

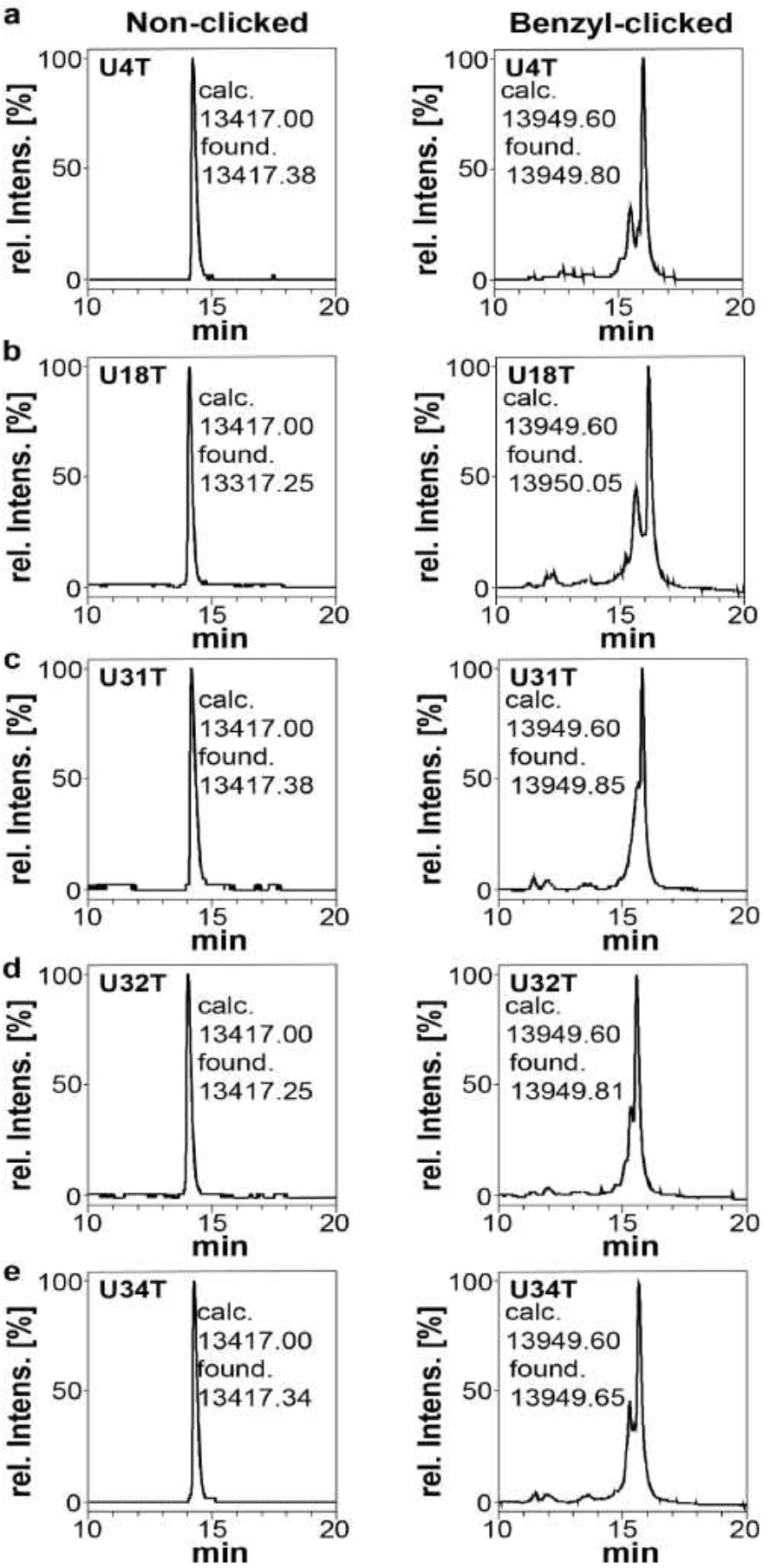

Fig. A6. Detected masses of point mutants. Non-clicked and benzyl-clicked U4T (a), U18T (b), U31T (c), U32T (d), U34T (e).

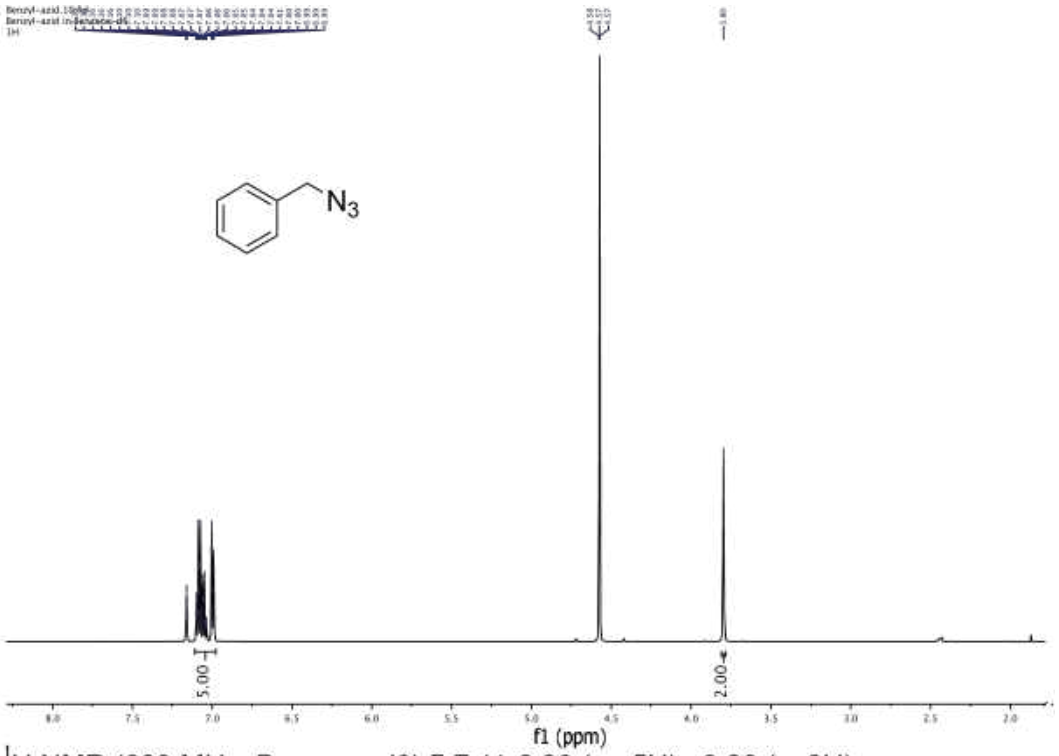

^{1}H NMR (600 MHz, Benzene-d6) δ 7.11-6.98 (m, 5H), 3.80 (s, 2H).

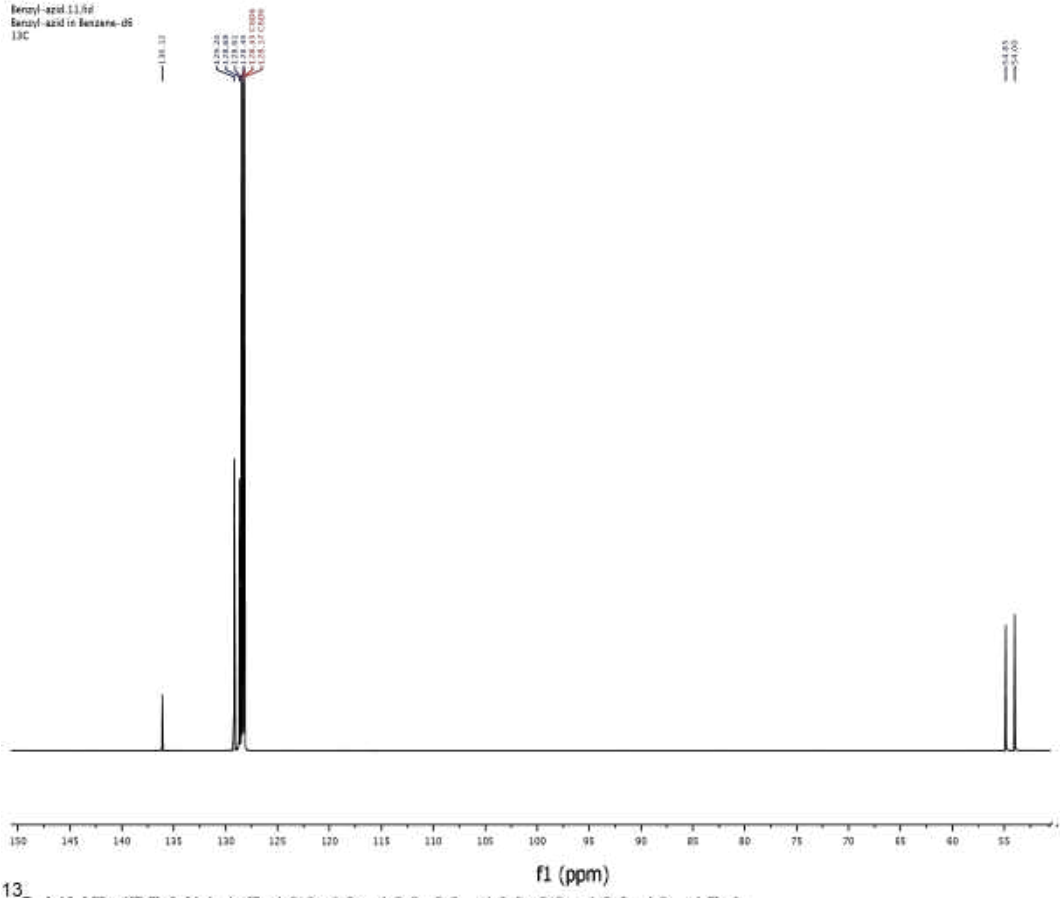

^{13}C NMR (75 MHz) δ 136.12, 129,20, 128.69, 128.49, 45.0.

Fig. A7. ^{1}H NMR and ^{13}C NMR of Benzyl-azide (Azide (1)).

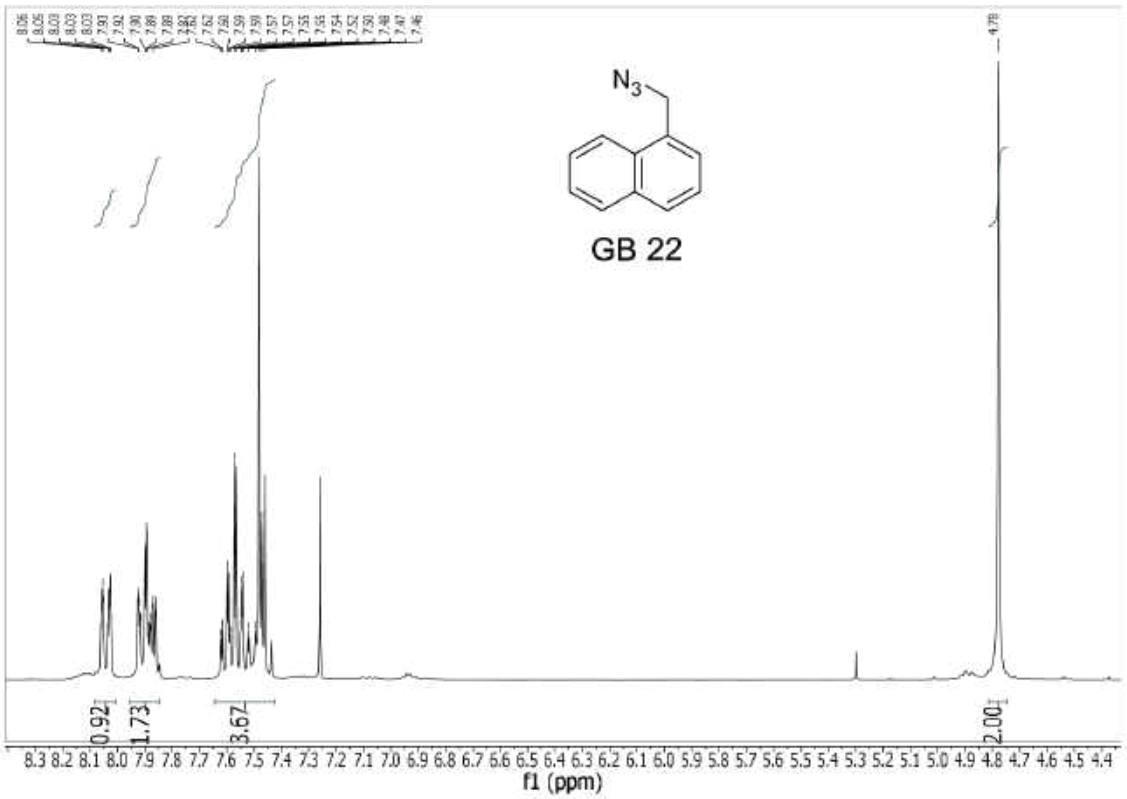

^{1}H NMR (300 MHz) δ 8.09-8.00 (m, 1H), 7,94-7.84 (m, 2H), 7.65-7.42 (m, 4H), 4.78 (s, 2H)

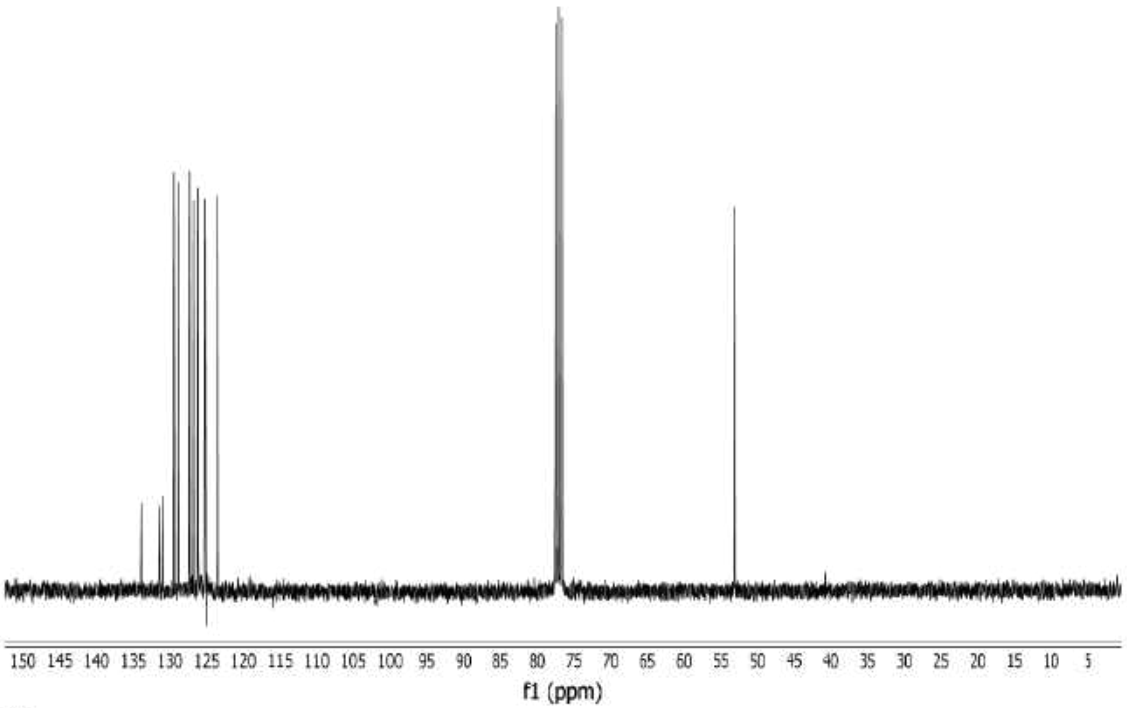

^{13}C NMR (75 MHz) δ 134.04, 131.49, 131.09, 129.57, 128.95, 127.42, 126.87, 126.30, 125.34, 123.62, 53.16

Fig. A8. ^{1}H NMR and ^{13}C NMR of 1-(2-azidomethyl) naphthalene (Azide (2); GB 22).

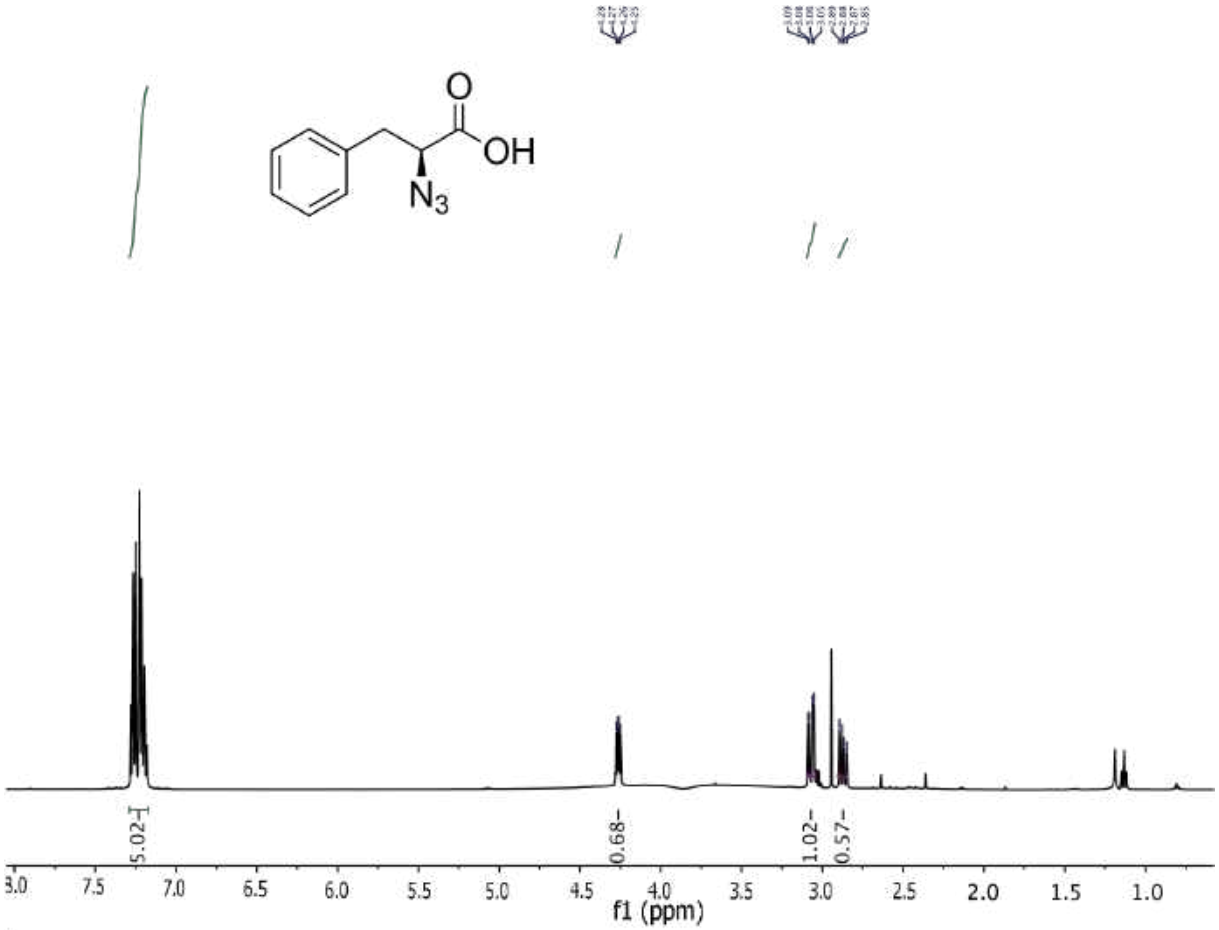

^{1}H NMR (300 MHz) δ 7.38 - 7.18 (br, m, 5H), 4.26 (dd, J = 4.9 Hz, 1H), 3.07 (dd, J = 4.9 Hz), 2.87 (dd, J = 8.9 Hz).

Fig. A9.^{1}H NMR of azido-benzenepropanoic acid (Azide (4)).

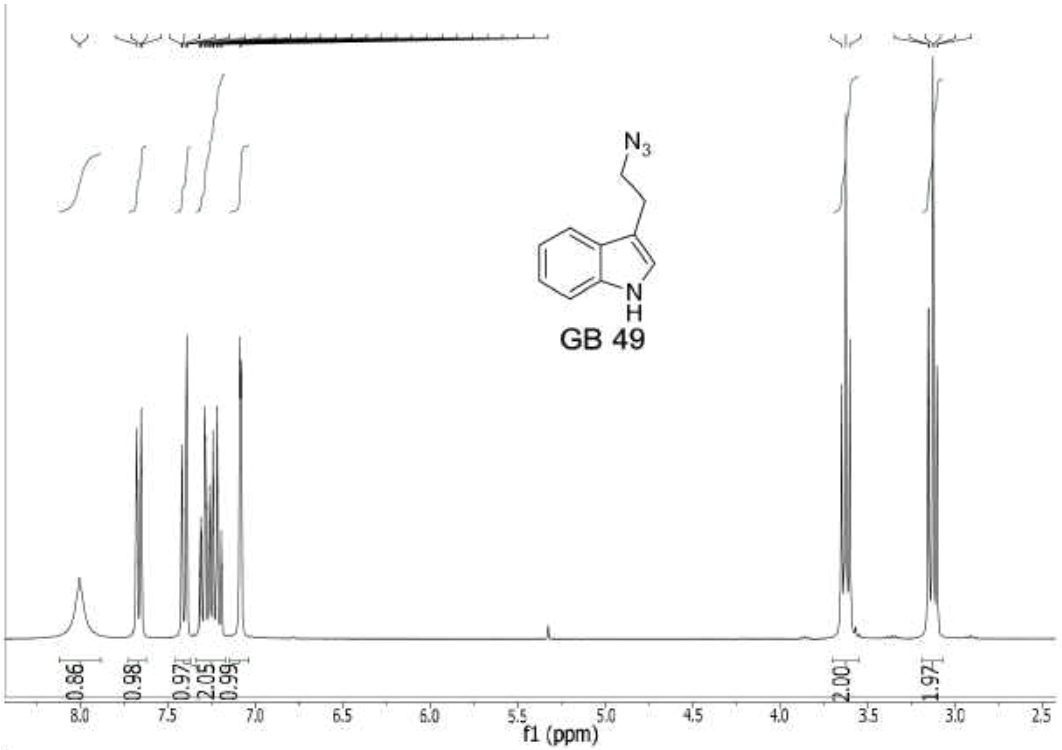

^{1}H NMR (300 MHz) δ 8.01 (br s, 1H), 7.67 (dt, J=7.8, 1.1 Hz, 1H), 7.40 (dt, J= 8.1, 1.0 Hz, 1H),7.34-7.17 (m, 2H), 7.08 (d, J=2.4 Hz, 1H), 3.62 (t, J=7.2, 2H), 3.13 (td, J=7.2, 0.9 Hz, 2H)

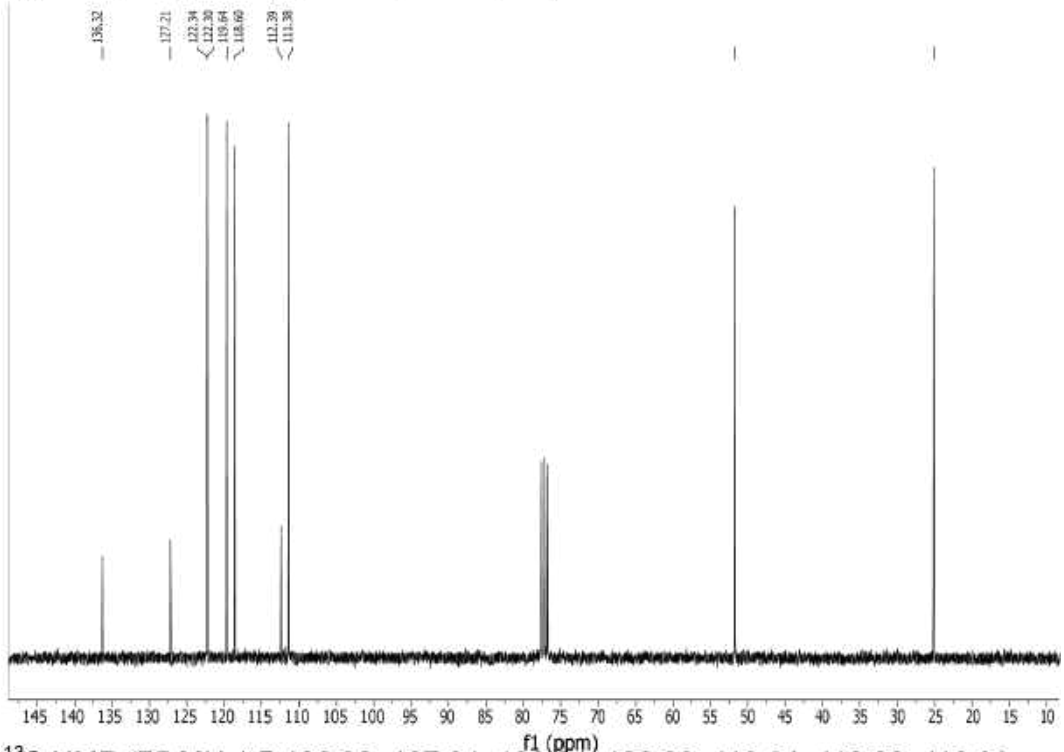

^{13}C NMR (75 MHz) δ 136.32, 127.21, 122.34, 122.30, 119.64, 118.60, 112.39, 111.38, 51.73, 25.16

Fig. A10. ^{1}H NMR and ^{13}C NMR of 3-(2-azidoethyl)-indole (Azide (5); GB 49).

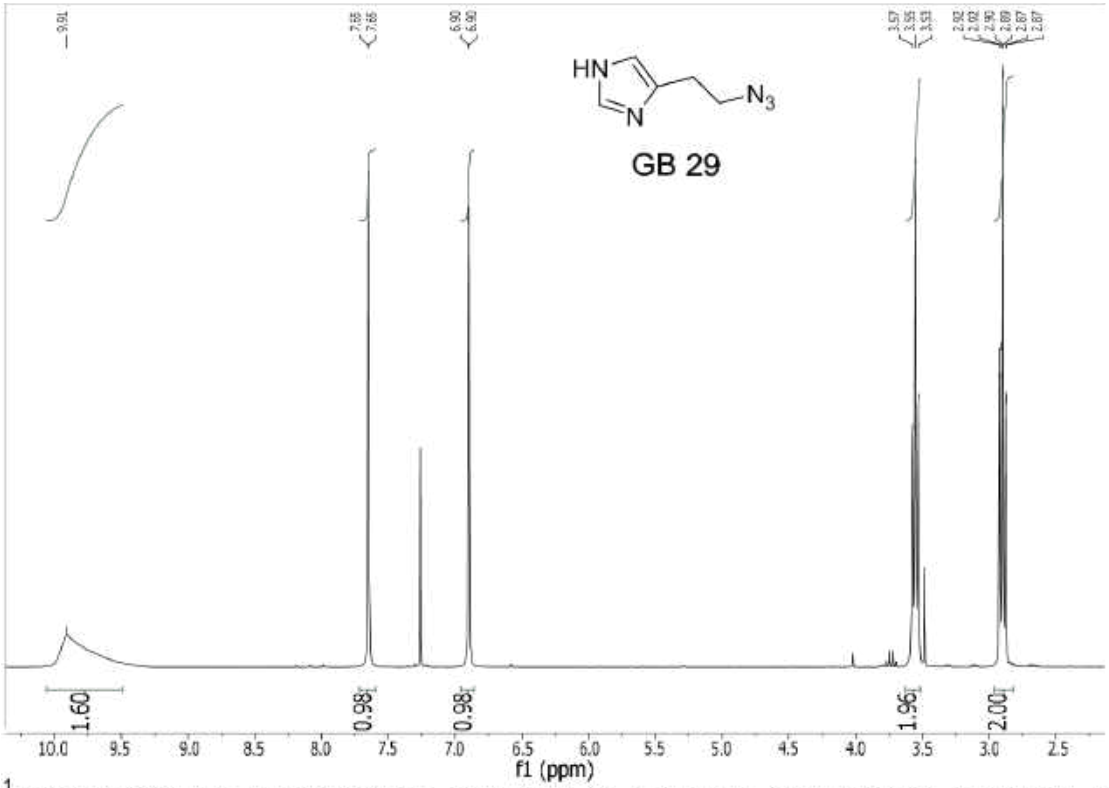

^{1}H NMR (300 MHz) δ 9.91 (br s, 2H), 7.65 (d, J=1.2 Hz, 1H), 6.90 (d, J=1.0 Hz, 1H) 3.55 (t,J=6.7 Hz, 2H), 2.89 (td, J=0.8 Hz, 2H).

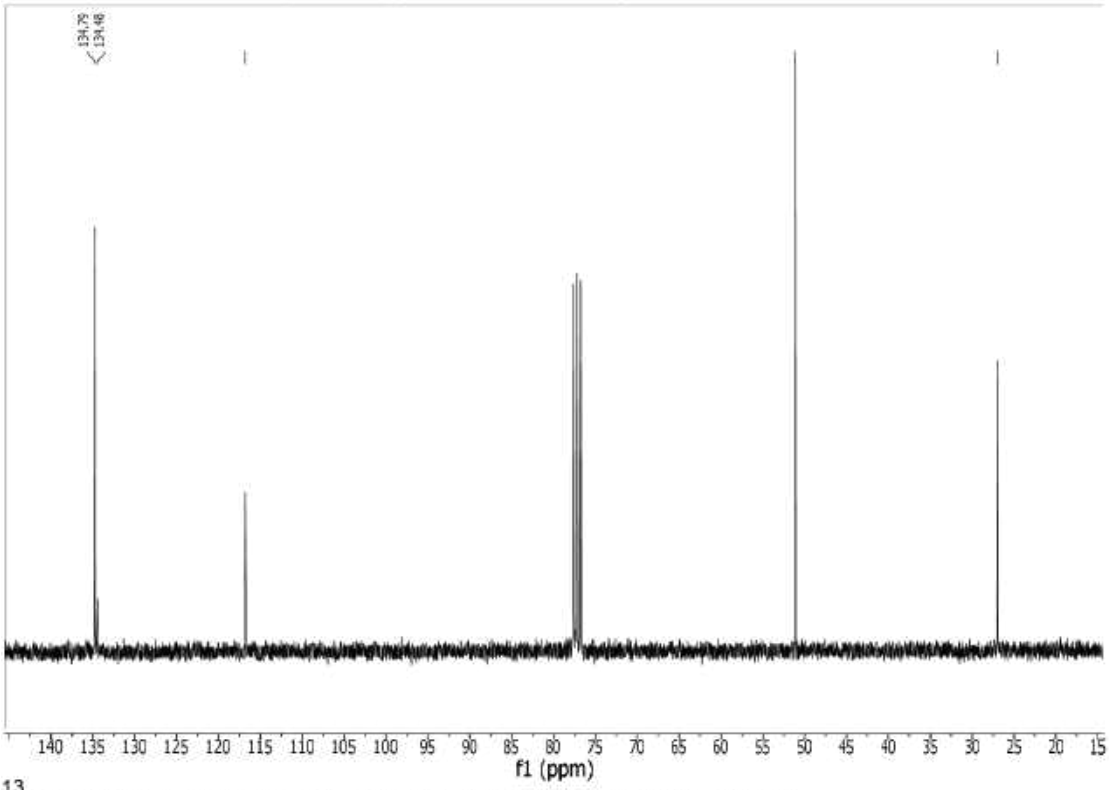

^{13}C NMR (75 MHz) δ 134.79, 134.48, 116.82, 51.05, 26.91.

Fig. A11. ^{1}H NMR and ^{13}C NMR of 4-(2-azidoethyl) imidazole (Azide (6); GB 29).

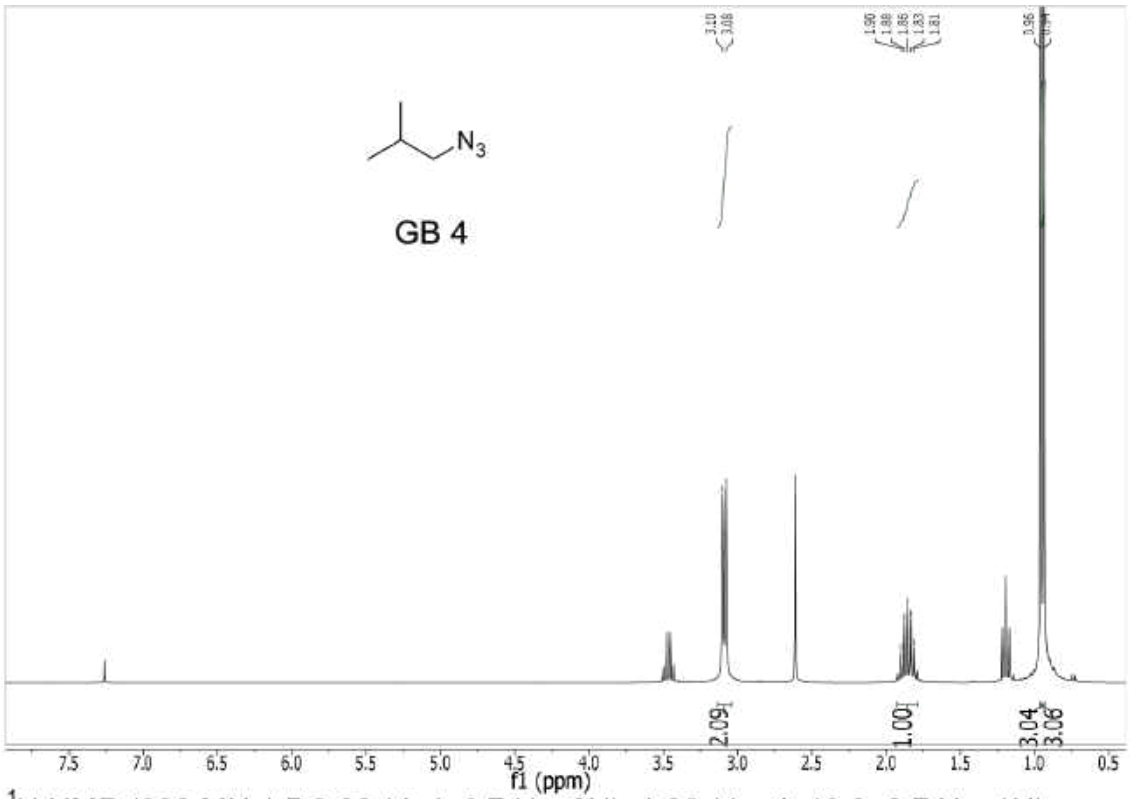

^{1}H NMR (300 MHz) δ 3.09 (d, J=6.7 Hz, 2H), 1.86 (dp, J=13.3, 6.7 Hz, 1H), 0.96 (s, 3H), 0.94 (s, 3H). (Et_2O impurity)

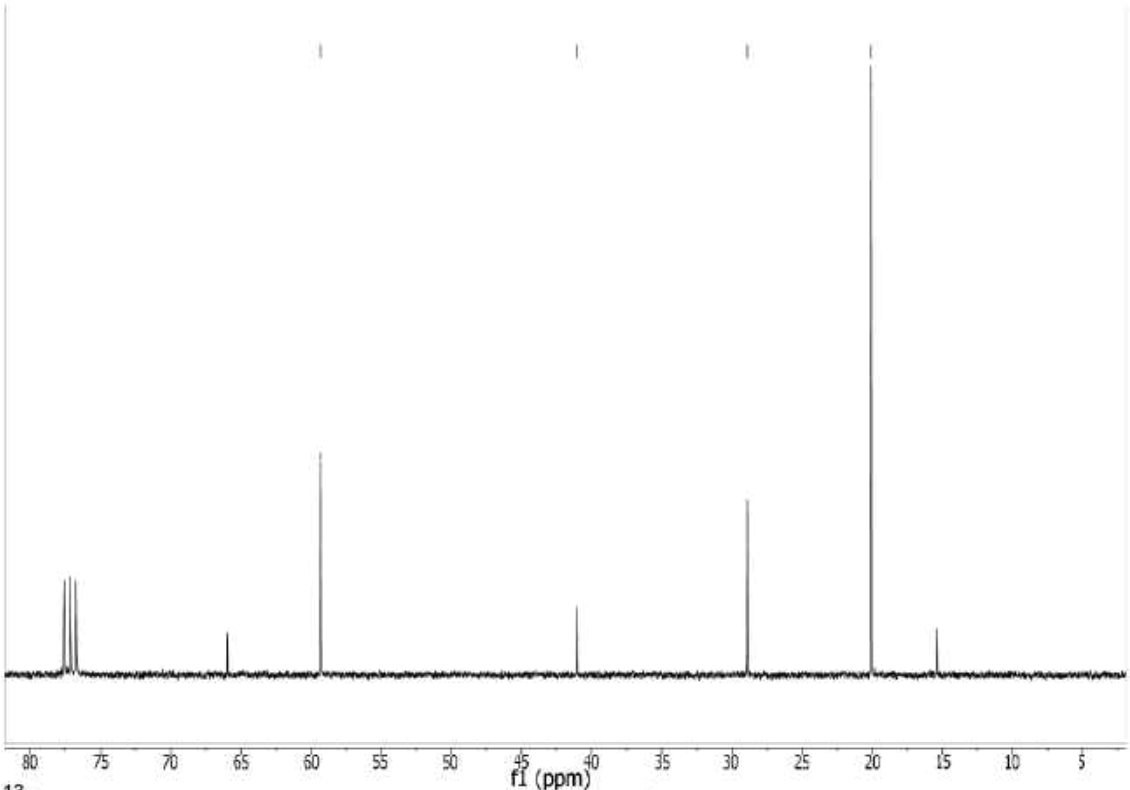

^{13}C NMR (75 MHz) δ 59.30, 28.91, 20.97. (Et_2O impurity)

Fig. A12. ^{1}H NMR and ^{13}C NMR of 1-azido-2-methylpropane (Azide (7); GB 4).

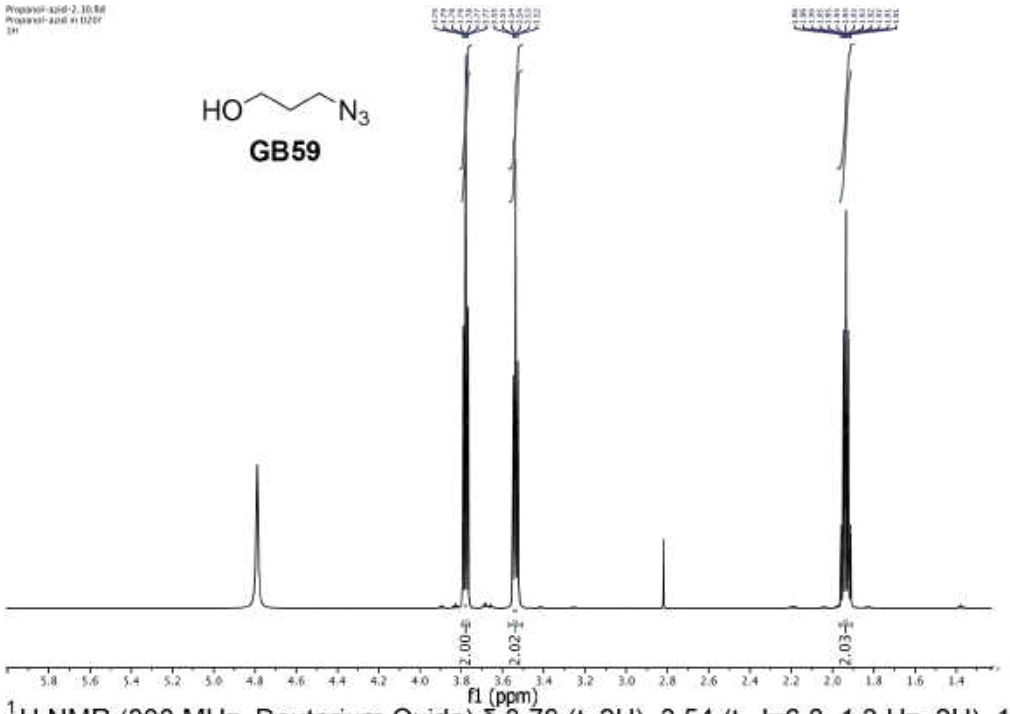

^{1}H NMR (300 MHz, Deuterium Oxide) δ 3.78 (t, 2H), 3.54 (t, J=6.8, 1.3 Hz, 2H), 1.98-1.9 (m, 2H).

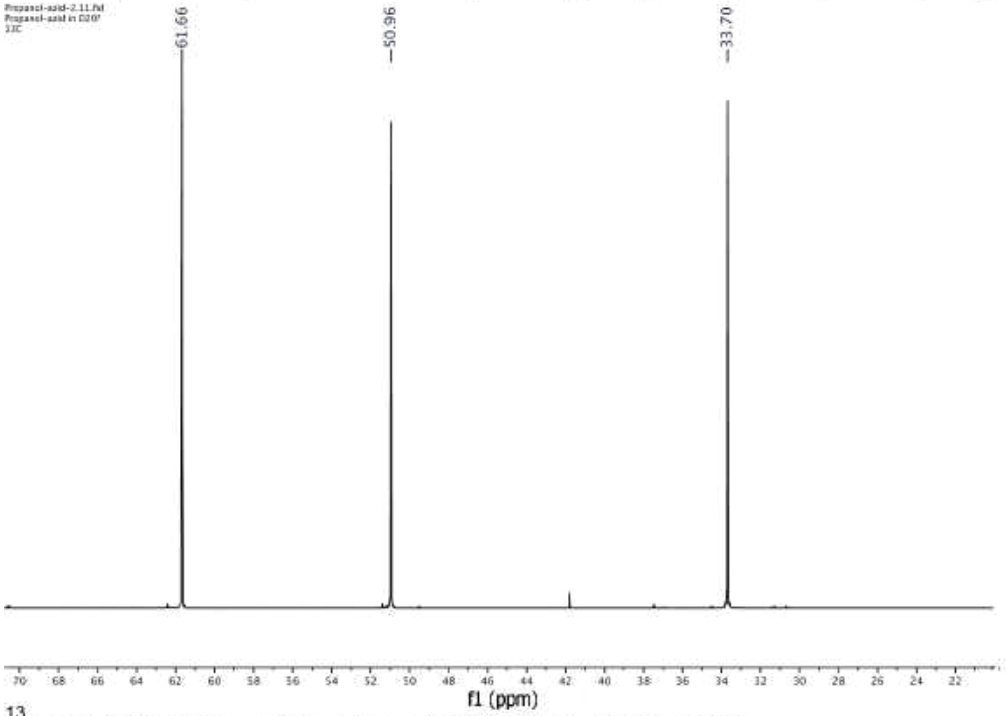

^{13}C NMR (151 MHz, Deuterium Oxide) δ 61.66, 50.96, 33.70.

Fig. A13. ^{1}H NMR and ^{13}C NMR of 3-azidopropan-1-ol (Azide (8); GB59).

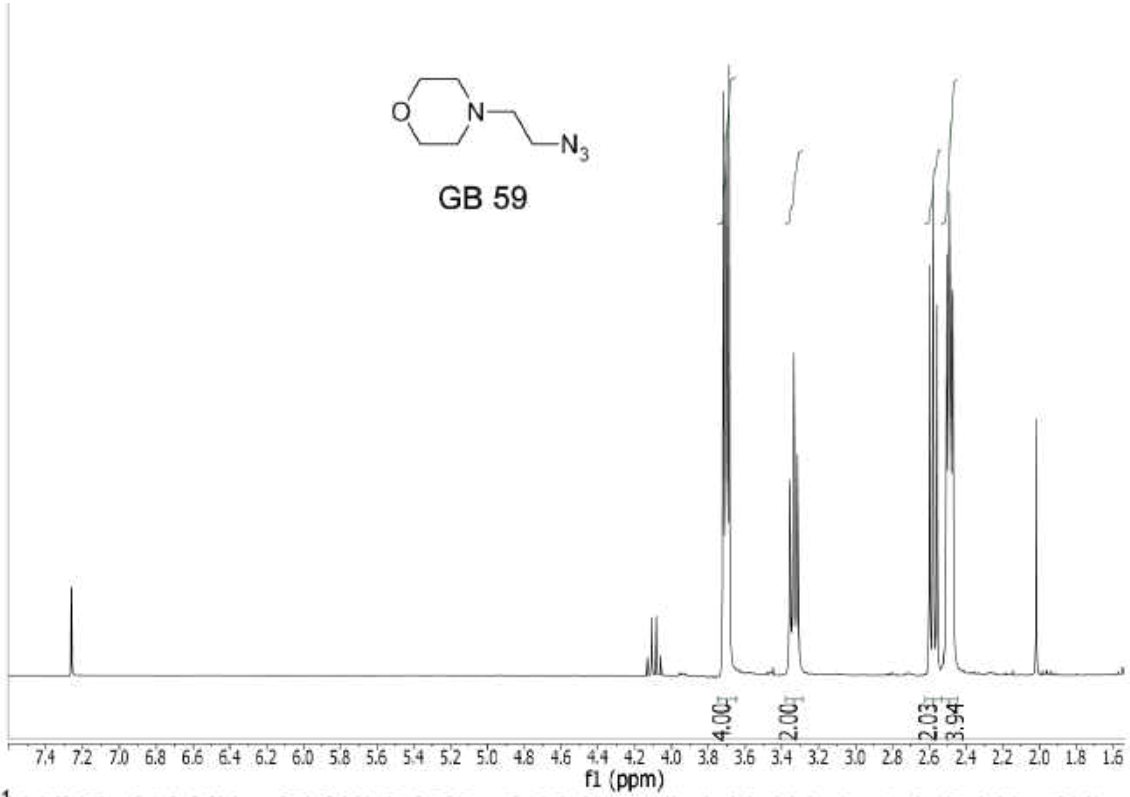

^{1}H NMR (300 MHz, CDCl3) δ 3.75 – 3.65 (m, 4H), 3.33 (dd, J = 6.6, 5.4 Hz, 2H), 2.58 (dd, J = 6.6, 5.4 Hz, 2H), 2.53 – 2.45 (m, 4H).

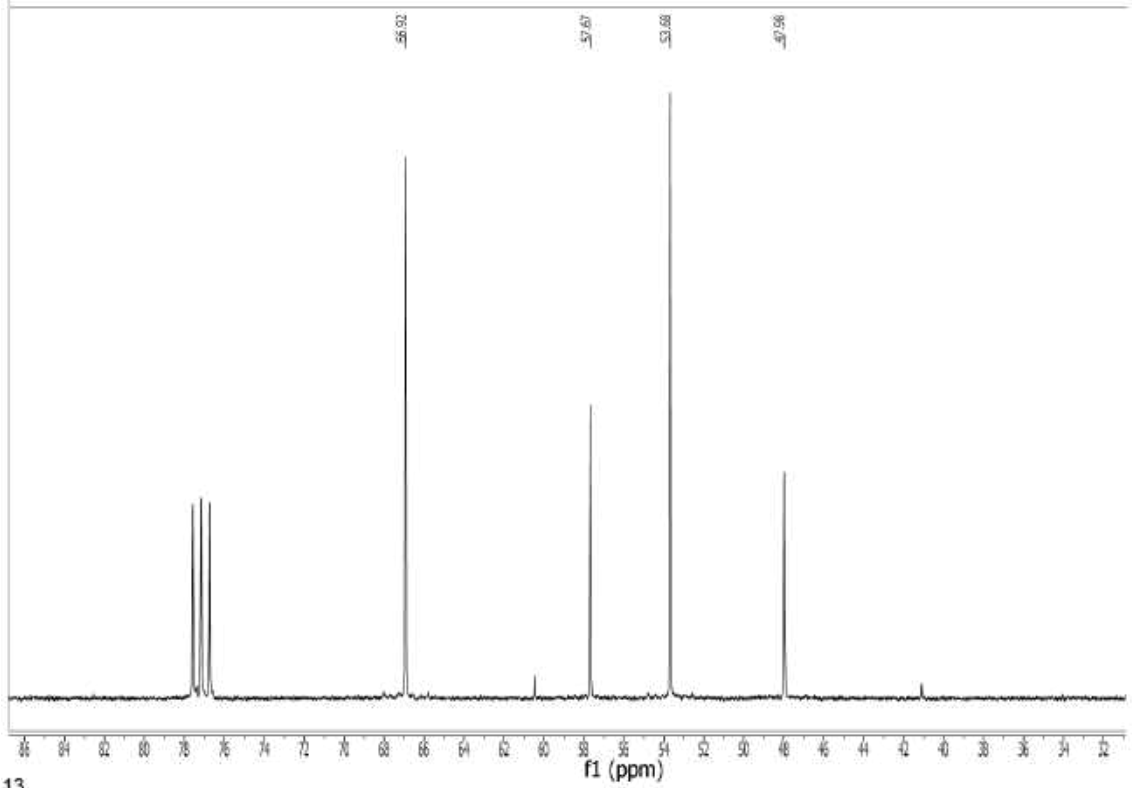

^{13}C NMR (75 MHz, CDCl3) δ 66.92, 57.67, 53.68, 47.98.

Fig. A14. ^{1}H NMR and ^{13}C NMR of 4-(2-azidoethyl)morpholine (Azide (9); GB59).

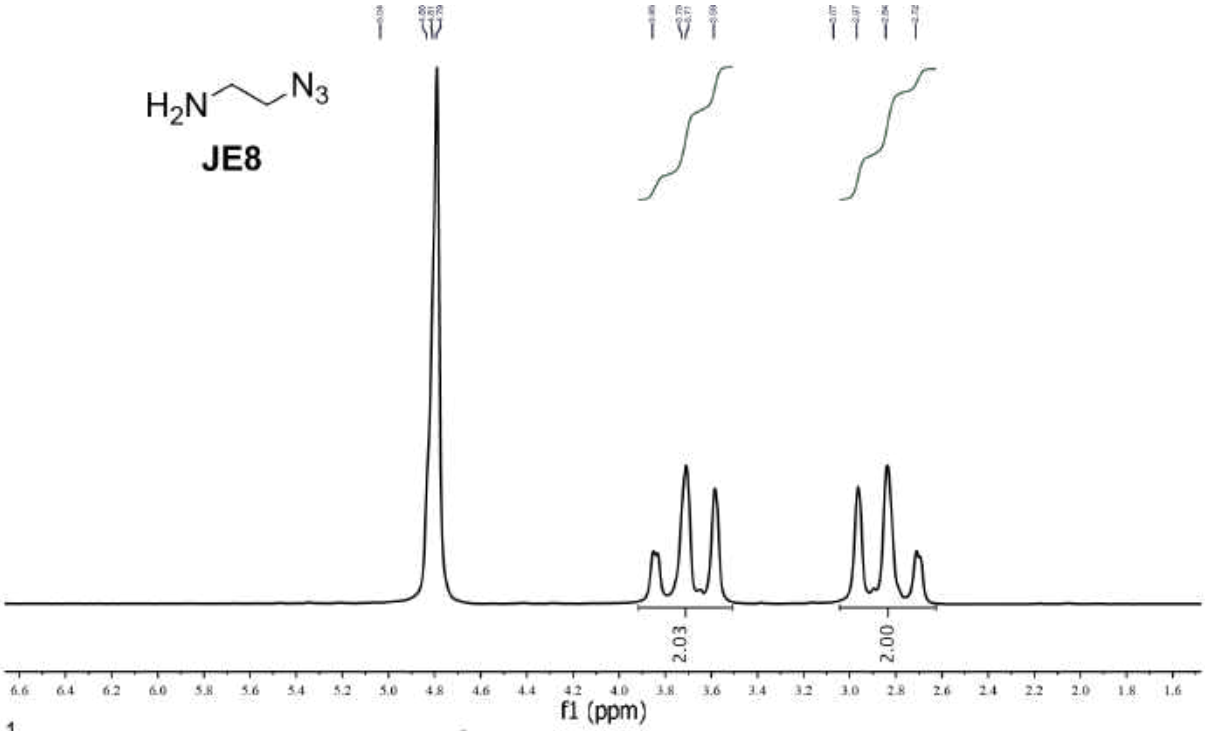

^{1}H NMR (43 MHz, Deuterium Oxide) δ 3.72 (t, 2H), 2.84 (t, 3.5 Hz, 2H).

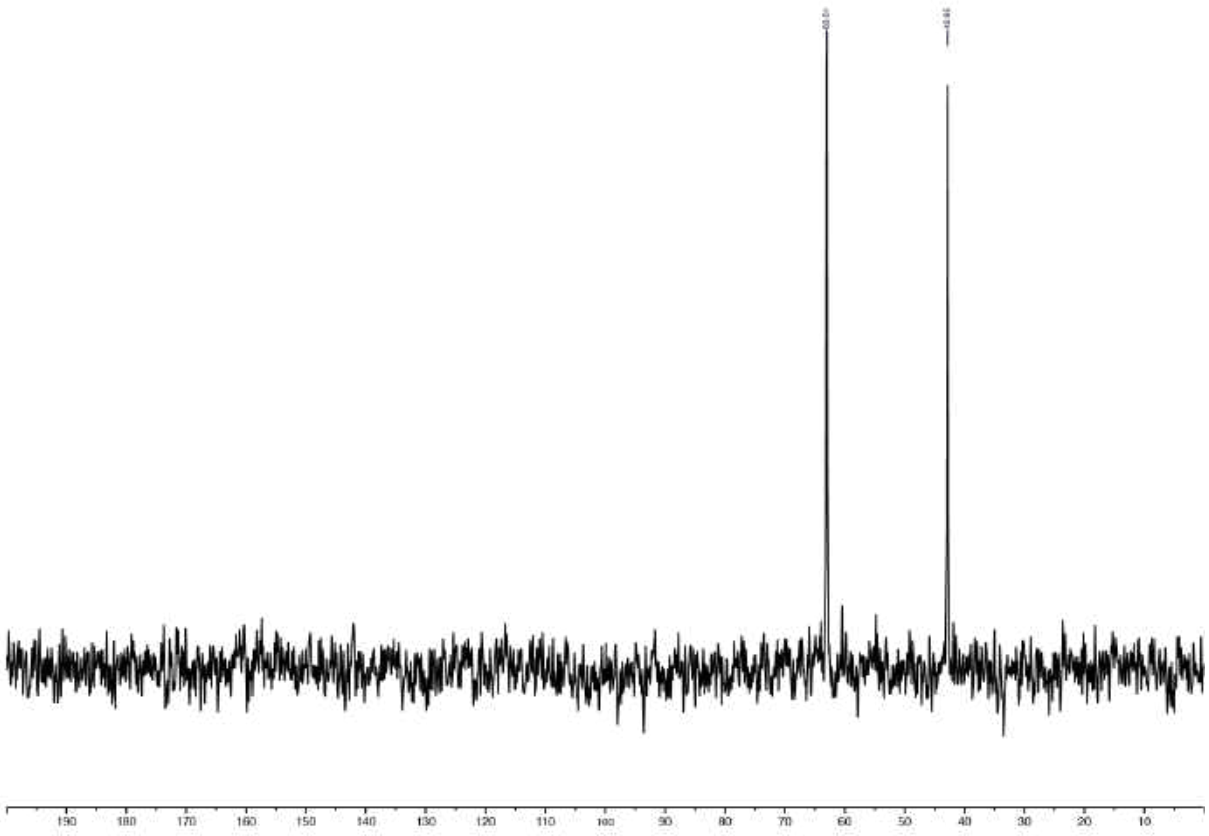

^{13}C NMR (11 MHz, Deuterium Oxide) δ 63.01, 42.85.

Fig. A15. ^{1}H NMR and ^{13}C NMR of 2-azido-ethanamine (Azide (10); JE8).

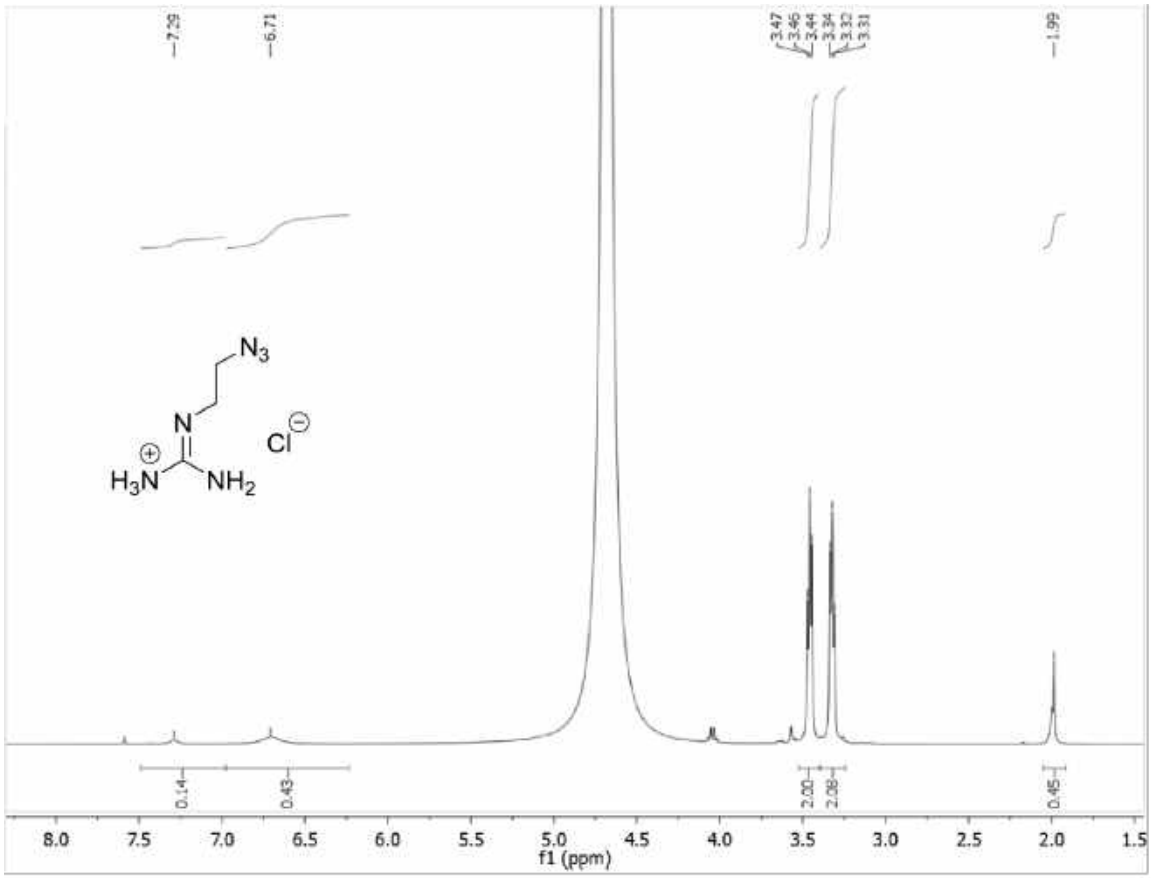

^{1}H NMR (400 MHz, Deuterium Oxide) δ 7.41 (br, s, 2H), 6.83 (br, s, 2H), 3.58 (t, 2H), 3.44 (t, 2H), 2.10 (s, 1H),

Fig. A16. ^{1}H NMR of 2-(azidoethyl)guanidine (Azide (11)).

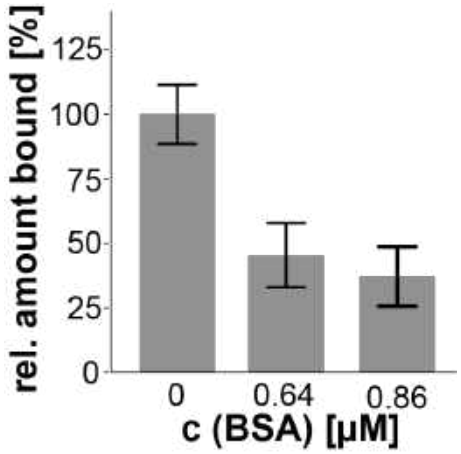

Fig. A17. Binding of C11.41 to THC-modified beads with increasing amounts of BSA in SELEX-buffer

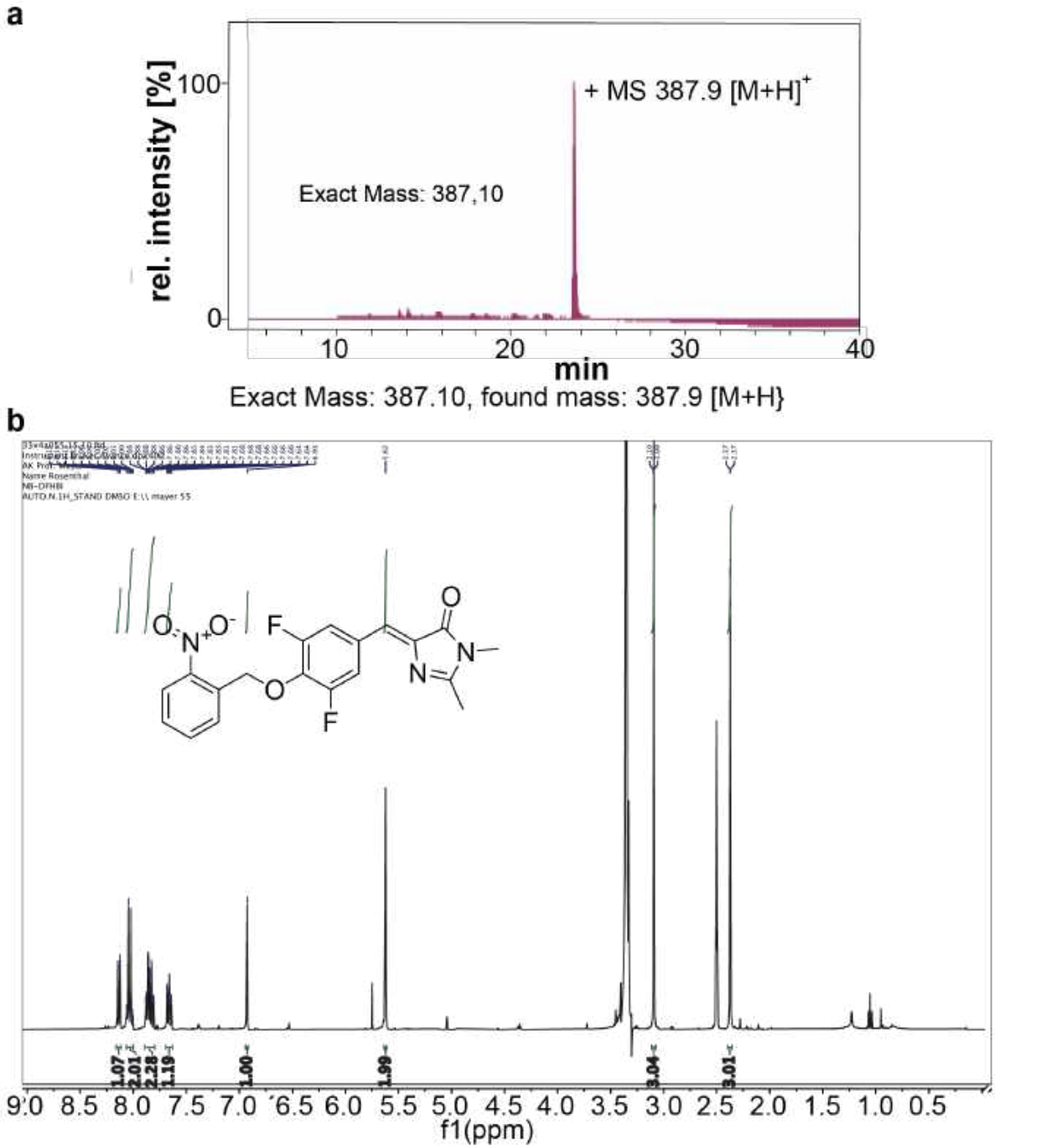

H NMR (400 MHz, DMSO-d6) δ 8.14 (dd, J = 8.2, 1.2 Hz, 1H), 8.04 (d, J = 9.9 Hz, 2H), 7.90 – 7.81 (m, 2H), 7.67 (ddd, J = 8.1, 7.2, 1.7 Hz, 1H), 6.93 (s, 1H), 5.63 (s, 2H), 3.10 (s, 3H), 2.38 (d, J = 0.7 Hz, 3H).

Fig. A18. HPLC-MS and ^{1}H-NMR of AP-DFHBI. a) HPLC-MS result of AP-DFHBI. A gradient of 5 – 100% ACN in 0.1 % FA in 50 min was applied. A singe UV-peak with the correct corresponding mass was observed. B) ^{1}H-NMR of AP-DFHBI.

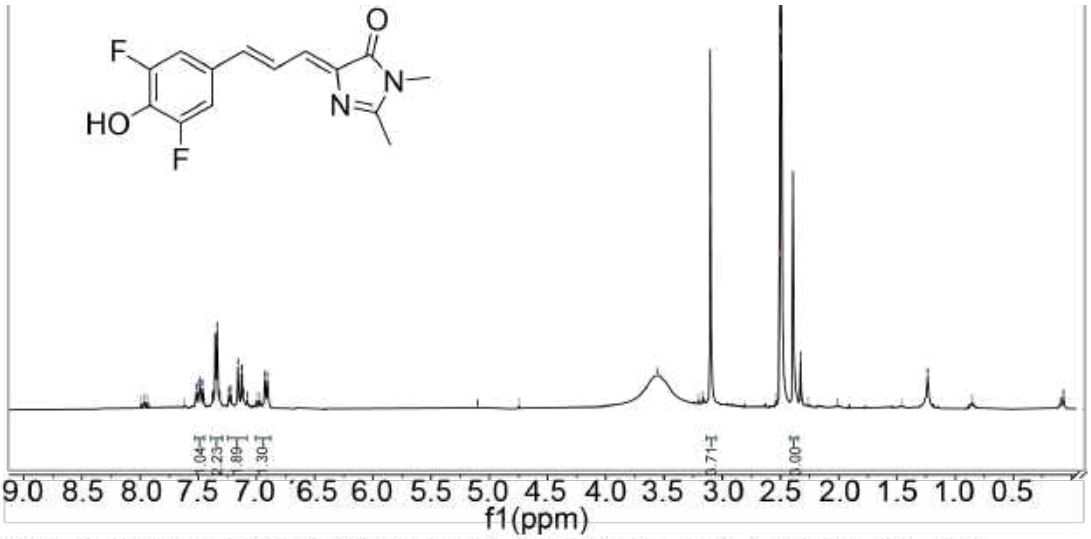

^{1}H NMR (500 MHz, DMSO-d6) δ 7.37 (d, 3J = 4.2 Hz, 1H), 7.19 (dd, 3J = 8.1, 4J =1.7 Hz, 1H), 7.06 (d, 3J = 15.7 Hz, 1H),7.01 (d, 3J = 15.7 Hz, 1H, H-3,), 6.90 (d,4J = 11.8 Hz, 2H, H-4), 6.79 (d, J = 11.5 Hz, 1H), 5.10 (s, 1H), 3.07 (s, 3H),2.30 (s, 3H).

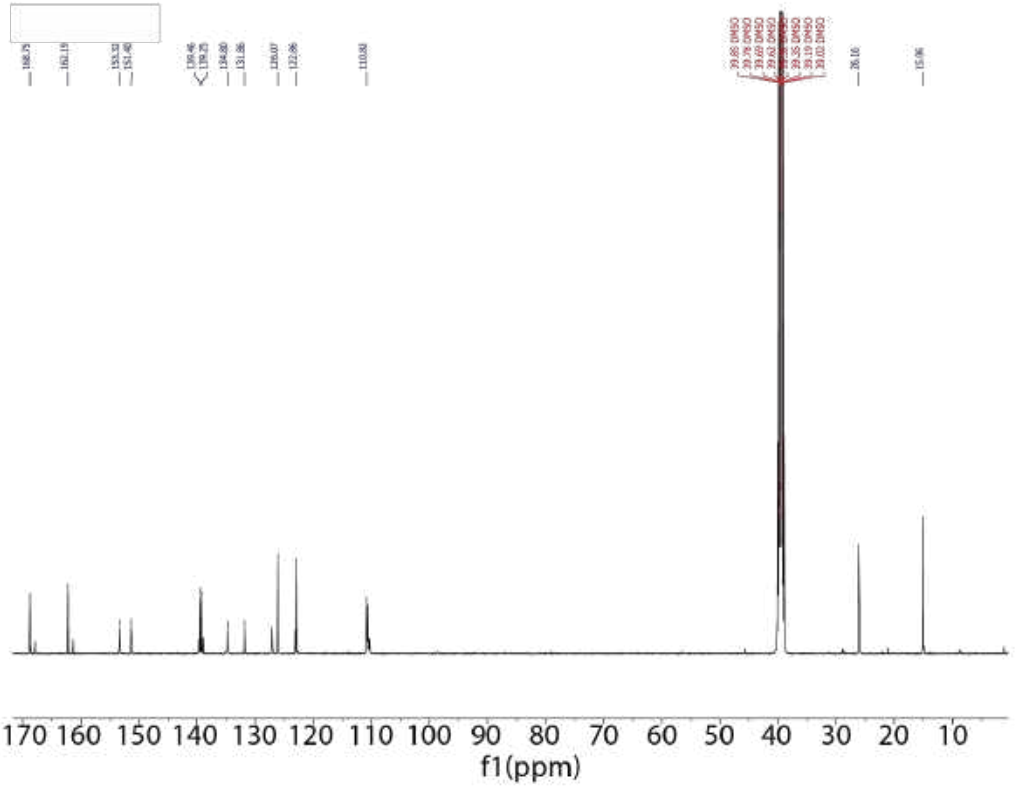

^{13}C NMR (126 MHz, DMSO) δ [ppm] = 168.75 (C-1), 162.19 (C-2), 153.32 (C-3), 151.40 (C-4),139.46 (C-5), 134.80 (C-6), 131.86 (C-7), 126.07 (C-8),122.86 (C-9), 110.82 (C-10), 26.16 (C-11), 15.06(C- 12).

Fig. A19. ^{1}H- and ^{13}C-NMR of eDFHBI.

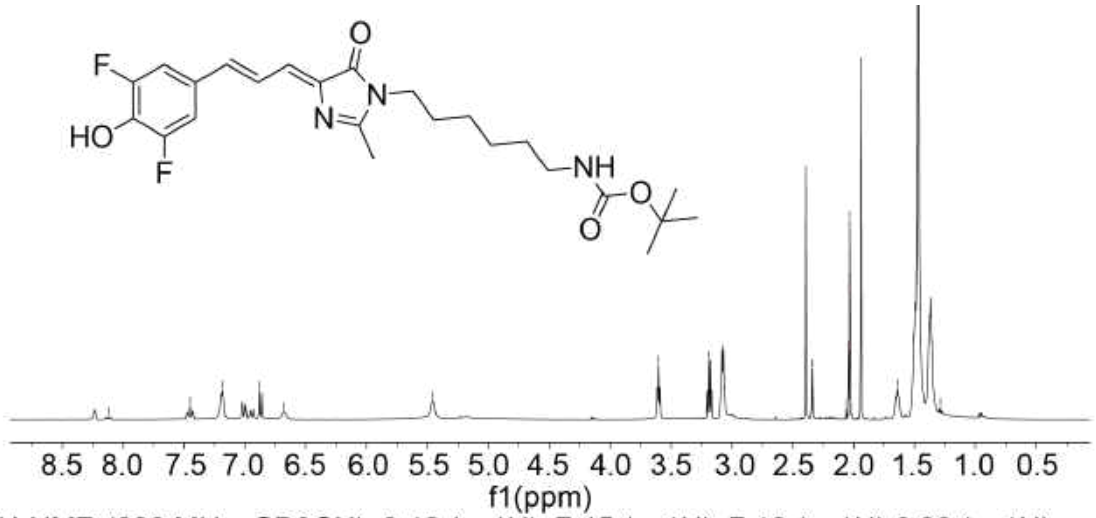

^{1}H-NMR (600 MHz, CD3CN) 8.12 (s, 1H), 7.45 (s, 1H), 7.18 (s, 1H),6.88 (s, 1H), 6.68 (s, 2H), 5.46 (s, 1H),3.60 (s, 2H), 3.19 (s, 2H), 2.34 (s, 3H),1.64 (s, 2H, H-10), 1.53 – 1.41 (m, 2H), 1.38 (s,9H, H-12), 1.29 (s, 4H, H-13).

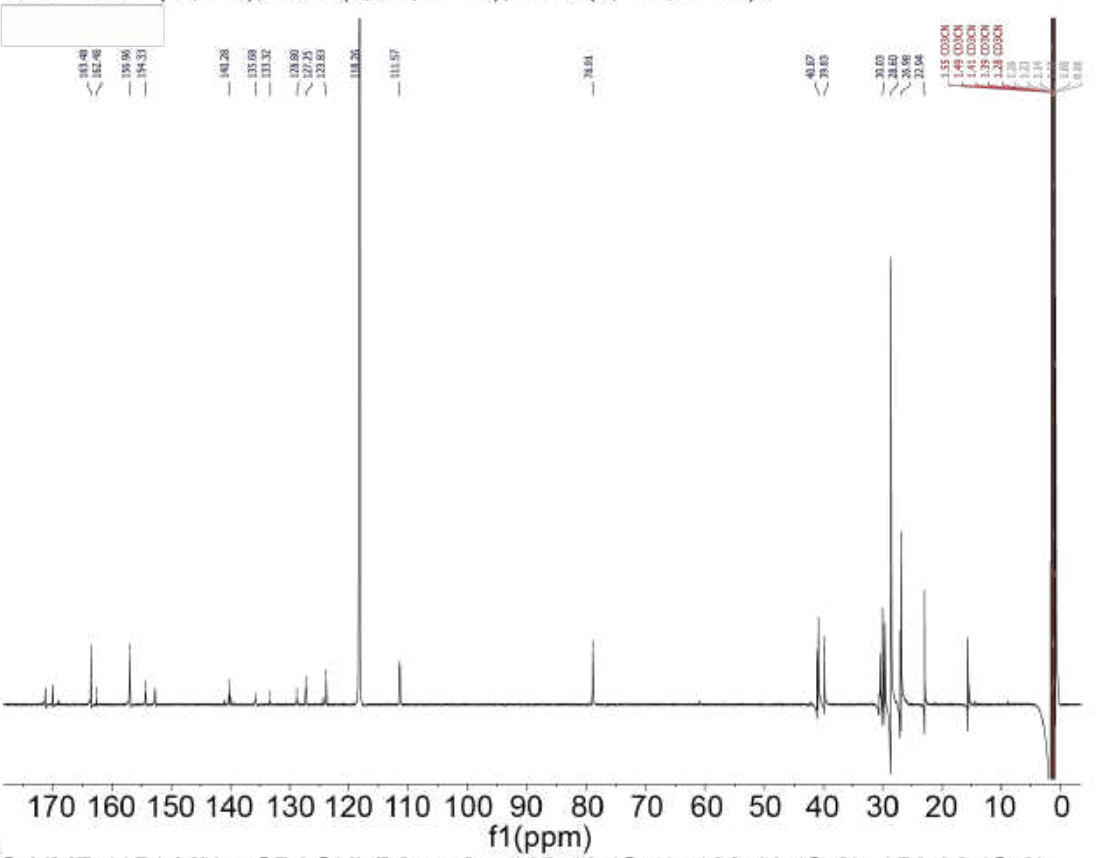

^{13}C-NMR (151 MHz, CD3CN) δ [ppm] = 163.48 (C-1), 162.48 (C-2), 156.96 (C-3), 154.33 (C-4),140.28 (C-5), 135.68 (C-6), 133.32 (C-7), 128.80 (C-8),127.25 (C-9), 123.83 (C-10), 111.57 (C-11), 78.91 (C-12) 40.87 (C-13), 39.83 (C-14), 30.03 (C-15), 28.60 (C-16), 26.98 (C-17), 22.94 (C-18).

Fig. A20. ^{1}H-NMR and ^{13}C-NMR of eDFHBI containing a Boc-protected linker.

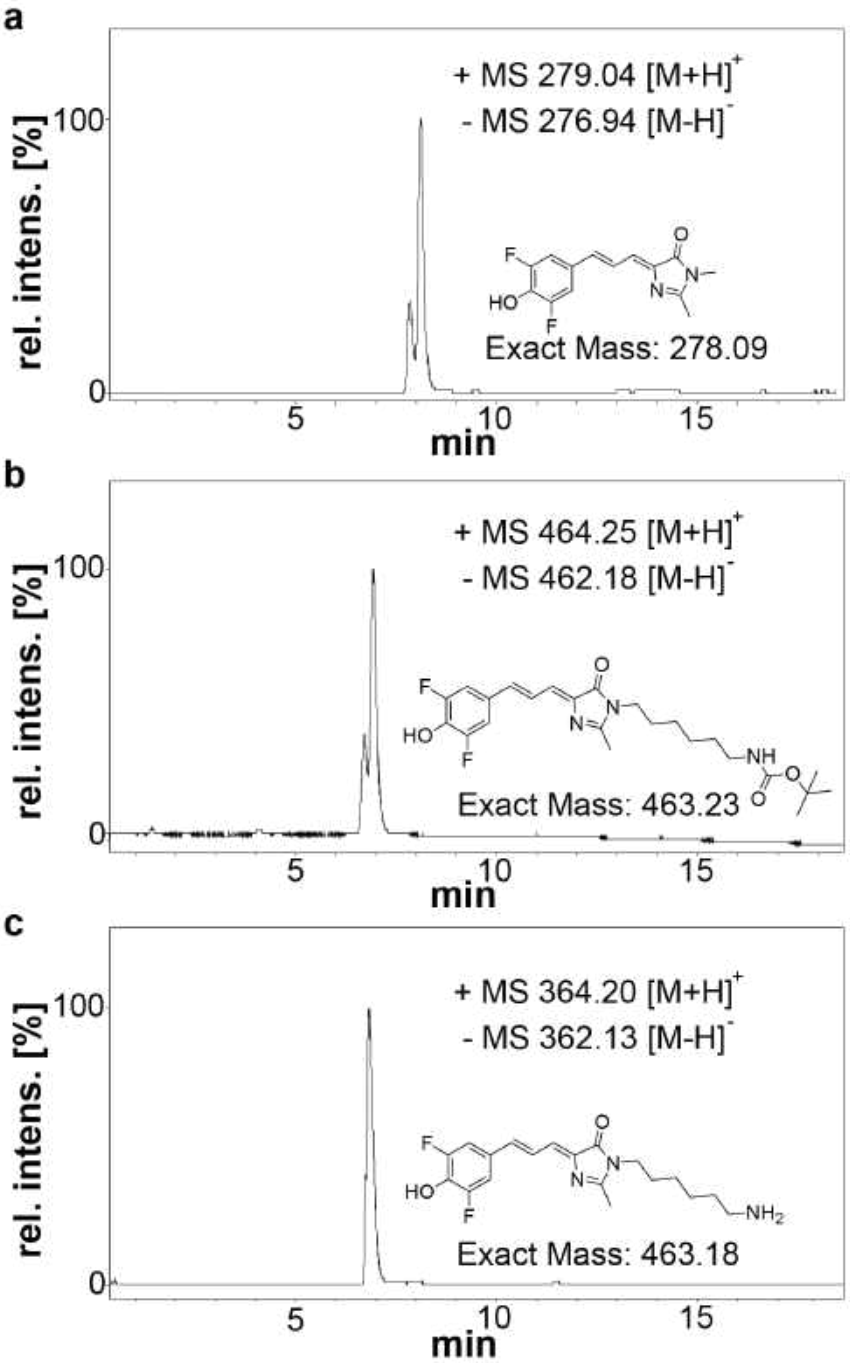

Fig. 21. HPLC-MS of eDFHBI with and without the linker. A gradient of 20-100% ACN in 0.1% FA in 30 min was applied. a) HPLC chromatogram with corresponding detected masses of eDFHBI. b) HPLC chromatogram with corresponding detected masses of eDFHBI carrying a Boc-protected linker. c) HPLC chromatogram with corresponding detected masses of eDFHBI carrying the linker after removal of the Boc group.

References

1. World-Health-Organisation. Management of substance abuse. vol. 2018.

2. Kai Macdonald, K. P. why not pot? A Review of the BrainbasedRisks of Cannabis. *Innov. Clin. Neurosci.* **13**, (2016).

3. Roffman, R. A. Legalization of marijuana: unraveling quandaries for the addiction professional. *Front Psychiatry* **4**, 50 (2013).

4. Mary Barna Bridgeman BCPS, BCGP; and Daniel T. Abazia, P. Medicinal Cannabis: History, Pharmacology, And Implications for the Acute Care Setting. *Pharm. Ther.* **42**, 180 (2017).

5. National Institute on Drug Abuse. https://www.drugabuse.gov/related-topics/college-age-young-adults.

6. Crime, U. N. O. o. D. a. World Drug Report 2017. https://www.unodc.org/wdr2017/field/WDR_2017_presentation_lauch_version.pdf.

7. Murphy, J. Canada becomes second country to legalise recreational cannabis. https://www.bbc.com/news/world-us-canada-45806255.

8. Cressey, D. The cannabis experiment. *Nature* **524**, 280–283 (2015).

9. Onvista. https://www.onvista.de/aktien/APHRIA-INC-Aktie-CA03765K1049.

10. William C. Kerr Meenakshi Sabina Subbaraman, Edwina Williams, *Yuye & Greenfield, & T. K. Changes in Marijuana Use Across the 2012 Washington State Recreational Legalization: Is Retrospective Assessment of Use Before Legalization More Accurate? *J. Stud. Alcohol Drugs* **97**, 495–502.

11. Pacula, R. L., Powell, D., Heaton, P. & Sevigny, E. L. Assessing the Effects of Medical Marijuana Laws on Marijuana Use The Devil is in the Details. *J. Policy Anal. Manag.* **34**, 7–31.

12. Wen Hefei, Hockenberry Jason M & Cummings Janet R. The effect of medical marijuana laws on adolescent and adult use of marijuana, alcohol, and other substances. *J. Health Econ.* **42**, 64–80 (2015).

13. Anderson, D. M., Hansen, B. & Rees, D. I. Medical marijuana laws and teen marijuana use. (2014).

14. Kim, H. S. & Monte, A. A. Colorado Cannabis Legalization and Its Effect on Emergency Care. *Ann Emerg Med* **68**, 71–75 (2016).

15. Andre, C. M., Hausman, J. F. & Guerriero, G. Cannabis sativa: The Plant of the Thousand and One Molecules. *Front Plant Sci* **7**, 19 (2016).

16. McPartland, J. M., Duncan, M., Di Marzo, V. & Pertwee, R. G. Are cannabidiol and Delta(9) -tetrahydrocannabivarin negative modulators of the endocannabinoid system? A systematic review. *Br J Pharmacol* **172**, 737–753 (2015).

17. L.M., B., K.L., F., A.M., N. & G.S., W. The pharmacologic and clinical effects of medical cannabis. *Pharmacotherapy* **33**, 195–209 (2013).

18. Mechoulam, R. & Parker, L. The Endocannabinoid System and the Brain. *Ssrn* (2013) doi:10.1146/annurev-psych-113011-143739.

19. Pacher, P., Batkai, S. & Kunos, G. The endocannabinoid system as an emerging target of pharmacotherapy. *Pharmacol Rev* **58**, 389–462 (2006).

20. Fattore, L. *et al.* An endocannabinoid mechanism in relapse to drug seeking: a review of animal studies and clinical perspectives. *Brain Res Rev* **53**, 1–16 (2007).

21. Kaur, R., R. Ambwani, S. & Singh, S. Endocannabinoid System: A Multi-Facet Therapeutic Target. *Curr. Clin. Pharmacol.* **11**, 110–117 (2016).

22. Howlett, A. C. & Abood, M. E. CB1 and CB2 Receptor Pharmacology. *Adv Pharmacol* **80**, 169–206 (2017).

23. Pertwee, R. G. The diverse CB 1 and CB 2 receptor pharmacology of three plant cannabinoids: Δ 9-tetrahydrocannabinol, cannabidiol and Δ 9-tetrahydrocannabivarin. *Br. J. Pharmacol.* **153**, 199–215 (2008).

24. Burstein, S. H. *et al.* Synthetic nonpsychotropic cannabinoids with potent antiinflammatory, analgesic, and leukocyte antiadhesion activities. *J. Med. Chem.* **35**, 3135–3141 (2005).

25. Russo, E. B. Current Therapeutic Cannabis Controversies and Clinical Trial Design Issues. *Front Pharmacol* **7**, 309 (2016).

26. Pertwee, R. G. Cannabinoid receptors and pain. *Prog. Neurobiol.* **63**, 569–611.

27. M Herkenham M D Little, M R Johnson, L S Melvin, B R de Costa, and K C Rice, A. B. L. Cannabinoid receptor localization in brain. *Proc Natl Acad Sci U S A* **87**, 1932–1936.

28. Mackie, K. Mechanisms of CB1 receptor signaling: endocannabinoid modulation of synaptic strength. *Int J Obes* **30 Suppl 1**, S19-23 (2006).

29. Shim, J. Y., Bertalovitz, A. C. & Kendall, D. A. Identification of essential

cannabinoid-binding domains: structural insights into early dynamic events in receptor activation. *J Biol Chem* **286**, 33422–33435 (2011).

30. Kapur, A. *et al.* Mutation studies of Ser7.39 and Ser2.60 in the human CB1 cannabinoid receptor: evidence for a serine-induced bend in CB1 transmembrane helix 7. *Mol Pharmacol* **71**, 1512–1524 (2007).

31. López-Rodríguez, S. O.-G. and M. L. CB1 and CB2 Cannabinoid Receptor Binding Studies Based on Modeling and Mutagenesis Approaches. *Mini-Reviews Med. Chem.* **5**, 651–658.

32. Schoepp, N. G. *et al.* Crystal structures of agonist-bound human cannabinoid receptor CB1. *Nature* **55**, 9557–9561 (2017).

33. Hua, T. *et al.* Crystal Structure of the Human Cannabinoid Receptor CB1. *Cell* **167**, 750-762 e14 (2016).

34. Shao, Z. *et al.* High-resolution crystal structure of the human CB1 cannabinoid receptor. *Nature* **540**, 602–606 (2016).

35. Zuardi, A. W. History of cannabis as a medicine: a review. *Rev. Bras. Psiquiatr.* **28**, 153–157.

36. Andrew Hand, A. B., Paul Kerrigan, P. S. & Friedberg, and J. History of medical cannabis. *J. Pain Manag.* **9**, 387–394 (2016).

37. Mikuriya, T. H. Marijuana in medicine: past, present and future. *Calif. Med.* **110**, 34–40 (1996).

38. Mcmeens, B. Y. R. R. Report of the Ohio State Medical Committee on cannabis Indica. *Sulphur* 117–140 (1860).

39. Mikuriya, T. H. & Aldrich, M. R. Cannabis 1988. Old drug, new dangers. The potency question. *J Psychoact. Drugs* **20**, 47–55 (1988).

40. Gaoni Y, M. R. J. Isolation structure and partial synthesis of an active constituent of hashish. *J Am Chem Soc.* **86**, 1646–1647.

41. Monika Fellermeier Adelbert Bacher and Meinhart H. Zenk, W. E. Biosynthesis of cannabinoids Incorporation experiments with 13C-labeled glucoses. *Eur. J. Biochem.* **268**, 1596–1604.

42. Raharjo, T. J., Chang, W.-T., Choi, Y. H., Peltenburg-Looman, A. M. G. & Verpoorte, R. Olivetol as product of a polyketide synthase in Cannabis sativa L. *Plant Sci.* **166**, 381–385 (2004).

43. Degenhardt, F., Stehle, F. & Kayser, O. *The Biosynthesis of Cannabinoids*. *Handbook of Cannabis and Related Pathologies: Biology, Pharmacology, Diagnosis, and Treatment* (Elsevier Inc., 2017). doi:10.1016/B978-0-12-800756-3.00002-8.

44. Munro S. Abu-Shaar M., T. K. L. Molecular characterization of a peripheral receptor for cannabinoids. *Nature* **365**, 61–65 (1993).

45. Matsuda LA Brownstein MJ, Young AC, Bonner TI., L. S. J. Structure of a cannabinoid receptor and functional expression of the cloned cDNA. *Nature* **346**, 561–564 (1990).

46. Devane WA Johnson MR, Melvin LS, Howlett AC, D. F. A. Determination and Characterization of a Cannabinoid Receptor in Rat Brain. *Mol Pharmacol.* **34**, 605–613.

47. Hughes, B. Cannabis legislation in Europe. *Luxemb. Publ. Off. Eur. Union* (2018) doi:10.2810/930744 10.2810/566650.

48. Mahnert, J. Canopy Growth-Aktie: Marktführer mit weiterem Potenzial! – Videoanalyse. https://www.finanztrends.info/canopy-growth-marktfuehrer-mit-weiterem-potenzial/.

49. Kanadas skurriler Cannabisplantagenbauwettbewerb. https://www.leafly.de/kanada-cannabisplantagenbauwettbewerb/.

50. Habekuß, F. Holy Shit! https://www.zeit.de/2018/15/cannabis-anbau-arzneimittel-deutschland-kanada.

51. Campos, A. C., Moreira, F. A., Gomes, F. V, Del Bel, E. A. & Guimaraes, F. S. Multiple mechanisms involved in the large-spectrum therapeutic potential of cannabidiol in psychiatric disorders. *Philos Trans R Soc L. B Biol Sci* **367**, 3364–3378 (2012).

52. Hill, K. P. Medical Marijuana for Treatment of Chronic Pain and Other Medical and Psychiatric Problems: A Clinical Review. *JAMA* **313**, 2474–2483 (2015).

53. Hammell, D. C. *et al.* Transdermal cannabidiol reduces inflammation and pain-related behaviours in a rat model of arthritis. *Eur J Pain* **20**, 936–948 (2016).

54. Hasenoehrl, C., Storr, M. & Schicho, R. Cannabinoids for treating inflammatory bowel diseases: where are we and where do we go? *Expert Rev. Gastroenterol. Hepatol.* **11**, 329–337 (2017).

55. Ware, M. A. *et al.* Smoked cannabis for chronic neuropathic pain: a randomized controlled trial. *CMAJ* **182**, E694-701 (2010).

56. Top 14 Marijuana Strains for Different Kinds of Pain. https://www.hellomd.com/health-wellness/562150d03232620006450000/top-14-marijuana-strains-for-different-kinds-of-pain.

57. Leonard, J. What are the best cannabis strains for chronic pain.

https://www.medicalnewstoday.com/articles/322051.php.

58. Rahn, B. The Best Cannabis Strains for Pain. https://www.leafly.com/news/strains-products/best-cannabis-strains-for-treating-pain.

59. Krcevski-Skvarc, N., Wells, C. & Häuser, W. Availability and approval of cannabis-based medicines for chronic pain management and palliative/supportive care in Europe: A survey of the status in the chapters of the European Pain Federation. *Eur. J. Pain (United Kingdom)* **22**, 440–454 (2018).

60. Fact sheet - Sativex (Tetranabinex and Nabidiolex). https://www.canada.ca/en/health-canada/services/drugs-health-products/drug-products/notice-compliance/conditions/fact-sheet-sativex-tetranabinex-nabidiolex.html.

61. Treat, L., Chapman, K. E., Colborn, K. L. & Knupp, K. G. Duration of use of oral cannabis extract in a cohort of pediatric epilepsy patients. *Epilepsia* **58**, 123–127 (2017).

62. Porsteinsson, A. P. & Antonsdottir, I. M. An update on the advancements in the treatment of agitation in Alzheimer's disease. *Expert Opin Pharmacother* **18**, 611–620 (2017).

63. Ohlsson A Wahlen A, Agurell S, Hollister LE, Gillespie HK, L. J. E. Plasma delta-9 tetrahydrocannabinol concentrations and clinical effects after oral and intravenous administration and smoking. *Clin Pharmacol Ther.* **28**, 409–416.

64. Berghaus, G., Sheer, N. & Schmidt, P. Effects of cannabis on psychomotor skills and driving performance - a metaanalysis of experimental studies. *Proc. 13th Int. Conf. Alcohol, Drugs Traffic Saf.* 403–409 (1995).

65. G. Berghaus W. Grellner, D. Lenz , Th. Nauman and S. Wiesenmüller, G. S. Meta-analysis of empirical studies concerning the effects of medicines and illegal drugs including pharmacokinetics on safe driving. *DRUID 6TH Framew. Program.* (2010).

66. Lanz, C., Mattsson, J., Soydaner, U. & Brenneisen, R. Medicinal Cannabis: In Vitro Validation of Vaporizers for the Smoke-Free Inhalation of Cannabis. *PLoS One* **11**, (2016).

67. Russo, E. B. History of Cannabis and Its Preparations in Saga, Science, and Sobriquet. *Chem. Biodiveraity* **4**, 1614–1648.

68. Gieringer, D., St. Laurent, J. & Goodrich, S. Cannabis Vaporizer Combines Efficient Delivery of THC with Effective Suppression of

Pyrolytic Compounds. *J. Cannabis Ther.* **4**, 7–27 (2004).

69. Earleywine, M. & Barnwell, S. S. Decreased respiratory symptoms in cannabis users who vaporize. *Harm Reduct J* **4**, 11 (2007).

70. Karschner, E. L., Darwin, W. D., Goodwin, R. S., Wright, S. & Huestis, M. A. Plasma Cannabinoid Pharmacokinetics following Controlled Oral ∆9-Tetrahydrocannabinol and Oromucosal Cannabis Extract Administration. *Clin. Chem.* **57**, 66–75 (2010).

71. Should marijuana be a medical option? ProCon.org.

72. Coffey, C. & Patton, G. C. Cannabis Use in Adolescence and Young Adulthood. *Can. J. Psychiatry* **61**, 318–327 (2016).

73. Evren, C. *Chapter 8 - Cannabis Use and Cognitive Function*. *Handbook of Cannabis and Related Pathologies* (Elsevier Inc., 2017). doi:10.1016/B978-0-12-800756-3/00009-0.

74. Volkow, N. D., Baler, R. D., Compton, W. M. & Weiss, S. R. Adverse health effects of marijuana use. *N Engl J Med* **370**, 2219–2227 (2014).

75. Hauet, P. M. P. K. V. D. S. R. T. THC Can Be Detected in BrainWhile Absent in Blood. *J. Anal. Toxicol.* **29**, 842–843.

76. Hall, W. & Lynskey, M. Why it is probably too soon to assess the public health effects of legalisation of recreational cannabis use in the USA. *The Lancet Psychiatry* **3**, 900–906 (2016).

77. Hartman, R. L. *et al.* Cannabis effects on driving lateral control with and without alcohol. *Drug Alcohol Depend* **154**, 25–37 (2015).

78. Summary of Main DRUID Results. https://www.bast.de/Druid/EN/Dissemination/downloads_and_links/2012_Washington_Brochure.html?nn=613804.

79. Jones, A. W., Holmgren, A. & Kugelberg, F. C. Driving under the influence of cannabis: A 10-year study of age and gender differences in the concentrations of tetrahydrocannabinol in blood. *Addiction* **103**, 452–461 (2008).

80. Addiction, E. M. C. for D. and D. Drug use, impaired driving and traffic accidents, second edition. *Publ. Off. Eur. Union, Luxemb.* (2014).

81. Battistella, G. *et al.* Weed or wheel! FMRI, behavioural, and toxicological investigations of how cannabis smoking affects skills necessary for driving. *PLoS One* **8**, e52545 (2013).

82. Martin, J. L., Gadegbeku, B., Wu, D., Viallon, V. & Laumon, B. Cannabis, alcohol and fatal road accidents. *PLoS One* **12**, e0187320 (2017).

83. Cannabis and driving: questions and answers for policymaking. *Eur. Monit. Cent. Drugs Drug Addict. Can. Cent. Subst. Use Addict.* (2018) doi:10.2810/729865 10.2810/090451.

84. Beirness, D. J. & Porath, A. J. Clearing the Smoke on Cannabis, Cannabis Use and Driving - An Update. *Can. Cent. Subst. Use Addict.* 1–7 (2017).

85. Bondallaz, P. *et al.* Cannabis and its effects on driving skills. *Forensic Sci Int* **268**, 92–102 (2016).

86. Ronen, A. *et al.* Effects of THC on driving performance, physiological state and subjective feelings relative to alcohol. *Accid. Anal. Prev.* **40**, 926–34 (2008).

87. Kelly, E., Darke, S. & Ross, J. A review of drug use and driving: epidemiology, impairment, risk factors and risk perceptions. *Drug Alcohol Rev* **23**, 319–344 (2004).

88. Ramaekers, J. G., Berghaus, G., van Laar, M. & Drummer, O. H. Dose related risk of motor vehicle crashes after cannabis use. *Drug Alcohol Depend.* **73**, 109–119 (2004).

89. Rogeberg, O. & Elvik, R. The effects of cannabis intoxication on motor vehicle collision revisited and revised. *Addiction* **111**, 1348–1359 (2016).

90. Salomonsen-Sautel, S., Min, S. J., Sakai, J. T., Thurstone, C. & Hopfer, C. Trends in fatal motor vehicle crashes before and after marijuana commercialization in Colorado. *Drug Alcohol Depend* **140**, 137–144 (2014).

91. Amy Berning and Kathryn Wochinger, R. C. Results of the 2013–2014 National Roadside Survey of Alcohol and Drug Use by Drivers. *Natl. Highw. Traffic Saf. Adm.* (2015).

92. Zaid, J. & Valleriani, J. Medical Cannabis and Impaired Driving : Preliminary Research Review. 1–30 (2017).

93. Blows, S. *et al.* Marijuana use and car crash injury. *Addiction* **100**, 605–611 (2005).

94. Huestis, M. A. & Smith, M. L. Cannabinoid Markers in Biological Fluids and Tissues: Revealing Intake. *Trends Mol Med* **24**, 156–172 (2018).

95. Owusu-Bempah, A. Cannabis Impaired Driving: An Evaluation of Current Modes of Detection. *Can. J. Criminol. Crim. Justice* **56**, 219–240 (2014).

96. Karschner, E. L. *et al.* Do Delta9-tetrahydrocannabinol concentrations indicate recent use in chronic cannabis users? *Addiction* **104**, 2041–2048 (2009).

97. Gallardo, E. & Queiroz, J. A. The role of alternative specimens in toxicological analysis. *Biomed Chromatogr* **22**, 795–821 (2008).

98. Lee, D. *et al.* Oral fluid cannabinoids in chronic, daily Cannabis smokers during sustained, monitored abstinence. *Clin Chem* **57**, 1127–1136 (2011).

99. Erin L. Karschner Ross H. Lowe, W. David Darwin, Ronald I. Herning, Jean Lud Cadet, and Marilyn A. Huestis, E. W. S. Implications of Plasma Δ9 Tetrahydrocannabinol, 11-Hydroxy- THC, and 11-nor-9-Carboxy-THC Concentrations in Chronic Cannabis Smokers. *J Anal Toxicol* **33**, 469–477.

100. Huestis, M. A. Pharmacokinetics and Metabolism of the Plant Cannabinoids, delta-9-THC, Cannabidiol and Cannabinol. *Cannabinoids* 657–690 (2005).

101. Bosker, W. M. & Huestis, M. A. Oral fluid testing for drugs of abuse. *Clin. Chem.* **55**, 1910–1931 (2009).

102. Hughes, B. Contemporary challenges for regulatory models Which approach to take? A conceptual overview. in *Third international symposium on drugs and driving* (2017).

103. Williams PL, M. A. C. Identification in human urine of delta 9-tetrahydrocannabinol-11-oic acid glucuronide: a tetrahydrocannabinol metabolite. *J Pharm Pharmacol* **32**, 445–448.

104. Agius, R., Nadulski, T., Kahl, H. G. & Dufaux, B. Comparison of LUCIO®-direct ELISA with CEDIA immunoassay for ‘zero tolerance’ drug screening in urine as required by the German re-licensing guidelines. *Drug Test. Anal.* **5**, 390–399 (2013).

105. Kauert, G. F., Toennes, S. W., Theunissen, E. L., Ramaekers, J. G. & Moeller, M. R. Comparison of Cannabinoid Pharmacokinetic Properties in Occasional and Heavy Users Smoking a Marijuana or Placebo Joint. *J. Anal. Toxicol.* **32**, 470–477 (2013).

106. Ramaekers, J. G. *et al.* High-potency marijuana impairs executive function and inhibitory motor control. *Neuropsychopharmacology* **31**, 2296–2303 (2006).

107. Nicholson, A. N., Turner, C., Stone, B. M. & Robson, P. J. Effect of Δ-9-tetrahydrocannabinol and cannabidiol on nocturnal sleep and early-morning behavior in young adults. *J. Clin. Psychopharmacol.* **24**, 305–313 (2004).

108. Desrosiers, N. A. *et al.* Urinary cannabinoid disposition in occasional and frequent smokers: is THC-glucuronide in sequential urine samples a

marker of recent use in frequent smokers? *Clin Chem* **60**, 361–372 (2014).

109. R. Sam Niedbala Dean F. Fritch, Stephanie Kardos, Tiffany Fries, and Joe Waga, K. W. K. Detection of Marijuana Use by Oral Fluid and Urine Analysis Following Single-Dose Administration of Smoked and Oral Marijuana. *J. Anal. Toxicol.* **25**, 289–303.

110. Robert S. Goodwin C. Nora Chiang, Ming Shih, Shou-Hua Li, and Marilyn A. Huestis, W. D. D. Urinary Elimination of 11-Nor-9-carboxy- 9-tetrahydrocannnabinol in Cannabis Users During Continuously Monitored Abstinence. *J Anal Toxicol* **32**, 562–569.

111. Andås, H. T. *et al.* Detection Time for THC in Oral Fluid After Frequent Cannabis Smoking. *Ther. Drug Monit.* **36**, 808–814 (2014).

112. Milman, G. *et al.* Cannabinoids and metabolites in expectorated oral fluid after 8 days of controlled around-the-clock oral THC administration. *Anal Bioanal Chem* **401**, 599–607 (2011).

113. Lee, D. *et al.* Can oral fluid cannabinoid testing monitor medication compliance and/or cannabis smoking during oral THC and oromucosal Sativex administration? *Drug Alcohol Depend* **130**, 68–76 (2013).

114. Lee, D. *et al.* Cannabinoid disposition in oral fluid after controlled smoked cannabis. *Clin Chem* **58**, 748–756 (2012).

115. Milman, G. *et al.* Disposition of cannabinoids in oral fluid after controlled around-the-clock oral THC administration. *Clin. Chem.* **56**, 1261–1269 (2010).

116. R.S., N. *et al.* Passive cannabis smoke exposure and oral fluid testing. II. Two studies of extreme cannabis smoke exposure in a motor vehicle. *J. Anal. Toxicol.* **29**, 607–615 (2005).

117. Kauert, G. F., Ramaekers, J. G., Schneider, E., Moeller, M. R. & Toennes, S. W. Pharmacokinetic properties of Δ9-tetrahydrocannabinol in serum and oral fluid. *J. Anal. Toxicol.* **31**, 288–293 (2007).

118. Sebastien Anizan Nathalie Desrosiers, Allan J. Barnes, David A.Gorelick, and Marilyn A. Huestis, G. M. Oral fluid cannabinoid concentrations following controlled smoked cannabis in chronic frequent and occasional smokers. *Anal Bioanal Chem.* **405**, (2013).

119. Wille, S. M. R., Samyn, N., Ramírez-Fernández, M. del M. & De Boeck, G. Evaluation of on-site oral fluid screening using Drugwipe-5+®, RapidSTAT® and Drug Test 5000® for the detection of drugs of abuse in drivers. *Forensic Sci. Int.* **198**, 2–6 (2010).

120. Huestis, M. A. & Cone, E. J. Relationship of Δ9-tetrahydrocannabinol

concentrations in oral fluid and plasma after controlled administration of smoked cannabis. *J. Anal. Toxicol.* **28**, 394–399 (2004).

121. Stefan W. Toennes Eef L. Theunissen, Manfred R. Moeller, and Gerold F. Kauert, J. G. R. Pharmacokinetic Properties of Δ9 Tetrahydrocannabinol in Oral Fluid of Occasional and Chronic Users. *J. Anal. Toxicol.* **34**, 216–221.

122. David B. Menkes George F.S. Spears, and Eric R. Cairns, R. C. H. Salivary THC following cannabis smoking correlates with subjective intoxication and heart rate. *Psychopharmacol.* **103**, 277–279.

123. Ramaekers, J. G. *et al.* Cognition and motor control as a function of Delta9-THC concentration in serum and oral fluid: limits of impairment. *Drug Alcohol Depend* **85**, 114–122 (2006).

124. A., M. *et al.* Assessment of driving capability through the use of clinical and psychomotor tests in relation to blood cannabinoids levels following oral administration of 20 mg dronabinol or of a cannabis decoction made with 20 or 60 mg Delta9-THC. *J. Anal. Toxicol.* **29**, 327–338 (2005).

125. Lenne, M. G. *et al.* The effects of cannabis and alcohol on simulated arterial driving: Influences of driving experience and task demand. *Accid Anal Prev* **42**, 859–866 (2010).

126. Hart CL Haney M, Foltin RW, Fischman MW., van G. W. Effects of acute smoked marijuana on complex cognitive performance. *Neuropsychopharmacology.* **25**, 757–767.

127. Milman, G. *et al.* Cannabinoids and metabolites in expectorated oral fluid after 8 days of controlled around-the-clock oral THC administration. *Anal. Bioanal. Chem.* **401**, 599–607 (2011).

128. Quintela, O., Crouch, D. J. & Andrenyak, D. M. Recovery of drugs of abuse from the immunalysis Quantisal™ oral fluid collection device. *J. Anal. Toxicol.* **30**, 614–616 (2006).

129. Cohier, C., Megarbane, B. & Roussel, O. Illicit Drugs in Oral Fluid: Evaluation of Two Collection Devices. *J Anal Toxicol* **41**, 71–76 (2017).

130. Desrosiers, N. A. *et al.* Cannabinoids in oral fluid by on-site immunoassay and by GC-MS using two different oral fluid collection devices. *Anal Bioanal Chem* **406**, 4117–4128 (2014).

131. Moore, C. *et al.* Cannabinoids in oral fluid following passive exposure to marijuana smoke. *Forensic Sci Int* **212**, 227–230 (2011).

132. Strano-Rossi, S. *et al.* Evaluation of four oral fluid devices (DDS(R), Drugtest 5000(R), Drugwipe 5+(R) and RapidSTAT(R)) for on-site monitoring drugged driving in comparison with UHPLC-MS/MS analysis.

Forensic Sci Int **221**, 70–76 (2012).

133. Bosker, W. M. *et al.* A placebo-controlled study to assess standardized field sobriety tests performance during alcohol and cannabis intoxication in heavy cannabis users and accuracy of point of collection testing devices for detecting thc in oral fluid. *Psychopharmacology (Berl).* **223**, 439–446 (2012).

134. Handbuch, T. & Manual, T. *Dräger DrugTest ® 5000 Testsystem*.

135. Tao Wanga Leon M. Larchera, Roberto A. Barreroa, Rakesh N. Veedua, C. C. Three decades of nucleic acid aptamer technologies: Lessons learned, progress and opportunities on aptamer development. *Biotechnol. Adv.* **37**, 28–50 (2018).

136. Ruscito, A. & DeRosa, M. C. Small-Molecule Binding Aptamers: Selection Strategies, Characterization, and Applications. *Front. Chem.* **4**, 1–14 (2016).

137. Bock LC1 Latham JA, Vermaas EH, Toole JJ., G. L. C. Selection of single-stranded DNA molecules that bind and inhibit human thrombin. *Nature* **355**, 564–566.

138. Hofmann, H. P., Limmer, S., Hornung, V. & Sprinzl, M. Ni2+-binding RNA motifs with an asymmetric purine-rich internal loop and a G-A base pair. *RNA* **3**, 1289–300 (1997).

139. Cerchia, L. & de Franciscis, V. Targeting cancer cells with nucleic acid aptamers. *Trends Biotechnol* **28**, 517–525 (2010).

140. Davydova, A. *et al.* Aptamers against pathogenic microorganisms. *Crit. Rev. Microbiol.* **42**, 847–865 (2016).

141. Ana Cláudia Graziani Ana Luisa Kalb Lopes, Pedro Henrique Caires Schluga, M. I. S., Soledad Marton Antero Silva Ribeiro de Andrade, Marco Aurélio Krieger, and, I. M. F. & Cardoso, J. High efficiency binding aptamers for a wide range of sepsis bacterial agents. *J. Microbiol. Biotechnol.* **27**, 838–843.

142. Pusuluri, A. *et al.* Treating Tumors at Low Drug Doses Using an Aptamer–Peptide Synergistic Drug Conjugate. *Angew. Chemie - Int. Ed.* **58**, 1437–1441 (2019).

143. Zhu, H. *et al.* Aptamer-PEG-modified Fe3O4 @Mn as a novel T1-and T2-dual-model MRI contrast agent targeting hypoxia-induced cancer stem cells. *Sci. Rep.* **6**, 1–12 (2016).

144. Zhou, J. & Rossi, J. Aptamers as targeted therapeutics: Current potential and challenges. *Nat. Rev. Drug Discov.* **16**, 181–202 (2017).

145. Bradbury, A. & Plückthun, A. Reproducibility: Standardize antibodies used in research. *Nature* **518**, 27–29 (2015).

146. Shukla, A. A., Wolfe, L. S., Mostafa, S. S. & Norman, C. Evolving trends in mAb production processes. *Bioeng. Transl. Med.* **2**, 58–69 (2017).

147. AlShamaileh, H. *et al.* Aptamer-mediated survivin RNAi enables 5-fluorouracil to eliminate colorectal cancer stem cells. *Sci Rep* **7**, 5898 (2017).

148. Tan, L., Neoh, K. G., Kang, E. T., Choe, W. S. & Su, X. PEGylated anti-MUC1 aptamer-doxorubicin complex for targeted drug delivery to MCF7 breast cancer cells. *Macromol Biosci* **11**, 1331–1335 (2011).

149. Ciancio, D. R. *et al.* Aptamers as diagnostic tools in cancer. *Pharmaceuticals* **11**, 1–23 (2018).

150. Khan, N. I., Maddaus, A. G. & Song, E. A low-cost inkjet-printed aptamer-based electrochemical biosensor for the selective detection of lysozyme. *Biosensors* **8**, (2018).

151. Famulok, M. & Mayer, G. Aptamer modules as sensors and detectors. *Acc. Chem. Res.* **44**, 1349–1358 (2011).

152. Ng, E. W. M. *et al.* Pegaptanib, a targeted anti-VEGF aptamer for ocular vascular disease. *Nat. Rev. Drug Discov.* **5**, 123–132 (2006).

153. Keefe, A. D., Pai, S. & Ellington, A. Aptamers as therapeutics. *Nat. Rev. Drug Discov.* **9**, 537–550 (2010).

154. Shahid M. Nimjee Richard C. Becker, and Bruce A. Sullenger, R. R. W. Aptamers as therapeutics. *Annu Rev Pharmacol Toxicol* **57**, 61–79 (2017).

155. Kaur, H., Bruno, J. G., Kumar, A. & Sharma, T. K. Aptamers in the therapeutics and diagnostics pipelines. *Theranostics* **8**, 4016–4032 (2018).

156. Hoellenriegel, J. *et al.* The Spiegelmer NOX-A12, a novel CXCL12 inhibitor, interferes with chronic lymphocytic leukemia cell motility and causes chemosensitization. *Blood* **123**, 1032–1039 (2014).

157. Marasca, R. & Maffei, R. NOX-A12: Mobilizing CLL away from home. *Blood* **123**, 952–953 (2014).

158. Ninichuk, V. *et al.* Late onset of Ccl2 blockade with the Spiegelmer mNOX-E36-3′PEG prevents glomerulosclerosis and improves glomerular filtration rate in db/db mice. *Am. J. Pathol.* **172**, 628–637 (2008).

159. Kulkarni, O. *et al.* Spiegelmer Inhibition of CCL2/MCP-1 Ameliorates

Lupus Nephritis in MRL-(Fas)lpr Mice. *J. Am. Soc. Nephrol.* **18**, 2350–2358 (2007).

160. Schwoebel, F. *et al.* The effects of the anti-hepcidin Spiegelmer NOX-H94 on inflammation-induced anemia in cynomolgus monkeys. *Blood* **121**, 2311–2315 (2013).

161. Darmostuk, M., Rimpelova, S., Gbelcova, H. & Ruml, T. Current approaches in SELEX: An update to aptamer selection technology. *Biotechnol. Adv.* **33**, 1141–1161 (2014).

162. Gold, L. & Tuerk, C. Systematic evolution of ligands by exponential enrichment: RNA ligands to bacteriophage T4 DNA polymerase. *Science (80-.).* **249**, 505–510 (1990).

163. Ellington, A. D. & Szostak, J. W. In vitro selection of RNA molecules that bind specific ligands. *Nature* **346**, 818–822 (1990).

164. Stoltenburg, R., Reinemann, C. & Strehlitz, B. SELEX-A (r)evolutionary method to generate high-affinity nucleic acid ligands. *Biomol. Eng.* **24**, 381–403 (2007).

165. Sun, H. & Zu, Y. A Highlight of Recent Advances in Aptamer Technology and Its Application. *Molecules* **20**, 11959–11980 (2015).

166. Paniel, N. *et al.* Selection of DNA aptamers against penicillin G using Capture-SELEX for the development of an impedimetric sensor. *Talanta* **162**, 232–240 (2017).

167. Sunghan Yoo, and W. S. D. Characterization of the RNA Binding Properties of Ku Protein. *Biochemistry* **37**, 1336–1343.

168. Stoltenburg, R., Nikolaus, N. & Strehlitz, B. Capture-SELEX: Selection of DNA aptamers for aminoglycoside antibiotics. *J. Anal. Methods Chem.* **1**, (2012).

169. Tenhunen, J. Hydrolysis of single-stranded RNA in aqueous solutions-effect on quantitative hybridizations Jukka Tenhunen. *Mol. Cell. Probes* **3**, 391–396 (1989).

170. Maier, K. E. & Levy, M. From selection hits to clinical leads: progress in aptamer discovery. *Mol. Ther. - Methods Clin. Dev.* **3**, 16014 (2016).

171. Sousa, R. P. and R. Efficient synthesis of nucleic acids heavily modified with non-canonical ribose 2′-groups using a mutant T7 RNA polymerase (RNAP). *Nucleic Acids Res.* **27**, 1561–1563.

172. Judy Ruckman Jim Beeson, Sheela Waugh, Wendy L. Gillette,Dwight D. Henninger, Lena Claesson-Welsh, and Nebojsa Janjic, L. S. G. 20-Fluoropyrimidine RNA-based aptamers to the 165-amino acid form of

vascular endothelial growth factor (VEGF165). Inhibition of receptor binding and VEGF-induced vascular permeability through interactions requiring the exon 7-encoded domain. *J. Biol. Chem.* **273**, 20556–20567.

173. Shum, K. T. & Tanner, J. A. Differential inhibitory activities and stabilisation of DNA aptamers against the SARS coronavirus helicase. *Chembiochem* **9**, 3037–3045 (2008).

174. Dougan, H. *et al.* Extending the lifetime of anticoagulant oligodeoxynucleotide aptamers in blood. *Nucl. Med. Biol.* **27**, 289–297 (2000).

175. Darfeuille, F., Hansen, J. B., Orum, H., Di Primo, C. & Toulmé, J. J. LNA/DNA chimeric oligomers mimic RNA aptamers targeted to the TAR RNA element of HIV-1. *Nucleic Acids Res.* **32**, 3101–3107 (2004).

176. Campbell, M. A. & Wengel, J. Locked vs. unlocked nucleic acids (LNA vs. UNA): contrasting structures work towards common therapeutic goals. *Chem Soc Rev* **40**, 5680–5689 (2011).

177. Purschke, W. G., Eulberg, D., Buchner, K., Vonhoff, S. & Klussmann, S. An L-RNA-based aquaretic agent that inhibits vasopressin in vivo. *Proc. Natl. Acad. Sci. U. S. A.* **103**, 5173–5178 (2006).

178. Denekas, T., Tröltzsch, M., Vater, A., Klussmann, S. & Messlinger, K. Inhibition of stimulated meningeal blood flow by a calcitonin gene-related peptide binding mirror-image RNA oligonucleotide. *Br. J. Pharmacol.* **148**, 536–543 (2006).

179. Wlotzka, B. *et al.* In vivo properties of an anti-GnRH Spiegelmer: An example of an oligonucleotide-based therapeutic substance class. *Proc. Natl. Acad. Sci. U. S. A.* **99**, 8898–8902 (2002).

180. El-Sagheer, A. H. & Brown, T. Click chemistry with DNA. *Chem Soc Rev* **39**, 1388–1405 (2010).

181. Mutisya, D., Selvam, C., Kennedy, S. D. & Rozners, E. Synthesis and properties of triazole-linked RNA. *Bioorg Med Chem Lett* **21**, 3420–3422 (2011).

182. Sau, S. P. & Hrdlicka, P. J. C2'-pyrene-functionalized triazole-linked DNA: universal DNA/RNA hybridization probes. *J Org Chem* **77**, 5–16 (2012).

183. Abeydeera, N. D. *et al.* Evoking picomolar binding in RNA by a single phosphorodithioate linkage. *Nucleic Acids Res.* **44**, 8052–8064 (2016).

184. Zandarashvili, L. *et al.* Entropic Enhancement of Protein-DNA Affinity by Oxygen-to-Sulfur Substitution in DNA Phosphate. *Biophys. J.* **109**, 1026–1037 (2015).

185. Healy, J. M. *et al.* Pharmacokinetics and biodistribution of novel aptamer compositions. *Pharm. Res.* **21**, 2234–2246 (2004).

186. Hoffmann, S., Hoos, J., Klussmann, S. & Vonhoff, S. RNA aptamers and spiegelmers: Synthesis, purification, and post-synthetic PEG conjugation. *Curr. Protoc. Nucleic Acid Chem.* 1–30 (2011) doi:10.1002/0471142700.nc0446s46.

187. Macugen, A. M. D. S. G. *et al.* Pegaptanib 1-year systemic safety results from a safety-pharmacokinetic trial in patients with neovascular age-related macular degeneration. *Ophthalmology* **114**, 1702–1712 (2007).

188. Famulok, M. & Mayer, G. Aptamers and SELEX in chemistry & biology. *Chem. Biol.* **21**, 1055–1058 (2014).

189. Zhuo, Z. *et al.* Recent advances in SELEX technology and aptamer applications in biomedicine. *Int. J. Mol. Sci.* **18**, 1–19 (2017).

190. Gold, L. *et al.* Aptamer-based multiplexed proteomic technology for biomarker discovery. *PLoS One* **5**, e15004 (2010).

191. Ramaraj, Thiruvarangan, Thomas Angel, Edward A. Dratz, Algirdas J. Jesaitis, and B. M. Antigen–antibody interface properties: Composition, residue interactions, and features of 53 non-redundant structures. *Biochim Biophys* **1824**, 520–532 (2013).

192. Young, L., Jernigan, R. L. & Covell, D. G. A role for surface hydrophobicity. *Protein Sci.* **3**, 717–729 (1994).

193. Pfeiffer, F., Rosenthal, M., Siegl, J., Ewers, J. & Mayer, G. Customised nucleic acid libraries for enhanced aptamer selection and performance. *Curr Opin Biotechnol* **48**, 111–118 (2017).

194. Davies, D. R. *et al.* Unique motifs and hydrophobic interactions shape the binding of modified DNA ligands to protein targets. *Proc. Natl. Acad. Sci.* **109**, 19971–19976 (2012).

195. Betz, K. *et al.* KlenTaq polymerase replicates unnatural base pairs by inducing a Watson-Crick geometry. *Nat Chem Biol* **8**, 612–614 (2012).

196. Ma, Q., Lee, D., Tan, Y. Q., Wong, G. & Gao, Z. Synthetic genetic polymers: Advances and applications. *Polym. Chem.* **7**, 5199–5216 (2016).

197. Piccirilli JA Moroney SE, Benner SA., K. T. Enzymatic incorporation of a new base pair into DNA and RNA extends the genetic alphabet. *Nature* **343**, 33–37.

198. Kimoto, M., Yamashige, R., Matsunaga, K. I., Yokoyama, S. & Hirao, I. Generation of high-affinity DNA aptamers using an expanded genetic

alphabet. *Nat. Biotechnol.* **31**, 453–457 (2013).

199. Kwame Sefaha Kevin M. Bradleyc, Shuichi Hoshikac, Elizabeth Jiméneza, Liqin Zhanga, Z. Y. & Guizhi Zhua Fahong Yue, Diane Tureka, Weihong Tana and Steven A. Bennerc, S. S. In vitro selection with artificial expanded genetic information systems. *PNAS* **111**, 1449–1454 (2013).

200. Biondi, E. *et al.* Laboratory evolution of artificially expanded DNA gives redesignable aptamers that target the toxic form of anthrax protective antigen. *Nucleic Acids Res.* **44**, 9565–9577 (2016).

201. Futami, K., Kimoto, M., Lim, Y. W. S. & Hirao, I. Genetic Alphabet Expansion Provides Versatile Specificities and Activities of Unnatural-Base DNA Aptamers Targeting Cancer Cells. *Mol. Ther. - Nucleic Acids* **14**, 158–170 (2019).

202. Kimoto, M., Matsunaga, K. & Hirao, I. DNA Aptamer Generation by Genetic Alphabet Expansion SELEX (ExSELEX) Using an Unnatural Base Pair System. in *Nucleic acid aptamers* vol. 1380 47–60 (2016).

203. Matsunaga, K. I., Kimoto, M. & Hirao, I. High-Affinity DNA Aptamer Generation Targeting von Willebrand Factor A1-Domain by Genetic Alphabet Expansion for Systematic Evolution of Ligands by Exponential Enrichment Using Two Types of Libraries Composed of Five Different Bases. *J Am Chem Soc* **139**, 324–334 (2017).

204. Kimoto, M., Nakamura, M. & Hirao, I. Post-ExSELEX stabilization of an unnatural-base DNA aptamer targeting VEGF165 toward pharmaceutical applications. *Nucleic Acids Res.* **44**, 7487–7494 (2016).

205. Latham, J. A., Johnson, R. & Toole, J. J. The application of a modified nucleotide in aptamer selection: Novel thrombin aptamers containing -(1 -pentynyl)-2′-deoxyuridine. *Nucleic Acids Res.* **22**, 2817–2822 (1994).

206. Pagano, B., Martino, L., Randazzo, A. & Giancola, C. Stability and binding properties of a modified thrombin binding aptamer. *Biophys. J.* **94**, 562–569 (2008).

207. Rohloff, J. C. *et al.* Nucleic acid ligands with protein-like side chains: Modified aptamers and their use as diagnostic and therapeutic agents. *Mol. Ther. - Nucleic Acids* **3**, e201 (2014).

208. Gawande, B. N. *et al.* Selection of DNA aptamers with two modified bases. *Proc Natl Acad Sci U S A* **114**, 2898–2903 (2017).

209. Joshi, A. & Mayr, M. In Aptamers They Trust: The Caveats of the SOMAscan Biomarker Discovery Platform from SomaLogic. *Circulation* **138**, 2482–2485 (2018).

210. Candia, J. *et al.* Assessment of Variability in the SOMAscan Assay. *Sci Rep* **7**, 14248 (2017).

211. Ashley, S. L. *et al.* Six-SOMAmer Index Relating to Immune, Protease and Angiogenic Functions Predicts Progression in IPF. *PLoS One* **11**, e0159878 (2016).

212. Jason Webber Evaldas Katilius, Breanna C. Smith, Bridget Gordon, Malcolm D. Mason, Zsuzsanna Tabi, Ian A. Brewis and Aled Clayton, T. C. S. Proteomics Analysis of Cancer Exosomes Using a Novel Modified Aptamer-based Array (SOMAscanTM) Platform. *Mol. Cell. Proteomics* **13**, 1050–1064.

213. Albaba, D., Soomro, S. & Mohan, C. Aptamer-Based Screens of Human Body Fluids for Biomarkers. *Microarrays (Basel)* **4**, 424–431 (2015).

214. Yetrib Hathout Paula R. Clemens, Linda Cripe, Robert Kirk DeLisle, Pat Furlong, Heather Gordish-Dressman, Lauren Hache, Erik Henricson, Eric P. Hoffman, Yvonne Monique Kobayashi, Angela Lorts, Jean K. Mah, Craig McDonald, Bob Mehler, Sally Nelson, Malti, E. B. Large-scale serum protein biomarker discovery in Duchenne muscular dystrophy. *PNAS* **112**, 7135–7158.

215. Kraemer, S. *et al.* From SOMAmer-based biomarker discovery to diagnostic and clinical applications: A SOMAmer-based, streamlined multiplex proteomic assay. *PLoS One* **6**, (2011).

216. Gelinas, A. D. *et al.* Crystal structure of interleukin-6 in complex with a modified nucleic acid ligand. *J Biol Chem* **289**, 8720–8734 (2014).

217. Jarvis, T. C. *et al.* Non-helical DNA Triplex Forms a Unique Aptamer Scaffold for High Affinity Recognition of Nerve Growth Factor. *Structure* **23**, 1293–1304 (2015).

218. Ren, X., Gelinas, A. D., von Carlowitz, I., Janjic, N. & Pyle, A. M. Structural basis for IL-1alpha recognition by a modified DNA aptamer that specifically inhibits IL-1alpha signaling. *Nat Commun* **8**, 810 (2017).

219. Eaton, B. E. *et al.* Expanding the Chemistry of DNA for in Vitro Selection. *J. Am. Chem. Soc.* **132**, 4141–4151 (2010).

220. Hartmuth C. Kolb and K. Barry Sharpless, M. G. F. Click Chemistry: Diverse Chemical Function from a Few Good Reactions. *Angew Chem Int Ed Engl* **40**, 2004–2021.

221. Christian W. Tornøe and Morten Meldal, C. C. Peptidotriazoles on Solid Phase: [1,2,3]-Triazoles by Regiospecific Copper(I)-Catalyzed 1,3-Dipolar Cycloadditions of Terminal Alkynes to Azides. *J. Org. Chem* **67**, 3057–3067.

222. Vsevolod V. Rostovtsev, L. G. G. & Valery V. Fokin, * and K Barry Sharpless*. A Stepwise Huisgen Cycloaddition Process: Copper(_)-Catalyzed Regioselective ™Ligation∫ of Azides and Terminal Alkynes**. *Angew. Chem. Int. Ed.* **41**, 2596–2599.

223. Sletten, E. M. & Bertozzi, C. R. Bioorthogonal chemistry: fishing for selectivity in a sea of functionality. *Angew Chem Int Ed Engl* **48**, 6974–6998 (2009).

224. Lim, R. K. & Lin, Q. Bioorthogonal chemistry: recent progress and future directions. *Chem Commun* **46**, 1589–1600 (2010).

225. Johannes Gierlich Philipp M. E. Gramlich, David M. Hammond, and Thomas Carell*, G. A. B. Click Chemistry as a Reliable Method for the High-Density Postsynthetic Functionalization of Alkyne-Modified DNA. *Org. Lett* **8**, 3639–3642.

226. Gramlich, P. M. E., Wirges, C. T., Manetto, A. & Carell, T. Postsynthetic DNA modification through the copper-catalyzed azide-alkyne cycloaddition reaction. *Angew. Chemie - Int. Ed.* **47**, 8350–8358 (2008).

227. Gierlich, J. *et al.* Synthesis of highly modified DNA by a combination of PCR with alkyne-bearing triphosphates and click chemistry. *Chem. - A Eur. J.* **13**, 9486–9494 (2007).

228. Burley, G. A. *et al.* Directed DNA metallization. *J. Am. Chem. Soc.* **128**, 1398–1399 (2006).

229. Abel Jr., G. R., Calabrese, Z. A., Ayco, J., Hein, J. E. & Ye, T. Measuring and Suppressing the Oxidative Damage to DNA During Cu(I)-Catalyzed Azide-Alkyne Cycloaddition. *Bioconjug Chem* **27**, 698–704 (2016).

230. Eric F. V. Scriven, and K. T. Azides: their preparation and synthetic uses. *Chem. Rev.* **88**, 297–368.

231. Held, H. A. Challenging artificial genetic systems: thymidine analogs with 5-position sulfur functionality. *Nucleic Acids Res.* **30**, 3857–3869 (2002).

232. Tolle, F., Brändle, G. M., Matzner, D. & Mayer, G. A Versatile Approach Towards Nucleobase-Modified Aptamers. *Angew. Chemie - Int. Ed.* **54**, 10971–10974 (2015).

233. Baker, B. R. *et al.* An electronic, aptamer-based small-molecule sensor for the rapid, label-free detection of cocaine in adulterated samples and biological fluids. *J. Am. Chem. Soc.* **128**, 3138–3139 (2006).

234. Qiu, Y., Tang, Y., Li, B. & He, M. Rapid detection of cocaine using aptamer-based biosensor on an evanescent wave fibre platform. *R Soc Open Sci* **5**, 180821 (2018).

235. Pfeiffer, F. *et al.* Identification and characterization of nucleobase-modified aptamers by click-SELEX. *Nat Protoc* **13**, 1153–1180 (2018).

236. Zhang, W., Liu, Q. X., Guo, Z. H. & Lin, J. S. Practical application of aptamer-based biosensors in detection of low molecular weight pollutants in water sources. *Molecules* **23**, 12–16 (2018).

237. McKeague, M. *et al.* Selection and characterization of a novel DNA aptamer for label-free fluorescence biosensing of ochratoxin A. *Toxins (Basel).* **6**, 2435–2452 (2014).

238. Wang L Ma W, Liu L, Ma W, Zhao Y, Zhu Y, Xu L, Kuang H, Xu C., C. W. Fluorescent strip sensor for rapid determination of toxins. *Chem Commun* **47**, 1574–1576.

239. McLoughlin, N. M., Mueller, C. & Grossmann, T. N. The Therapeutic Potential of PTEN Modulation: Targeting Strategies from Gene to Protein. *Cell Chem. Biol.* **25**, 19–29 (2018).

240. Licatalosi, D. D. & Darnell, R. B. Resolving RNA complexity to decipher regulatory rules governing biological networks. *Nat. Rev. Genet.* **11**, 75–87 (2010).

241. Amann, R. & Fuchs, B. M. Single-cell identification in microbial communities by improved fluorescence in situ hybridization techniques. *Nat. Rev. Microbiol.* **6**, 339–348 (2008).

242. Orjalo, A. V. J. & Johansson, H. E. Stellaris ® RNA Fluorescence In Situ Hybridization for the Simultaneous Detection of Immature and Mature Long Noncoding RNAs in Adherent Cells. *Long Non-Coding RNAs Methods Protoc.* **1402**, 119–134 (2016).

243. Querido, E. & Chartrand, P. Using Fluorescent Proteins to Study mRNA Trafficking in Living Cells. *Methods Cell Biol.* **85**, 273–292 (2008).

244. Bann, D. V. & Parent, L. J. Application of live-cell RNA imaging techniques to the study of retroviral RNA trafficking. *Viruses* **4**, 963–979 (2012).

245. Huber, D., Voith von Voithenberg, L. & Kaigala, G. V. Fluorescence in situ hybridization (FISH): History, limitations and what to expect from micro-scale FISH? *Micro Nano Eng.* **1**, 15–24 (2018).

246. Lim. Imaging transcriptional dynamics. *Curr Opin Biotechnol* **52**, 49–55 (2018).

247. Neubacher, S. & Hennig, S. RNA Structure and Cellular Applications of Fluorescent Light-Up Aptamers. *Angewandte Chemie - International Edition* vol. 58 1266–1279 (2019).

248. You, M., Litke, J. L. & Jaffrey, S. R. Imaging metabolite dynamics in living cells using a Spinach-based riboswitch. *Proc. Natl. Acad. Sci. U. S. A.* **112**, E2756–E2765 (2015).

249. Paige, J. S., Nguyen-Duc, T., Song, W. & Jaffrey, S. R. Fluorescence imaging of cellular metabolites with RNA. *Science (80-.).* **335**, 1194 (2012).

250. Strack, Rita L., S. R. J. New approaches for sensing metabolites and proteins in live cells using RNA. *Curr Opin Chem Biol* **17**, 651–655 (2013).

251. Sun, Z., Nguyen, T., McAuliffe, K. & You, M. Intracellular imaging with genetically encoded RNA-based molecular sensors. *Nanomaterials* **9**, (2019).

252. Paige, J. S., Wu, K. Y. & Jaffrey, S. R. RNA mimics of green fluorescent protein. *Science (80-.).* **333**, 642–646 (2011).

253. Warner, K. D. *et al.* Structural basis for activity of highly efficient RNA mimics of green fluorescent protein. *Nat. Struct. Mol. Biol.* **21**, 658–663 (2014).

254. Huang, H. *et al.* A G-quadruplex-containing RNA activates fluorescence in a GFP-like fluorophore. *Nat. Chem. Biol.* **10**, 686–691 (2014).

255. RY, T. The green fluorescent protein. *Annu. Rev. Biochem* **76**, 509–44 (1998).

256. Arpino, J. A., Rizkallah, P. J. & Jones, D. D. Crystal structure of enhanced green fluorescent protein to 1.35 A resolution reveals alternative conformations for Glu222. *PLoS One* **7**, e47132 (2012).

257. Autour, A., Westhof, E. & Ryckelynck, M. iSpinach: a fluorogenic RNA aptamer optimized for in vitro applications. *Nucleic Acids Res* **44**, 2491–2500 (2016).

258. Strack, R. L., Disney, M. D. & Jaffrey, S. R. A superfolding Spinach2 reveals the dynamic nature of trinucleotide repeat-containing RNA. *Nat Methods* **10**, 1219–1224 (2013).

259. Okuda, M., Fourmy, D. & Yoshizawa, S. Use of Baby Spinach and Broccoli for imaging of structured cellular RNAs. *Nucleic Acids Res.* **45**, 1404–1415 (2017).

260. Fernandez-Millan, P., Autour, A., Ennifar, E., Westhof, E. & Ryckelynck, M. Crystal structure and fluorescence properties of the iSpinach aptamer in complex with DFHBI. *Rna* **23**, 1788–1795 (2017).

261. Filonov, G. S., Moon, J. D., Svensen, N. & Jaffrey, S. R. Broccoli: Rapid

selection of an RNA mimic of green fluorescent protein by fluorescence-based selection and directed evolution. *J. Am. Chem. Soc.* **136**, 16299–16308 (2014).

262. Wenjiao Song*, 1, Grigory S. Filonov*, 1, Hyaeyeong Kim1, Markus Hirsch1, Xing Li1, Jared D. Moon1, and S. R. J. Imaging RNA polymerase III transcription using a photostable RNA-fluorophore complex. *Nat Chem Biol* **13**, 1187–1194 (2017).

263. Guet, D. *et al.* Combining Spinach-tagged RNA and gene localization to image gene expression in live yeast. *Nat. Commun.* **6**, (2015).

264. Sharma, S., Zaveri, A., Visweswariah, S. S. & Krishnan, Y. A fluorescent nucleic acid nanodevice quantitatively images elevated cyclic adenosine monophosphate in membrane-bound compartments. *Small* **10**, 4276–4280 (2014).

265. Song, W., Strack, R. L. & Jaffrey, S. R. Imaging bacterial protein expression using genetically encoded RNA sensors. *Nat. Methods* **10**, 873–875 (2013).

266. Murata, A., Sato, S. I., Kawazoe, Y. & Uesugi, M. Small-molecule fluorescent probes for specific RNA targets. *Chem. Commun.* **47**, 4712–4714 (2011).

267. Information, S. Universal Aptamer-Based Real-Time Monitoring of Enzymatic RNA Synthesis. *JACS* **153**, 13692–13694 (2013).

268. Mishin, A. S. & Lukyanov, K. A. Live-Cell Super-resolution Fluorescence Microscopy. *Annu Rev Biochem* **87**, 993–1016 (2009).

269. Huang, B., Babcock, H. & Zhuang, X. Breaking the diffraction barrier: Super-resolution imaging of cells. *Cell* **143**, 1047–1058 (2010).

270. Mayer, G. Nucleic Acid Aptamers : Selection, Characterization, and Application. *Methods Mol. Biol.* **1380**, 113–125 (2016).

271. Maria Angela Gomes de Castro , Burkhard Rammner, and F. O. Aptamer Stainings for Super-resolution Microscopy. in *Methods in Molecular Biology* (ed. Mayer, G.) vol. 1380 197–210 (Humana Press, New York, NY, 2016).

272. Betzig, E. *et al.* Imaging intracellular fluorescent proteins at nanometer resolution. *Science (80-.).* **313**, 1642–1645 (2006).

273. Honglin, L. and V. Switchable Fluorophores for Single-Molecule Localization Microscopy. *Chem Rev* **118**, 9412–9454 (2018).

274. Klar, T. A. & Hell, S. W. Subdiffraction resolution in far-field fluorescence microscopy. *Opt. Lett.* **24**, 954 (1999).

275. Hell, S. W. & Wichmann, J. Breaking the diffraction resolution limit by stimulated emission: stimulated-emission-depletion fluorescence microscopy. *Opt. Lett.* **19**, 780 (1994).

276. Hofmann, M., Eggeling, C., Jakobs, S. & Hell, S. W. Breaking the diffraction barrier in fluorescence microscopy at low light intensities by using reversibly photoswitchable proteins. *Proc. Natl. Acad. Sci. U. S. A.* **102**, 17565–17569 (2005).

277. Schermelleh, L., Heintzmann, R. & Leonhardt, H. A guide to super-resolution fluorescence microscopy. *J. Cell Biol.* **190**, 165–175 (2010).

278. Xu, K., Babcock, H. P. & Zhuang, X. Dual-objective STORM reveals three-dimensional filament organization in the actin cytoskeleton. *Nat. Methods* **9**, 185–188 (2012).

279. Kozma, E. & Kele, P. Fluorogenic probes for super-resolution microscopy. *Org. Biomol. Chem.* **17**, 215–233 (2019).

280. Brakemann, T. *et al.* A reversibly photoswitchable GFP-like protein with fluorescence excitation decoupled from switching. *Nat. Biotechnol.* **29**, 942–950 (2011).

281. Post, J. N., Lidke, K. A., Rieger, B. & Arndt-Jovin, D. J. One- and two-photon photoactivation of a paGFP-fusion protein in live Drosophila embryos. *FEBS Lett.* **579**, 325–330 (2005).

282. Subach, F. V. *et al.* Photoactivatable mCherry for high-resolution two-color fluorescence microscopy. *Nat. Methods* **6**, 153–159 (2009).

283. Chang, H. *et al.* A unique series of reversibly switchable fluorescent proteins with beneficial properties for various applications. *Proc. Natl. Acad. Sci. U. S. A.* **109**, 4455–4460 (2012).

284. Hell, S. W. Microscopy and its focal switch. *Nat. Methods* **6**, 24–32 (2009).

285. Ali, M. H., Elsherbiny, M. E. & Emara, M. Updates on aptamer research. *Int. J. Mol. Sci.* **20**, 1–23 (2019).

286. De Castro, M. A. G., Hobartner, C. & Opazo, F. Aptamers provide superior stainings of cellular receptors studied under superresolution microscopy. *PLoS One* **12**, 1–16 (2017).

287. Yan, Q. *et al.* Using an RNA aptamer probe for super-resolution imaging of native EGFR. *Nanoscale Adv.* **1**, 291–298 (2019).

288. Xiao, H. *et al.* Obtaining More Accurate Signals: Spatiotemporal Imaging of Cancer Sites Enabled by a Photoactivatable Aptamer-Based Strategy. *ACS Appl. Mater. Interfaces* **8**, 23542–23548 (2016).

289. Bates, P. J., Laber, D. a, Miller, D. M., Thomas, S. D. & Trent, J. O. Discovery and Development of the G-rich Oligonucleotide AS1411 as a Novel Treatment for Cancer. *Exp. Mol. Pathol.* **86**, 151–164 (2009).

290. Kim, S. *et al.* Bioimaging of nucleolin aptamer-containing 5-(N -benzylcarboxyamide)- 2′-deoxyuridine more capable of specific binding to targets in cancer cells. *J. Biomed. Biotechnol.* **2010**, (2010).

291. Gupta, S. *et al.* Rapid histochemistry using slow off-rate modified aptamers with anionic competition. *Appl. Immunohistochem. Mol. Morphol.* **19**, 273–278 (2011).

292. Jaffrey, M. Y. and S. R. Structure and Mechanism of RNA Mimics of Green Fluorescent Protein. *Annu Rev Biophys* **44**, 187–206 (2015).

293. Ha*†‡‖, K. Y. H. B. J. L. J. F. J. Z. T. H. Understanding the Photophysics of the Spinach–DFHBI RNA Aptamer–Fluorogen Complex To Improve Live-Cell RNA Imaging. *J. AM. CHEM. SOC.* **135**, 19033–19038 (2013).

294. Pengcheng Wang, Jérôme Querard, Sylvie Maurin, a Sarang S. Nath, Thomas Le Saux, A. G. and L. J. Photochemical properties of Spinach and its use in selective imaging. *Chem. Sci.* **4**, 2865–2873 (2013).

295. Wang, L., Brock, A., Herberich, B. & Schultz, P. G. Expanding the genetic code of Escherichia coli. *Science (80-.).* **292**, 498–500 (2001).

296. Groff, D., Wang, F., Jockusch, S., Turro, N. J. & Schultz, P. G. A New Strategy to Photoactivate GFP. *Angew Chem Int Ed Engl Oct.* **11**, 7677–7679 (2010).

297. Chudakov, D. M., Matz, M. V., Lukyanov, S. & Lukyanov, K. A. Fluorescent proteins and their applications in imaging living cells and tissues. *Physiol. Rev.* **90**, 1103–1163 (2010).

298. Day, R. N. & Davidson, M. W. The fluorescent protein palette: tools for cellular imaging. *Chem Soc Rev* **38**, 2887–2921 (2009).

299. Olenych, S. G., Claxton, N. S., Ottenberg, G. K. & Davidson, M. W. The Fluorescent Protein Color Palette. *Curr. Protoc. Cell Biol.* **36**, 21.5.1-21.5.34 (2007).

300. Dolgosheina, E. V *et al.* RNA Mango Aptamer-Fluorophore - A Bright, High-Affinity Complex for RNA Labeling and Tracking. (2014).

301. Autour, A. *et al.* Fluorogenic RNA Mango aptamers for imaging small non-coding RNAs in mammalian cells. *Nat. Commun.* **9**, (2018).

302. Jeng, S. C. Y., Chan, H. H. Y., Booy, E. P., McKenna, S. A. & Unrau, P. J. Fluorophore ligand binding and complex stabilization of the RNA Mango and RNA Spinach aptamers. *Rna* **22**, 1884–1892 (2016).

303. Robert J. Trachman, Amir Abdolahzadeh, Alessio Andreoni, Razvan Cojocaru, Jay R. Knutson, Michael Ryckelynck, Peter J. Unrau, and Adrian R. Ferré-D'Amaré Robert J. Trachman, Amir Abdolahzadeh, Alessio Andreoni, Razvan Cojocaru, Jay R. K, and A. R. F.-D. Crystal structures of the Mango-II RNA aptamer reveal heterogeneous fluorophore binding and guide engineering of variants with improved selectivity and brightness. *Biochemistry* **57**, 3544–3548 (2018).

304. Trachman, R. J. *et al.* Structure and functional reselection of the Mango-III fluorogenic RNA aptamer. *Nat. Chem. Biol.* **15**, 472–479 (2019).

305. Katherine Deigan Warner1, Ljiljana Sjekloća1, Wenjiao Song2, Grigory S. Filonov2, Samie R. Jaffrey2, and A. R. F.-D. A homodimer interface without base pairs in an RNA mimic of red fluorescent protein. *Nat Chem Biol* **13**, 1195–1201 (2017).

306. Song, W., Strack, R. L., Svensen, N., Ja, S. R. & Jaffrey, S. R. Plug-and-Play Fluorophores Extend the Spectral Properties of Spinach. *J. Am. Chem. Soc.* **136**, 22–25 (2013).

307. Sachin Asaram Ingale Peter Leonard, and Frank Seela, H. M. Ethynyl Side Chain Hydration During Synthesis and Work-up of "Clickable" Oligonucleotides: Bypassing Acetyl Group Formation by Triisopropylsilyl Protection. *J. Org. Chem.* **78**, 11271–11282 (2013).

308. Pfeiffer, F. Click-SELEX enables the selection of Δ 9-tetrahydrocannabinol-binding nucleic acids Dissertation. (2018).

309. Zuker, M. Mfold web server for nucleic acid folding and hybridization prediction. *Nucleic Acids Res.* **31**, 3406–3415 (2003).

310. Kosman, J. & Juskowiak, B. Peroxidase-mimicking DNAzymes for biosensing applications: a review. *Anal Chim Acta* **707**, 7–17 (2011).

311. Travascio, P., Li, Y. & Sen, D. DNA-enhanced peroxidase activity of a DNA aptamer-hemin complex. *Chem. Biol.* **5**, 505–517 (1998).

312. Kong, D. M., Yang, W., Wu, J., Li, C. X. & Shen, H. X. Structure-function study of peroxidase-like G-quadruplex-hemin complexes. *Analyst* **135**, 321–326 (2010).

313. Cheng, X., Liu, X., Bing, T., Cao, Z. & Shangguan, D. General peroxidase activity of G-quadruplex-hemin complexes and its application in ligand screening. *Biochemistry* **48**, 7817–7823 (2009).

314. Ekaterina N. Kadnikova, N. M. K. Oxidation of ABTS by hydrogen peroxide catalyzed by horseradish peroxidase encapsulated into sol–gel glass. Effects of glass matrix on reactivity. *J. Mol. Catal.* **18**, 39–48.

315. S. HUNIG H . CONRAD, A. SCHOTT, H. B. 2.2'-Azine aromatischer

heterocycle und ihre höheren Oxidationsstufen. *European J. Org. Chem.* **676**, 36–50.

316. Gallati, H. Peroxidase aus Meerrettich: Kinetische Studien sowie Optimierung der Aktivitätsbestimmung mit den Substraten H2O2 und 2,2′-Azino-di-(3-ethyl-benzthiazolinsulfonsäure-(6)) (ABTS). *Clin. Chem. Lab. Med.* **17**, 1–8 (1979).

317. Opazo, F. *et al.* Modular Assembly of Cell-targeting Devices Based on an Uncommon G-quadruplex Aptamer. *Mol Ther Nucleic Acids* **4**, e251 (2015).

318. Vorlíčková, M. *et al.* Circular dichroism and guanine quadruplexes. *Methods* **57**, 64–75 (2012).

319. del Villar-Guerra, R., Trent, J. O. & Chaires, J. G-quadruplex secondary structure from circular dichroism spectroscopy. *Angew. Chemie Int. Ed.* (2017) doi:10.1101/184390.

320. Karsisiotis, A. I. *et al.* Topological characterization of nucleic acid G-quadruplexes by UV absorption and circular dichroism. *Angew. Chemie - Int. Ed.* **50**, 10645–10648 (2011).

321. Gray, D. M. *et al.* Measured and calculated CD spectra of G-quartets stacked with the same or opposite polarities. *Chirality* **20**, 431–440 (2008).

322. Baaske, P., Wienken, C. J., Reineck, P., Duhr, S. & Braun, D. Optical thermophoresis for quantifying the buffer dependence of aptamer binding. *Angew Chem Int Ed Engl* **49**, 2238–2241 (2010).

323. Duhr, S. & Braun, D. Why molecules move along a temperature gradient. *Proc Natl Acad Sci U S A* **103**, 19678–19682 (2006).

324. Entzian, C. & Schubert, T. Mapping the Binding Site of an Aptamer on ATP Using MicroScale Thermophoresis. *J Vis Exp* (2017) doi:10.3791/55070.

325. Entzian, C. & Schubert, T. Studying small molecule-aptamer interactions using MicroScale Thermophoresis (MST). *Methods* **97**, 27–34 (2016).

326. Jerabek-Willemsen, M. *et al.* MicroScale Thermophoresis: Interaction analysis and beyond. *J. Mol. Struct.* **1077**, 101–113 (2014).

327. Lakowicz, Joseph R, E. *Principles of fluorescence Spectroscopy*. *Principles of fluorescence Spectroscopy* (1999).

328. Adam J. Kimple Mark Hughes, Ajit Jadhav, Francis S. Willard, Robin E., A. Y., Muller James Inglese, Gordon C. Ibeanu, David P. Siderovski, C. P. A. & Simeonov*, and A. A High-Throughput Fluorescence

Polarization Assay for Inhibitors of the GoLoco Motif:G-alpha Interaction. *Comb. Chem. High Throughput Screen.* **11**, 396–409.

329. Rossi, A. M. & Taylor, C. W. Analysis of protein-ligand interactions by fluorescence polarization. *Nat Protoc* **6**, 365–387 (2011).

330. Ma, X., Wang, J. & Cheng, Z. Cerenkov radiation: a multi-functional approach for biological sciences. *Front. Phys.* **2**, (2014).

331. Ciarrocchi, E. & Belcari, N. Cerenkov luminescence imaging: physics principles and potential applications in biomedical sciences. *EJNMMI Phys* **4**, 14 (2017).

332. Cho, J. S. *et al.* Cerenkov radiation imaging as a method for quantitative measurements of beta particles in a microfluidic chip. *Phys Med Biol* **54**, 6757–6771 (2009).

333. Zhang, G., Gurtu, V. & Kain, S. R. An enhanced green fluorescent protein allows sensitive detection of gene transfer in mammalian cells. *Biochem. Biophys. Res. Commun.* **227**, 707–711 (1996).

334. Ponchon, L. & Dardel, F. Recombinant RNA technology: The tRNA scaffold. *Nat. Methods* **4**, 571–576 (2007).

335. Jaffrey. Live-cell imaging of mammalian RNAs with Spinach2. *Methods Enzym.* **550**, 129–146 (2015).

336. Hahn, J. Synthese elongierter DFHBI-Varianten. (2016). doi:10.1017/CBO9781107415324.004.

337. Trapp, S. Synthese einer elongierten DFHBI-Variante Bachelorarbeit in der Chemie. (2017).

338. Rohrbach, F. *et al.* Chemical maturation of a bivalent aptamer by single domain variation. *Chembiochem* **13**, 631–634 (2012).

339. Patel, D. J. & Suri, A. K. Structure, recognition and discrimination in RNA aptamer complexes with cofactors, amino acids, drugs and aminoglycoside antibiotics. *Rev. Mol. Biotechnol.* **74**, 39–60 (2002).

340. Gordon, C. K. L. *et al.* Click-Particle Display for Base-Modified Aptamer Discovery. *ACS Chem. Biol.* (2019) doi:10.1021/acschembio.9b00587.

341. Jinpeng Wang, Qiang Gong, Nupur Maheshwari, Michael Eisenstein, Mary Luz Arcila, Kenneth S. Kosik, and H. T. S. Particle Display: A Quantitative Screening Method for Generating High-Affinity Aptamers. *Angew. Chemie* **126**, 1–6 (2014).

342. J.P Wang, J. McDermott, J. Yu, R. Lagrois, Q. Gong, W. Greenleaf, M. Eisenstein, B.S. Ferguson, and H. T. S. Multiparameter Particle Display

(MPPD): A Quantitative Screening Method for the Discovery of Highly Specific Aptamers. *Angew. Chemie Int. Ed.* **56**, 37–39 (2017).

343. Minyong Li, Na Lin, Zhen Huang, Lupei Du, Craig Altier, Hao Fang, and B. W. Selecting Aptamers for a Glycoprotein through the Incorporation of the Boronic Acid Moiety. *J Am Chem Soc* **130**, 12636–12638 (2008).

344. Bull SD, Davidson MG, van den Elsen JM, Fossey JS, Jenkins AT, Jiang YB, Kubo Y, Marken F, Sakurai K, Zhao J, J. T. Exploiting the Reversible Covalent Bonding of Boronic Acids: Recognition, Sensing, and Assembly. *Acc Chem Res.* **46**, 312–326 (2013).

345. Whyte, G. F., Vilar, R. & Woscholski, R. Molecular recognition with boronic acids-applications in chemical biology. *J. Chem. Biol.* **6**, 161–174 (2013).

346. Eriksson AE Zhang XJ, Heinz DW, Blaber M, Baldwin EP, Matthews BW, B. W. A. Response of a Protein Structure to Cavity Creating Mutations and Its Relation to theHydrophobic Effect. *Science (80-.).* **255**, 173–181.

347. Pace CN McNutt M, Gajiwala K., S. B. A. Forces contributing to the conformational stability of proteins. *FASEB J* **10**, 75–83.

348. David M. Huang, and D. C. The Hydrophobic Effect and the Influence of Solute-Solvent Attractions. *J. Phys. Chem* **106**, 2042–2053.

349. Noel T. Southall and A. D. J. Haymet, K. A. D. A View of the Hydrophobic Effect. *J. Phys. Chem.* **106**, 521–533.

350. Pfeiffer, F. *et al.* Systematic evaluation of error rates and causes in short samples in next-generation sequencing. *Sci. Rep.* **8**, 10950 (2018).

351. Gupta, S. *et al.* Pharmacokinetic Properties of DNA Aptamers with Base Modifications. *Nucleic Acid Ther* **27**, 345–353 (2017).

352. Kwok, C. K. & Merrick, C. J. G-Quadruplexes: Prediction, Characterization, and Biological Application. *Trends Biotechnol.* **35**, 997–1013 (2017).

353. Wong, H. M., Stegle, O., Rodgers, S. & Huppert, J. L. A toolbox for predicting g-quadruplex formation and stability. *J Nucleic Acids* **2010**, (2010).

354. Kikin, O., D'Antonio, L. & Bagga, P. S. QGRS Mapper: a web-based server for predicting G-quadruplexes in nucleotide sequences. *Nucleic Acids Res* **34**, W676-82 (2006).

355. Cowperthwaite, M. C. & Ellington, A. D. Bioinformatic analysis of the contribution of primer sequences to aptamer structures. *J. Mol. Evol.* **67**,

95–102 (2008).

356. Coleman, T. M. & Huang, F. Optimal random libraries for the isolation of catalytic RNA. *RNA Biol.* **2**, (2005).

357. Gupta, S. *et al.* Chemically modified DNA aptamers bind interleukin-6 with high affinity and inhibit signaling by blocking its interaction with interleukin-6 receptor. *J. Biol. Chem.* **289**, 8706–8719 (2014).

358. Contents, P. & Description, P. Dynabeads M-280 Tosylactivated. 1–2 https://assets.thermofisher.com/TFS-Assets/LSG/manuals/dynabeads_m280tosylactivated_man.pdf.

359. Widlanski, B. T. B. and T. S. An Intuitive Look at the Relationship of Ki and IC50: A More General Use for the Dixon Plot. *J. Chem. Educ.* **80**, (2003).

360. Hulme, E. C. & Trevethick, M. A. Ligand binding assays at equilibrium: validation and interpretation. *Br J Pharmacol* **161**, 1219–1237 (2010).

361. Tanious, F. A., Nguyen, B. & Wilson, W. D. Biosensor-Surface Plasmon Resonance Methods for Quantitative Analysis of Biomolecular Interactions. *Methods Cell Biol.* **84**, 53–77 (2008).

362. Liu, Y. & Wilson, W. D. Quantitative analysis of small molecule-nucleic acid interactions with a biosensor surface and surface plasmon resonance detection. *Methods Mol Biol* **613**, 1–23 (2010).

363. Hui Xu Qingxiang Zeng, Shengfu Wang, Abdel-Nasser Kawde and Guodong Liu, X. M. Aptamer-Functionalized Gold Nanoparticles as Probes in a Dry-Reagent Strip Biosensor for Protein Analysis. **81**, 669–675.

364. Liu, G. *et al.* Aptamer-nanoparticle strip biosensor for sensitive detection of cancer cells. *Anal Chem* **81**, 10013–10018 (2009).

365. Liu, J., Mazumdar, D. & Lu, Y. A simple and sensitive ‘dipstick’ test in serum based on lateral flow separation of aptamer-linked nanostructures. *Angew. Chemie - Int. Ed.* **45**, 7955–7959 (2006).

366. Wong, P. T. *et al.* Control of an Unusual Photo-Claisen Rearrangement in Coumarin Caged Tamoxifen through an Extended Spacer. *ACS Chem. Biol.* **12**, 1001–1010 (2017).

367. Rodionov, V. I., Lim, S. S., Gelfand, V. I. & Borisy, G. G. Microtubule dynamics in fish melanophores. *J. Cell Biol.* **126**, 1455–1464 (1994).

368. Cramer, L. & Mitchison, T. J. Moving and stationary actin filaments are involved in spreading of postmitotic PtK2 cells. *J. Cell Biol.* **122**, 833–843 (1993).

369. Vincent, J. and ’Farrell P. The State of engrailed Expression Is Not Clonally Transmitted during Early Drosophila Development. *1Cell* **68**, 923–931 (992).

370. John R.Giudicessi, BA.Michael J.Ackerman., 2013. Photoactivatable fluorophores and techniques for biological imaging applications. *Photochem Photobiol Sci* **11**, 460–471 (2012).

371. Aujard, I. *et al.* O-nitrobenzyl photolabile protecting groups with red-shifted absorption: Syntheses and uncaging cross-sections for one- And two-photon excitation. *Chem. - A Eur. J.* **12**, 6865–6879 (2006).

372. John R.Giudicessi, BA.Michael J.Ackerman., 2013. A New Method for the Cleavage of Nitrobenzyl Amides and Ethers. *Tetrahedron Lett.* **55**, 6467–6469 (2014).

373. Heckman, L. M. *et al.* Design and Synthesis of a Calcium-Sensitive Photocage. *Angew. Chemie - Int. Ed.* **55**, 8363–8366 (2016).

374. Hauke, S., Von Appen, A., Quidwai, T., Ries, J. & Wombacher, R. Specific protein labeling with caged fluorophores for dual-color imaging and super-resolution microscopy in living cells. *Chem. Sci.* **8**, 559–566 (2016).

375. Yan, Q. *et al.* Efficient substrate screening and inhibitor testing of human CYP4Z1 using permeabilized recombinant fission yeast. *Biochem. Pharmacol.* **146**, 174–187 (2017).

376. Tan, X. *et al.* Fluoromodules Consisting of a Promiscuous RNA Aptamer and Red or Blue Fluorogenic Cyanine Dyes: Selection, Characterization, and Bioimaging. *J. Am. Chem. Soc.* **139**, 9001–9009 (2017).

377. Ageely, E. A., Kartje, Z. J., Rohilla, K. J., Barkau, C. L. & Gagnon, K. T. Quadruplex-Flanking Stem Structures Modulate the Stability and Metal Ion Preferences of RNA Mimics of GFP. *ACS Chem. Biol.* **11**, 2398–2406 (2016).

378. Feng, G. *et al.* DNA mimics of red fluorescent proteins (RFP) based on G-quadruplex-confined synthetic RFP chromophores. *Nucleic Acids Res.* **45**, 10380–10392 (2017).

379. Spiga, F. M., Maietta, P. & Guiducci, C. More DNA-Aptamers for Small Drugs: A Capture-SELEX Coupled with Surface Plasmon Resonance and High-Throughput Sequencing. *ACS Comb Sci* **17**, 326–333 (2015).

380. Chen, A. & Yang, S. Replacing antibodies with aptamers in lateral flow immunoassay. *Biosens. Bioelectron.* **71**, 230–242 (2015).

381. Hwang, S. I. *et al.* Tetrahydrocannabinol Detection Using Semiconductor-Enriched Single-Walled Carbon Nanotube

Chemiresistors. *ACS Sensors* **4**, 2084–2093 (2019).

382. Maxi, N. X. Plasmid DNA Purification User Manual Extraction. *Culture* (2010).

383. Five-minute cloning of Taq polymerase-amplified PCR products. https://assets.thermofisher.com/TFS-Assets/LSG/manuals/topota_man.pdf.

384. Alex Apffel Steven Fischer, Kay Lichtenwalter, and William S. Hancock, J. A. C. Analysis of Oligonucleotides by HPLC-Electrospray Ionization Mass Spectrometry. *Anal. Chem.* **69**, 1320–1325.

Acknowledgement

I would like to thank a multitude of people who contributed to the development of this thesis in one way or another.

First, my special thanks go to Prof. Dr. Günter Mayer for the opportunity to work on this project. His encouraging support and helpful advices and inputs had an enormous impact in my development as a scientist.

I am very thankful to Prof. Dr. Christoph Thiele and Prof. Dr. Matthias Geyer for their willingness to be part of my committee.

My greatest thanks also go to Franziska Ersoy, who provided me with helpful information and advices throughout the whole project.

Thank you to our cooperation partners Christoph Protzek and Bern Tiemann from Protzek Gesellschaft für biomedizinische Technik mbH for providing us with help when needed, and the lateral flow THC-test stripes.

In addition, I am very grateful to my proofreading team containing Franziska Ersoy, Anna Esser, Julia Siegl, Georg Pietruschka and Jörg Ewers. Thank you all for your fruitful remarks.

I want to thank all current and former members of the Mayer-, Famulok., and Kath-Schorr groups for the nice time in the lab, the great colleagueship and their constant willingness for help and support, whenever needed. This particularly includes the coffee break team: Franziska Ersoy, Gerhard Brändle, Anna Esser, Julia Siegl, Anna Weber, and Jörg Ewers. Special thanks for their patience and useful advice also go to Fabian Tolle, Frank Eggert, Daniel Matzner, Mark Kerzhner, and Jeffrey Hannam.

Finally, thanks to my family, my parents Xaver and Elfi Rosenthal, as well as my brother Gerrit Rosenthal, for the constant motivation and mental support during this time. I know that you will always support me.